

Linking Parkinson's Disease and Melanoma:
The role of alpha-synuclein in DNA double-strand break repair

By

Moriah R. Arnold

A DISSERTATION

Presented to the Program in Biomedical Science and the Oregon Health & Science
University School of Medicine in partial fulfillment of the requirements for the degree of
Doctor of Philosophy

January 31st, 2025

CERTIFICATE OF APPROVAL

This is to certify the PhD dissertation of

Moriah R. Arnold

has been approved by

Mentor/Advisor: Vivek Unni, MD, PhD

Committee Chair: Amanda McCullough, PhD

Member: Pamela Cassidy, PhD

Member: Stephan Witt, PhD

Member: Philip Copenhaver, PhD

Member: Dorthe Payne-Larsen, PhD

Table of Contents

List of Abbreviations	11
Acknowledgements	14
Abstract	16
Chapter 1: Introduction	17
1.1 Parkinson's Disease	18
<i>Prevalence</i>	18
<i>Symptoms and Diagnosis</i>	21
<i>Neuropathology</i>	24
<i>Treatment</i>	26
1.2 Melanoma	27
<i>Prevalence</i>	27
<i>Symptoms, Pathology, and Diagnosis</i>	28
<i>Melanomagenesis Mechanisms</i>	32
<i>Treatment</i>	35
1.3 Parkinson's Disease and Melanoma	37
<i>Epidemiological Studies</i>	37
<i>Current Molecular Hypotheses</i>	39
1.4 Alpha-synuclein	45
<i>Alpha-Synuclein in PD</i>	47
<i>Alpha-Synuclein in Melanoma</i>	50
<i>Functional Studies</i>	52
1.5 Alpha-Synuclein and DNA Double-Strand Break Repair	54
<i>Role in the Nucleus</i>	54
<i>DNA Double-Strand Break Repair Pathways</i>	56
<i>Alpha-Synuclein in the Nucleolus and the Nucleolar DNA Damage Response</i>	60
1.6 Conclusion	66
Chapter 2:	
<i>PD-THRESHOLD: Melanocytic lesions and co-occurring disorders associated with future risk of Parkinson's Disease</i>	68
2.1 Abstract	69
2.2 Introduction	70
2.3 Results	72
<i>Cohort</i>	72
<i>Elevated PD Incidence after Diagnosis of Melanoma Precursors and Certain Subtypes</i>	74
<i>Positive Interaction of Melanocytic Lesions with Other Disorders</i>	76
<i>Lower Melanoma Stage if preceding PD</i>	79
2.4 Discussion	81
2.5 Methods	84

2.6 Acknowledgements	86
2.7 Author Contributions	87
2.8 Supplemental Material	88

Chapter 3:

Alpha-synuclein regulates nucleolar DNA double-strand break repair in melanoma **95**

3.1 Abstract	96
3.2 Introduction	97
3.3 Results	99
<i>Alpha-Synuclein Localizes to the Granular Component of the Nucleolus</i>	99
<i>Alpha-Synuclein Knockout Increases γH2AX Levels in the Nucleus and Nucleolus in an ATM- and ATR-Dependent Manner</i>	103
<i>Alpha-Synuclein Regulates Nucleolar Double-Strand Break Repair of Ribosomal DNA</i>	111
<i>Alpha-Synuclein is Recruited near Nucleolar Caps and Regulates the Rate of DSB Repair</i>	118
<i>Alpha-Synuclein Knockout Impairs MDC1-Mediated 53BP1 Recruitment to Nucleolar Caps and Leads to Micronuclei Formation and Growth Dysregulation</i>	120
<i>Transcriptomic Analysis Reveals Alpha-Synuclein Involvement in Nucleolar DNA Binding Regulation and Damage Repair Pathways</i>	123
3.4 Discussion	125
3.5 Methods	130
3.6 Acknowledgements	144
3.7 Author Contributions	145
3.8 Supplemental Material	146

Chapter 4:

Alpha-synuclein knockout impairs melanoma development and alters DNA damage repair in the TG3 mouse model in a sex-dependent manner **157**

4.1 Abstract	158
4.2 Introduction	159
4.3 Results	161
<i>Loss of Alpha-Synuclein Delays Melanoma Onset and Decreases Tumor Growth in vivo</i>	161
<i>Experimental Genotypes Display Similar Pigment Formation and Grm1 Expression</i>	164
<i>Loss of Alpha-Synuclein Decreases DNA Damage Signatures in the Melanoma Tumor</i>	165
<i>DNA Damage Signature Correlates to Cell Death Phenotypes</i>	168
4.4 Discussion	171
4.5 Methods	177
4.6 Acknowledgements	181
4.7 Author Contributions	182
4.8 Supplemental Material	183

Chapter 5: Discussion	185
5.1 Summary	185
5.2 DNA Damage Repair Pathways	186
<i>Mechanistic Insight</i>	186
<i>Other Forms of DNA DSB Repair</i>	191
<i>DSB Inducer Limitations</i>	193
5.3 Forms of Synuclein	197
<i>Phosphorylated Alpha-Synuclein</i>	198
<i>PD-Associated Mutations</i>	199
<i>Conformational Strains</i>	200
<i>Beta- and Gamma-Synuclein</i>	202
5.4 Liquid-Liquid Phase Separation	203
5.5 Downstream Cellular Phenotypes	206
<i>Apoptosis</i>	206
<i>Senescence</i>	208
<i>Autophagy</i>	212
5.6 Melanoma Models	214
<i>Limitations (in vitro)</i>	214
<i>Limitations (in vivo)</i>	216
<i>Alternative Disease Models</i>	219
5.7 Clinical Implications	220
5.8 Conclusions	224
Appendix A (unpublished)	225
A.1 Primary Melanocytes	225
<i>Introduction</i>	225
<i>Results</i>	225
<i>Discussion</i>	228
<i>Methods</i>	230
A.2 SK-Mel28 Cells	232
<i>Introduction</i>	232
<i>Results</i>	232
Neutral Comet Assay: DNA DSB Levels (Figure A.2.1)	232
HR and NHEJ Repair Pathways (Figure A.2.2)	233
Localization and Interaction with Nucleolar Proteins (Figure A.2.3)	234
53BP1 Recruitment and Western Blot Analysis (Figure A.2.4)	235
Kinase Dysregulation in DDR Pathways (Figures A.2.5 and A.2.6)	236
rDNA Copy Number and Ribosome Biogenesis (Figure A.2.7)	238
Ferroptosis and Lipid Peroxidation (Figure A.2.8)	240
EMT and Metastatic Potential (Figure A.2.9)	242
Replication Stress and Caspase-3 Activity (Figure A.2.10)	243
<i>Discussion</i>	244
<i>Methods</i>	254
A.3 In Vivo Class Switch Recombination	262
<i>Introduction</i>	262

Results	263
Discussion	264
Methods	265

Appendix B:

α-synuclein seed amplification in CSF and brain from patients with different brain distributions of pathological α-synuclein in the context of co-pathology and non-LBD diagnoses _____ **267**

B.1 Abstract _____ **268**

B.2 Introduction _____ **269**

B.3 Results _____ **270**

Neuropathological αSyn Analysis and Comparison _____ 270

Sensitivity and Specificity of the αSyn-SAA using CSF Samples _____ 274

Comparisons of Subjects with Positive vs Negative CSF αSyn-SAA Results _____ 279

Clinical Significance of Incidental Synuclein Pathology _____ 280

Detection of αSyn Seeds from Frontal Cortex and amygdala brain samples _____ 281

B.4 Discussion _____ **283**

B.5 Methods _____ **288**

B.6 Acknowledgements _____ **294**

B.7 Author Contributions _____ **295**

B.8 Supplemental Material _____ **296**

References _____ **302**

Table of Figures

Chapter 1: Introduction	17
<i>Figure 1.3.1. Biosynthesis of Melanin and Neuromelanin</i>	42
<i>Figure 1.4.1. Structure of αSyn</i>	47
<i>Figure 1.5.1. Proposed Loss-of-Function (PD) and Gain-of-Function (melanoma) Hypothesis</i>	56
<i>Figure 1.5.2. DSB Repair Pathways</i>	59
<i>Figure 1.5.3. αSyn is enriched in DAPI-poor regions of the nucleolus</i>	62
<i>Figure 1.5.4. Nucleolar DNA Double-Strand Break Repair Pathway.</i>	65
Chapter 2:	
<i>PD-THRESHOLD: Melanocytic lesions and co-occurring disorders associated with future risk of Parkinson's Disease</i>	68
<i>Figure 2.3.1. Schematic outlining analysis workflow</i>	72
<i>Figure 2.3.2. Cancer and risk of developing Parkinson's Disease</i>	74
<i>Figure 2.3.3. Impact of risk lesions for melanoma, melanoma subtypes, and pre-melanotic lesions on incidence of PD</i>	76
<i>Figure 2.3.4. Positive interaction of melanocytic lesion with other non-melanocytic skin disorders and prodromal-PD disorders upon incidence of PD</i>	78
<i>Table 2.3.1. Comparison of cancer registry data for melanoma with and without subsequent PD diagnosis</i>	80
<i>Table 2.8.1. Baseline characteristics of VA database populations</i>	88
<i>Table 2.8.2. Cancer counts in VA Oncology registry, medical notes, and pathology reports</i>	89
<i>Table 2.8.3. Added cases of Parkinson's Disease (per 10000 people) after melanocytic lesion versus control</i>	90
<i>Figure 2.8.1. Melanoma diagnosis and PD Incidence</i>	91
<i>Table 2.8.4. Added cases of Parkinson's Disease (per 1000 people) from interaction of a melanocytic lesion and another skin disorder</i>	92
<i>Table 2.8.5. Added cases of Parkinson's Disease (per 1000 people) from interaction of a melanocytic lesion and another prodromal PD disorder</i>	93

Chapter 3:

Alpha-synuclein regulates nucleolar DNA double-strand break repair in melanoma

95

Figure 3.3.1. Alpha-synuclein localizes to the granular component of the nucleolus in melanoma cells _____ 103

Figure 3.3.2. Alpha-synuclein interacts with γ H2AX in the nucleolus and knocking out alpha-synuclein leads to increased ATM/ATR-driven H2AX phosphorylation. _____ 105

Figure 3.3.3. Alpha-synuclein is important in bleomycin and IR-induced DNA damage response pathways _____ 111

Figure 3.3.4. Inducing rDNA DSBs increases alpha-synuclein levels and localization to sites of damage and alpha-synuclein knockout significantly increases γ H2AX _____ 115

Figure 3.3.5. Alpha-synuclein knockout significantly impairs recovery of rDNA damage downstream of ATM signaling _____ 117

Figure 3.3.6. Alpha-synuclein localizes to DSB-induced nucleolar caps and is important for nucleolar cap recovery _____ 119

Figure 3.3.7. Alpha-synuclein knockout leads to reduced recruitment of MDC1 and 53BP1 to nucleolar caps and is associated with impaired cellular growth and dysregulated expression of transcripts associated with DNA repair pathways _____ 123

Figure 3.4.1. Potential molecular mechanism by which α Syn facilitates nucleolar DDR and the downstream cellular consequences _____ 126

Figure 3.8.1. Alpha-synuclein localizes to nucleolar markers in melanoma cells and primary melanocytes _____ 146

Figure 3.8.2. Knockout and reintroduction validation of alpha-synuclein in SK-Mel28 cells _____ 147

Figure 3.8.3. Alpha-synuclein localizes with γ H2AX in melanoma cells & primary melanocytes and γ H2AX increases in alpha-synuclein knockout cells _____ 148

Figure 3.8.4. γ H2AX increase is driven by ATM and ATR in alpha-synuclein knockout cells _____ 149

Figure 3.8.5. Representative Images of ICW plates _____ 150

Figure 3.8.6. Increase in alpha-synuclein following bleomycin treatment is not due to transcriptional regulation _____ 151

Figure 3.8.7. Representative images of BRCA1 staining _____ 152

Figure 3.8.8. Alpha-synuclein is not involved in nucleolar DDR-mediated transcriptional silencing _____ 153

Table 3.8.1. Differentially expressed nucleolar transcripts in alpha-synuclein knockout cells _____ 156

Table 3.8.2. TaqMan assay probes _____ 156

Chapter 4:	
Alpha-synuclein knockout impairs melanoma development and alters DNA damage repair in the TG3 mouse model in a sex-dependent manner	157
<i>Figure 4.3.1. Alpha-synuclein knockout significantly delays tumor onset and slows tumor progression</i>	163
<i>Figure 4.3.2. Alpha-synuclein knockout does not interfere with Grm1 expression and results in possible decrease in lymph node metastasis</i>	165
<i>Figure 4.3.3. Alpha-synuclein loss-of-function leads to lower DNA damage signature in P110 perianal tumors</i>	168
<i>Figure 4.3.4. Alpha-synuclein knockout increases apoptosis, autophagy, and senescence marker expression</i>	171
<i>Figure 4.4.1. Schematic summary of proposed mechanism.</i>	173
<i>Figure 4.8.1. Alpha-synuclein knockout does not affect mouse weight.</i>	183
<i>Figure 4.8.2. Representative images and description of pinna tumor grading scale</i>	183
<i>Table 4.8.1. Primers used in qRT-PCRs</i>	184
Chapter 5: Discussion	185
<i>Figure 5.2.1. Proposed model for how α-syn regulates 53BP1 recruitment to sites of DSBs</i>	187
Appendix A (unpublished)	225
<i>Figure A.1.1 Response of γH2AX after UV radiation</i>	227
<i>Figure A.1.2. Alpha-synuclein is important in bleomycin and IR-induced DNA damage response pathways</i>	227
<i>Figure A.1.3. Alpha-MSH removal significantly diminished alpha-synuclein levels and its response to UV radiation</i>	228
<i>Figure A.2.1. Alpha-synuclein KO does not affect DNA DSB levels as measured by neutral comet assay</i>	233
<i>Figure A.2.2. Alpha-synuclein KO does not affect HR or NHEJ reporter plasmid repair efficiency</i>	234
<i>Figure A.2.3. Alpha-synuclein interacts with multiple nucleolar proteins</i>	235
<i>Figure A.2.4. Alpha-synuclein KO does not affect 53BP1 total protein expression as measured by western blot</i>	236
<i>Figure A.2.5. Volcano plot of dysregulated kinases after alpha-synuclein loss-of-function</i>	237
<i>Figure A.2.6. Heat maps of the identified phosphosites from 4 kinases of interest (Figure A.2.5)</i>	238

Figure A.2.7. Alpha-synuclein KO does not affect rDNA copy number _____	240
Figure A.2.8. Alpha-synuclein KO does not affect ferroptosis levels _____	241
Figure A.2.9. Alpha-synuclein KO increases mesenchymal marker, vimentin _____	243
Figure A.2.10. Alpha-synuclein KO decreases Caspase-3 activity after etoposide treatment _____	244
Table A.2.1. Primers used in qRT-PCRs _____	260
Figure A.3.1. A model of immunoglobulin class switch recombination _____	263
Figure A.3.2. Alpha-synuclein loss-of-function does not influence IgG2b class switch recombination _____	264

Appendix B:

α-synuclein seed amplification in CSF and brain from patients with different brain distributions of pathological α-synuclein in the context of co-pathology and non-LBD diagnoses _____	267
Table B.3.1. α S-SAA positivity as a function of pathology diagnosis _____	273
Table B.3.2. Sensitivity, specificity, and predictive values for antemortem and postmortem CSF α Syn-SAA against α Syn-pathology _____	275
Figure B.3.1. Kinetic parameters of Research SAA stratified by alpha-synuclein distribution _____	277
Figure B.3.2. Differences in neuropathology scores between synuclein-pathology groups as a function of SAA result _____	278
Figure B.3.3. Clinical and pathological differences between True Positive and False Negative _____	280
Table B.3.3. Patient categorization from brain homogenate samples _____	282
Table B.8.1. Summary of patient information _____	299
Table B.8.2. Summary of statistical analysis between α Syn pathology groups _____	301

List of Abbreviations

53BP1	p53-Binding Protein 1
α Syn	Alpha-synuclein
AD	Alzheimer's Disease
aNHEJ	Alternative NHEJ
ATM	Ataxia-Telangiectasia Mutated
ATR	Ataxia-Telangiectasia and Rad3-related protein
β Syn	Beta-synuclein
CNS	Central Nervous System
CRISPR	Clustered Regularly Interspaced Short Palindromic Repeats
CSF	Cerebrospinal Fluid
CSR	Class Switch Recombination
DDR	DNA Damage Response
DLB	Dementia with Lewy Bodies
DNA-PK	DNA-dependent Protein Kinase
DMSO	Dimethyl Sulfoxide
DSB	Double-strand Break
EMT	Epithelial-to-Mesenchymal Transition
γ Syn	Gamma-synuclein
GBA1	Glucocerebrosidase (lysosomal enzyme gene code)
GFP	Green Fluorescent Protein
HAP1	Human Haploid Cell Line
HR	Homologous Recombination

ICC	Immunocytochemistry
IDP	Intrinsically Disordered Protein
IF	Immunofluorescence
IHC	Immunohistochemistry
IR	Ionizing Radiation
KI	Knockin
KO	Knockout
LB	Lewy Body
LID	Laser-Induced Damage
LLPS	Liquid-Liquid Phase Separation
MAO B	Monoamine Oxidase Type B
MDC1	Mediator of DNA Damage Checkpoint Protein 1
MET	Mesenchymal-to-Epithelial Transition
MPTP	1-methyl-4-phenyl-1,2,3,6-tetrahydropyridine
MSA	Multiple System Atrophy
NAC	Non-Amyloid-beta Component
NHEJ	Non-homologous End-joining
NOR	Nucleolar Organizer Regions
PAR	Poly ADP Ribose
PD	Parkinson's Disease
PDD	Parkinson's Disease Dementia
PFF	Preformed Fibril
PLA	Proximity Ligation Assay

PLK	Polo-like Kinase
pPD	Prodromal-Parkinson's Disease
PSP	Progressive Supranuclear Palsy
pSyn	S129 Phosphorylated Alpha-synuclein
RBD	REM Sleep Behavior Disorder
rDNA	Ribosomal DNA
REM	Rapid Eye Movement
RPA32	Replication Protein A2
SAA	Seed Amplification Assay
SASP	Senescence-Associated Secretory Phenotype
SNCA	Gene encoding for Alpha-synuclein
SSB	Single-strand Break
TH	Tyrosine Hydroxylase
TNM	Tumor, Node, Metastasis
TYR	Tyrosinase
UVR	Ultra-Violet Radiation
WB	Western Blot
WT	Wild-Type

Acknowledgements

First and foremost, I want to thank my incredible PI, Vivek Unni, who has been the most wonderful mentor I could have hoped for. Your guidance has shaped me into the scientist I am today, and your unwavering support has carried me through every challenge. You taught me not just how to do good science but how to think critically and approach problems with creativity and rigor. Lastly, your love for things outside of science and medicine inspired me to prioritize those things as well, despite being a busy graduate student. I couldn't have done this without you, and I'll always be grateful for everything you've done for me. I hope that one day I will be even a fraction of the kind of physician scientist that you are.

I also want to express my deepest gratitude to my Dissertation Advisory Committee, Dr. Amanda McCullough, Dr. Stephan Witt, Dr. Pamela Cassidy, and Dr. Dorte Helena Larsen. Meeting with you all every six months was an incredible privilege, and I learned so much from each of you. You are brilliant scientists and inspiring role models, and your passion for science and your belief in my project pushed me to think bigger and do better. Thank you for your thoughtful feedback, challenging questions, and steadfast support. Your guidance has been instrumental in shaping this work and in shaping me as a scientist. To all of the other incredible mentors that I have met along the way: thank you to Dr. Joseph Quinn, Dr. Gregory Scott, Dr. Sancy Leachman, Dr. Sarah Meerts, Dr. Philip Copenhaver, Dr. David Jacoby, Dr. Todd Vanderah, Dr. Samuel Miller.

To my lab mates—thank you for being my problem-solving crew. Whether it was troubleshooting experiments, lending an extra set of hands, or commiserating over failed assays, you all made the grind bearable. Science is hard as hell, but it's easier with good people by your side. Valerie Osterberg, Dr. Sydney Weber-Boutros, Dr. Elizabeth Rose, Anna Bowman, Dr. Carlos Soto Faguas, Elias Wisdom, Jessica Keating, Samuel Kim, and Allison Zhou.

Dr. Mike Cohen, I don't even know where to start. You were one of the most influential mentors I've ever had. You didn't just spark my interest in science; you set me on the path that brought me here. The MD/PhD idea, the training at OHSU, the confidence to tackle big questions—it all started with you. I owe so much of this journey to your belief in me. Thank you for seeing my potential before I saw it myself.

Now, to the people who have kept me sane and laughing through this rollercoaster ride—my friends. You distracted me when I needed it most, brought joy and absurdity into my life, and reminded me there's more to the world than pipettes and data analysis. You're the reason I've smiled and laughed even during the most stressful times. Thank you to Parham Diba, Landon Bayless-Edwards, Zoe Beach, Simone Woodruff, Mizan Gaillard, Chris Taves, Olivia Decelles, Cole Brashaw, Gabby Thuillier.

Staci, my therapist, you deserve a damn medal. Thank you for listening to my endless rants, helping me untangle the chaos in my head, and always reminding me that

I'm strong enough to handle whatever comes next. I wouldn't have made it through this PhD—or life, frankly—without you.

Libby, my best friend and lab mate, you're the MVP of my PhD experience. Sharing this journey with you has been one of the greatest gifts. We got to do badass science together during the day and then leave it behind to just be us—laughing, venting, and being best friends. You made the tough days better and the good days even brighter. I'm so damn lucky to have had you by my side.

Scott, my lub, you came into my life at the most chaotic time of the PhD, and somehow you made it all feel manageable. The past 9 months have been hard but coming home to you and our little family with our two ridiculous dogs has been the absolute best part of my day, every day. You've made me feel so loved, supported, and understood, and I love you more than words can say. 

Hapa, this journey wouldn't have been the same without you. You have been there every single day of this PhD, greeting me with your wagging tail when I come home, forcing me to step away from my desk and think beyond science during our walks, and curling up next to me when I've cried through the hard moments. You've been my constant source of laughter, comfort, and unconditional love. You're my everything, and I'm so grateful to have had you by my side through it all (you are asleep next to me as I write this).

Finally, to my family. You are the reason I am who I am today. Every quality I possess, every dream I dared to chase, every strength I've leaned on through this journey, it all comes back to you. You cheered me on through every wild adventure, supported me through every tough moment, and gave me the space and resources to explore science and pursue my passions. You are my foundation, my safety net, my biggest cheerleaders, and my inspirations. Mom, Dad(s), and Mimi, you taught me to be bold and confident, never dimming my light—even when it shone as "bossiness" in my younger years. Max, your support from afar has meant everything to me. I'm so proud of you and the life you've built for yourself. All of your guys' love and support in the last 30 years have been unmatched, and I'll always cherish the way you stepped up when I needed you most.

This dissertation is for all of you. It's been a hell of a ride, but I didn't do it alone.

Thank you, from the bottom of my heart.

Abstract

There are clear links between genomic instability, aging, and diseases of aging, like neurodegeneration and cancer. In Chapter 1, background information on Parkinson's Disease, melanoma, and the clinical connection between these two diseases is explored. Furthermore, rationale for studying the neurodegeneration-associated protein, α Syn, and its role in the DNA damage response pathway is discussed as a potential molecular connection between the two diseases.

Chapter 2 through 4 dive into these topics experimentally, investigating the links between Parkinson's Disease and melanoma clinically (Chapter 2) and cellularly through both *in vitro* (Chapter 3) and *in vivo* (Chapter 4) methodologies. Through this dissertation, I conclude that there are distinct clinical characteristics in Parkinson's Disease-associated melanoma and that the upregulation of α Syn in melanoma is important in functional DNA double-strand break repair, essential for cell growth phenotypes *in vitro* and *in vivo*. In Chapter 5, I explore the limitations of this work as well as future directions for investigation; I ultimately propose a rationale for the co-occurrence of disease, in that individuals with high levels of α Syn expression are susceptible to both Parkinson's Disease and melanoma through similar loss-of-function and gain-of-function hypotheses, respectively.

Lastly, Appendix A highlights unpublished work focusing on the role of α Syn in DNA double-strand break repair using various models. Appendix B is adapted from published work indicating the use of α Syn-based seed amplifications assays in the diagnosis of incidental Lewy body pathology in other neurodegenerative diseases.

Chapter 1: Introduction

Neurodegeneration and cancer are two of the most debilitating medical conditions. They are often thought of as opposite processes, whereby neurodegeneration is characterized as neuronal cell death, and cancer is characterized as hyperproliferation of cells. One could think of these phenomena, at the opposite extremes of cellular survival, as having minimal overlap, but evidence suggests otherwise. Strong associations link neurodegeneration and cancer in autopsy studies (1), epidemiological work (2), and monogenic syndromes (3). Interestingly, there is a general decrease in overall cancer incidence in neurodegenerative disease patients (2), but an increased risk of selected cancer types (4). The best studied neurodegeneration-cancer relationship comes from epidemiological work on Parkinson's Disease (PD) and the skin cancer melanoma. Many studies report an increase in melanoma risk among individuals with PD compared to healthy individuals (2, 5-20). This risk is bidirectional, since there is also increased risk of developing PD in melanoma patients (12, 15, 21-23). Altogether, the association between PD and melanoma is well-established clinically, yet the cause is poorly understood. A potential mechanistic convergence in these two diseases provides new avenues to study both of these age-related conditions and address an urgent need for therapeutic options. The next sections of Chapter 1 will summarize some key points about these diseases individually and together, as well as introduce an alpha-synuclein (α Syn)-based hypothesis for understanding the underlying molecular connection between these two diseases.

1.1 Parkinson's Disease

Prevalence

Parkinson's Disease (PD) is a movement disorder that affects more than 10 million people worldwide. The estimated prevalence is 94 cases per 100,000 people, or approximately 0.3% in the general population in people 40 years or older (24) and nearly 2% in those over 65 years of age in industrialized countries (25). The yearly incidence of new cases ranges from 8 to 18.6 people per 100,000. These numbers are rising, as the estimated global prevalence of PD was 2.5 million in 1990, compared to the 10 million reported in 2022 (26). By 2040, the global prevalence of PD is expected to double from 6.2 million cases in 2015 to 12.9 million cases (27).

There are several risk factors associated with PD development and diagnosis, including age, sex, environmental exposures, medical comorbidities, and genetics, which will be discussed below. Of these, age is the most important risk factor for PD. Both incidence and prevalence rise significantly in adults beginning at the age of 50 (24), with the mean age of diagnosis at 70.5 years (28), although other studies have found varying mean ages at diagnosis around 60 years. Furthermore, men have a significantly higher risk of developing PD than females by a ratio of approximately 1.4:1 (26), which is paired with higher mortality rates and faster progression than women (29-31). Both males and females show differing parkinsonism phenotypes, where men may develop a postural instability-dominant phenotype, which includes freezing of gate and falling, whereas females exhibit a more tremor-dominant phenotype (32, 33). Lastly, men experience more cognitive issues associated with the disease, such as rapid eye movement (REM) sleep behavior disorder (RBD) (33) and mild cognitive impairment with a rapid progression to

dementias (34, 35). Sexual dimorphism in PD will be more extensively discussed in Chapter 4. Many environmental exposures have been identified as risk factors for PD as well, including exposure to certain pesticides (36-43), air pollution (44-46), high consumption of dairy products (47, 48), hydrocarbon solvents (49, 50), living in rural areas associated with agriculture work (36), high intake of iron (51), and reduced vitamin D (52-54). PD also interacts with several other diseases, where individuals afflicted with particular medical illnesses in early or mid-life have an increased risk of PD. Among the most consistently identified are: metabolic syndrome (55, 56), type 2 diabetes mellitus (57-59), traumatic brain injury (60-62), constipation (63), and depression (64-69).

In PD, 90% of all patient cases are idiopathic. However, 10% of PD cases are caused by genetic mutations, sometimes occurring in familial cohorts. These monogenic forms of PD span autosomal dominant, autosomal recessive, and X-linked inheritance patterns. Most patients with familial PD have a younger age of onset compared to sporadic PD (70-72). The first gene linked to PD was *SNCA*, which encodes α Syn (73). This protein and will be discussed at length in Chapter 1.4. In addition to *SNCA*, other mutations in other genes have been since linked to PD, including *LRRK2*, *GBA1*, *PRKN*, *PINK1*, and *DJ-1*.

The most common autosomal-dominant form of PD is a genetic point mutation in *LRRK2* (leucine-rich repeat kinase 2) (74). Epidemiological studies have found that the G2019S mutation in the *LRRK2* gene is the most prevalent and accounts for 5-6% of autosomal-dominant cases and 1% of idiopathic cases (75). However, genetic screening studies have found a race-specific incidence of *LRRK2*-associated familial PD. Studies suggest that *LRRK2* pathogenic variants account for 3-13% of autosomal dominant forms

of PD in Europe (76-80), but up to 50% of familial PD in people of North African and Middle Eastern origin (77, 81-84). The *LRRK2*-associated phenotype is often correlated to late-onset diseases (79, 85-87) and symptoms are almost indistinguishable from idiopathic PD (88, 89). *LRRK2* is a gene that encodes a protein called dardarin, which functions as a cytoplasmic kinase involved in phosphorylation of proteins (74, 81, 85). It is also associated with a variety of membrane and vesicular structures, important in vesicular transport, membrane turnover, and the lysosomal degradation pathway (90).

Monogenic mutations in *PRKN*, *PINK1*, and *DJ-1* have been associated with rare autosomal recessive forms of PD (91-93). These forms of disease are associated with early-onset of symptoms (before the age of 50), a slowly progressive course, and respond well to medications (94-98). The *PRKN* gene expresses a protein that is important in proteasomal pathways that functions in clearance of accumulating aggregated proteins; therefore, loss-of-function due to mutations can cause a significant impairment in this proteasomal pathway, leading to increase in neurodegenerative-associated aggregates (99, 100). Both *PINK1* and *DJ-1* genes are involved in mitochondrial function, therefore these variants may cause mitochondrial dysfunction-induced parkinsonism (93, 101-103).

Other than the aforementioned point mutations associated with familial forms of PD, mutations in the gene *GBA1* make up the most prevalent genetic risk factor for idiopathic PD. About 5-15% of PD patients will have mutations in the *GBA1* gene (104) and the risk of PD among *GBA1* pathogenic variant carriers is increased 2- to 7-fold over noncarriers (105-109). When compared to patients who had PD but lacked a *GBA1* pathogenic variant, those who carried a variant were significantly more likely to have a younger age of onset, less prominent motor symptoms, lower frequency of asymmetric

onset, higher frequency of family history of PD, and greater likelihood of cognitive impairment (105, 110-116). Because *GBA* mutations are the most widespread genetic risk factor for PD, substantial attention in the field is focused on this area of investigation. Altogether, although these genetic mutations are rare in comparison to the entire PD patient population, they can provide critical insight into the mechanisms of neurodegeneration.

Symptoms and Diagnosis

PD is traditionally thought of as a movement disorder, where most patients present with a “classical triad” of motor signs. These three signs include bradykinesia, resting tremor, and muscle rigidity. Postural instability is often mentioned as an additional cardinal feature, but typically occurs much later in the disease (117). Bradykinesia can often be described by patients as “weakness”, “incoordination”, and “tiredness”, but is typically associated with decrementing amplitude and decreased manual dexterity of the fingers, and dragging or shuffling of the feet when walking, and affects 80% of patients at the onset of disease (118). Resting tremor is the presenting symptom in 70-80% of patients with PD and affects 80 to 100% of patients at some point in the course of the disease (118). Rigidity occurs in approximately 75 to 90% of patients with PD (118) and usually refers to an increased resistance to passive movement at a joint and manifests typically as decreased arm swing when walking and stooped posture (119). Classically, these three PD-associated motor signs start unilaterally and spread contralaterally several years after the onset of symptoms. Although disease progression and severity

are variable between patients, the motor symptoms associated with PD universally worsen over time.

There are three major clinical subtypes of PD: 1) tremor-dominant, 2) akinetic-rigid, and 3) postural instability and gait difficulty (120-122). Generally, individuals with the tremor-dominant subtype show slower progression and less neuropsychologic impairment than the other two groups (123-129). However, it is worth noting that there is large variability of parkinsonism symptoms between patients, and initial course progression does not allow clinicians to accurately predict the future course of PD for any given individual (129, 130). However, studies suggest that mortality is significantly increased for patients with PD compared to age-matched controls (30, 127, 131-135).

In addition, PD patients will experience non-motor symptoms as well, with many of these arising years or even decades before the onset of classic motor symptoms (136), and are commonly referred to as prodromal-PD (pPD) disorders. These include RBD (137-142), constipation, and hyposmia (143-146). pPD disorders and their synergistic effect with melanocytic lesions in predicting PD will be discussed in Chapter 2. In addition, other non-motor symptoms during the course of disease include cognitive dysfunction and dementia (147-149), mood disorders (150, 151), sleep disturbances (152, 153), fatigue (154, 155), autonomic dysfunction (144, 156-160), olfactory dysfunction (143), and pain and sensory disturbances (161). In a multicenter survey, 97% of PD patients reported non-motor symptoms, with an average of 8 symptoms (152). Another single-center survey study found that PD patients reported the most troublesome non-motor symptoms to be mood disorders, pain, and sleep problems (152). Altogether, the presence or absence of certain non-motor symptoms can help aid in the diagnosis of PD

and distinguish various synucleinopathies that may otherwise present similarly, including Dementia with Lewy Bodies (DLB) or multiple system atrophy (MSA).

Because of the symptom variability between patients described above, definitive antemortem diagnosis for PD remains difficult, as physicians rely almost exclusively on patient history and physical exam. Currently, clinical diagnosis for PD follows criteria assigned by the Movement Disorder Society. Diagnosis requires the presence of parkinsonism (bradykinesia plus tremor or rigidity) as the central feature (117). In addition, supportive criteria can further increase the confidence of PD diagnosis, such as clear benefit from treatment with dopaminergic drugs, the presence of levodopa-induced dyskinesia, asymmetric resting tremor of a limb, and/or the presence of either olfactory loss or cardiac sympathetic denervation (117). Lastly, there are a set of absolute exclusion criteria and “red flags” that are specific signs of alternative diagnoses. The diagnosis of clinically established PD requires all of the following: 1) presence of parkinsonism, 2) no absolute exclusion criteria, 3) at least two supportive criteria, and 4) no red flags. Studies have shown that the overall accuracy of diagnosis based on the MDS criteria was 93% (162).

Although there are no physiologic, radiologic, or blood tests available to confirm the clinical diagnosis of PD, some diagnostic modalities are currently being developed. Striatal dopamine transporter imaging (DaTscan) can be used for patients whom clinical diagnosis is unclear. This modality can detect a decrease in the number of dopaminergic neuron terminals in the striatum and reliably distinguishes parkinsonian syndromes from control patients with essential tremor (163-166). In addition, positron emission tomography (PET) in combination with ligands that bind to dopamine transporters can act

as a marker of uptake in various brain regions. Studies have shown decreased uptake in the caudate and putamen in patients with early PD compared to controls (167-169). Ligands that detect α Syn for PET are currently in development (170). Lastly, testing for α Syn via cerebrospinal fluid (CSF) or skin biopsies is available although not routinely utilized. These tests employ seed amplification assays (SAAs) to identify abnormal clusters of α Syn aggregation. Many of these modalities are uncovering a striking amount of overlap between multiple neurodegenerative diseases, suggesting the comorbidity of these diseases pathologically is higher than originally thought based solely on antemortem clinical examination. The SAA modality and the overlap in synucleinopathy between differing clinical diseases is further discussed in Appendix B.

Neuropathology

As mentioned above, the gold-standard for PD diagnosis is confirmation of neuropathology during postmortem brain autopsy. On gross-pathology, PD patients will exhibit loss of a subset of dopamine neurons in the substantia nigra pars compacta that projects to the dorsal putamen (171). These cells are pigmented with neuromelanin, so a loss of these neurons corresponds to a decrease in pigment within this brain region. The substantia nigra is a critical movement center in the brain and a loss of this neuronal population is what causes the motor symptoms seen in PD. It is estimated that by the time first symptoms of PD emerge, approximately 60-80% of the neurons in the substantia nigra pars compacta have been lost (172, 173). In the surviving neurons, there are cytoplasmic inclusions called Lewy bodies (LBs), which are the pathological hallmark for PD. LBs are round, eosinophilic, intracytoplasmic neuronal inclusions that consist of a

dense granular core and loosely arranged in fibrillary elements. LBs are comprised primarily of aggregated and misfolded forms of α Syn and ubiquitin but can also contain other protein elements as well (174, 175). Although a pathological hallmark for PD, LBs are not specific for PD since they are found in other neurodegenerative diseases and as many as 10% of brains of otherwise healthy adults (176).

The current neuropathological staging of PD does not follow the traditionally held view that pathology begins in the substantia nigra. Neuropathologist Heiko Braak, proposed an alternative six-stage process, whereby pathologic changes in PD start in the medulla of the brainstem and in the olfactory bulb (Braak Stages 1-2), progressing rostrally over many years to the substantia nigra and other clusters of the midbrain and basal forebrain (Braak Stages 3-4), and eventually to the cerebral cortex and temporal and frontal lobes (Braak Stages 5-6) (177). Stages 1 and 2 could represent clinically pre-symptomatic phenotypes, whereas stages 3 and 4 generally associate with the time at which classic motor symptoms of PD first appear, followed by end-stages of PD during stages 5 and 6. Although Braak staging is widely used clinically, the validity and predictive utility of this staging has been questioned for multiple reasons, yet it remains the gold-standard.

In addition to this disease-specific pathology found in the substantia nigra, some patients will show a degeneration of various non-dopamine neurons in other nervous system regions, which correlates to non-motor symptoms. These include the internal globus pallidus, the centeromedian-perifascicular complex, the pedunculopontine tegmental nucleus, and the glutamatergic caudal intralaminar thalamic nuclei (178).

Concepts associated with α Syn neuropathology and downstream molecular dysregulation as a consequence of LB formation in PD will be introduced more thoroughly in Chapter 1.4.

Treatment

To date, the most effective therapeutic treatment option for patients with idiopathic PD is carbidopa-levodopa. Levodopa is a catecholamine precursor to dopamine synthesis that helps replenish its levels when dopaminergic neurons are reduced in the substantia nigra. Carbidopa is given in combination as it acts as a peripheral decarboxylase inhibitor to block levodopa conversion to dopamine in the systemic circulation before crossing the blood-brain barrier. This generally prevents nausea, vomiting, and orthostatic hypotension. Alternatively, monoamine oxidase type B (MAO B) inhibitors, dopamine agonists, or amantadine may be offered as an alternative, on a case-by-case basis. However, multiple studies have documented the benefit of levodopa over placebo and other dopaminergic therapies, with one showing a positive change in clinical scoring from baseline to 42 weeks on levodopa therapy (179), and another showing increased patient-rated quality of life over seven years of follow-up, with less patients needing add-on therapy compared to patients on other therapies (180). Motor symptoms can be highly responsive to levodopa early in the disease course, but motor fluctuations and “wearing off” develop in 30-40% of patients by 5 years. Because of these features, patients on levodopa require education of risks and consistent monitoring to establish minimum effective dose.

The therapies described above are not disease-modifying therapies, but rather compensate for the loss of dopaminergic neurons associated with PD pathology. However, several anti-synuclein strategies are being investigated in clinical trials currently, but all to date remain unsuccessful (181). Trials of two monoclonal antibodies, cinpanemab and prasinezumab, showed similar clinical and radiographic outcomes in the treatment and placebo groups at 52 weeks in early-stage PD patients (182, 183). In addition, active immunotherapy-based modalities directed against α Syn are in early stages of development (184, 185). Despite these recent advances, no disease-modifying therapies are currently clinically available.

1.2 Melanoma

Prevalence

Melanoma is the fifth most common cancer in males and females and is the most serious form of skin cancer (186). It is estimated that roughly 100,000 new cases of invasive melanoma were diagnosed just within the United States in 2023 and about 325,000 new cases worldwide in 2020 (187). Incidence rates in the United States continue to increase in adults ages 50 and older by approximately 1% per year from 2015 to 2019 or 12-fold increase between 1970 to 2020 (188). Although the incidence of melanoma is rising worldwide, most likely due to increasing numbers of skin biopsies (189, 190), the mortality rates are beginning to decrease, likely because of early detection efforts and advancements in treatments. It is estimated that in the United States, the overall mortality has declined by around 5% per year between 2011 to 2020.

Certain risk factors are associated with the development of melanoma, including family history, excessive sun exposure (191-196), immunosuppression (197-200), light-complexion (191, 201), red or blond hair (201), and light eye color (201). In addition, several syndromes can increase chances of developing melanoma, including familial atypical mole and melanoma syndrome (202, 203) and xeroderma pigmentosum.

Symptoms, Pathology, and Diagnosis

The current classifications of cutaneous melanoma are influenced by site of origin and various other pathological, clinical, and genetic characteristics, making up the revised 2018 World Health Organization classifications of melanoma tumors: high or low cumulative sun damage melanoma, desmoplastic melanoma, Spitz melanoma, acral melanoma, mucosal melanoma, melanoma arising in congenital nevus, melanoma arising in blue nevus, and uveal melanoma (186, 204). However, the traditionally classified melanoma subtypes based on previously described clinicopathological subtypes are superficial spreading, nodular, lentigo maligna, and acral lentiginous (205). For the scope of this dissertation, only these four melanoma subtypes and their associated pathological features will be discussed below.

Superficial spreading melanoma is the most common subtype, accounting for ~70% of all melanomas (204). These tumors are generally thin with ≤ 1 mm in thickness (206) and are most likely found on the back in males and the lower extremities in females. Most melanomas arise de novo without an associated nevus (207), yet superficial spreading melanoma is the subtype most likely to be associated with a pre-existing nevus (207). Histologically, superficial spreading melanoma presents as a variably pigmented macule or thin plaque with irregular border and lacks cellular maturation. In the radial

growth phase, there is a single-cell spread of epithelioid, neoplastic melanocytes through the layers of the epidermis. During the vertical growth phase, an epidermal component extends into the dermal component and mitosis is evident.

Nodular melanoma is the second most common type of melanoma accounting for 15-30% of all melanomas. These tumors appear as darkly pigmented, pedunculated, or polypoid papules (206-212). Unlike superficial spreading melanomas, nodular melanoma frequently presents with uniform color and are usually thicker than 2mm at the time of diagnosis (212). While the other subtypes can exist as a precursor lesion (melanoma in situ) or in the radial growth phase, nodular melanoma cannot and begins a vertical growth phase on inception. Histologically, dermal growth of epithelioid or spindled neoplastic cells occurs in isolation without an epidermal component.

Lentigo maligna melanoma is the subtype most closely associated with sun-damaged areas of the skin in older individuals and accounts for 10-15% of all melanomas (213). These tumors begin as tan or brown macules (214) and lesions gradually grow larger over the course of years, although vertical transformation of these tumors is slow (214, 215). Histologically, neoplastic melanocytes are present along the dermo-epidermal junction in a lentiginous pattern. Additional epidermal atrophy and solar elastosis is also commonly seen in these tumors. The hallmark of vertical growth is the formation of dermal nodules and fascicles and it is frequent that lentiginous proliferation extends down external root sheaths of hair follicles.

Lastly, acral lentiginous melanoma accounts for less than 5% of all melanomas, however, makes up the majority of melanomas among non-white individuals (216). The

anatomical location of these tumors is unique, in that they commonly arise on palmar, plantar, and subungual surfaces and first appear as dark brown irregular pigmented macules or patches (217). This subtype is the least likely to have radial growth and commonly, raised areas with ulceration and bleeding signify deeper invasion in the dermis. These tumors are generally diagnosed at later stages due to imitative qualities with other benign diseases and difficult-to-detect sites (218). Histologically, lentiginous melanomas are characterized by a lentiginous array of atypical melanocytes along the dermo-epithelial junction. Invasive lesions show the presence of neoplastic single cells or nests in the dermis.

Although clinical diagnosis for these melanoma subtypes is confirmed by biopsy and pathological analysis, early diagnostic criteria for melanoma follows key shared prediction rules. Many physicians use the widely adopted ABCDE checklist, which includes determination of asymmetry, border irregularity, color variegation, diameter >6mm, and evolution (219, 220). In addition, inpatient comparative analysis is important, where suggestion of melanoma comes with a lesion that does not match the patient's nevus phenotype, often referred to as the "ugly duckling" sign (221-224). Both the ABCDE rule and "ugly duckling" sign can be used by the patient and their primary care clinicians to detect suspicious lesions necessary for dermatological referral (225-227). It is important to note that these criteria apply most commonly to the superficial spreading subtype of melanoma and are less applicable to nodular and desmoplastic subtypes. In addition, because the ABCDE criteria are likely to miss early nodular or subungual melanomas, the EFG rule (228) (elevation, firm on palpation, and continuous growth) and ABCDEF rule (229) (age, brown band, change in nail band, digits commonly

involved, extension of pigment onto nail fold, family history of melanoma) were proposed to facilitate the detection of these subtypes, respectively.

Once melanoma has been suspected, dermatology referral is necessary with diagnostic confirmation using biopsy and histopathologic analysis. No single pathologic feature of melanoma is diagnostic, but rather based on a combination of features, like atypical melanocytes and architectural disorder. Although melanoma subtype classification is helpful for diagnosis, it is not informative about the biological behavior of the tumor and necessary management. Recognized prognostic factors for melanoma follow the tumor, node, metastasis (TNM) staging system (230). The American Joint Committee on Cancer in collaboration with the Union for International Cancer Control developed the TNM staging system that is now widely accepted by dermatologists (231). The “T” stands for tumor thickness and is defined as: T0 (unknown or regressed), T1 (≤ 1 mm), T2 (>1 to 2mm), T3 (>2 to 4mm), and T4 (>4 mm), with subdivision in each category for presence or absence of ulceration (231-234). The “N” category details the involvement of regional lymph nodes and is defined as: N0 (no regional metastasis), N1 (one involved lymph node), N2 (2-3 tumor-involved nodes), and N3 (4+ tumor-involved nodes, with subdivision in each category for method of detection and location of disease (231). Lastly, the “M” stands for distant metastases and is defined as: M1a (metastasis to distant skin or lymph nodes), M1b (metastasis to lung), M1c (metastasis to other visceral sites, excluding the CNS), and M1d (metastasis to the CNS). Based on the TNM parameters, patients are grouped into 4 prognostic stages: Stage I (T1-1N0M0), Stage II (T2-4N0M0), Stage III (T2-4N1-3M0), and Stage IV (T2-4N1-3M1a-d) (231). Additional

independent prognostic factors include age (235, 236), sex (237-240), anatomic location (237, 241, 242), and mutation status (243).

In difficult-to-confirm lesions, immunohistochemistry can be used with markers specific for melanoma (S-100, Sox10, MART-1, HMB-45, MITF, and tyrosinase) as well as molecular techniques (comparative genomic hybridization, fluorescence in situ hybridization, and gene expression profiling) (244-247). Overall, these approaches can be particularly useful when distinguishing between atypical melanoma, precursor melanocytic lesions, and nonmelanocytic lesions. This becomes critically important in order to combat such an aggressive neoplasm and minimize morbidity and mortality. Together, TNM staging parameters and these additional prognostic factors help providers develop individualized clinical care and treatment plans for their melanoma patients. However, the underlying molecular mechanisms of melanoma progression are important in understanding these diagnostic criteria.

Melanomagenesis Mechanisms

Melanocyte biology and its perturbation in the context of melanomagenesis and progression is an extensively studied area of research, with the ultimate goal of developing targeted therapies and improving outcomes for melanoma patients. Many studies have demonstrated that UV exposure is a major risk factor for melanoma. There are two independent pathogenic pathways for UV-induced melanomagenesis that have been postulated: 1) a melanin-independent pathways associated with UVB-induced DNA damage and 2) a UVA-initiated melanin-dependent pathway associated with indirect

oxidative DNA damage (248, 249). Both pathways however will create cyclobutane pyrimidine dimers in DNA (250) and are linked to *BRAF*-mediated melanomagenesis (251). In addition, the “divergent pathway” model describes a theory that individuals with the propensity to develop fewer melanocytic lesions require more sun exposure to begin melanomagenesis, and this usually occurs on chronically sun-exposed sites. In contrast, individuals with large numbers of nevi may require less UV exposure to induce melanomagenesis, and therefore development melanoma in sites where large nevi are found. This model suggests that melanoma on different sites of the body may occur via different mechanisms, like the ones described above (252-255).

Multiple genetic mutations are necessary to lead to melanocytic transformation and melanomagenesis, also known as the “multi-hit” model (256). One study, utilizing the Cancer Genome Atlas program, found that in 331 metastatic and primary melanoma samples, there were three main mutated genes, including *BRAF*, *RAS*, *NF1*, and the triple wildtype, which is defined as *BRAF*, *RAS* and *KIT* wild type (257). Later studies confirmed these findings and postulated that these specific melanoma genetic subtypes develop along distinct evolutionary pathways, driven by mutations in different genes, and that these paths diverge depending on amount of sun exposure (204). The initiating events of melanomagenesis are typically gain-of-function mutations in driver oncogenes (*BRAF*, *NRAS*, *GNAQ*, *GNA11*), followed by secondary loss-of-function mutations in tumor suppressor genes (*CDNK2A*, *TP53*, *PTEN*, *BAP1*) (204, 205, 256). In other words, the initial oncogenic mutations are not founder events, but rather facilitate malignant transformation with the acquisition of subsequent oncogenic stimuli. Divergence in these pathways can give rise to different surface antigen expression, cytogenetic profiles, and

growth characteristics between patients of the same melanoma subtype, that can lead to differing metastatic propensities and prognosis (258-262). For example, cutaneous melanomas, arising from sun-exposed skin, are often associated with *BRAF* mutations, whereas acral melanomas are less commonly linked to *BRAF* mutations and more likely have amplifications in genes like *CCND1* and *CDK4* (263-265).

Specifically, 25-30% of cutaneous melanomas will harbor a mutation in the oncogene, *NRAS* (257, 266). A somatic mutation in *NRAS* can cause constitutive activity of the NRAS protein, which in turn leads to serial activation of serine-threonine kinases, promoting cell cycle progression and melanocytic transformation. In about 14% of melanoma cases, loss of function of the *NF1* tumor suppressor gene, which directly suppresses NRAS signaling, is found in combination with *NRAS* mutations (257, 266-270). Of the serine-threonine kinases activated downstream of RAS activity, BRAF and CRAF are arguably the most important in melanoma pathobiology. Following activation, RAF homo- and hetero-dimers interact with the MAPK/ERK kinase MEK to initiate phosphorylation and subsequent activating phosphorylation of ERK (271-273). This MAPK pathway signaling cascade ultimately results in pro-growth and melanoma transforming signal (274). In addition to *NRAS* mutations, RAS-independent pathway growth signaling can be activated directly with *BRAF* mutations and in fact, approximately 50% of cutaneous melanomas have an activating V600 mutation in the *BRAF* gene (275-277). Among melanomas that are *BRAF* mutation-positive, up to 95% are *BRAF* V600 alterations to -E or -K (278, 279). These point mutations result in BRAF monomers, instead of homo- or hetero-dimers, which leads to insensitivity to ERK-mediated feedback inhibition.

In addition to somatic mutations associated with the multi-hit model of melanomagenesis, 10% of melanoma are familial and are a consequence of germline mutations (280). However, there is considerable heterogeneity between different families, suggesting the importance of multiple genes that can contribute to familial melanomagenesis (281). The three most commonly linked familial melanoma genes are *CDKN2A*(282, 283), *BAP1*(284-287), and *MCR1* (288-290).

Treatment

The diagnostic, prognostic, and genetic information provided by pathologic review of the biopsied lesion influences the selection of treatment for patients (291). During the radial growth phase, the melanoma is almost always curable by surgical excision alone (98.4% 5-year survival rate) (292). These melanomas are called melanoma in situ or microinvasive melanomas. However, tumors that infiltrate deep into the dermis are considered to be in a vertical growth phase and have metastatic potential (293). Vertical growth phase tumors can arise de novo or from radial growth phase melanoma, but require more extensive treatment modalities, especially in the setting of metastasis. In patients with limited number of metastases, surgical metastasectomy can be beneficial with or without the addition of adjuvant systemic therapy.

Immunotherapy is a common treatment option and the most common systemic treatment for metastatic melanoma. “Typical” systemic anti-cancer treatment options, like radiation therapy and cytotoxic chemotherapy, have not been shown to improve overall survival in patients with melanoma and are therefore not widely used. In fact, in multiple

randomized phase III clinical trials in *BRAF* wild-type metastatic melanoma, single-agent immunotherapy improved overall survival compared to chemotherapy (294, 295). Checkpoint immunotherapy inhibition with a PD-1 inhibitor (pembrolizumab or nivolumab) in combination with a T cell activator (ipilimumab or relatlimab) has been reported to be more efficacious than single-agent anti-PD-1 therapy (296, 297), however responses to immunotherapy may develop slowly. PD-1 is a transmembrane protein expressed on T cells, B cells, and natural killer cells that binds to the ligands PD-L1 and PD-L2, which are present on many tumor cells. This interaction directly inhibits apoptosis of the tumor cell, therefore inhibition of PD-1 through treatment with antibodies like pembrolizumab or nivolumab, lead to downstream activation of apoptosis of cancer cells (298, 299). Unfortunately, the use of these systemic treatment modalities is associated with a variety of clinically significant autoimmune side effects, including fatigue, infusion-related reactions, cytokine release syndrome, dermatologic toxicity, diarrhea, hepatotoxicity, pneumonitis, autoimmune thyroid disease, adrenal insufficiency, type 1 diabetes mellitus, and increased risk of opportunistic infections.

In patients where melanoma tumors have been sampled and specific point mutations have been identified, targeted therapy is the preferential treatment option. In *BRAF* V600 mutation-positive melanoma, *BRAF* inhibition is highly effective in producing rapid tumor regression, especially in combination with MEK inhibition (300-303). These combination regimens include dabrafenib plus trametinib, vemurafenib plus cobimetinib, and encorafenib plus binimetinib. Unfortunately, virtually every patient treated with a *BRAF* inhibitor will eventually have resistance and disease progression. No consistent mechanism for resistance has been identified, but studies have suggested bypass

mechanisms within the MAPK pathway (304-312), altered RNA processing of BRAF (313), and signaling through the parallel cell growth pathway, PI3K (314, 315).

1.3 Parkinson's Disease and Melanoma

Chapter 1.3 will focus on the clinical association between PD and melanoma. However, it is important to contextualize this disease connection within the broader trends between PD and other common cancers. Many epidemiological studies have indicated an inverse association between the risk of developing cancers and PD. Bajaj et al. found in a meta-analysis of 29 studies that PD was associated with an overall 27% decreased risk of all cancers and 31% decreased risk after exclusion of melanoma (2). Similarly, another meta-analysis study found a 17% decreased risk of cancer in PD patients (316). These trends extend to other neurodegenerative diseases as well, including Alzheimer's Disease (AD) (317-320). However, these studies have collectively found an increased prevalence of a select few cancers in PD, including breast (4-6, 321), brain (4, 322, 323), non-melanoma skin cancer (5-7, 322, 323), and melanoma. Chapter 2 will further address the differences in incidence between PD-melanoma and PD-other cancers.

Epidemiological Studies

In 1972, Skibba et al. first reported the unusual development of multiple melanomas in a patient suffering from PD (324). Since this initial report, many epidemiological studies have further elucidated a clinical connection between PD and melanoma, where there is an increased incidence of melanoma in PD patients compared to healthy individuals. These reports found an increased incidence ranging from 1.41-

20.9, depending on the study, which included a variety of cohort sizes and demographic characteristics (2, 5-7, 10-15, 17, 18, 32, 325). A meta-analysis from 12 studies showed that the risk of developing melanoma in individuals with PD was 3.6-fold higher than controls individuals, with a pooled odds ratio of 2.1 (326). Another meta-analysis from 22 studies reported a 2.4-fold increased risk of melanoma in PD, with a pooled odds ratio of 1.83 (327).

This clinical relationship is bi-directional, whereby individuals with melanoma are at an increased risk of developing PD. Although less well-studied, multiple investigations have reported an increased fold change of developing PD in melanoma patients ranging from 1.5 to 4.2 (7, 12, 15, 21-23). Interestingly, this increase in incidence of PD not only included patients with melanoma, but also their first-degree relatives. Gao et al. found that individuals with a first-degree family history of melanoma had a 1.85-fold higher risk in developing PD than those without a family history of melanoma (22), and this association extends to third-degree relatives, as well (12). Lastly, PD-associated mortality is significantly higher in individuals with melanoma compared to individuals with other types of cancer (12, 21, 23). Despite overwhelming evidence that the clinical relationship between melanoma and PD is bi-directional, the difference in melanoma disease presentation, characteristics, and prognosis in pPD is not well characterized, but it could provide substantial clinical insight and prompt development of clinical criteria that allow for better monitoring in a high-risk pPD population. Chapter 2 investigates the melanoma characteristics and other melanocytic and non-melanocytic precursor lesions associated with pPD, to address this gap in epidemiological research.

There have been documented shared risk factors between PD and melanoma which include: 1) Age- the risk of developing both diseases increases with age; 2) Family history- having a close relative with PD increases one's risk for PD, and having a close relative with melanoma increases one's risk for melanoma (328); 3) Gender- men are 1.5 times more likely to develop PD (329) or melanoma (330) compared to women; and 4) Ethnicity- both PD (28) and melanoma (329) are more common in white populations. Furthermore, melanoma and PD patients can share certain clinical prodromal features, like vitamin D deficiency (331-335) and sleep disorders (336-338). Altogether, the bidirectionality of this relationship and the shared clinical risk factors suggest that there are common genetic, environmental, and/or molecular mechanisms contributing to this phenomenon.

Current Molecular Hypotheses

Initial reports, like Skibba et al. (324), suggested that the increased incidence of melanoma among PD patients could arise from levodopa treatment. This was hypothesized based on the concept that levodopa is fundamentally involved in both dopamine and melanin biosynthetic pathways in dopaminergic neurons and melanocytes, respectively (339-341). Furthermore, although bidirectional, the risk for PD in melanoma patients has consistently been lower than that for melanoma in PD patients, indicating additional factors, like levodopa therapy, could be contributing to the latter. Clinically, melanoma history is still listed as a contraindication to levodopa use. However, reports showing an increased incidence of PD in melanoma patients and an increased risk of melanoma in first-degree relatives of PD patients, two populations that are not taking

levodopa, overwhelmingly suggest that the clinical relationship between PD and melanoma is not due to levodopa treatment, but rather other genetic, environmental, and molecular factors.

Some studies have investigated the underlying genetic links between PD and melanoma, given work linking family-history of melanoma to PD risk (12, 22). A meta-analysis of four genome-wide association studies found a positive genetic correlation between melanoma and PD (342). They identified 7 melanoma and PD-associated genes, including *GPATCH8*, *MYO9A*, *PIEZO1*, *SOX6*, *TRAPPC2L*, *ZNF341*, and *ZNF778*. Another study performed whole-exome sequencing of 246 cutaneous melanoma tissue samples and found that roughly 50% of the samples contained one of 14 somatic mutations in genes that had previously been associated with PD (110). These included the genes, *LRRK2*, *PRKN*, *EIF4G1*, and *SYNJ1*. In fact, other studies have validated these findings of *PRKN* somatic mutations within melanoma tissue (343, 344). Conversely, various melanoma-related gene mutations have been identified in PD patients. These include *TRPM7* (345), *PTEN* (346), *GPNMB* (347, 348), and *MC1R* (22). Two gene polymorphisms in *MC1R*, variants *R151C* and *R160W*, which are responsible for fair skin phenotypes with reduced UV protection, has been linked to an increased incidence of PD (22, 349-352) and increased incidence of melanoma (353-355). Interestingly, the location of these correlated genes in melanoma and PD plays a role in the susceptibility of mutations. For example, fragile regions on chromosome 6 are home to *PRKN* as well as other tumor suppressor genes that are commonly mutated in melanoma. This region is especially susceptible to deletions and mutations (356). In addition, *PINK1* is located on chromosome 1p36, a region frequently deleted in human

cancers and mutated in familial forms of PD (357-359). Further investigation is necessary to uncover the molecular and cellular pathways affected by these genetic mutations and how dysregulation of these pathways lead to both melanoma and PD pathogenesis.

Beyond the genetic connection between melanoma and PD, it is intriguing to consider the pathway convergences between these two diseases. One such pathway that has garnered interest in the context of melanoma and PD co-incidence is the pigmentation synthesis pathways. Melanin is the main determinant of skin pigment in melanocytes, but also exists as neuromelanin in dopaminergic neurons in the substantia nigra. Melanin synthesis disorders can lead to melanoma, while neuromelanin abnormalities have been linked to PD, suggesting a common correlation between both diseases (360, 361). These synthesis pathways share conserved precursors, where phenylalanine is converted to tyrosine (Figure 1.3.1). At this stage, pathways will diverge, where tyrosine hydroxylase (TH) converts tyrosine to the dopamine precursor levodopa, while tyrosinase (TYR) converts tyrosine to the melanin precursor dopaquinone. Neuromelanin is ultimately produced from dopamine in dopaminergic neurons and eumelanin and pheomelanin is produced from dopaquinone in the melanosome of melanocytes (362).

radicals can lead to DNA damage, ultimately increasing the risk of PD and melanoma respectively (365, 366). Furthermore, aggregated α Syn, as seen in PD, has been shown to disrupt melanin biosynthesis, namely the catalytic activity of TYR (Figure 1.3.1) (367-369). In fact, the TYR melanogenesis pathway was identified as the top significant pathway for PD in a GWAS study (370) and treatment with TYR inhibitor, S05014, protected neurons from MPTP-induced impairment *in vitro* and attenuated movement abnormalities *in vivo* (371). Overall, researchers have hypothesized that in the melanocytes of patients suffering from PD, increased α Syn causes inhibition of TYR, which leads to decreased melanin synthesis, leading in turn to the increased risk for melanoma (367, 372). However, aggregated α Syn may regulate other components of the melanin synthesis pathway, as well. In fact, Dean and Lee proposed an alternative mechanism by which α Syn modulates Pmel17 function, a premelanosomal protein which forms a fibrillar matrix that serves as a scaffold for melanin polymerization (373). α Syn has also been shown to regulate glycosphingolipids, which are responsible for the sorting of tyrosinase to melanosomes, and the dysregulation of glycosphingolipids has been associated with both melanoma and PD (374-379). Lastly, it has been proposed that the connection between PD and melanoma arises from pheomelanin levels; where neuromelanin is made of a pheomelanin core that becomes more exposed with age and therefore increases the selective vulnerability of the pigmented dopaminergic neurons to oxidative reagents or dopaminergic toxins in PD (380, 381), while increased peripheral pheomelanin is also associated with increased risk of melanomagenesis (382).

Regardless of the cause of melanin/neuromelanin biosynthesis dysregulation suggested above, it is unclear whether the presence of neuromelanin in dopaminergic

neurons is toxic or protective. The loss of neuromelanin in the substantia nigra, as seen on autopsy in PD patients (383), could be the result of the loss of neurons, or indicate that the death of neurons is triggered by loss of neuromelanin when the synthesis pathway is compromised (360, 384). However, in melanoma, it has been found that transformed melanocytes increase expression of melanin, which inversely correlates with overall survival and tumor progression in patients with advanced melanoma (361), suggesting its role in melanoma is not protective. Further studies are needed to elucidate the role of CNS and periphery pigmentation in the PD-melanoma association, especially in racial populations where melanomas most likely form on sun-protected areas.

In addition to the pigmentation pathway hypothesis, researchers have proposed the immune system as a contributing factor in the PD-melanoma association. Melanoma has traditionally been thought of as an immunogenic tumor, where cell proliferation is associated with immune system dysfunction (385, 386). In addition, neuroinflammation plays a role in the pathogenesis of PD (387-389). On autopsy, PD patients will exhibit elevated levels of pro-inflammatory factors in their brains, which are believed to play a role in neurodegeneration within the CNS (390). Furthermore, there is evidence that supports the involvement of the peripheral immune system in melanoma and PD pathogenesis and progression (391, 392). For example, PD patients have altered gut microbiomes, which may increase inflammation (391), and the intestinal flora plays a role in the response of patients treated with anti-PD-1 therapies (393). Overall, immune dysregulation may represent one of the convergent mechanisms leading to neurodegeneration in dopaminergic neurons and tumorigenesis in melanocytes, however more studies are needed to explore immune dysregulation in the PD-melanoma link.

Lastly, the shared role of α Syn in melanoma and PD is of great interest. Although α Syn is traditionally thought of as a neurodegeneration-associated protein, it is also found outside of the CNS and is highly upregulated in melanoma. Studies have found an increased amount of α Syn deposition in skin biopsies of patients with melanoma, compared to melanocytes in healthy individuals(394-396), with an estimated 86% of primary metastatic melanoma tissue samples being positive for α Syn (397). In addition, gene expression analysis found that *SNCA* expression was around 3-fold higher in metastatic melanoma tissue samples compared with healthy controls (398). Lastly, immortalized human melanoma cell lines highly upregulate endogenous α Syn expression when compared to multiple other cell lines (339, 397-401). Altogether, these observations suggest that this PD-associated protein could represent a molecular link between these two diseases and will be the focus for the remainder of this dissertation.

1.4 Alpha-synuclein

α Syn is a small 140 amino acid long protein that is abundant in the CNS, accounting for about 1% of total soluble CNS protein (402). As shown in Figure 1.4.1, the N-terminal segment (residues 1-60) of the protein takes on an alpha-helical shape in the presence of synaptic vesicles (403, 404), which allows for α Syn to act as a chaperone when bound to these docked synaptic vesicles to form SNARE complexes for downstream neurotransmitter release from the presynaptic membrane (405-407). The hydrophobic Non-amyloid-beta Component (NAC) domain (residues 61-95) allows for α Syn to form β sheet structures and is the region responsible for pathologic α Syn

oligomerization. This region can either be membrane-bound or exposed to the cytosol, where it can recruit monomer α Syn and induce accumulation (408, 409). Finally, the C-terminal segment (residues 96-140) inhibits aggregation but contains post-translational modification sites that are important in α Syn biology. These properties of α Syn's structure suggest that it is an intrinsically disordered protein (IDP) that can fold into alpha-helical conformations and undergo other disease-associated reorganizations (described later in Chapter 1.4 and Chapter 5.4), yet there remains controversy as to whether it can also exist physiologically as a tetramer (410). α Syn is located throughout the cell body but enriched in the synapse and nucleus of the cell. Its role at the synapse has been highly studied, and it is involved in synaptic vesicle release and plasticity of the synapse via its N-terminal alpha-helical structure. Its role in the nucleus is poorly understood but will be discussed in length in Chapter 1.5, and is the basis for Chapters 3 and 4.

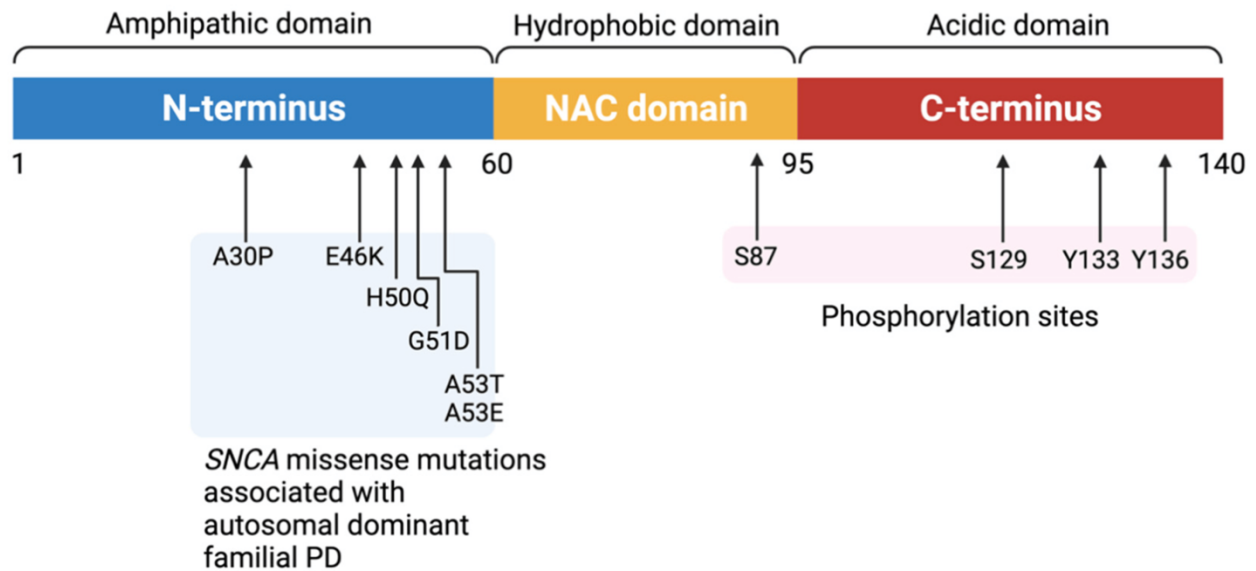


Figure 1.4.1. Structure of α Syn. Adapted from Fan et. al 2021 (411). This figure illustrates the domain organization of alpha-synuclein, a 140-amino-acid protein central to synucleinopathies. The N-terminal region (residues 1–60) features amphipathic helices that enable membrane binding and contains key mutations (e.g., A30P, E46K, A53T) linked to familial Parkinson’s disease. The non-amyloidogenic (NAC) domain (residues 61–95) drives aggregation into amyloid fibrils, a hallmark of pathological inclusion bodies. The C-terminal region (residues 96–140) modulates aggregation through its acidic residues and is a site for phosphorylation and truncation. Together, these domains underpin alpha-synuclein’s role in physiological functions, such as synaptic vesicle regulation, and its misfolding in neurodegenerative diseases.

Alpha-Synuclein in PD

As described in Chapter 1.1, aggregated and insoluble forms of α Syn are a major component of LBs in PD and other synucleinopathies (412-414). The mechanisms by which α Syn aggregates is not well understood. It is thought that an alteration in secondary structure causes the natively unfolded α Syn to self-aggregate after being targeted for proteasomal degradation by ubiquitin (415). Observations from both human and rodent models suggest that misfolded forms of α Syn can be transmitted from diseased neurons to healthy ones (416). Additionally, pathologic and aggregated α Syn can act as a template

that corrupts monomeric α Syn. This “seeding” phenomenon, similar to prion diseases and therefore coined the “prion-like hypothesis”, further spreads the disease from an affected neuron or glial cell to a normal one, which in turn becomes diseased. This is based, in part, on studies in which injection of pre-formed fibrils (PPFs) of α Syn into the brains of normal mice leads to LB-like pathology with progressive loss of dopaminergic neurons and impaired motor coordination (417, 418). Furthermore, in long-term studies of patients with PD who received human fetal nigral neuron transplantation, autopsy revealed that the grafted nigral neurons contain LBs that stain positive for α Syn (419, 420).

Throughout the past few decades of research, scientists have questioned whether α Syn aggregation itself causes cell death and ultimately neurodegeneration (421, 422), or if LBs are merely byproducts and may actually serve a protective rather than toxic function (423-426). This issue is still under debate; however, recent evidence utilizing longitudinal *in vivo* multiphoton imaging in mice injected with pre-formed fibrils (PPFs) suggests that neurons that bear these inclusions are the ones that eventually degenerate (427). This data strongly supports a model where LBs are tightly paired with cellular death. However, how these aggregates are promoting cell death is still an active area of investigation. Some studies suggest that misfolded and aggregated α Syn can “clog” cellular protein homeostasis and impair proteolysis, through dysregulation of molecular chaperone, ubiquitin-proteasome, and autophagy-lysosomal pathways (428-430). Other studies suggest that α Syn aggregation causes mitochondrial dysfunction. In 32 to 38% of sporadic PD patients, mitochondrial complex I activity is decreased in the substantia nigra (431, 432). In addition, mitochondrial toxicity in PD has been utilized to develop multiple murine-based PD models. These agents include 1-methyl-4-phenyl-1,2,3,6-

tetrahydropyridine (MPTP) (433, 434) and rotenone (435). Lastly, other cellular insults have been reported as a consequence of LB formation upstream of neurodegeneration, including oxidative stress (432, 436), iron metabolism (437-439), inflammation (440, 441), and DNA damage (442, 443).

Not only is α Syn pathologically connected to PD, but it is also genetically connected to PD. *SNCA* gene missense mutations and multiplications are rare causes of autosomal dominant parkinsonism (76). The symptomatic phenotype of individuals harboring these mutations range from classic PD to DLB (444-446); however, the clinical features of the majority of *SNCA* mutations show younger age of onset, greater cognitive decline, and more rapid progression of disease (88, 447, 448). The first *SNCA* mutation to be associated with parkinsonism was a single base pair substitution leading to a point mutation, A53T, on chromosome 4q21-q23 in a Greek-Italian kindred (73, 449). Since this discovery, several additional mutant variants have been found in familial kindreds linking the *SNCA* gene to parkinsonism, including A30P, E46K, A53E, H50Q, and G51D. Since their discovery, there have been PD mouse models created utilizing the A30P, E46K, and A53T mutations (450).

Interestingly, all of these missense mutations are located within a specific region of the N-terminal segment of α Syn (Figure 1.4.1), which suggests a functional role for this region in PD pathogenesis. Studies have found that the A30P mutations disrupts alpha-helical formation of the N-terminal segments, and the A53T mutation enhances the formation of β sheet-like conformations in the N-terminal segment (451, 452). Mechanistic insight into the pathophysiology of these mutations has uncovered a role for the NAC domain, as well. The A30P and G51Q mutations have been shown to increase cytosol

exposure of the NAC domain, prompting α Syn misfolding and aggregation (453). The difference in protein dynamics between the PD-associated point mutations helps increase our understanding of PD pathophysiology and α Syn aggregation; however, requires further investigation.

Similarly, overexpression of *SNCA* can also lead to parkinsonism features. Duplications and triplications were first discovered in rare familial cohorts that display phenotypic symptoms of early-onset parkinsonism (454). In general, duplications in *SNCA* can lead to early-onset PD with an approximate average age of onset of 50, and triplications can lead to early-onset PD at around age 35, with rapid progression of disease (455). In addition, triplications have been studied in multiple family cohorts, associated with autosomal dominant, young-onset parkinsonism, dysautonomia, cardiac denervation, DLB, and neuropathological features similar to MSA (456). Pathophysiologically, *SNCA* duplications and triplications may cause the natively unfolded α Syn protein to alter its secondary structure and self-aggregate (415). These genetic variations may promote the hydrophobic portion of α Syn to spontaneously form fibrillar protein aggregates as described above (457).

Overall, α Syn biology and its aggregation properties are clearly linked to PD and other synucleinopathies. Yet its expression outside of the CNS is intriguing and allows us to consider its role in other diseases and physiological conditions as well.

Alpha-Synuclein in Melanoma

Although traditionally thought of as a neurodegeneration-associated protein, α Syn is also present in the periphery of the body and in cell-types seemingly unrelated to the

brain. In PD patients, researchers have found evidence for the deposition of pathologic α Syn within peripheral tissues (394, 458-473), which has been proposed as a pPD diagnostic tool for PD (474). In fact, a meta-analysis by Tsukita et al. found that the detection of pathologic α Syn in skin samples had enhanced selectivity in identifying PD versus healthy individuals (474). α Syn has also been found in specific skin cell types, including fibroblasts (475, 476), keratinocytes (394, 395, 458, 473), and melanocytes (395, 464, 477) within PD patients compared to healthy controls (395). Not only is α Syn found in the skin of PD patients, but endogenous α Syn seems to be highly upregulated in melanoma samples as mentioned in Chapter 1.3. Studies have found that ~85% or more of primary and metastatic melanoma biopsies from patients were positive for α Syn (5, 395-397), and this has been validated in multiple other studies (395, 473). In addition, gene expression analysis has found that *SNCA* expression is ~3-fold higher in metastatic growth phase melanomas compared with healthy controls (398). Finally, human melanoma cell lines that are commonly utilized in research show upregulation of α Syn compared to other cell lines (367, 397-401).

A handful of studies have followed up this observation with functional studies for the role of α Syn in melanoma. Exploiting The Cancer Genome Atlas melanoma mRNA expression dataset, one study found that melanoma patients with high *SNCA* expression had lower survival probabilities (478), suggesting that α Syn expression is important in the growth and potentially aggressiveness of the melanoma tumor. Other studies have supported this result and have found that α Syn is critical for melanoma growth and proliferation in both *in vitro* and *in vivo* models. Overexpression of α Syn causes increased cell proliferation in B16 melanoma cells (479) and increased tumor growth in a mouse

xenograft model (479). Conversely, knocking out α Syn suppresses melanoma proliferation (478), migration (480), and invasion (480) *in vitro*, while decreasing tumor growth in a mouse xenograft model (478, 481). Furthermore, inhibiting α Syn oligomerization with anle138b (3-(1,3-benzodioxol-5-yl)-5-(3-bromophenyl)-1*H*-pyrazole, a molecule that binds to fibrils and destabilizes oligomers) significantly inhibits melanoma cell proliferation *in vitro* (398) and the growth of xenograft melanoma tumors (398). Overall, these results suggest that endogenous α Syn expression plays a functional role within the melanoma cell to promote growth phenotypes, yet what this role may be is not well understood.

Functional Studies

With the aforementioned data suggesting that LB formation contributes to neuronal death, and conversely, the upregulation of α Syn in melanoma is important for cell survival, this begs the question: what is α Syn doing inside of the cell to play a role in these disparate outcomes?

Within PD research, there are two opposing hypotheses to explain the observation that LB formation correlates to neuronal cell death: the α Syn “gain-of-function” hypothesis and the α Syn “loss-of-function” hypothesis. The more widely studied “gain-of-function” hypothesis postulates that α Syn aggregates can have toxic properties that can lead to problems within the cell. These downstream problems, which were briefly mentioned earlier in this section, include oxidative stress (432, 436), mitochondrial malfunction (482), synaptic dysfunction (483), ubiquitin proteasome system impairment (484, 485), iron metabolism (437-439), autophagic dysregulation (430, 486, 487), and inflammation (440,

441). Although more robustly studied, these “gain-of-function” hypotheses do not perfectly fit the complex nature of PD progression, and there has been building evidence for the validity of the “loss-of-function” hypothesis in PD.

The less-studied “loss-of-function” hypothesis in PD research postulates that the normal role of endogenous monomeric α Syn within the cell is perturbed during pathologic aggregation and LB formation. The absence of this upstream α Syn function ultimately leads to neuronal death. Data supporting this hypothesis includes the detection of interrupted synaptic transmission and dysregulated neuronal function in α Syn KO mice (488, 489). Furthermore, as mentioned earlier, longitudinal *in vivo* multiphoton imaging in PFF-injected WT Syn-GFP-expressing mice revealed tight correlation between inclusion formation and neuronal cell death (427). However, this study also revealed that prior to mature inclusion development, soluble Syn-GFP was present in both the cytoplasm and nucleus of the neuron. Upon somatic inclusion formation, the soluble Syn-GFP disappears from the nucleus of the cell. This finding was further confirmed in an analogous experiment utilizing an A53T Syn-GFP mouse line (442). Multiple studies have also shown endogenous expression of α Syn in the nucleus of the cell in PD patients’ brains, mouse models of PD, and immortalized cell lines (427, 442, 490-502). Altogether, these studies further advocate for the “loss-of-function” hypothesis, whereby the loss of soluble nuclear α Syn and the impairment of its potential function within the nucleus potentially contributes to neurodegeneration in PD.

With this in mind, it is also plausible that this “loss-of-function” hypothesis in PD and the nuclear function of α Syn could inform melanoma biology and help explain the PD-melanoma association. Multiple studies have shown that the upregulation of α Syn,

which is important for proliferation in melanoma cells, extends to expression within the nucleus (373, 395, 398, 401, 473, 503-506). The loss-of-function of nuclear α Syn as a consequence of LB formation in neurons can simultaneously exist with a gain-of-function of nuclear α Syn as a consequence of overexpression in melanoma cells, ultimately leading to both cell death and hyperproliferation, respectively. This potential explanation for the PD-melanoma association raises the question: what is the nuclear function of α Syn?

1.5 Alpha-Synuclein and DNA Double-Strand Break Repair

Role in the Nucleus

Few studies have investigated the normal role of α Syn in the nucleus. Some of these have uncovered functions, including the modulation of gene expression by interacting with nucleosomes (507), histones (508-512), and regulatory regions of genes (513, 514), protecting against replication stress in yeast (510), and binding to DNA *in vitro* (442, 502, 515, 516). There is additional evidence that α Syn facilitates DNA double-strand break (DSB) repair.

The role of α Syn in DNA DSB repair is first based on the observation of reported increases in DNA DSB signatures in brains of PD patients, that is directly correlated with LB pathology (442, 517, 518). Additionally, in one study, researchers found that in individuals with Ataxia Telangiectasia, a rare DSB repair deficiency disorder due to the mutation in DSB repair protein Ataxia Telangiectasia Mutated (ATM), LB-like inclusions were present in brain samples on autopsy (519). ATM knockout (KO) mice also display

increased α Syn aggregation and progressive loss of dopaminergic neurons in the substantia nigra (520). Furthermore, direct evidence has implicated α Syn as a functional component of the DSB repair pathway. Nuclear α Syn foci have been shown to colocalize with γ H2AX and poly ADP-ribose (PAR), both DSB response markers important in the early stages of the repair process (442). In mouse cortical neurons, *in vivo* laser-induced DNA damage rapidly recruited 142E Syn-GFP to the sites of damage (442). Moreover, α Syn KO in human haploid (HAP1) cells showed a significant increase in γ H2AX after widespread DNA damage via bleomycin treatment (442) and an increase in percent of deletion frequency after CRISPR/Cas9 DSB induction (443). *In vivo* studies showed a significant increase in γ H2AX and PAR signals in α Syn KO mice, as well (442). Mechanistically, there is evidence that α Syn facilitates DSB repair via the non-homologous end-joining (NHEJ) pathway (443).

These findings thus far link DSB repair to PD. Yet additional evidence suggests that DSB repair plays an important role in melanoma. During melanomagenesis, there is an increased amount of DSBs (521, 522), and studies have shown that melanoma cells upregulate DSB repair components, allowing for improved DSB repair critical for cell survival (523, 524). In addition, melanoma is known as a relatively radiotherapy-resistant cancer because of this increased DSB repair capacity (525, 526), whereby the addition of DSB repair inhibitors have been effective at treating melanoma (527, 528).

Overall, these findings further support the loss-of function (PD) and gain-of-function (melanoma) hypothesis (Figure 1.5.1): The loss of nuclear α Syn in dopaminergic neurons as a consequence of LB formation in PD leads to decreased DSB repair efficiency, an increased DNA damage burden seen in PD, and ultimately contributes to

degeneration of this population of neurons; Conversely, as an additional mechanism to evade replication-induced DNA damage, melanoma cells upregulate α Syn to increase DSB repair efficiency, and ultimately promote cell proliferation, tumor growth, and metastatic potential. However, it is still unclear the mechanism by which α Syn could be involved in DSB repair within the nucleus and how this connects PD and melanoma progression. This question is the basis for Chapters 3 and 4 and will be investigated during this dissertation.

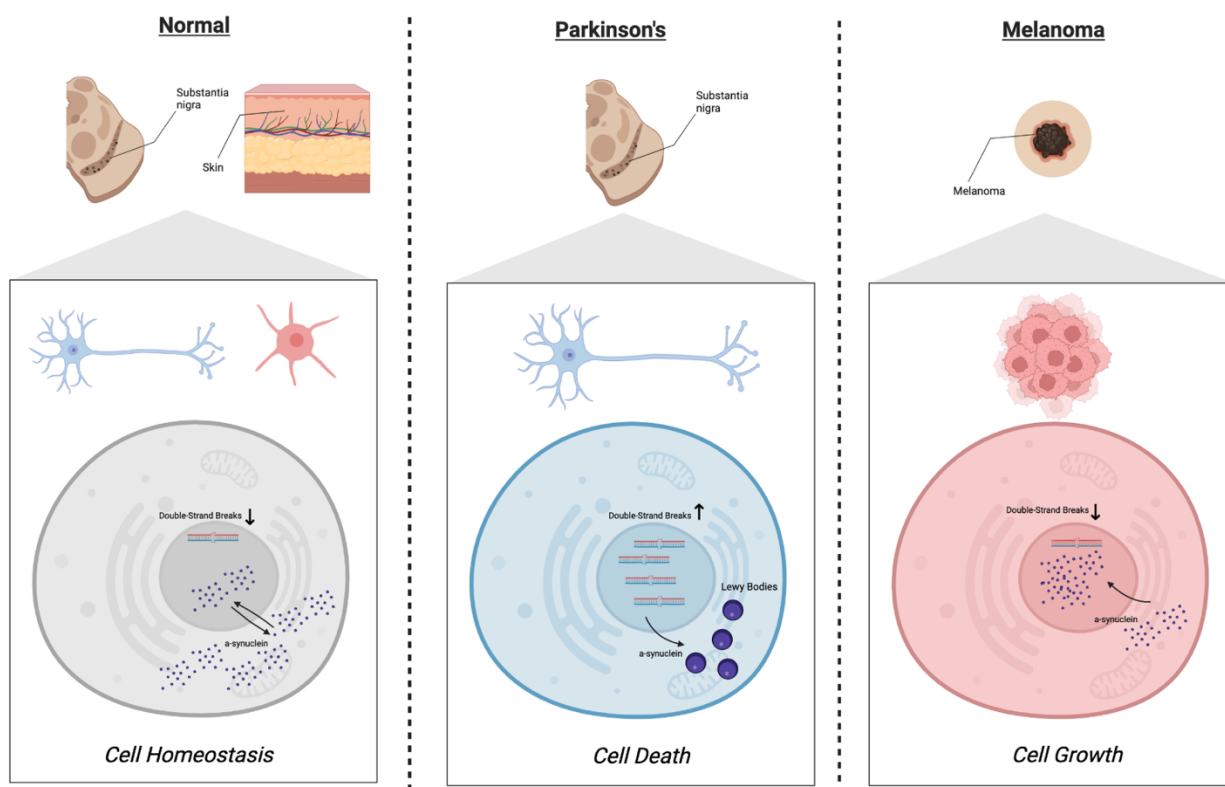


Figure 1.5.1. Proposed Loss-of-Function (PD) and Gain-of-Function (melanoma) Hypothesis

DNA Double-Strand Break Repair Pathways

Cells have developed conserved mechanisms to repair DNA damage, collectively referred to as the DNA damage response (DDR). These highly complex pathways have

adapted different DNA damage mechanisms specific to the type of insult and cell state. These types of insults include base pair mismatch, base oxidation, deamination and alkylation, single-strand breaks, intra-strand crosslinks, inter-strand crosslinks, and DSBs. Of these lesions, DSBs are the most toxic form of DNA damage and at baseline, 10-50 DSBs occur during each cell cycle (529). DSBs arise from not only endogenous sources such as reactive oxygen species during metabolism, collapsed replication forks, collisions between replication and transcription machineries, incomplete separation of sister chromatids during mitosis, and nucleases, but also from exogenous sources, including ionizing radiation and compounds used in chemotherapy. The proper functioning of these pathways is critical, because if left unrepaired or if the level of damage exceeds the repair capacity, the outcome is either cell senescence or death. Therefore, the DSB DDR becomes especially important in the context of diseased states when cells are under highly stressful conditions that increase genomic instability. The two most-common pathways to repair DSBs are homologous recombination (HR) and non-homologous end-joining (NHEJ) (Figure 1.5.2).

HR is named for this pathway's ability to copy genetic information from a homologous (sister) chromatid. First, after recognition of the DSB site, a large 5' to 3' resection on one strand of the DNA is created, resulting in a single-stranded overhang. The MRN complex, consisting of MRE11, Rad50, and Nbs1, initiates short-range resection along with CtIP and BRCA1. Long-range resection is performed by EXO1 and BLM helicase. RPA will localize to the single-stranded overhangs until Rad51 is recruited, at which point a D-loop is created on the sister chromatid. The DSB is resolved by either synthesis dependent strand annealing (SDSA) or double Holliday junction (dHJ)

formation, ultimately resulting in non-crossover or crossover events. Because HR depends on templating of a sister chromatid, this pathway is relatively faithful and “error-free”. However, this process is contingent on DNA replication and is therefore constrained to late S and G2 phases of the cell cycle when the duplicated sister chromatid is accessible. Because of these features, HR is traditionally found in proliferating cell types and not within post-mitotic populations, like neurons.

Unlike HR, NHEJ does not rely on a sister chromatid and therefore is thought to be the only DSB repair pathway relevant to post-mitotic cells. First, Ku70/80 recognizes the DSB and recruits DNA-PK to the site of damage. DNA-PK then interacts with Artemis to form a complex, which autophosphorylates. After Artemis-mediated end processing, XRCC4 and XLF repair the DSB. Both XRCC4 and XLF can function in template-dependent and template-independent synthesis, therefore leading to base pair mutations. Compared to the error-free nature of HR, NHEJ is traditionally thought of as “error-prone”; however, recent studies have suggested that its actual propensity towards inaccurate repair may be overestimated(530, 531). Because NHEJ is not dependent on sister chromatid templating, NHEJ can operate throughout the cell cycle and at a much faster rate than HR (532).

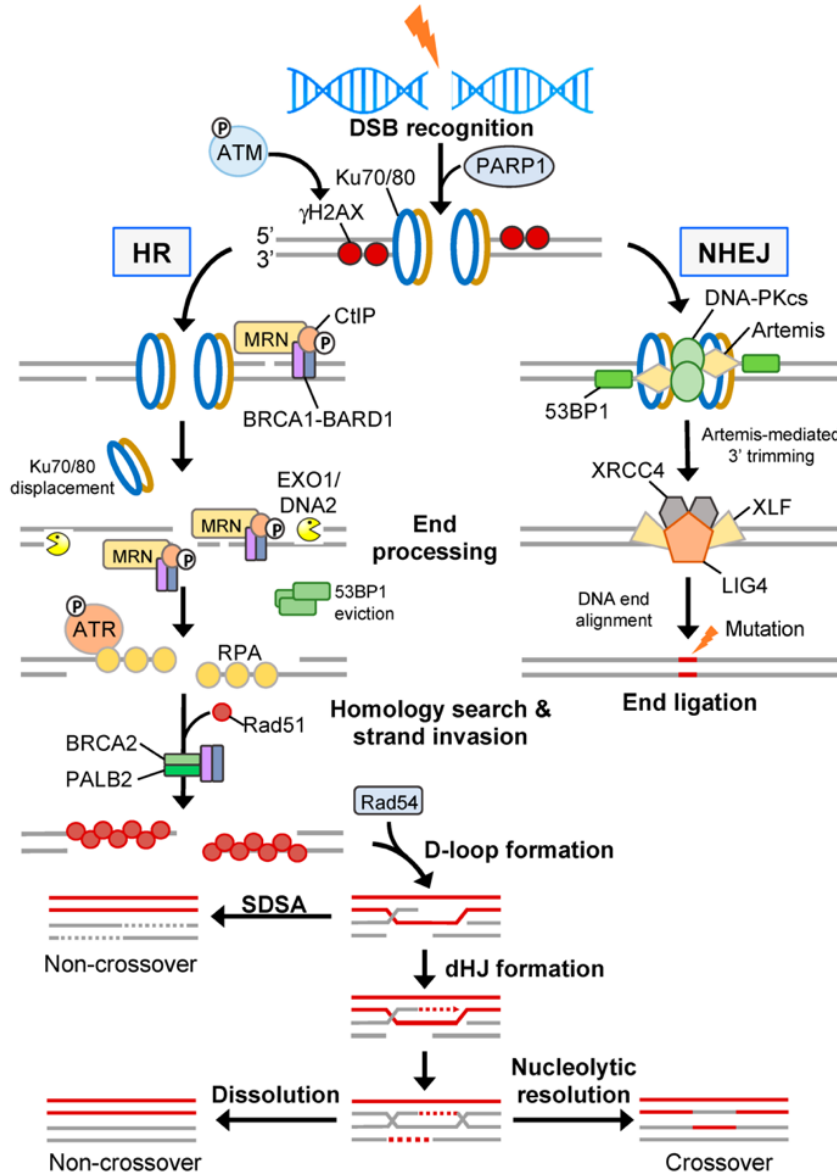


Figure 1.5.2. DSB Repair Pathways. Adapted from Gillespie et al. 2023 (533). This schematic depicts the two main pathways for repairing double-strand breaks (DSBs) in DNA: non-homologous end-joining (NHEJ) and homologous recombination (HR). NHEJ is active throughout the cell cycle and involves direct ligation of DNA ends with minimal processing, making it rapid but error-prone. Key steps include recognition by the Ku70/Ku80 heterodimer, end processing by DNA-PKcs and Artemis, and ligation by XRCC4-LIG4. HR is active during the S and G2 phases when a sister chromatid is available as a template, ensuring error-free repair. This pathway includes end resection by the MRN complex, recruitment of RPA and RAD51, and strand invasion mediated by BRCA1/BRCA2. The pathways are tightly regulated by cell cycle-specific factors to maintain genome stability and prevent mutagenesis.

The choice between HR and NHEJ during any given insult is an active area of study, but include factors like cell cycle stage, chromatin structure and accessibility, repair protein expression, availability of homologous repair templates, and DNA damage type (534-537). Researchers have also found that although HR and NHEJ are mutually exclusive, a number of repair proteins are involved in and influence both pathways, including MRN complex, BRCA1, H2AX, PARP1, RAD18, ATM, and DNA-PK (537). For example, pathway choice is partly regulated by the balance of 53BP1 and BRCA1 (538). 53BP1 protects the DNA ends against resection and promotes NHEJ, while BRCA1 promotes resection and HR (539). DNA-PK can also play a role in pathway choice via its kinetics, enzymatic competition, and/or autophosphorylation checkpoints with Artemis (534, 540). This area of investigation, HR versus NHEJ, becomes especially pertinent in the context of the association between PD and melanoma. Both neurodegeneration and cancer utilize these DSB repair pathways differently, which have substantial implications for the role of α Syn in these repair mechanisms. This topic will be discussed in Chapters 3, 4, and 5.

Alpha-Synuclein in the Nucleolus and the Nucleolar DNA Damage Response

Preliminary data from multiple cell lines indicate a potential role for α Syn in the nucleolus of the cell. Immunocytochemistry staining of primary melanocytes and human melanoma cell lines, SK-Mel28 and A375, for α Syn (Syn1) revealed an enrichment of discrete foci in the DAPI-poor regions of the nucleus (Figure 1.5.3). Traditionally in immunofluorescence, DAPI-poor regions have been associated with the nucleolus of the cell. DAPI binds to double-stranded DNA that is A-T rich, therefore it preferentially stains

heterochromatin more intensely than euchromatin due to its highly condensed nature. The nucleolus is a membraneless subcompartment of the nucleus where ribosome biosynthesis primarily occurs. Ribosomal DNA (rDNA) occur in repetitive gene clusters, called nucleolar organizer regions (NORs). The actively transcribed rDNA genes are located within euchromatic regions, allowing for efficient access by transcription machinery. However, heterochromatin is typically found in the regions between the repeating units of the rDNA gene cluster, which help regulate transcription and maintain the structural integrity of the rDNA array (541). Furthermore, rDNA does not have a particularly high proportion of adenine and thymine bases, the nucleolus is not considered A-T rich, but rather G-C rich. Lastly, although the nucleolus contains rDNA, it is primarily composed of rRNA and proteins involved in the process of ribosome assembly, ultimately leading to a low density of DNA found in the nucleolus. Altogether, this supports the notion that the enrichment of α Syn seen in the DAPI-poor regions of the primary melanocytes and melanoma cells is most likely within the nucleoli of the cell and require further investigation.

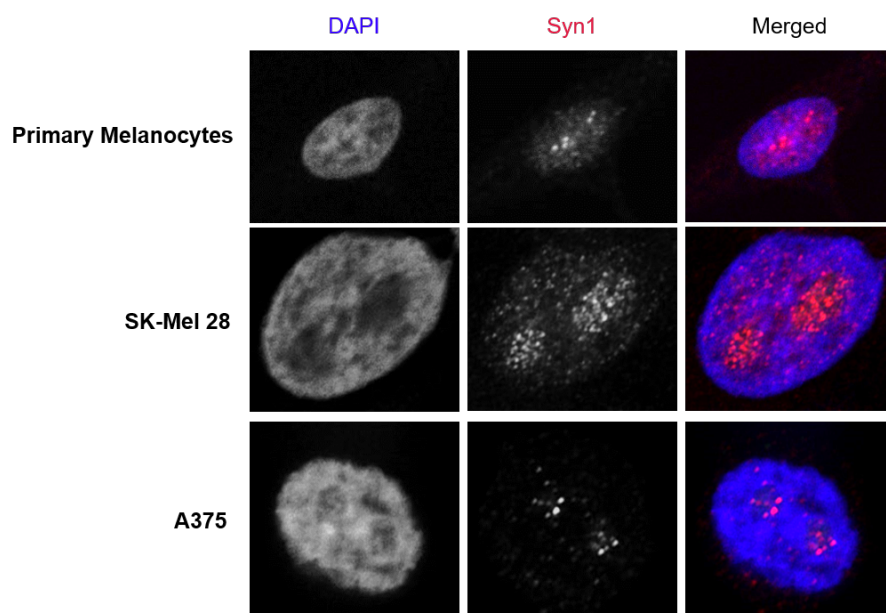


Figure 1.5.3. α Syn is enriched in DAPI-poor regions of the nucleolus. Primary melanocytes, SK-Mel28 cells, and A375 cells were seeded on coverslips and stained for alpha-synuclein (Syn1) and DAPI. Cells were imaged on the Zeiss 980 confocal microscope. Images produced by M. Arnold (unpublished).

The formation of the nucleolus is driven largely by the presence of intrinsically disordered proteins (IDPs), which readily undergo liquid-liquid phase separation (LLPS), allowing them to associate and form the distinct, membraneless compartment that is the nucleolus (542, 543). As stated above, the nucleolus is best known as the intranuclear compartment where rDNA genes are transcribed and rRNA is processed as part of ribosome biogenesis. Nucleoli form around tandem arrays of ribosomal DNA repeats, called nucleolar organizer regions (NORs). In humans, NORs are located on the p-arms of acrocentric chromosomes 13, 14, 15, 21, and 22 (544, 545). Within the nucleolus, three distinct subcompartments have been discovered, each with different biological functions: the fibrillar center, dense fibrillar component, and the granular component. These different regions are thought to represent the progressive stages of ribosome biogenesis. The rDNA genes are located in the fibrillar centers, with transcription occurring at the interface between the fibrillar center and dense fibrillar component. Processing of the pre-rRNA is initiated in the dense fibrillar component and continues into the granular component, where rRNA is assembled to form pre-ribosomal subunits, eventually exported into the cytoplasm for functional ribosomal assembly. The presence of rRNA is important in the phase separation necessary to establish the different subcompartments. When rRNA transcription is disrupted, for example from RNA polymerase I inhibition by treatment with Actinomycin D, the nucleolus will undergo drastic morphological changes. The formation of these subcompartments not only reflect ribosome biogenesis processes, but also arise

from the different combinations of IDPs with unique sequence characteristics that are important for facilitating these different processes of ribosome biogenesis (546). For example, pre-rRNA processing factor, fibrillarin, form clusters via its IDP properties that assemble into the dense fibrillar component. This self-association immobilize its interactions with rRNA to promote directional trafficking in the dense fibrillar component and pre-rRNA processing (547).

The nucleolus is a structure important in the pathophysiology of human disease. There are a growing number of papers that investigate the role of nucleolar DSBs in the context of various disease states, such as neurodegeneration and cancer, that are prone to genome instability (548-550). The structure of the nucleolus is highly sensitive to various types of DNA damage (551-556), partly because rDNA is an intrinsically unstable genomic region due to its high level of transcriptional activity and repetitive sequences. Estimates suggest that up to 60% of all transcription within a normal mammalian cell occurs at rDNA (557), and faithful ribosome biogenesis is even more important to sustain the high rates of cell division and growth that occur in malignant cells (558, 559). Additionally, G-C rich DNA, like NORs, are highly stable, which leads to polymerase stalling, slippage, and increased susceptibility to damage from reactive oxygen species during replication, giving rise to SSBs and DSBs (560, 561).

DSB repair within nucleoli involves distinct mechanisms from those operative in the larger nucleoplasm (Figure 1.5.4) where breaks are recognized by the ATM-phosphorylated protein treacle (562-564), along with the MRN complex (MRE11-RAD50-NBS1) (565, 566). The recruitment of the MRN complex suppresses transcription through inhibition of RNA polymerase I (563, 565, 567, 568), with this process being dependent

on ATM (569, 570), and triggers the translocation of ATR into the nucleolus. This in turn results in large-scale reorganization of nucleolar structure characterized by the movement of damaged rDNA to the nucleolar periphery and the formation of nucleolar “caps” consisting of the damaged rDNA and other proteins important for DSB repair (564, 565, 569-571). The purpose for these nucleolar caps is to facilitate the accessibility of the damaged rDNA to repair components normally found in the nucleoplasm (572), including RPA, 53BP1, BRCA1, CtIP, and RAD51/52. It is thought that rapid repair with NHEJ is the prominent rDNA DSB repair pathway within the nucleolar interior at subthreshold levels of DSBs prior to transcriptional inhibition or nucleolar cap formation. However, this pathway choice shifts to HR when transcriptional silencing occurs and rDNA DSBs are recruited to the nucleolar caps (570). Furthermore, although HR is traditionally considered “error-free”, emerging evidence highlights that HR in clustered repetitive loci, like NORs, may be deleterious, as it can lead to chromosomal translocations and DNA repeat aberrations (573). Therefore, it has been argued that HR occurring at the nucleolar cap utilizes templated *cis* undamaged rDNA repeats present in the same NOR, which may limit interchromosomal recombination and translocations and allow for rDNA DSB repair in all phases of the cell cycle, as opposed to nucleoplasmic *trans*-based HR (569).

The role of α Syn in the nucleolus has not been well-studied, especially in the context of DNA damage repair, and there have only been a handful of studies linking α Syn to the nucleolus, although most are indirect functional studies. Researchers have found that remaining neurons in the substantia nigra and peripheral blood of PD patients showed reduced mRNA expression of key nucleolar DDR proteins, diminished rRNA levels, less expression of key mRNAs encoding for ribosomal protein subunits, and

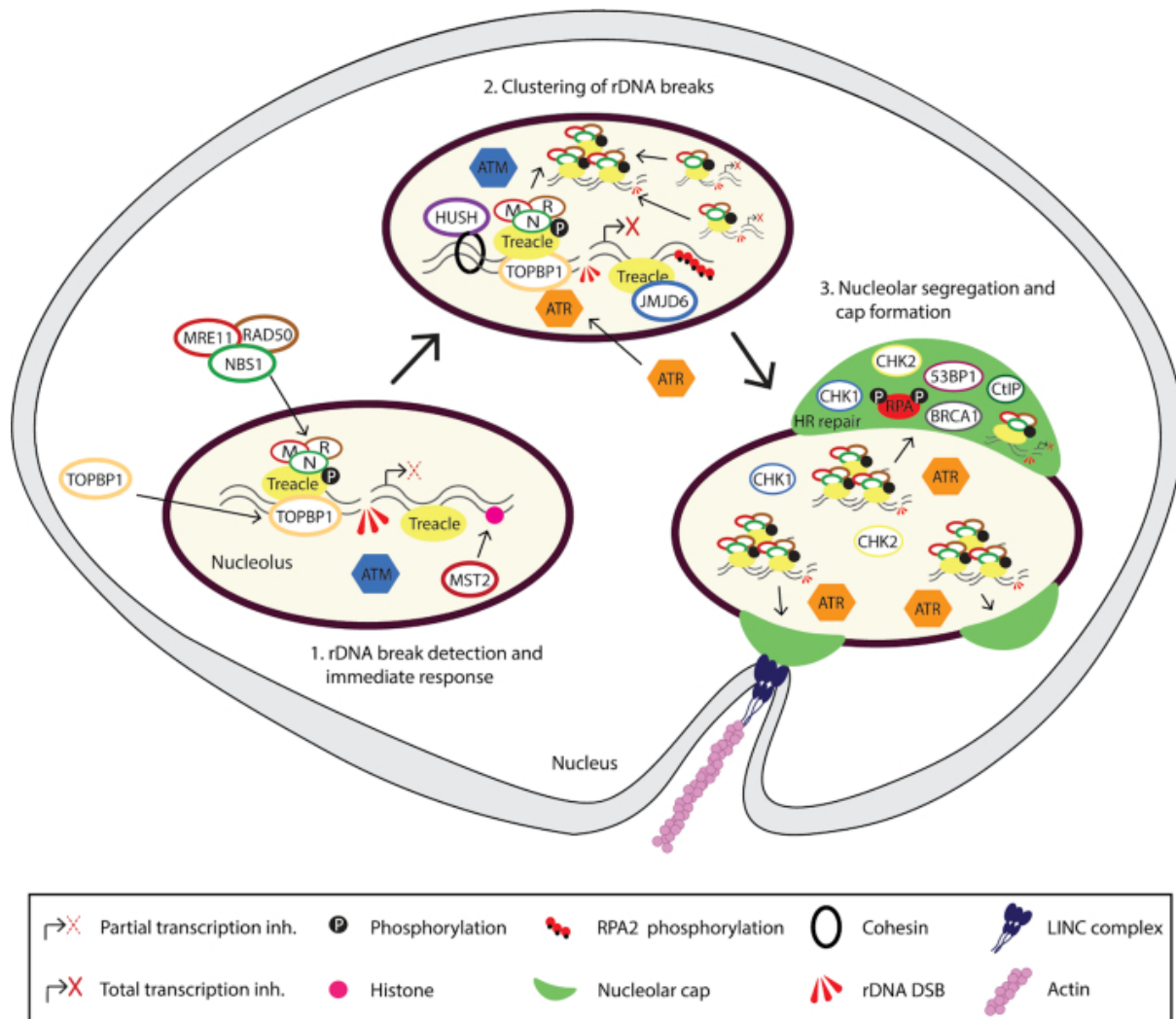


Figure 1.5.4. Nucleolar DNA Double-Strand Break Repair Pathway. Adapted from Korsholm et al. 2020 (574). This figure illustrates the nucleolar response to DNA double-strand breaks (DSBs) in ribosomal DNA (rDNA). Upon DSB induction, the ATM kinase is activated, initiating local transcriptional inhibition in the nucleolus. Treacle (TCOF1) recruits the MRN complex (MRE11-RAD50-NBS1), which is essential for DNA end resection and activation of ATR. ATR further suppresses transcription and facilitates nucleolar reorganization. Damaged rDNA loci translocate to the nucleolar periphery, forming nucleolar caps where homologous recombination (HR) repair factors, such as BRCA1, RAD51, and CtIP, assemble. This repair mechanism contrasts with non-homologous end joining (NHEJ), which occurs in the nucleolar interior during active transcription. These pathways underscore the specialized processes ensuring rDNA stability while protecting the nucleolar architecture.

abnormal nucleolar morphology (501, 555, 575). Nucleolar RNA helicase DDX10 stabilizes α Syn oligomeric species in yeast (576) and overexpressed nuclear pathological

α Syn has been shown to alter rRNA processing in the mouse embryonic fibroblast via nucleolin malfunction-mediated nucleolar segmentation (577). Given the data suggesting that α Syn facilitates DNA DSB repair outside of the nucleolus (442, 443) and the preliminary data that α Syn may be enriched within the nucleolus (Figure 1.5.3), whether or not α Syn facilitates nucleolar DDR needs to be further investigated and is the basis for Chapter 3.

1.6 Conclusion

The dissertation work that I will be presenting herein fits into the intersection between genomic instability, aging, and diseases of aging, like neurodegeneration and cancer. Genomic instability has long been implicated as an important factor in cellular aging (578). Dividing cells are constantly exposed to various sources of DNA damage, with an accumulation of such damage sufficient to cause the phenotypic changes associated with aging. In the context of neurodegeneration, post-mitotic cells, like neurons, are especially vulnerable to genomic instability generally due to their inability to undergo homologous recombination and their high metabolic rates that lead to increased production of DNA damage-inducing reactive oxygen species (579). In the context of cancer, hyperproliferation is a serious stressor that induces high levels of DNA damage within the cell. Taken together, and the fact that DNA repair efficiency decreases with age, it is possible that the underlying pathophysiology of neurodegeneration and cancer are more similar than originally thought. Furthermore, the PD-melanoma association highlights the need to study common molecular components important in genomic

stability, one being α Syn. It is plausible that in the general population, individuals with high expression of α Syn are 1) more predisposed to LB formation in PD and 2) more predisposed to melanocytic transformation in melanoma. I hypothesize that the consequence of both phenomena is a dysregulation in α Syn-mediated DSB repair function (loss-of-function in PD and gain-of-function in melanoma) (Figure 1.5.1). Chapter 2 will further characterize the PD-melanoma association via epidemiological analysis of patient cohorts. Chapters 3 and 4 will dive into the mechanism of α Syn in melanomagenesis and growth via its role in DNA damage repair *in vitro* and *in vivo* respectively.

[Jump Back to Table of Contents](#)

Chapter 2:
**PD-THRESHOLD: Melanocytic lesions and co-occurring disorders
associated with future risk of Parkinson's Disease**

Moriah R. Arnold^{1,2}, Lee E. Neilson^{2,3,4}, Erin F. Foster⁵, Reid F. Thompson^{6,7}, Wesley Y. Yu^{5,8}, Vivek K. Unni^{2,4}, Sancy Leachman⁵, Gregory D. Scott^{9,10}

¹ Medical Scientist Training Program, Oregon Health and Science University, Portland, OR, USA

² Department of Neurology and Jungers Center for Neurosciences Research, Oregon Health and Science University, Portland, OR, USA

³ Neurology and Research Service, VA Portland Health Care System, Portland, OR, USA

⁴ OHSU Parkinson Center, Oregon Health and Science University, Portland, OR, USA

⁵ Department of Dermatology, Oregon Health and Science University, Portland, OR, USA

⁶ Department of Radiation Medicine, Oregon Health & Science University, Portland

⁷ Division of Hospital and Specialty Medicine, VA Portland Healthcare System, Portland, Oregon

⁸ Operative Care Division, VA Portland Health Care System, Portland, OR

⁹ Department of Pathology, Oregon Health and Science University, Portland, OR, USA

¹⁰ Pathology and Laboratory Services, VA Portland Health Care System, Portland, OR, USA

In preparation for submission to *Journal of the American Academy of Dermatology*

2.1 Abstract

Background: Surveillance of melanoma survivors will increasingly involve diseases of older age such as Parkinson's Disease (PD) due to lengthening survival from modern therapies. The association of melanoma and subsequent PD is unverified and clinicopathologic features driving this association are unknown.

Objective: Determine melanoma characteristics and interactions associated with PD incidence.

Methods: Retrospective cohort study of US Veterans (n=5,890,509) using cancer registry, administrative codes, and notes. PD incidence adjusted for competing risk of death and confounders.

Results: Diagnosis of multiple nevi, atypical nevi, melanoma in-situ, lentigo maligna and superficial-spreading melanoma was associated with 15.9 [10.1,21.7], 34.3 [21.7,46.8], 39.0 [6.9,71.1], 34.4 [17.3,51.4], 16.4 [-0.1,33.0] additional PD cases per 10,000 people at year 10. Co-occurring dermatophytosis, hyperhidrosis, orthostatic hypotension, and REM-sleep behavior disorder amplified the melanoma-PD association adding 3.3 [0.2,6.3], 4.6 [1.2,7.9], 10.0 [5.7,14.3], 50.3 [36.8,63.9] extra PD cases. Other disorders (e.g. seborrheic dermatitis, constipation, anxiety) also increased the melanoma-PD association.

Limitations: Lower proportion of females and non-whites

Conclusion: Melanocytic lesions and co-occurring disorders associated with PD risk are summarized "PD-THRESHOLD": GI-**T**ract (constipation), mental **H**Health (depression, anxiety), **R**EM-Sleep-Behavior Disorder, **S**eborrheic dermatitis, **H**yperhidrosis, **O**rthostatic-hypotension, **L**ower-stage melanoma, **D**ermatophytosis. Clinicians should

consider asking about these symptoms to help identify early PD patients for neuroprotective trials.

2.2 Introduction

Melanoma represents the 5th most common malignancy with incidence rising among adults greater than 40 years old (580, 581). The advent of modern immunotherapies has revolutionized melanoma treatment such that 5-year relative survival for metastatic disease has more than doubled (582). Consequently, with substantially increased prevalence, it is now necessary to pivot toward surveillance strategies for these long-term survivors (583).

The expanding role of melanoma surveillance raises the prospect of catching the neurodegenerative disease, Parkinson's Disease (PD), years before it is currently diagnosed during an opportune time for preventative clinical trials. Early detection of PD not only improves quality of life and reduces treatment costs (584) but by the time most PD diagnoses are made, significant brain damage has also occurred (e.g. up to 68% loss of neurons in certain regions of the substantia nigra) (585), so early detection of PD offers hope for a better treatment window. Due to aging, shared genetic underpinnings (22, 586, 587), environmental exposures (588), and biological mechanisms, melanoma survivors are at particular risk for developing PD. Although the increased incidence of melanoma in PD populations has been well-studied, the incidence of PD in melanoma patients is less established. While an early meta-analysis of nine case-control studies showed no association between melanoma and a later diagnosis of PD (OR 1.09, 95 %

CI 0.78–1.54 (327)), updated studies have yielded more mixed results (12, 589-591). However, the positive studies were either under-powered, utilized minimal follow-up times, did not control for important confounders such as smoking history, or were susceptible to misclassification. Given the strong evidence of high rates of melanoma in manifest PD (373), the biologically plausible mechanisms implicating alpha-synuclein – the main PD pathologic protein – in melanoma (398, 478-481, 504, 506, 592) and shared precursors in the melanin (in melanocytes) and neuromelanin (in dopaminergic neurons) synthesis pathways (373, 593), this association demands a re-examination.

The current electronic health records (EHR)-based cohort study aims to overcome prior limitations by leveraging the database of the United States Department of Veterans Affairs. These data allow for accurate and orthogonal ascertainment of both commonly coded entities like melanoma and uncoded clinical and clinicopathologic entities such as multiple nevi and dysplastic nevi. The study expands the level of detail collected about melanomas (e.g. precursor lesions, subtyping, and staging) to more closely reflect a dermatologist's assessment and add prevalence data to contribute to PD risk assessment. To further aid dermatologists in their risk assessment, we also explore important modifiers of association including non-motor symptoms such as co-occurring orthostatic hypotension and constipation (594) and common skin conditions (144) which have all previously been shown to elevate risk of PD. Filling this knowledge gap will provide more precise estimates of PD risk and will help elucidate the shared pathophysiology between melanoma and PD.

2.3 Results

Cohort

1,317,418 Veterans were identified in the cancer registry for initial screening for their association with PD (Figure 2.3.1). 4,573,091 Veterans were identified with medical charts and paired pathology reports for analysis of melanocytic lesions and interactions (Figure 2.3.1). Participants were predominately white (97%), non-Hispanic (99%), and male (97% male and 3.1% female) (Table 2.8.1).

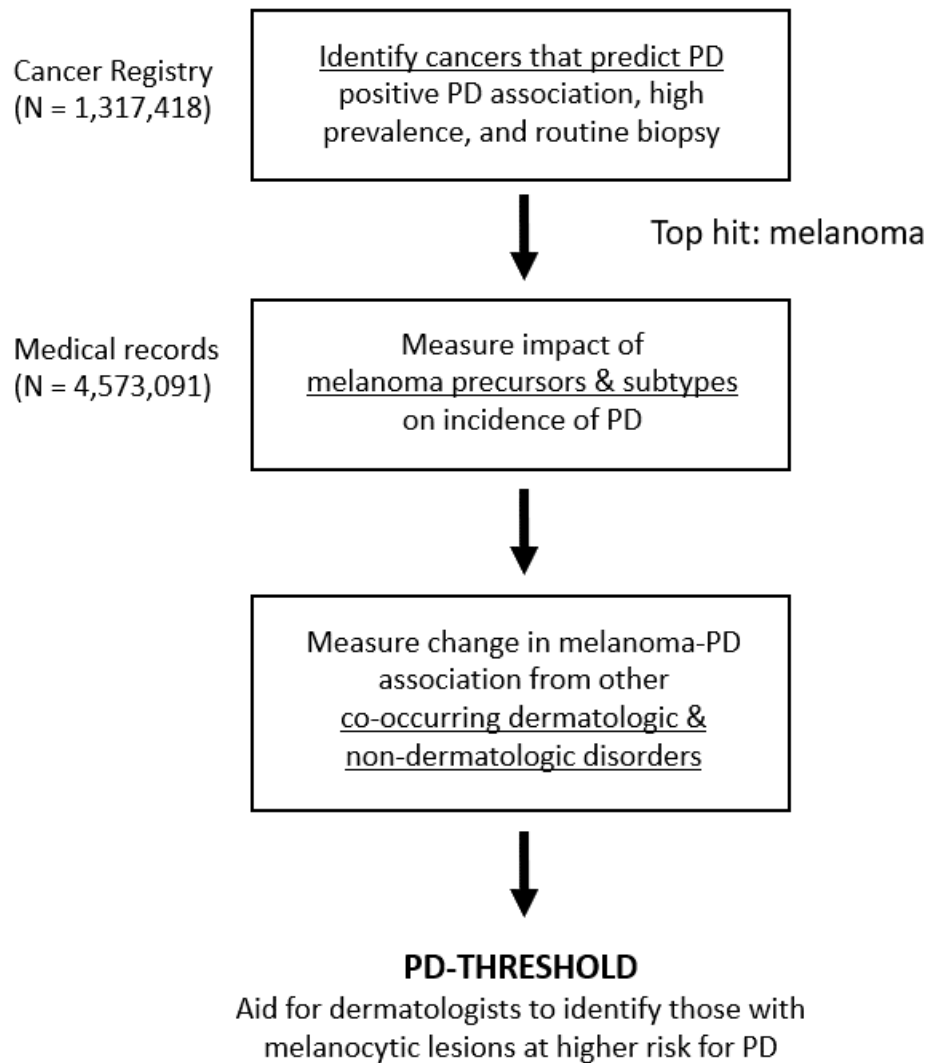


Figure 2.3.1. Schematic outlining analysis workflow.

Association of Melanoma and PD in Registry Data

In the cancer registry, there were 45,758 diagnoses of melanoma and 1.1% (498) had subsequent diagnosis of PD (Table 2.8.1). Diagnosis of melanoma (HR = 1.66 [1.49, 1.84]) and melanoma in situ (HR = 1.71 [1.46, 1.99]) were positively associated with PD. Other cancers with positive association with subsequent PD included cancers of the thyroid (HR = 2.44 [1.88, 3.15]), female breast (HR = 1.70 [1.07, 2.73]), and nervous system (HR = 1.63 [1.29, 2.05]) (Figure 2.3.2). In contrast, most cancers were negatively associated with PD such as colon (HR = 0.89 [0.80, 0.99]), respiratory (HR = 0.37 [0.29, 0.47]), and pancreatic cancers (HR = 0.18 [0.09, 0.33]). When comparing prevalence amongst cancers positively associated with PD, melanoma cancers were more common than thyroid (n=10,022), breast (n=16,220), and nervous system (n=15,782) in both the cancer registry and in pathology reports (Table 2.8.2).

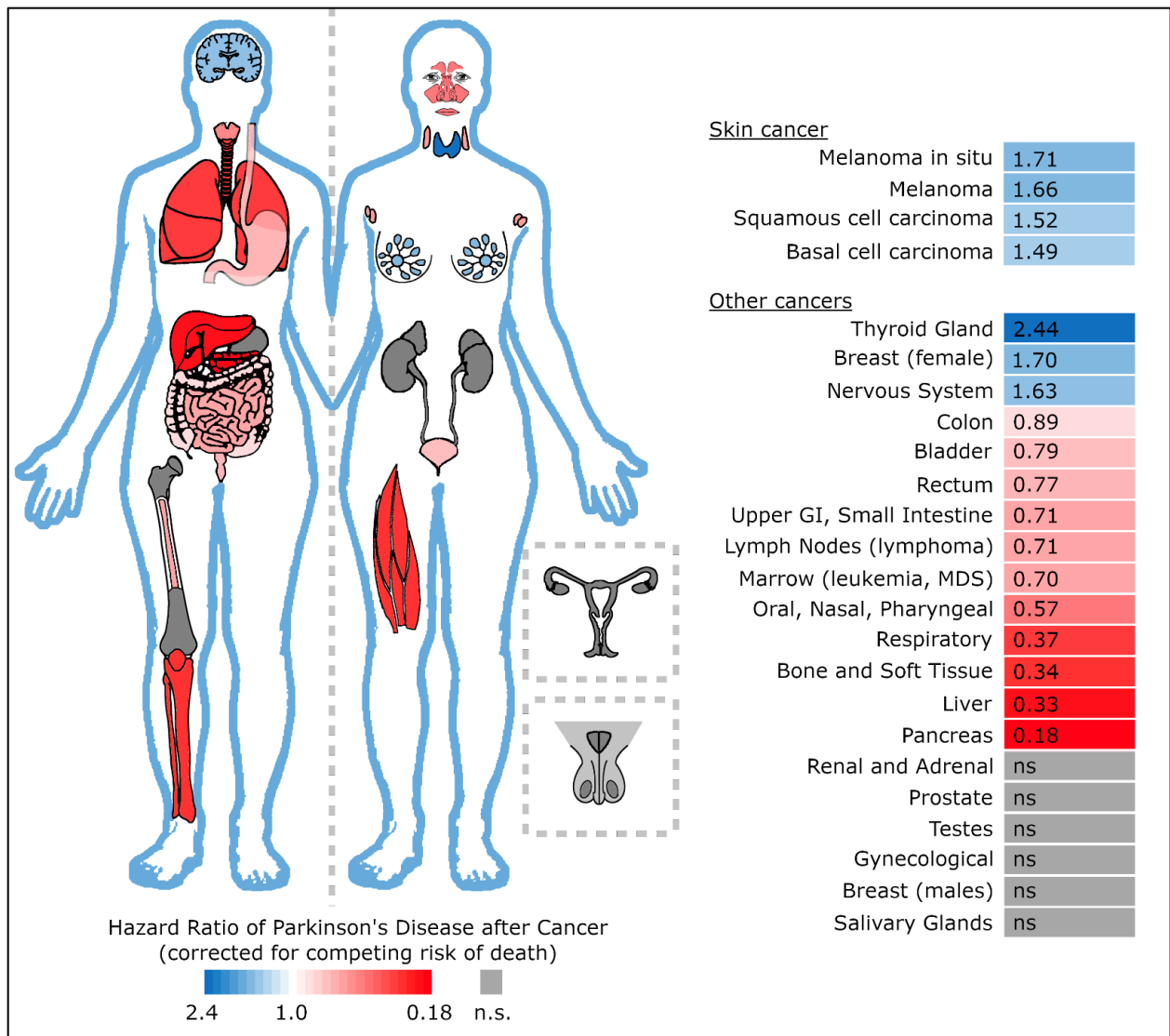


Figure 2.3.2. Cancer and risk of developing Parkinson's Disease. Participants with cancer of a specific site were propensity matched 4-to-1 with controls using birth year, sex, race, ethnicity, and smoking status. The human body diagram (left) and heatmap table (right) show significant hazard ratios ($p < 0.05$) after adjustment for competing risk of death and multiple comparisons. Inset shows male and female reproductive organs. Adapted from images primarily provided by Wikimedia commons (sources in supplement text). Formal analysis performed by Gregory Scott.

Elevated PD Incidence after Diagnosis of Melanoma Precursors and Certain Subtypes

Melanoma identified through clinical notes and pathology reports was associated with PD (Figure 2.3.3a) similar to the registry definition of melanoma (Figure 2.8.1). At 5 and 10 years after diagnosis, melanoma was associated with an extra 29.9 [8.9, 51] and

37.3 [13.6, 61] cases of PD per 10,000 people (Table 2.8.3). Lentigo maligna showed similar effect sizes to melanoma overall with 18.3 [6.7, 29.9] and 34.4 [17.3,51.4] added PD cases per 10,000 at years 5 and 10. Superficial-spreading melanoma showed borderline significant ($p = 0.051$ and $p = 0.07$) and lower magnitude PD risk of 10.6 [-1.2, 22.5] and 16.4 [-0.1, 33] added PD cases at years 5 and 10, respectively. PD incidence was not significantly increased after diagnosis of nodular, desmoplastic, or acral lentiginous subtypes of melanoma. Affirmative mentions in the clinical notes of multiple/many nevi, atypical/dysplastic nevi, and melanoma in situ showed an ascending pattern of association with PD; for example, each accounting for 15.9 [10.1, 21.7], 34.3 [21.7, 46.8] and 39 [6.9,71.1] cases of added PD per 10000 people at year 10, respectively (Figure 2.3.3b, Table 2.8.3). Dysplastic/atypical nevi, melanoma in-situ, and melanoma had similar PD association effect sizes with greater collective prevalence than melanoma alone ($n=359,163$ in pathology reports), and so were combined and called “melanocytic lesions” in later analyses.

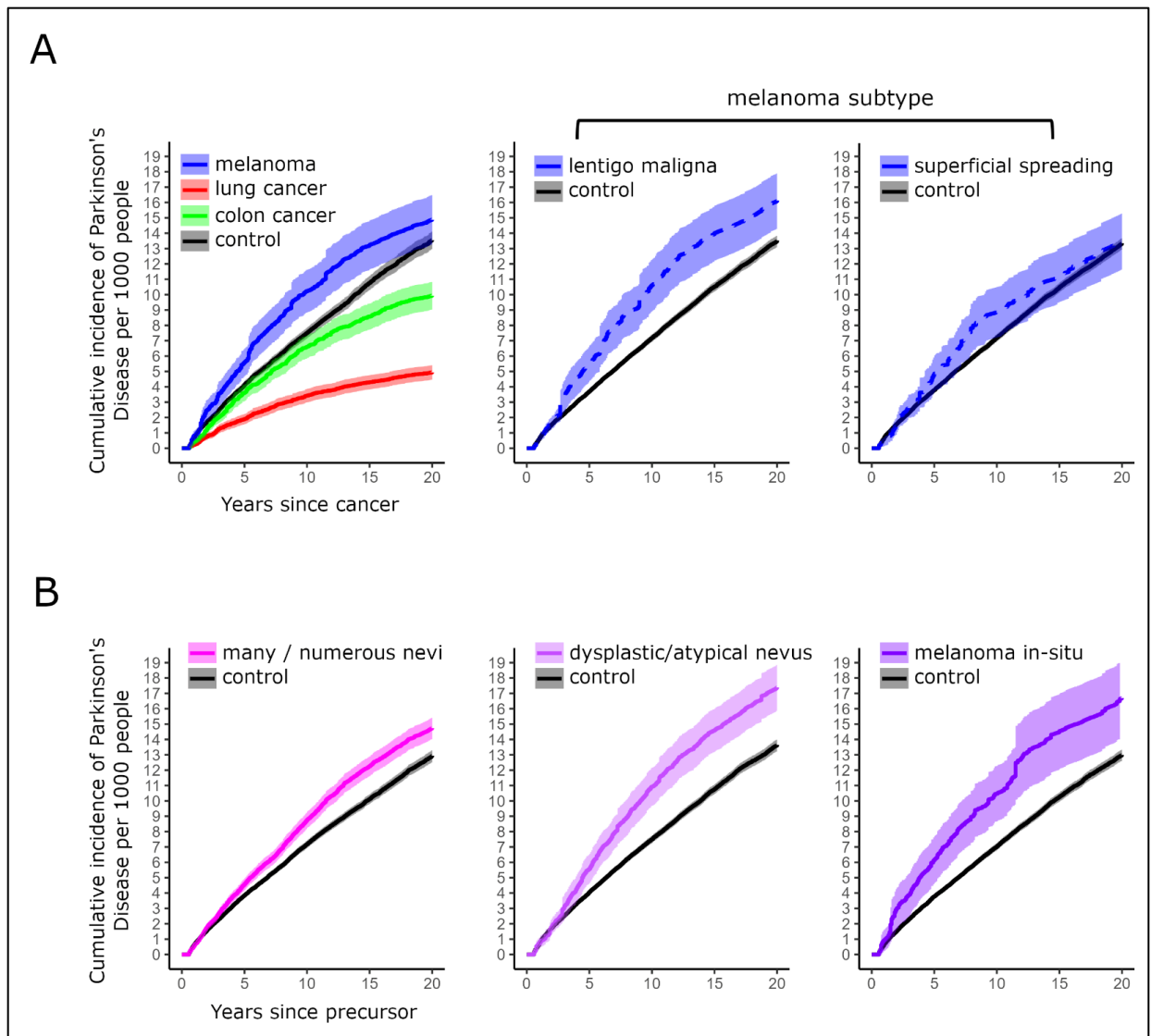


Figure 2.3.3. Impact of risk lesions for melanoma, melanoma subtypes, and pre-melanotic lesions on incidence of PD. A) Cumulative incidence of PD is shown for those diagnosed with melanoma (blue) and cancer-free controls (black), lung cancer (red), or colon cancer (green) over twenty years. Desmoplastic, acral lentiginous, and nodular subtypes (not shown) were not significantly different from controls. B) Cumulative incidence of PD is shown for those diagnosed with any of three pre-melanotic lesions (pink or purple) and cancer-free controls (black) over twenty years. Formal analysis performed by Gregory Scott.

Positive Interaction of Melanocytic Lesions with Other Disorders

Having a combined diagnosis of a melanocytic lesion and another disorder was tested for positive interactions to further increase PD incidence. Three out of twelve

dermatologic disorders showed positive interactions including hyperhidrosis, dermatophytosis, and seborrheic dermatitis (Figure 2.3.4a, Table 2.8.4). Hyperhidrosis exhibited a longer duration (from year 9 to 20) of positive interaction with 3.6 [0.4,6.9], 5.5 [2.1, 9], and 7.1 [3.5, 10.6] extra cases of PD per 1000 people due to positive interaction at years 10, 15, and 20. Dermatophytosis and seborrheic dermatitis were significant at a later timepoint and shorter duration with 4.0 [0.7, 7.2] and 4.3 [1.5,7.2] cases of PD per 1000 people at year 20, respectively.

Melanocytic lesions also showed positive interaction with multiple non-dermatologic disorders at increasing future PD incidence. The longest duration (17 and 14 year) and greatest effects were seen for REM sleep behavior disorder and orthostatic hypotension which ranged from 20.5 [10.4, 30.7] to 60.6 [46, 75.3] and 7.1 [3.4, 10.7] to 14.8 [10.1, 19.6] added cases of PD per 1000 people (Figure 2.3.4b, Table 2.8.5). Other disorders exhibited effect sizes and durations similar to dermatologic conditions including anxiety, constipation, depression, and urinary dysfunction with 5.0 [1.4, 8.5], 6.0 [3.5, 8.4], 4.7 [1.6, 7.8], 3.8 [1.7, 5.9] added PD cases per 1000 people at year 20, respectively.

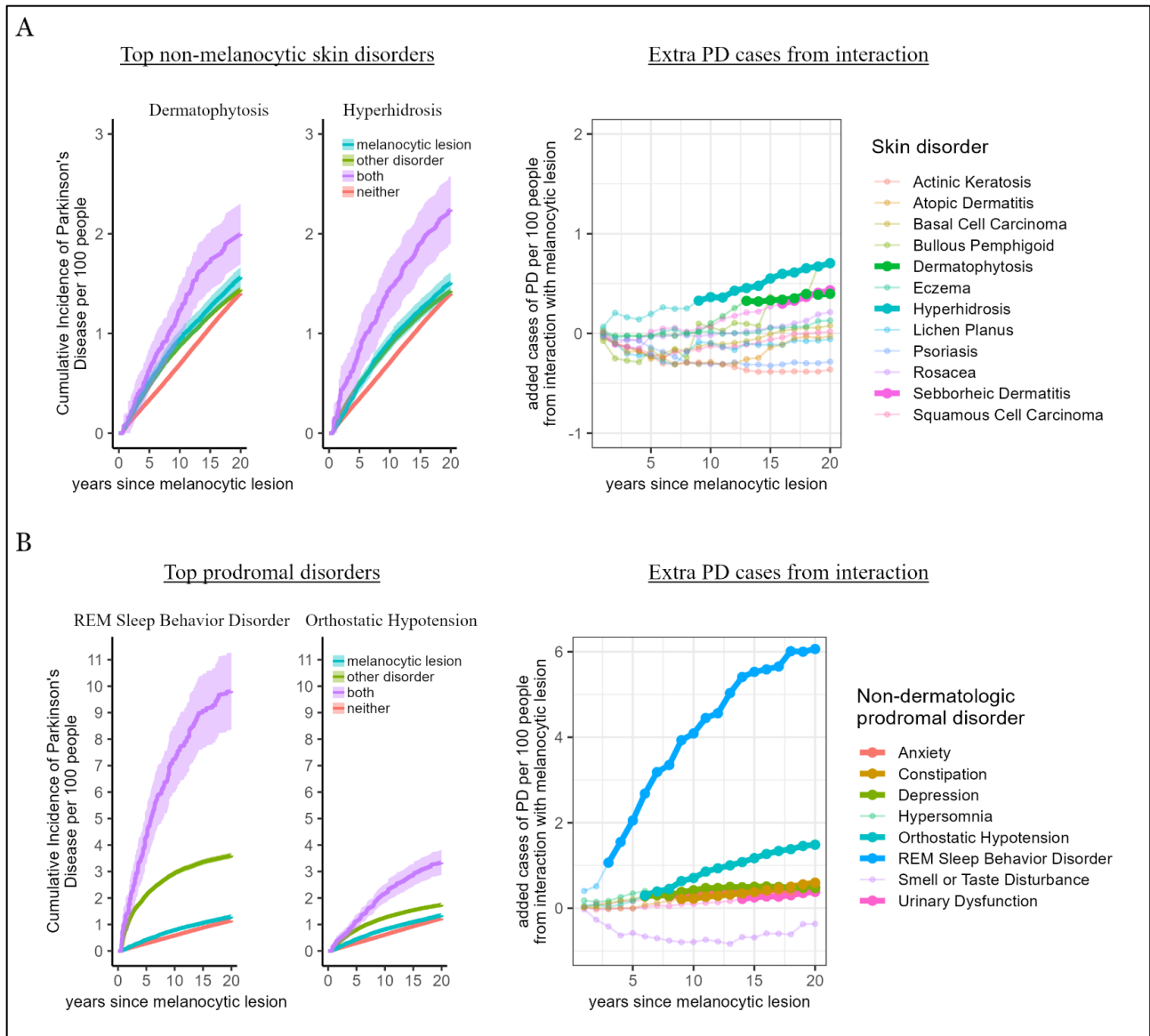


Figure 2.3.4. Positive interaction of melanocytic lesion with other non-melanocytic skin disorders and prodromal-PD disorders upon incidence of PD. LEFT: Representative graphs of individual skin (A) and prodromal (B) disorders with greatest positive interaction with melanoma showing cumulative incidence of PD over 20 years in melanocytic lesion only (blue), other disorder only (green), both melanocytic lesion and other disorder (purple), or neither (red). RIGHT: plot of all non-melanocytic skin disorders (A) or prodromal-PD disorders (B) showing the extra cases of PD from interaction with melanoma above that of adding risk of individual disorders. Bolded lines represent statistical significance. Formal analysis performed by Gregory Scott.

Lower Melanoma Stage if preceding PD

Registry data was compared between melanoma associated with subsequent PD versus unassociated melanoma (Table 2.3.1). Data completeness was above 80% for AJCC stage, tumor status, and therapies and was lower for lymphovascular invasion (54%), venous invasion (23%), pathologic stage (42%), and clinical stage (55%). Melanoma antecedent to PD showed a greater proportion with early stage pathology compared to melanoma after PD in terms of overall AJCC stage (88.5% vs 84.2%), clinical stage (91.8% vs. 86.1%), and a trend for pathologic stage (84.9% vs 80.2%, $p = 0.09$). Melanoma antecedent to PD also showed an increased proportion of patients with no evidence of tumor at the final report when compared to melanoma after PD (93.6% vs. 85.7%). There were no significant differences in SEER stage, laterality, venous invasion, lymphovascular invasion, or the occurrence of various therapeutics (including radiation, chemotherapy, or immunotherapy). There were also no differences in BRAF and NRAS mutational status in both the VA registry and pathology reports (data not shown).

		Melanoma, no PD after	Melanoma w/ PD after	Comparison	p
	N	42951	473		
AJCC Stage	Total records	34568 (80.5%)	393 (83.1%)		
	Stage 0	15132 (43.8%)	187 (47.6%)	0-I vs. II-IV	< 0.05
	Stage I	13979 (40.4%)	161 (41%)		
	Stage II	3312 (9.6%)	32 (8.1%)		
	Stage III	1655 (4.8%)	13 (3.3%)		
	Stage IV	490 (1.4%)	0 (0%)		
Clinical Stage	Total records	23768 (55.3%)	294 (62.2%)		
	Stage 0	11037 (46.4%)	152 (51.7%)	0-1 vs. 2-3	< 0.05
	Stage 1	9446 (39.7%)	118 (40.1%)		
	Stage 2	2259 (9.5%)	19 (6.5%)		
	Stage 3	1026 (4.3%)	5 (1.7%)		
Pathologic Stage	Total records	18359 (42.7%)	232 (49%)		
	Stage 0	7243 (39.5%)	89 (38.4%)	0-1 vs. 2-4	0.1
	Stage 1	7487 (40.8%)	108 (46.6%)		
	Stage 2	2162 (11.8%)	25 (10.8%)		
	Stage 3	1141 (6.2%)	10 (4.3%)		
	Stage 4	326 (1.8%)	0 (0%)		
Venous Invasion	Total Records	10038 (23.4%)	137 (29%)		
	Yes	143 (1.4%)	2 (1.5%)	Yes vs. No	0.9
	No	9895 (98.6%)	135 (98.5%)		
Lymphovascular Invasion	Total Records	23281 (54.2%)	215 (45.5%)		
	Yes	571 (2.5%)	3 (1.4%)	Yes vs. No	0.4
	No	22710 (97.5%)	212 (98.6%)		
Last Tumor Status	Total Records	42169 (98.2%)	467 (98.7%)		
	Evidence of Tumor	6019 (14.3%)	30 (6.4%)	Yes evidence of tumor vs. No	< 0.05
	No Evidence of Tumor	36150 (85.7%)	437 (93.6%)		
Radiation Therapy	Total Records	40876 (95.2%)	461 (97.5%)		
	Yes	346 (0.8%)	3 (0.7%)	Yes vs. No	0.8
	No	40530 (99.2%)	458 (99.3%)		
Chemotherapy	Total Records	40864 (95.1%)	461 (97.5%)		
	Yes	294 (0.7%)	3 (0.7%)	Yes vs. No	1
	No	40570 (99.3%)	458 (99.3%)		
Immunotherapy	Total Records	40877 (95.2%)	461 (97.5%)		
	Yes	965 (2.4%)	5 (1.1%)	Yes vs. No	0.1
	No	39912 (97.6%)	456 (98.9%)		

Table 2.3.1. Comparison of cancer registry data for melanoma with and without subsequent PD diagnosis. Formal analysis performed by Gregory Scott.

2.4 Discussion

Clinical surveillance of patients with an atypical or malignant melanocytic lesion will continue to increase with the rising incidence and survivorship of melanoma and the growing awareness of dysplastic nevus/atypical moles from tools like the “What to Look For: ABCDES of Melanoma” and “Body Mole Map” provided by the American Academy of Dermatology (595). These surveillance visits represent an opportunity to screen for melanoma and aging-associated diseases, such as PD, before significant neurodegeneration has occurred (585). Similar to early detection and prevention in dermatology, early detection and protection against neurodegenerative disorders is better than rewiring an already damaged brain (584, 585). This early window has been reinforced at the biologic level in a new PD definition that recognizes skin pathology occurring many years to decades before classic movement symptoms (596). It is also a stage of PD enriched for dermatologic disorders such as melanoma, dermatophytosis, seborrheic dermatitis, rosacea, and psoriasis (144, 597, 598)

This study overcomes limitations of prior investigations into an association with PD – deploying lengthier follow-up, adjusting of essential confounders, employing accurate and orthogonal definitions, including novel entities, and testing clinical interactions – to reveal that a diagnosis of a melanocytic lesion is tied to clinically meaningful increases in PD risk. Misclassification in prior studies results from the use of administrative data (e.g. ICD codes) that show poor PPV for PD (599) as well as low accuracy for dermatologic entities not in tumor registries such as 47% for non-melanocytic skin cancer (NMSC) (600) and 30% for atopic dermatitis (601). By using validated PD and melanoma subtyping definitions with much higher PPVs, searching for under-coded non-malignant

and melanocytic entities, and leveraging orthogonal definitions for melanoma (notes, registry), this study addresses these issues. Prior studies were also hampered by lack of studying precursors, pathologic data, interactions, and limited follow-up given that preceding skin disorders, such as melanoma, occur on average 8 years before PD (602). The current study addresses these issues by spanning twenty years and examining precursor lesions, clinicopathologic classification and measurement of clinical interactions. Overall, this study points to melanocytic lesions and specific comorbid disorders as components of a potential screening tool that is both sensitive and predictive for future PD. Data show there are far more registry diagnoses, clinical workups, and pathologic workups of melanoma and melanocytic lesions compared to other PD-associated malignancies and dermatologic entities (Table 2.8.2). Interactions dramatically increase PD prediction and will help dermatologists target the most impactful features since melanoma, when considered alone and without interactions confers an inadequately small effect size for screening (e.g. hazard ratio of 1.66 and 3 cases of PD per 10,000 people, Figure 2.3.2 and Table 2.8.5).

When taken together, these data can assist in eliciting a targeted history based on the mnemonic PD THRESHOLD: PD (**P**arkinson's **D**isease), T (GI **T**ract dysfunction, such as constipation), H (mental **H**ealth disorders, including anxiety and depression), RE (**RE**M Sleep Behavior Disorder, RBD), S (**S**eborrheic dermatitis), H (**H**yperhidrosis), O (**O**rthostatic hypotension), L (**L**ower melanoma stage), and D (**D**ermatophytosis). This encompasses synergistic, i.e. greater than additive, interactions that when present in combination with melanocytic lesions should raise awareness for the development of PD. Moreover, there are emerging confirmatory skin and cerebrospinal fluid assays that could

be used after clinical screening (603, 604). Most profoundly, asking the singular question “have you been told or suspected of acting out your dreams” for RBD allows dermatologists to predict an impressive 6 extra cases of PD per 100 people on top of the two cases predicted by RBD alone (605).

Finally, these data likely reflect shared pathophysiology between melanoma and PD and between melanoma and other disorders that serve to flag therapeutic targets for neuroprotective clinical trials. The current study specifically implicates PD targets shared with both earlier stages of melanomagenesis and sebaceous, autonomic and sleep-related systems as showing potential. For example, this study identifies dermatophytosis as a skin disorder that synergizes with melanocytic lesion to increase incidence of PD. Previous work has identified dermatophytosis as a pPD disorder (144) and 60% of acral melanoma patients contract dermatophytosis (606). While the exact cause of increased susceptibility to these fungi in PD and melanoma remains unclear, theories include lipid metabolism disruptions and immune system dysfunction (607, 608). Given the established connection between PD and melanoma, further research into shared pathways, such as immune dysregulation and lipid metabolism, may provide insight into whether these other disorders play a role in PD-related skin abnormalities.

Limitations of the current study include sampling bias, particular a skewing towards white and male populations in the VA, which may limit generalizability. Another limitation is lack of other melanoma risk factor data such as family history and UV light exposure which could potentially impact PD risk.

In summary, our study reveals the connection between melanoma and subsequent PD and arms the dermatologist with empirical data and a roadmap to guide patients

during a time of uncertainty. Patients may benefit from early diagnostic testing and neuroprotective trials, and this is especially pertinent in individuals that meet PD THRESHOLD risk factors that positively interact with melanocytic lesions to increase incidence of PD. As evidence accumulates, we submit this is one high-risk population in need of a clinical protocol for close monitoring.

2.5 Methods

Patient Population and Institutional Approval

For the VA cohort, all Veterans over the age of 40 years old as of October 1st, 2021 were included (n=21,882,307). Data was obtained from the Corporate Data Warehouse (CDW) under IRB approval (MIRB #04744) using a waiver of participant consent. All time periods were included in the study. The earliest ICD codes in the CDW were dated 1999.

Case Definitions and Data

PD was defined using a validated definition based on age, ICD code, medication, and record duration (609). Cancers were defined using the VA cancer registry (Oncology Domain) entered at the local level by registrars. Data include cancer type, site, overall stage, clinical stage, pathologic stage, venous invasion, lymphovascular invasion, last tumor status, radiation therapy, chemotherapy, and immunotherapy. Melanoma risk lesions (e.g. many nevi) are not coded or biopsied and so were defined based on affirmative mentions in clinical notes after removing negation and ambiguous statements.

Melanoma subtypes and precursors (e.g. superficial-spreading melanoma, dysplastic nevus) that are not coded but are typically biopsied were defined by both a) the presence of affirmative mention of the melanoma subtype in a clinical note and b) affirmative mention of melanoma in the associated pathology report. Accuracy of melanoma, atypical/dysplastic nevi, lentigo maligna melanoma, and acral lentiginous melanoma were manually validated in a randomized subset of 200 cases by M.A and showed positive predictive values (PPVs) of 98.5%, 99.5%, 97.5%, and 95% respectively.

Additional data collected included baseline characteristics (birth year, age, sex, race, ethnicity, smoking status), date of death, diagnosis of other skin disorders (actinic keratosis, atopic dermatitis, basal cell carcinoma, bullous pemphigoid, dermatophytosis, eczema, hyperhidrosis, lichen planus, psoriasis, rosacea, seborrheic dermatitis, squamous cell carcinoma) and early/prodromal PD disorders using ICD codes and free-text medical and pathology notes (609). Missing data for baseline characteristics was imputed using Multiple Imputation by Chained Equations (610).

Statistical Analysis

Initial screening of cancer and PD used a retrospective cohort design and 4-to-1 propensity score matching (caliper width = 0.2). Propensity score matching was done on birth year, race, ethnicity, sex, and smoking status and standardized mean differences were less than 0.1. Association between cancer and subsequent PD was calculated after adjusting for competing risk of death and reported as hazard ratios (HR) and 97.5% confidence intervals (611). Analysis of PD risk after diagnosis of melanocytic lesions used a retrospective cohort design and a pseudo-randomized control trial approach with

inverse probability of treatment weighting followed by measurement of cumulative incidence of PD adjusted for competing risk of death as described previously (612). Positive interactions between melanoma and another disorder are defined as a more-than-additive impact on PD incidence when co-occurring in the same patient. Analysis was conducted using RStudio (RStudio, Boston, MA).

2.6 Acknowledgements

We thank the patients who participated in this research, their families, and the investigators and staff at the Veterans Affairs Corporate Data Warehouse (CDW) and the University of Utah hospital and affiliated clinics Enterprise Data Warehouse (EDW).

This work was supported by VA Biomedical Laboratory Research and Development Career Development Award 1 IK2 BX005760-01A1 (to G.D.S.), John and Tami Marick Family Foundation, Collins Medical Trust Award (to G.D.S.), Oregon Health & Science University Medical Research Foundation New Investigator Award (to G.D.S.), and Oregon Parkinson's Center Research Pilot Award (to G.D.S.). VA Clinical Science Research and Development Career Development Award IK2 CX00253-01A1 (to L.E.N.). Ruth L. Kirschstein National Research Service Award 5F30AF082406-02 (to M.R.A.). HSR&D VA Career Development Award 1IK2CX002642-01A1 (to WYY), a US Department of Defense CDMRP Award W81XWH-21-1-0818 (to WYY), and a Kuni Foundation Cancer Discovery Grant and Kuni Cancer Research Fellows Award (to WYY). The funding sources had no role in the design and conduct of the study; collection,

management, analysis, and interpretation of the data; preparation, review of approval of the manuscript; and decision to submit the manuscript for publication.

2.7 Author Contributions

Conceptualization: MRA, GDS

Data Curation: SS, GDS

Formal Analysis: MRA, SS, GDS

Funding Acquisition: MRA, LEN, WYY

Investigation: MRA, SS, SL, GDS

Methodology: SS, GDS

Project Administration: MRA, GDS

Resources: SS, GDS

Software: SS, GDS, RFT

Supervision: VKU, SL, GDS

Validation: MRA, GDS

Visualization: MRS, GDS

Writing- original draft: MRA, GDS

Writing- review & editing: MRA, LEN, EFF, RFT, WYY, VKU, SL, GDS

2.8 Supplemental Material

	Oncology Registry		Path Reports & Charts	
Database size (N)	1,317,418		4,573,091	
Analysis	PSM		IPTW	
	Matched Controls	Melanoma	Controls	Melanoma
N	182972	45758	4556591	16500
BASELINE				
Birth Year	1943 (±12)	1943 (±12)	1948 (±14)	1943 (±12)
Sex				
Female	5633 (3.1%)	1413 (3.1%)	341399 (7.5%)	492 (3%)
Male	177339 (97%)	44345 (97%)	4215192 (93%)	16008 (97%)
Race				
African American, Black	2876 (1.6%)	715 (1.6%)	826753 (18%)	296 (1.8%)
Native American OR Alaskan Native	534 (0.29%)	157 (0.34%)	31844 (0.7%)	53 (0.32%)
White	178075 (97%)	44502 (97%)	3618302 (79%)	16000 (97%)
Ethnicity				
Not Hispanic or Latino	180653 (99%)	45176 (99%)	4299310 (94%)	16242 (98%)
Hispanic or Latino	2319 (1.3%)	582 (1.3%)	257281 (5.6%)	258 (1.6%)
Smoking				
Never Smoker	65624 (36%)	16400 (36%)	1412708 (31%)	5882 (36%)
Former Smoker	66210 (36%)	16568 (36%)	1350546 (30%)	6002 (36%)
Current Smoker	51138 (28%)	12790 (28%)	1793337 (39%)	4616 (28%)
FOLLOW-UP				
Duration (years)	16 (±5.7)	7.1 (±5)	14 (±6.6)	8.5 (±5.7)
Outcomes				
None	122311 (67%)	27086 (59%)	2876448 (63%)	9296 (56%)
Parkinson's disease	1500 (0.82%)	498 (1.1%)	55723 (1.2%)	213 (1.3%)
Death	59161 (32%)	18174 (40%)	1624420 (36%)	6991 (42%)

abbreviations: PSM = Propensity-Score Matching, IPTW = Inverse Probability Treatment Weighting. * = adjusted for competing risk of death

Table 2.8.1. Baseline characteristics of VA database populations. Data acquisition performed by Gregory Scott.

	Oncology registry	Medical notes	Pathology reports
Skin			2,350,719
Cancer	102,999	-	1,066,990
Melanoma	45,758	521,535	101,710
Melanoma, MIS, or nevus	-	-	359,163
Thyroid			30,885
Cancer	10,022	188,198	11,445
Breast*			47,723
Cancer	16,220		17,076
Nervous system			27,315
Cancer	15,782		8,421

* female sex under-represented in VA data

Table 2.8.2. Cancer counts in VA Oncology registry, medical notes, and pathology reports. Data acquisition performed by Gregory Scott.

	Time since melanocytic lesion (years)					
	1	3	5	10	15	20
melanoma	-- [-3, 18.6]	22.4 [3, 41.8]	29.9 [8.9, 51]	37.3 [13.6, 61]	33.9 [6.6, 61.1]	29.1 [1, 57.2]
<u>melanoma subtypes</u>						
lentigo maligna	-- [-2.4, 3]	11.3 [1, 21.6]	18.3 [6.7, 29.9]	34.4 [17.3, 51.4]	34.8 [16.7, 53]	26 [7.6, 44.5]
superficial spreading	-2.8 [-5.8, 0.2]	-- [-3.9, 11.4]	10.6* [-1.2, 22.5]	16.4* [-0.1, 33]	-- [-9.9, 25.7]	-- [-17.2, 20]
nodular	-- [-5.1, 5.9]	-- [-8.9, 16.1]	-- [-7.5, 23.6]	-- [-21.4, 17.3]	-- [-35.1, 8.1]	-25.6 [-47.7, -3.4]
desmoplastic	-- [-10.3, 3.9]	-- [-20.7, 18]	-- [-31.4, 11.8]	-- [-50.2, 9]	-- [-57.2, 16.7]	-- [-68.3, 5.9]
acral lentiginous	-6.4 [-7.1, -5.8]	-- [-37.8, 22]	-- [-34.7, 71.7]	-- [-54.6, 53.9]	-- [-65.7, 61.7]	-- [-69.6, 93.4]
<u>precursor lesions</u>						
many nevi	-- [-2.1, 1.2]	4.1 [0.9, 7.3]	7.3 [3.1, 11.4]	15.9 [10.1, 21.7]	21.4 [14.2, 28.5]	17.9 [10, 25.9]
atypical/dysplastic nevus	-- [-4, 3.5]	-- [-2.2, 14.3]	15.2 [5.6, 24.8]	34.3 [21.7, 46.8]	38.3 [24, 52.7]	37.4 [21.9, 52.8]
melanoma in situ	-- [-15.8, 30.2]	-- [-14.7, 36.6]	-- [-7, 47.4]	39 [6.9, 71.1]	41.4 [7.4, 75.3]	46.6 [10.9, 82.2]

* borderline significance: p = 0.07 and p = 0.051 for years 5 and 10 respectively

Table 2.8.3. Added cases of Parkinson's Disease (per 10000 people) after melanocytic lesion versus control. Formal analysis performed by Gregory Scott.

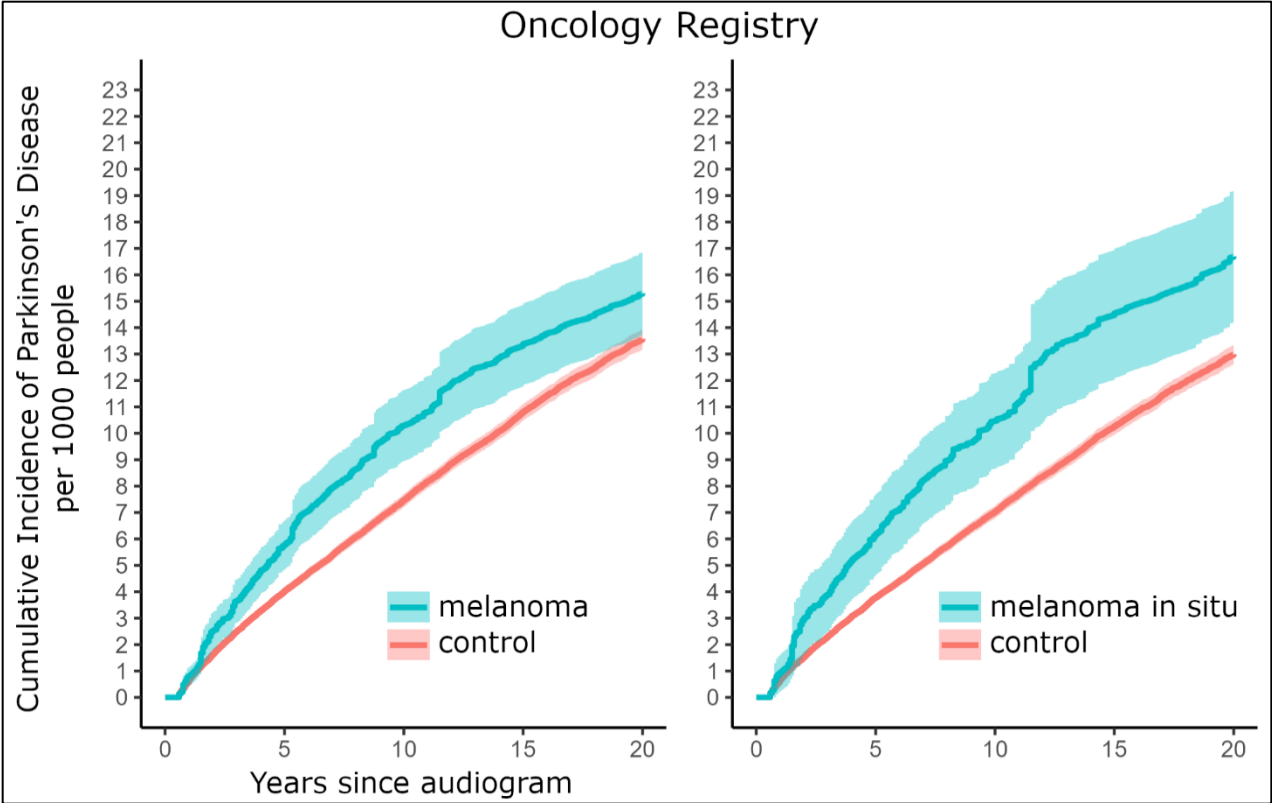


Figure 2.8.1. Melanoma diagnosis and PD Incidence. Melanoma defined by Oncology registry. Cumulative incidence of PD is shown for those diagnosed with melanoma (cyan) and controls (red) over twenty years. Formal analysis performed by Gregory Scott.

	Time since melanocytic lesion (years)					
	5	10	13	15	18	20
Actinic Keratosis	-- [-1, -3.5]	-- [-1.3, -4.7]	-- [-1.8, -5.5]	-- [-1.9, -5.7]	-- [-1.9, -5.8]	-- [-1.6, -5.6]
Atopic Dermatitis	-- [-0.8, -4.3]	-- [-0.2, -5.6]	-- [0.5, -5.7]	-- [2.1, -4.9]	-- [3.5, -4.1]	-- [3.6, -4.1]
Basal Cell Carcinoma	-- [-0.8, -3.9]	-- [1.3, -3.4]	-- [1.7, -3.2]	-- [2.4, -2.5]	-- [3.1, -1.9]	-- [3.4, -1.8]
Bullous Pemphigoid	-- [2.4, -5.6]	-- [8.5, -7.3]	-- [9.1, -7.2]	-- [12.8, -5.5]	-- [12.8, -5.6]	-- [17.9, -4]
Dermatophytosis	-- [2, -2.5]	-- [3.8, -1.7]	3.3 [6.3, 0.2]	3.3 [6.4, 0.2]	4 [7.2, 0.7]	4 [7.2, 0.7]
Eczema	-- [1.4, -2]	-- [2.3, -2]	-- [2.3, -2.3]	-- [2.9, -1.8]	-- [3.1, -1.7]	-- [3.8, -1.2]
Hyperhidrosis	-- [4.7, -0.8]	3.6 [6.9, 0.4]	4.6 [7.9, 1.2]	5.5 [9, 2.1]	6.5 [10.1, 3]	7.1 [10.6, 3.5]
Lichen Planus	-- [0.2, -4.5]	-- [2.6, -4.5]	-- [2.7, -4.7]	-- [2.6, -4.8]	-- [3, -4.6]	-- [3.2, -4.4]
Psoriasis	-- [0.5, -3.4]	-- [-0.7, -5.5]	-- [-0.5, -5.7]	-- [-0.6, -5.9]	-- [-0.2, -5.7]	-- [-0.1, -5.6]
Rosacea	-- [2.4, -3]	-- [2.8, -3.1]	-- [3.3, -2.9]	-- [3.8, -2.5]	-- [4.5, -1.9]	-- [5.6, -1.3]
Seborrheic Dermatitis	-- [2.1, -1.8]	-- [3, -1.6]	-- [4.8, -0.6]	-- [5.4, 0]	3.7 [6.4, 0.9]	4.3 [7.2, 1.5]
Squamous Cell Carcinoma	-- [-0.8, -3.3]	-- [0.5, -3]	-- [0.8, -3]	-- [1.4, -2.6]	-- [2, -2]	-- [2.2, -1.8]

Table 2.8.4. Added cases of Parkinson’s Disease (per 1000 people) from interaction of a melanocytic lesion and another skin disorder. PD risk from having both disorders concomitantly versus adding risk from each disorder alone. Formal analysis performed by Gregory Scott.

	Time since melanocytic lesion (years)					
	5	10	13	15	18	20
Anxiety	-- [4, -0.8]	3.1 [5.9, 0.3]	3.6 [6.9, 0.4]	3.9 [7.3, 0.6]	4.2 [7.6, 0.8]	5 [8.5, 1.4]
Constipation	-- [1.4, -1.5]	2.3 [4.3, 0.3]	3.2 [5.4, 1]	3.8 [6, 1.5]	5 [7.4, 2.7]	6 [8.4, 3.5]
Depression	-- [4.4, -0.2]	4.2 [6.9, 1.5]	5 [7.9, 2.1]	5 [8, 2.1]	4.9 [7.9, 1.8]	4.7 [7.8, 1.6]
Hypersomnia	-- [7.3, -0.3]	-- [8.2, -0.4]	-- [8.4, -0.5]	-- [8.8, -0.4]	-- [9.1, -0.3]	-- [9.3, -0.2]
Orthostatic Hypotension	-- [4.4, -1]	7.1 [10.7, 3.4]	10 [14.3, 5.7]	11.7 [16.2, 7.2]	13.8 [18.5, 9.1]	14.8 [19.6, 10.1]
REM Sleep Behavior Disorder	20.5 [30.7, 10.4]	40.9 [53.4, 28.3]	50.3 [63.9, 36.8]	55.3 [69.3, 41.3]	60.1 [74.7, 45.5]	60.6 [75.3, 46]
Smell or Taste Disturbance	-- [-2.2, -9.4]	-- [-3.1, -12.7]	-- [-2.9, -13.8]	-- [-0.8, -13]	-- [0.5, -12.7]	-- [3.7, -11]
Urinary Dysfunction	-- [1.2, -1.3]	-- [2.7, -0.8]	-- [3.6, -0.2]	2.5 [4.5, 0.6]	3 [5.1, 1]	3.8 [5.9, 1.7]

Table 2.8.5. Added cases of Parkinson’s Disease (per 1000 people) from interaction of a melanocytic lesion and another prodromal PD disorder. PD risk from having both disorders concomitantly versus adding risk from each disorder alone. Formal analysis performed by Gregory Scott.

Supplement Text

Images adapted for Figure 2 fall under the Creative Commons license and include:

https://commons.wikimedia.org/wiki/File:Anatomy_and_physiology_of_animals_Adrenal_glands.jpg

https://commons.wikimedia.org/wiki/File:Digestive_system_diagram_edit.svg

https://commons.wikimedia.org/wiki/File:Respiratory_system_-_Lungs_-_Smart-Servier.png

https://commons.wikimedia.org/wiki/File:Alzheimer%27s_disease_brain_preclinical.jpg

https://commons.wikimedia.org/wiki/File:Paranasal_sinuses.svg

https://commons.wikimedia.org/wiki/File:Human_leg_bones_labeled_ru.png

https://commons.wikimedia.org/wiki/File:Illu_cervix.jpg

GGanatogram, R library, skeletal muscle:

<https://pmc.ncbi.nlm.nih.gov/articles/PMC6208569/>

[https://commons.wikimedia.org/wiki/File:Sexual_organs_-_male_\(no_description\).svg](https://commons.wikimedia.org/wiki/File:Sexual_organs_-_male_(no_description).svg)

[Jump Back to Table of Contents](#)

Chapter 3: Alpha-synuclein regulates nucleolar DNA double-strand break repair in melanoma

Moriah R. Arnold^{1,2}, Gabriel M. Cohn³, Kezia Catharina Oxe⁴, Somarr N. Elliott², Cynthia Moore⁵, Allison May Zhou², Peter V. Laraia⁶, Sahar Shekoohi⁷, Dillon Brownell⁸, Rosalie C. Sears^{3,9,10}, Randall L. Woltjer¹¹, Charles K. Meshul^{5,12}, Stephan N. Witt^{7,13}, Dorthe H. Larsen⁴, Vivek K. Unni^{*2,14}

¹Medical Scientist Training Program, Oregon Health and Science University, Portland, OR, USA.

²Department of Neurology and Jungers Center for Neurosciences Research, Oregon Health and Science University, Portland, OR, USA.

³Department of Molecular and Medical Genetics, School of Medicine, Oregon Health and Science University, Portland, OR, USA.

⁴Danish Cancer Institute, Nucleolar Stress and Disease Group, Strandboulevarden 49, 2100 Copenhagen, Denmark.

⁵Research Services, Neurocytology Laboratory, Veterans Affairs Medical Center, Portland, OR, USA.

⁶Independent Collaborator.

⁷Department of Biochemistry and Molecular Biology, Louisiana State University Health Sciences Center, Shreveport, LA, USA.

⁸Department of Molecular Microbiology and Immunology, Oregon Health and Science University, Portland, OR, USA.

⁹Brenden-Colson Center for Pancreatic Care, Oregon Health & Science University, Portland, OR, USA.

¹⁰Knight Cancer Institute, Oregon Health & Science University, Portland, OR, USA.

¹¹Layton Aging & Alzheimer's Disease Research Center and Department of Pathology, Oregon Health and Science University, Portland, OR, USA.

¹²Departments of Behavioral Neuroscience and Pathology, Oregon Health and Science University, Portland, OR, USA.

¹³Feist-Weiller Cancer Center, Louisiana State University Health Sciences Center, Shreveport, LA, US.

¹⁴OHSU Parkinson Center, Oregon Health and Science University, Portland, OR, USA.

Published on bioRxiv January 14th, 2024

In Press at *Science Advances*

3.1 Abstract

Although an increased risk of the skin cancer melanoma in people with Parkinson's Disease (PD) has been shown in multiple studies, the mechanisms involved are poorly understood, but increased expression of the PD-associated protein alpha-synuclein (α Syn) in melanoma cells may be important. Our previous work suggests that α Syn can facilitate DNA double-strand break (DSB) repair, promoting genomic stability. We now show that α Syn is preferentially enriched within the nucleolus in melanoma, where it colocalizes with DNA damage markers and DSBs. Inducing DSBs specifically within nucleolar ribosomal DNA (rDNA) increases α Syn levels near sites of damage. Alpha-synuclein knockout increases DNA damage within the nucleolus at baseline, after specific rDNA DSB induction, and prolongs the rate of recovery from this induced damage. α Syn is important downstream of ATM signaling to facilitate MDC1-mediated 53BP1 recruitment to DSBs, reducing micronuclei formation and promoting cellular proliferation, migration, and invasion.

3.2 Introduction

Neurodegeneration and cancer are traditionally thought of as opposite processes, with the former characterized by neuronal death and the latter uncontrolled cellular proliferation. In general, neurodegenerative disease patients are at moderately decreased risk of developing most cancers (2), however exceptions exist. The best described positive association between a neurodegenerative disease and cancer risk is between Parkinson's Disease (PD) and the skin cancer melanoma (4). Since the initial observation by Skibba et al. (324), many epidemiological studies report an increase in melanoma risk ranging from 1.4- to 20-fold among individuals with PD compared to healthy individuals (2, 5-20). More malignant forms of melanoma that originate in the head or neck region (613) are also associated with sporadic and genetic forms of PD (602). This risk is bidirectional, since there is also increased risk of developing PD in melanoma patients (1.7-4.2-fold) (12, 15, 21-23). Altogether, the association between PD and melanoma is well-established, yet the cause is poorly understood.

One potential molecular link is the neurodegeneration-associated protein alpha-synuclein (α Syn) that aggregates into cytoplasmic inclusions called Lewy bodies in PD and other Lewy body disorders (LBDs) (614, 615). This Lewy pathology is associated with neuronal death in midbrain dopaminergic neurons, cortical glutamatergic neurons, and other vulnerable cell populations in LBDs (616). α Syn is not only abundant in the central nervous system, but is also found in other cell types in the body, including skin (617, 618). Given this connection between PD and melanoma, the presence of α Syn in the skin is intriguing. α Syn is not highly expressed in melanocytes of healthy individuals, but increased in melanocytes of people with PD (394, 395), and in ~85% of primary and

metastatic melanoma samples (5, 395-397). Many immortalized human melanoma cell lines also show high expression of α Syn (2, 5, 397, 401). These findings suggest that α Syn upregulation may be a key molecular link between PD and melanoma and an important contributor in both disease pathologies.

Our previous work using longitudinal *in vivo* multiphoton imaging in mice revealed that Lewy body formation in cortical neurons was associated with a loss of soluble α Syn from the nucleus and cytoplasm and that only neurons bearing Lewy bodies went on to die (427). This led us to hypothesize that loss of a normal nuclear α Syn function could contribute to these cells' demise. We unexpectedly found that α Syn colocalized with DNA double-strand break (DSB) repair components within the nucleus of human and mouse cells. Alpha-synuclein knockout (KO) increased DSBs and impaired DSB repair efficiency in human cells and mouse cortical neurons, which could be rescued by transgenic reintroduction of human α Syn in the mouse neuron α Syn KO background (442). Our previous findings are consistent with the work of others observing activation of DNA damage response (DDR) pathways in synucleinopathy models (500, 619, 620). We suggested that in neurodegenerative disease α Syn loss-of-function within the nucleus of inclusion-bearing neurons may contribute to their cell death (442). We also speculated that an α Syn gain-of-function in melanoma could play a potentially protective role against DNA damage. Consistent with this, the original report of α Syn localization to the nucleus in melanoma cell lines (401) has now been replicated in melanoma tissue samples from patients by multiple groups (395, 505). Within the epidermis in melanoma samples, α Syn was found in the nucleus, cytoplasm and even in the extracellular space (395), and present in oligomeric (506) and filamentous (505) aggregate forms. Although to our

knowledge, more mature discrete intracellular α Syn inclusions like Lewy pathology have not been described in melanoma. This contrasts with neuronal and glial α Syn aggregation found in LBDs and Multiple System Atrophy, where oligomeric forms and mature inclusions are present in the cytoplasm and nucleus (490, 491, 621). Consistent with the potential importance of nuclear α Syn in melanoma, work by others has shown that α Syn KO human melanoma cells implanted as xenografts in mice exhibit slower growth and increased apoptosis (478), paired with reduced tumor-induced mechanical allodynia (481). In addition, WT melanoma cells in α Syn overexpressing mice show increased metastasis (479), indicating potentially complex interactions between α Syn within melanoma cells and other tissues in the body. Alpha-synuclein expression is also correlated with poorer survival for patients with melanoma (478). Although numerous studies have described localization of α Syn to the nucleus in melanoma cells (373, 395, 398, 401, 503, 504), its nuclear function is still unclear. In order to better understand these interesting links between neurodegeneration and cancer, we set out to test the function of α Syn within the nucleus of melanoma cells.

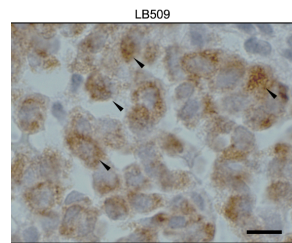
3.3 Results

Alpha-Synuclein Localizes to the Granular Component of the Nucleolus

In order to understand the spatial pattern of α Syn localization within melanoma cells, primary cutaneous melanoma (n=4) and brain metastatic melanoma (n=17) biopsies were stained for α Syn. We found that 4/4 primary cutaneous melanoma and 15/17 brain metastatic melanoma samples demonstrated obvious α Syn staining

(Figure 3.3.1A). Counterstaining with hematoxylin showed a moderate degree of α Syn staining in these samples localized to the cytoplasm as well as the nucleus. Next, a wide-excision biopsy from a primary melanoma tumor was stained for α Syn and various nuclear markers. Our immunofluorescence staining showed clear enrichment of α Syn near large, distinct replication protein A2 (RPA32) foci, which are reminiscent of similar large RPA32 foci seen within the nucleolus and required for the repair of ribosomal DNA (rDNA) DSBs (Figure 3.3.1B) (567, 574). We next stained a panel of primary and immortalized melanocytes and melanoma cell lines and detected clear α Syn enrichment within the nucleolar sub-compartment of the nucleus in the vast majority of cells in all of these lines. In the SK-Mel28 melanoma cell line, α Syn colocalized to DAPI-poor regions and with established nucleolar markers treacle, nucleophosmin, and nucleostemin (Figure 3.3.1C-1D, Figure 3.8.1A). Similar results were also seen in A375 (melanoma line), PIG1 (melanocyte line), and human primary melanocyte cells derived from foreskin (Figure 3.8.1B-D). We next used fluorescence deconvolution analysis to measure α Syn localization at higher spatial resolution within nucleolar sub-compartments. Mammalian nucleoli are comprised of three sub-compartments: the fibrillar center (FC), the dense fibrillar component (DFC), and the granular component (GC; rRNA transcription occurs at the interface of the FC and DFC, early rRNA processing occurs in the DFC, followed by additional rRNA processing and pre-ribosome assembly in the GC). These sub-compartments were visualized using antibodies specific for each of them (RPA194, FC; fibrillarin, DFC; nucleophosmin, GC). 3D reconstruction (Imaris) revealed the localization of α Syn primarily in the GC, directly adjacent to the DFC, and relatively excluded from FCs (Figure 3.31E). In order to obtain more detailed spatial information, we measured

α Syn localization with immunogold transmission electron microscopy (immuno-TEM). Immuno-TEM images in SK-Mel28 cells also showed particle labeling primarily in the GC and/or DFC, but relatively excluded from the FC, and this labeling was significantly increased when compared to α Syn KO SK-Mel28 cells previously described (478) (Figure 3.3.1F, Figure 3.8.2). Taken together, these data strongly suggest that α Syn localizes to the nucleolus in melanocytes and melanoma cells and is enriched within the GC of the nucleolus. These data are consistent with other work showing α Syn labeling within the nucleolus (401, 504), and extends it by demonstrating preferential enrichment within the GC.

A

Case number	Type	Age	Sex	Stain	Status	Comments
Primary cutaneous melanoma						
1		73 F		++		
2		70 M		++		
3		64 M		++		
4		85 F		++		
Metastatic melanoma						
5		66 M		++		
6		69 M		++		
7		67 F		++		
8		79 M		++		
9		58 M		++		
10		62 M		++		Largely necrotic
11		61 M		++		Largely necrotic
12		53 F		++		Nearly completely necrotic
13		72 M		++		Largely necrotic
14		49 M		++		
15		34 M		++		
16		73 F		++		Nearly completely necrotic
17		44 F		++		
18		68 M		++		
19		73 F		++		Largely necrotic

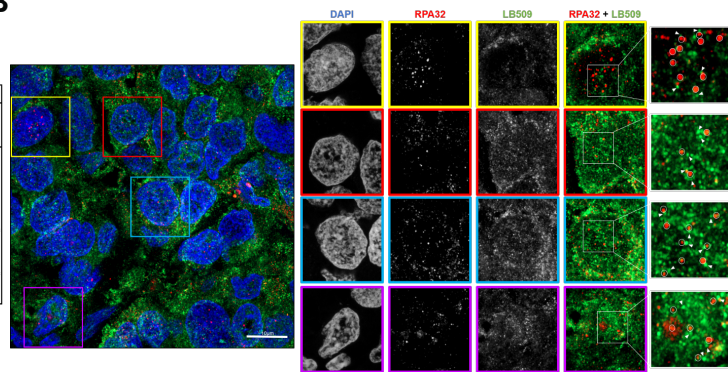
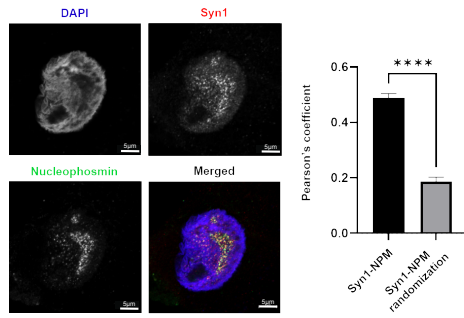
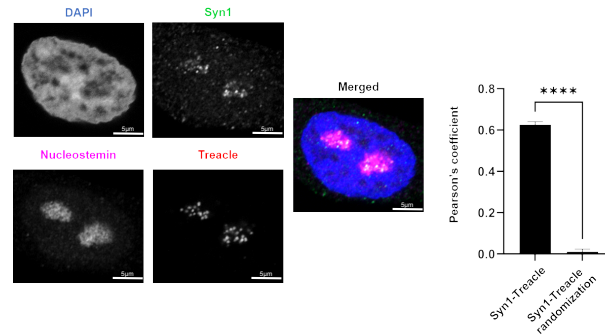
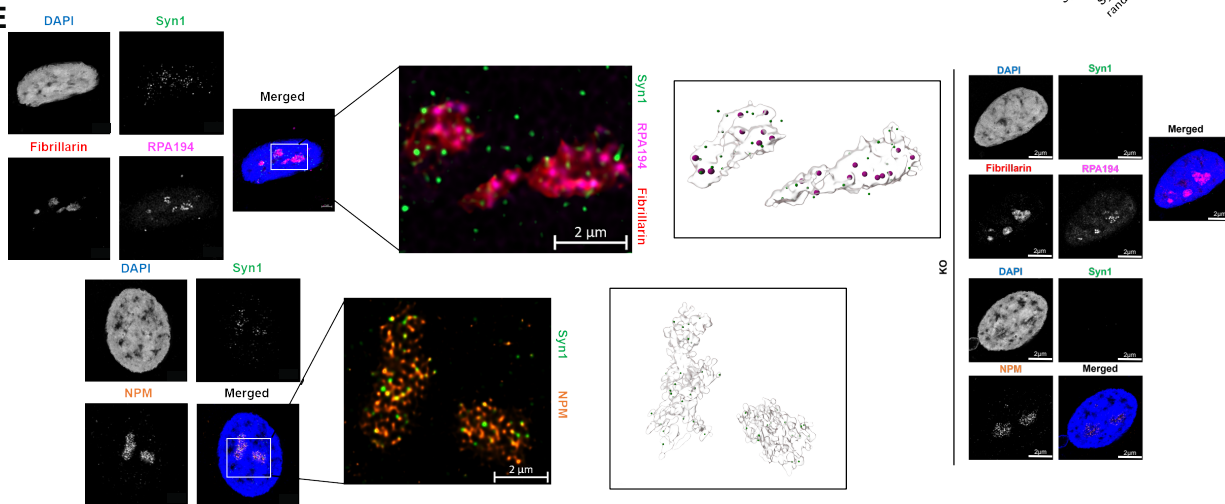
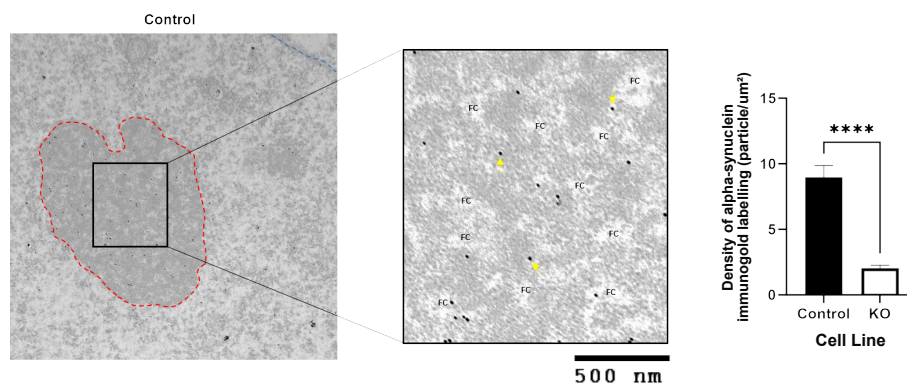
B**C****D****E****F**

Figure 3.3.1. Alpha-synuclein localizes to the granular component of the nucleolus in melanoma cells. A) Brown DAB pigment labels alpha-synuclein antibody (LB509) staining enriched in a subset of metastatic melanoma cells (arrowheads). Scale bar 10 μ m. Table showing demographic information and staining pattern detected. – no detectable staining, + light staining, ++ moderate staining. B) Formalin-fixed paraffin-embedded wide-excision patient biopsy was stained for alpha-synuclein (LB509), nuclear marker (RPA32), and DAPI. The sample was imaged on the Zeiss 980 confocal microscope with Airyscan. White circles indicate RPA32 foci and arrows denote LB509 foci. C, D) SK-Mel28 cells were stained for alpha-synuclein (Syn1), nucleolar markers (nucleophosmin, treacle, and nucleostemin), and DAPI. Cells were imaged on the Zeiss 980 confocal microscope with Airyscan and colocalization was analyzed in Imaris software. Error bars represent Standard Error of the Mean (SEM) with quantification from 3 biological replicates (total n=30-36 nuclei per condition). ****p<0.0001 by T-test. E) SK-Mel28 cells were stained for alpha-synuclein (Syn1), fibrillar center marker (RPA194), dense fibrillar component marker (fibrillarin), granular component marker (nucleophosmin), and DAPI. Cells were imaged on the Zeiss 980 confocal microscope with Airyscan oversampling and Joint Deconvolution and Channel Alignment post-processing. 3D renderings were produced using Imaris software. F) SK-Mel28 cell pellets were fixed for 2 hours at RT. Thin sections were cut on an ultramicrotome (EM UC7), stained for alpha-synuclein (MJFR1, 1:75) (12nm colloidal gold particles), and observed by a JEOL 1400 transmission electron microscope. Blue labeling denotes nuclear membrane. Red labeling denotes the outline of the nucleolus. FC=Fibrillar Center. Arrows point to representative MJFR1 staining. Quantification of 3 biological replicates (total n=28-35 nucleoli per genotype). ****p<0.0001 by T-test. Error bars denote SEM. The different alpha-synuclein antibodies utilized in panels A-E were chosen after tissue-type and methodology optimization to determine which produced the most distinct and specific nuclear labeling. Formal analysis of Figure 3.3.1A performed by Randy Woltjer. Staining of samples in Figure 3.3.1B performed by Allison Zhao. TEM imaging and formal analysis of Figure 3.3.1F performed by Cindy Moore.

Alpha-Synuclein Knockout Increases γ H2AX Levels in the Nucleus and Nucleolus in an ATM- and ATR-Dependent Manner

In order to understand the functional role of α Syn enrichment within the nucleolus, we measured levels of the phosphorylated histone marker of DSB repair γ H2AX within the nucleoplasmic and nucleolar compartments independently. α Syn and γ H2AX levels were both significantly greater in the nucleolus compared to the nucleoplasm and this γ H2AX strongly colocalized with α Syn foci in SK-Mel28 cells (Figure 3.3.2A). We also measured significant colocalization between α Syn and γ H2AX in PIG1 (melanocyte cell

line) and primary melanocytes (Figure 3.8.3A-3B). PLA analysis revealed significant α Syn and γ H2AX colocalization compared to proper controls, within the \sim 40nm resolution of this technique (Figure 3.3.2B, Figure 3.8.3C), suggesting close proximity of these two molecules in nuclear and nucleolar DSB repair-associated foci. Interestingly, α Syn KO cells exhibited increased γ H2AX immunocytochemical signal in the nucleus compared to control cells and this difference was even larger in the nucleolus (Figure 3.3.2C), suggesting that α Syn is even more important in the nucleolus for DSB repair than it is in the nucleoplasm. Importantly, stable reintroduction of wild-type human α Syn into the α Syn KO background (α Syn “rescue”) reduced both nucleolar and nuclear γ H2AX back down to control levels (Figure 3.3.2C, Figure 3.8.2). These specific patterns in γ H2AX levels were also seen using western blot analysis after nuclear fractionation and normalization to either total protein levels or total H2AX levels (Figure 3.3.2D, Figure 3.8.3D).

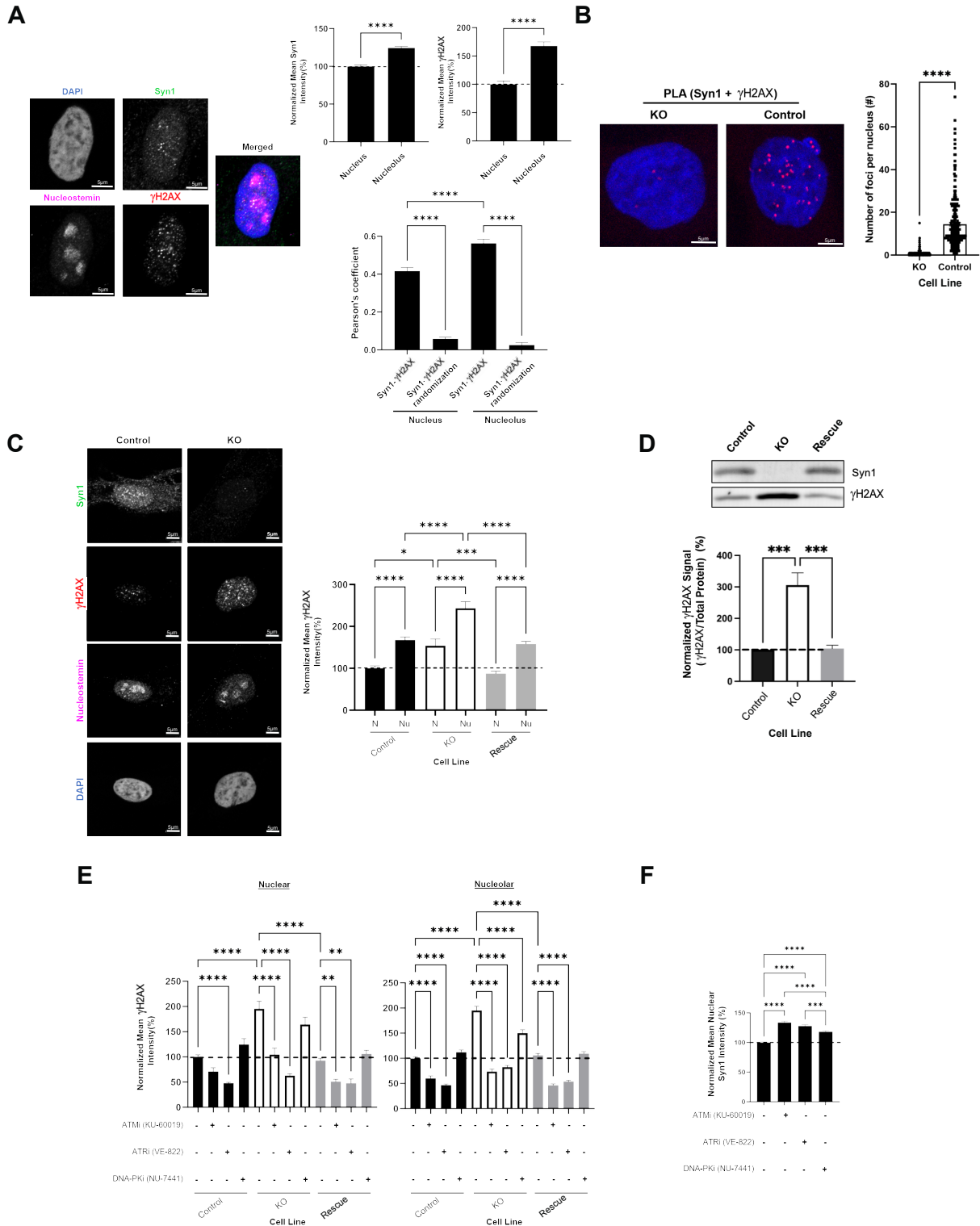


Figure 3.3.2. Alpha-synuclein interacts with γ H2AX in the nucleolus and knocking out alpha-synuclein leads to increased ATM/ATR-driven H2AX phosphorylation. A, C) SK-Mel28 cells were stained for alpha-synuclein (Syn1), DSB marker (γ H2AX),

nucleolar mask (nucleostemin), and DAPI. Cells were imaged on the Zeiss 980 confocal microscope with Airyscan and data was analyzed using FIJI (intensity) or Imaris (colocalization). Quantification represents 3 biological replicates (total n=71-172 nuclei or nucleoli per condition/genotype for intensity or n=30 nuclei per condition for colocalization). * p<0.05, *** p<0.001, **** p<0.0001 by T-test or ANOVA. Error bars denote SEM for all graphs. N=nucleus, Nu=nucleolus. Same γ H2AX quantification of control cells between A and C. B) SK-Mel28 cells were seeded on PDL-coated coverslips and then fixed in 4% paraformaldehyde. Proximity Ligation Assay (Duolink) was completed using antibodies against Syn1 and γ H2AX. Cells were imaged on the Zeiss 980 confocal microscope and number of foci per nucleus was measured using CellProfiler while masking for the nucleus using DAPI. Each figure shows representative images and quantification from 3 biological replicates (total n=283-306 nuclei per genotype). ****p<0.0001 by T-test. Error bars denote SEM. D) SK-Mel28 cells were lysed and a nuclear fractionation was performed. Nuclear protein was run out on SDS-PAGE and probed for γ H2AX and total protein. Western blots were imaged on Licor CLx imager. *** p<0.001 by ANOVA. Error bars denote SEM. Quantification from 4 biological replicates. E, F) SK-Mel28 cells were treated with DMSO, KU-60019 (10 μ M), VE-822 (0.1 μ M), or NU-7441 (1 μ M) for 24 hours. Cells were fixed and stained for Syn1, γ H2AX, nucleostemin and DAPI. Mean intensity of γ H2AX signal within DAPI and nucleostemin masks analyzed using FIJI. ** p<0.01, *** p<0.001, **** p<0.0001 by ANOVA. Error bars denote SEM. Quantification from 3 biological replicates (total n=517-615 nuclei or nucleoli per condition). Staining of Figure 3.3.2B performed by Gabe Cohn.

Three phosphoinositide 3-kinase (PI3K)-related kinase (PI3KK) family members are important for regulating γ H2AX levels, ataxia-telangiectasia mutated (ATM), ataxia-telangiectasia and Rad3-related (ATR), and DNA-dependent protein kinase (DNA-PK) (622). Pharmacologic ATR inhibition reduced γ H2AX levels in the nucleoplasm, and both ATM and ATR inhibition reduced γ H2AX levels in the nucleolus in control SK-Mel28 cells, while DNA-PK inhibition had no effect in either compartment (Figure 3.3.2E). In α Syn KO cells, both ATM and ATR inhibition reduced γ H2AX levels in the nucleus and nucleolus, while DNA-PK inhibition again had less prominent effects, and similar overall patterns were also seen in α Syn rescue and control cells (Figure 3.3.2E, Figure 3.8.4A). Interestingly, inhibition of ATM, ATR, or DNA-PK all moderately increased nuclear α Syn levels (Figure 3.3.2F, Figure 3.8.4A). Similar changes in nuclear γ H2AX levels after ATM,

ATR, or DNA-PK inhibition were also seen using the complementary In-Cell Western assay (Figure 3.8.4B, Figure 3.8.5A). Taken together, these results show that ATM and ATR are required for the increased phosphorylation of H2AX detected in the α Syn KO condition. Additionally, inhibiting any of these kinases—ATM, ATR, or DNA-PK—increases nuclear α Syn levels, potentially as part of a compensatory mechanism to improve DSB repair. We also attempted to test the potential effects of combined ATM, ATR and DNA-PK inhibition in our SK-Mel28 cell lines by applying inhibitors to all three kinases simultaneously, but unfortunately, this led to toxicity with greatly reduced cell viability and were not pursued further.

To directly test the role of α Syn in facilitating DSB repair, we induced DNA damage throughout the nucleoplasm and nucleolus (pan-nuclear) in SK-Mel28 cells with the chemotherapeutic agent bleomycin (100 μ g/ml, 1 hour). Bleomycin chemically induces DSBs, in addition to other forms of DNA damage like single-strand breaks (623). As expected, bleomycin treatment increased pan-nuclear γ H2AX immunocytochemical intensity (Figure 3.3.3A). Similar to our results with PI3KK inhibition, bleomycin also moderately increased pan-nuclear α Syn levels (Figure 3.3.3A). Pan-nuclear γ H2AX levels were higher in α Syn KO cells compared to control cells treated with bleomycin and this was attenuated in α Syn rescue cells (Figure 3.3.3A). Similar results were also seen using western blot (Fig. 3B) and In-Cell Western (Figure 3.3.3C, Figure 3.8.5A) analyses. Next, we used immunocytochemistry to compare γ H2AX levels between the nucleoplasm and nucleolus after bleomycin treatment, as we previously did in untreated cells (Figure 3.3.2C). Bleomycin significantly increased γ H2AX levels in both the nucleoplasm and in nucleoli (Figure 3.3.3D, Figure 3.8.6A) with no clear differences between the two

compartments, likely because bleomycin is a nonselective inducer of DNA damage throughout the nucleus with no preference for nucleolar versus nuclear DNA. Furthermore, we wanted to explore whether the increase in nuclear α Syn signal after bleomycin treatment via ICC was due to an upregulation of transcriptional activity or another mechanism. We performed qRT-PCR against *SNCA* and found that bleomycin treatment did not significantly change mRNA levels coding for α Syn, suggesting alternate downstream mechanisms such as increased cytoplasmic-to-nuclear transport or reduced α Syn degradation may be responsible for the increase in nuclear α Syn signal we detect after bleomycin treatment (Figure 3.8.6B).

In order to understand the spatial relationship between α Syn and DNA at the sites of DSBs, we used a recently developed modified PLA technique, DNA Damage In Situ Ligation Followed by Proximity Ligation Assay (DI-PLA) (624). This approach detects a protein of interest, in our case α Syn, and a hairpin-shaped biotinylated DNA oligonucleotide that only ligates to double-stranded DNA ends (found in DSBs) as the PLA partner. This allows sensitive detection of proteins located within \sim 40nm of a DSB site. We found a higher number of α Syn DI-PLA foci in SK-Mel28 cells treated with bleomycin compared to our controls (Figure 3.3.3E, Figure 3.8.3C), indicating that α Syn is located close to the site of DSBs after bleomycin treatment.

Although bleomycin treatment induces DNA DSBs, it also produces other types of DNA damage within the nucleus, including single-strand breaks. Therefore, we wanted to induce global nuclear DNA damage in a manner that more specifically created DSBs, so we next used ionizing radiation (IR). Upon X-ray IR, pan-nuclear γ H2AX levels were higher in α Syn KO cells compared to control cells treated with IR, and this effect was

slightly, but significantly, attenuated below control levels in α Syn rescue cells (Figure 3.3.3F). Altogether, these data indicate that α Syn is upregulated in response to DNA damage and may play a role in modulating DSB repair and that this might be particularly important in the nucleolus.

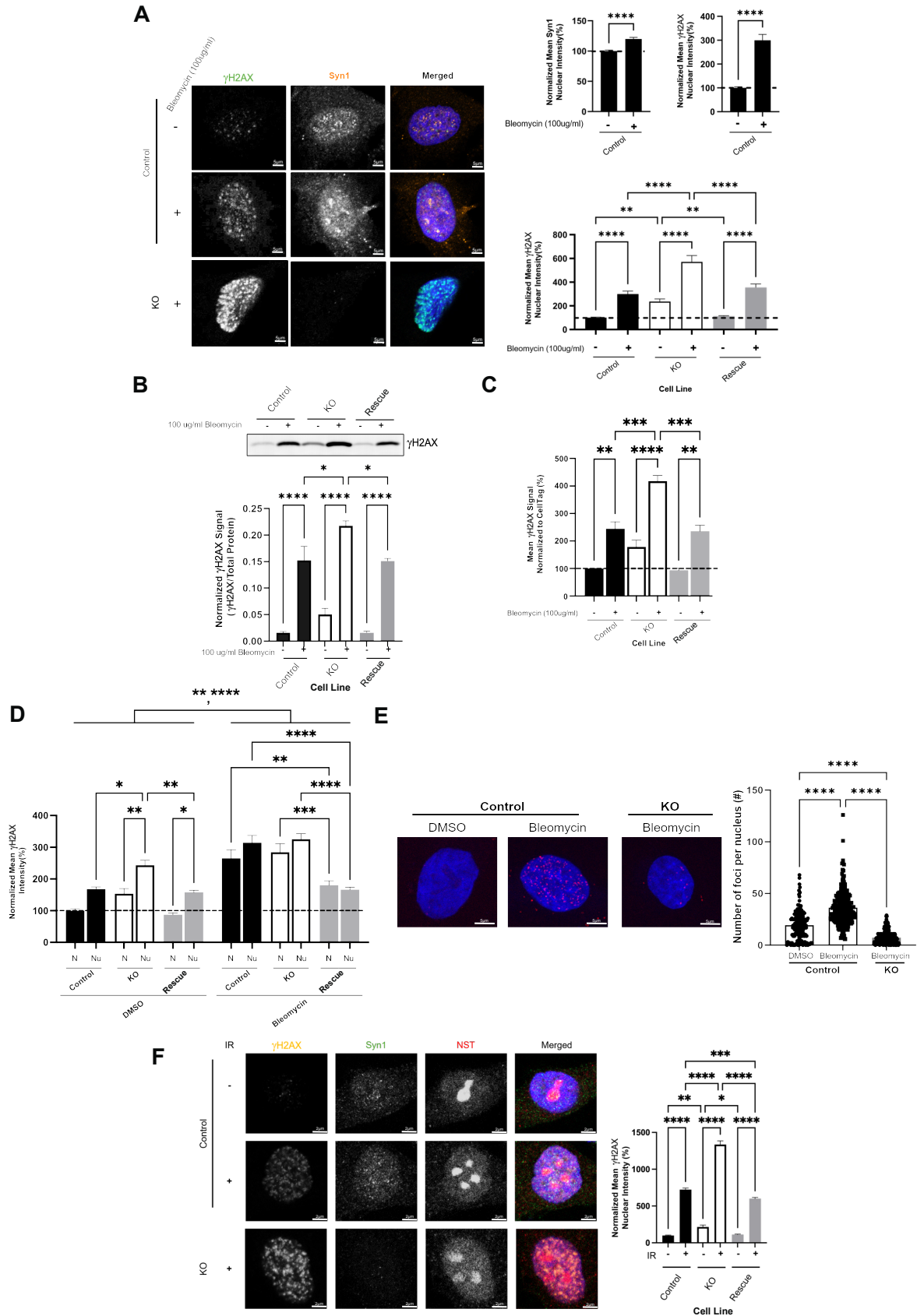


Figure 3.3.3. Alpha-synuclein is important in bleomycin and IR-induced DNA damage response pathways. A, D) SK-Mel28 cells were treated with DMSO or 100µg/ml bleomycin for 1 hour and stained for Syn1, γH2AX, and DAPI. Mean intensity of γH2AX signal within DAPI and/or nucleostemin masks were analyzed using FIJI. * p<0.05, ** p<0.01, ***p<0.001, **** p<0.0001 by ANOVA. Error bars denote SEM. N=nucleus, Nu=nucleolus. Quantification from 3 biological replicates (total n=45-757 nuclei or nucleoli per condition). Same γH2AX quantification between graphs in panel A with control cells. B) SK-Mel28 cells were treated with DMSO or 100µg/ml bleomycin and lysed and a nuclear fractionation was performed. Nuclear protein was run out on SDS-PAGE and probed for γH2AX and total protein. * p<0.05, **** p<0.0001. Error bars denote SEM. Quantification from 4 biological replicates. C) SK-Mel28 cells were treated with DMSO or 100µg/ml bleomycin. Cells were processed according to the In-Cell Western manufacturer instructions and stained for γH2AX (800) and CellTag (700). ** p<0.01, *** p<0.001, **** p<0.0001 by ANOVA. Error bars denote SEM. Quantification from 3 biological replicates (with 4 technical replicates per biological replicate). E) SK-Mel28 cells were treated with DMSO or 100µg/ml bleomycin. DNA Damage In Situ Ligation Followed by Proximity Ligation Assay (DI-PLA) was completed. Number of foci per nucleus was measured within nuclear masking. Quantification from 3 biological replicates (total n=171-231 nuclei per condition). ****p<0.0001 by ANOVA. Error bars denote SEM. F) SK-Mel28 cells were treated with 0Gy or 5Gy of X-ray ionizing radiation followed by a 20-minute recovery period and stained for Syn1, γH2AX, NST and DAPI. Mean intensity of γH2AX signal within DAPI masks were analyzed using FIJI. * p<0.05, ** p<0.01, ***p<0.001, **** p<0.0001 by ANOVA. Error bars denote SEM. Quantification from 3 biological replicates (total n=358-388 nuclei per condition). Staining of Figure 3.3.3E performed by Gabe Cohn.

Alpha-Synuclein Regulates Nucleolar Double-Strand Break Repair of Ribosomal DNA

Given that bleomycin is a non-selective inducer of DNA damage both in the nucleoplasm and nucleolus, and our data suggests that αSyn is particularly enriched within the nucleolus, we next used an approach to create nucleolar-specific DSBs in rDNA with the intron-encoded endonuclease I-Ppol (569) that recognizes a 13-15bp DNA sequence within the 28S rDNA coding region. I-Ppol-induced DSBs in rDNA lead to a large-scale reorganization of nucleolar structure, including the formation of nucleolar “caps” at the nucleolar periphery that allow DSB repair components that do not accumulate inside nucleoli to associate with damaged DNA for repair. After repair occurs,

the nucleolus returns to its normal structure and caps disappear. After transfecting SK-Mel28 cells with mRNA for I-Ppol WT or the catalytically inactive mutant H98A (negative control), we measured a clear increase in nuclear γ H2AX, with a pattern indicating nucleolar-specific DSBs in the I-Ppol WT condition (Figure 3.3.4A). There was also a significant increase in nuclear α Syn levels upon rDNA DSBs (Figure 3.3.4A), indicating that the cell may upregulate protein levels of α Syn as a consequence of rDNA damage, similar to that seen with PI3KK inhibition and bleomycin treatment (Figures 3.3.2F, 3.3.3A). Interestingly, γ H2AX levels in the α Syn KO condition following induction of rDNA DSBs by I-Ppol were significantly increased compared to control or α Syn rescue cells (Figure 3.3.4A). A similar pattern was also seen using western blot analysis (Figure 3.3.4B). Although I-Ppol is used extensively to study rDNA damage, the recognition sequence for this endonuclease is found in a small number of genomic locations outside of rDNA. In order to further test the role of α Syn in rDNA DSB repair, we next used an alternative CRISPR/Cas9 system to induce DSBs at a site only found in rDNA using gRNAs targeting the 28S rDNA subunit (565, 569). Similar to our I-Ppol experiments, CRISPR/Cas9-treated cells exhibited a high proportion of nucleolar caps (visualized by staining for the nucleolar protein treacle) and increase in γ H2AX signal directly surrounding the caps compared to a non-targeting gRNA negative control treated cells (Figure 3.3.4C). Similarly, γ H2AX levels were increased in the α Syn KO condition, compared to control and α Syn rescue cells, again indicating that α Syn loss-of-function impairs rDNA DSB repair (Figure 3.3.4C). To further test the role of nucleolar α Syn recruitment to sites of rDNA DSBs, DI-PLA analysis after nucleolar rDNA DSB induction with I-Ppol showed a higher number of α Syn DI-PLA foci compared to control conditions

(Figure 3.3.4D, Figure 3.8.3C), indicating that α Syn is recruited to within ~ 40 nm of rDNA DSBs. We also utilized laser-induced DNA damage using multiphoton laser illumination to generate small, sub-nucleolar regions of DNA DSBs and then measured the immediate response of GFP-tagged human α Syn (α Syn-GFP). Focal illumination of small nucleolar subregions with a short pulse of high intensity laser light induced the rapid redistribution of α Syn-GFP to the site of damage (Figure 3.3.4E).

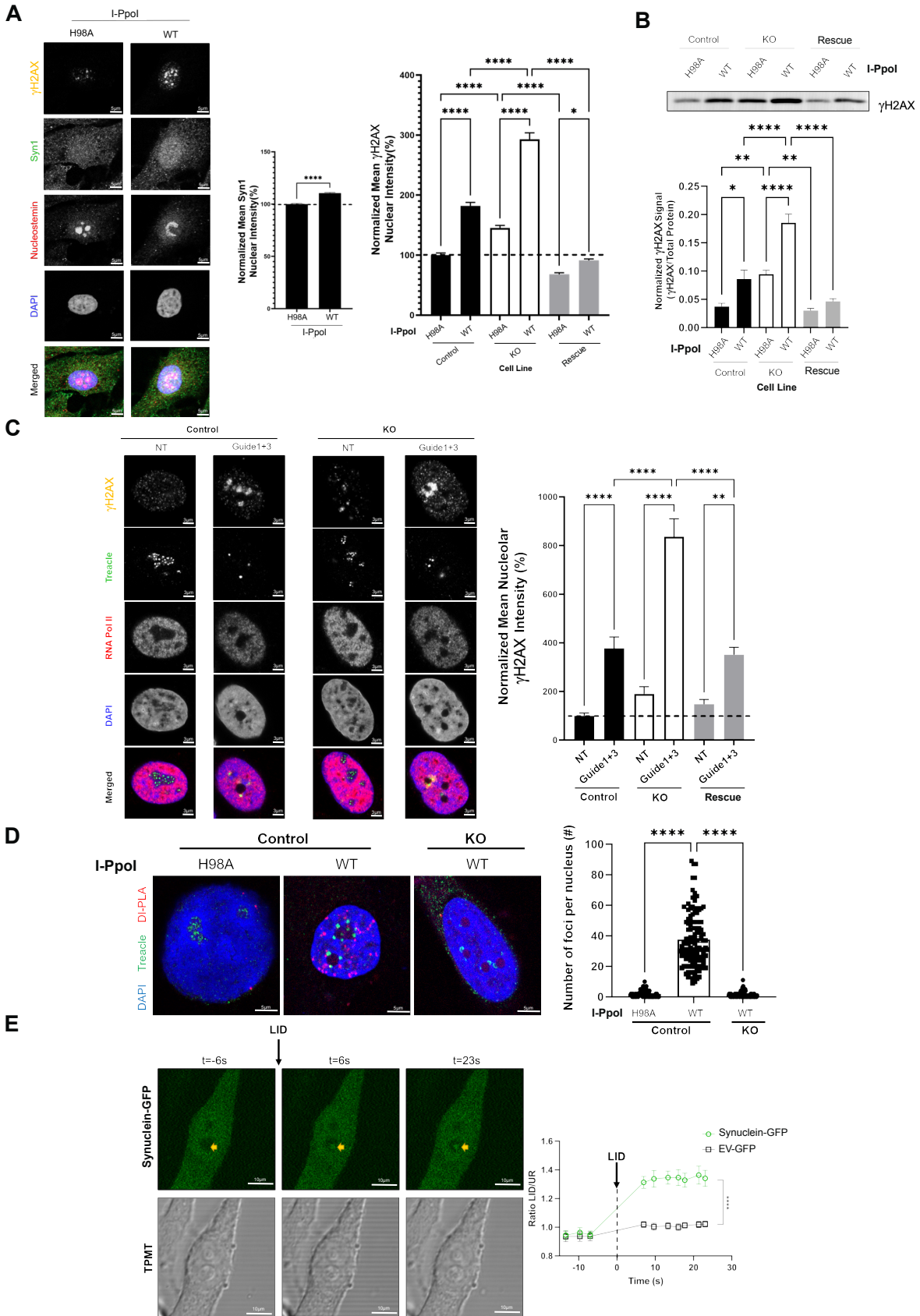


Figure 3.3.4. Inducing rDNA DSBs increases alpha-synuclein levels and localization to sites of damage and alpha-synuclein knockout significantly increases γ H2AX. A) SK-Mel28 cells were transfected with WT and H98A I-Ppol mRNA and stained for Syn1, γ H2AX, nucleostemin, and DAPI. Quantification from 3 biological replicates (total n=1867-2823 nuclei per condition). * $p < 0.05$, **** $p < 0.0001$ by ANOVA. Error bars denote SEM. B) SK-Mel28 cells were transfected with WT and H98A I-Ppol mRNA, cells were lysed and a nuclear fractionation was performed. Nuclear protein was run out on SDS-PAGE and probed for γ H2AX and total protein. Quantification from 4-6 biological replicates. * $p < 0.05$, ** $p < 0.01$, **** $p < 0.0001$ by ANOVA. Error bars denote SEM. C) SK-Mel28 cells were transfected with Cas9 and guide RNAs. Cells were stained for γ H2AX, treacle, RNA polymerase II, and DAPI. γ H2AX intensity was measured within a radius of treacle-identified nucleolar cap. Quantification from 3 biological replicates (total n=126 nucleoli per condition). ** $p < 0.01$, **** $p < 0.0001$ by ANOVA. Error bars denote SEM. D) SK-Mel28 cells were transfected with WT and H98A I-Ppol mRNA and the DNA Damage In Situ Ligation Followed by Proximity Ligation Assay (DI-PL) was completed. A treacle co-stain was included to identify nucleolar cap formation. Number of foci per nucleus was measured with DAPI masking. Each figure shows representative images and quantification from 3 biological replicates (total n=104-119 nuclei per condition). **** $p < 0.0001$ by ANOVA. Error bars denote SEM. E) SK-Mel28 control cells expressing Synuclein-GFP or Empty Vector-GFP (EV). Yellow arrows show targeting of laser-induced damage (LID) pulse in the nucleolus. Baseline (t=-6s) and after LID (t=6 and 23s) images show accumulation of Synuclein-GFP at DNA damage site. Data from graph shows calculated enrichment ratio at LID site (compared to an adjacent site in the nucleolus). Quantification from >20 cells over 2 biological replicates. **** $p < 0.0001$ by t-test. Error bars denote SEM. Quantification of Figure 3.3.4C performed by Kezia Catharina Oxe. Staining of Figure 3.3.4D performed by Gabe Cohn.

We next investigated which PI3KK family member/s are responsible for the increase in γ H2AX signal we detect in α Syn KO cells after I-Ppol induction of rDNA DSBs. This analysis revealed the largest decrease in γ H2AX intensity in cells treated with ATM inhibitor, and a less pronounced, but still substantial, decrease after ATR or DNA-PK inhibition (Figure 3.3.5A, Figure 3.8.5B). These results differ from baseline (Figure 3.3.2E), in that ATR inhibition no longer produced the largest γ H2AX signal reduction. This could be due to the prominence of replication stress-induced DSBs during baseline conditions that are repaired by ATR cascades, as opposed to a shift towards ATM cascades during I-Ppol-induced DSBs. These results indicate that the increase in γ H2AX

phosphorylation in control SK-Mel28 cells after I-Ppol treatment is driven primarily by ATM activity.

To understand the potential importance of α Syn in the kinetics of repair after I-Ppol-induced rDNA DSB formation, we measured the time course of γ H2AX changes. Using immunocytochemistry, we found a delay in recovery of γ H2AX levels after I-Ppol transfection in α Syn KO cells that lasts at least 24 hours compared to control or α Syn rescue cells (Figure 3.3.5B). Western blot analysis of γ H2AX at the 24-hour time point also confirmed a persistent elevation of γ H2AX in α Syn KO cells compared to either control group (Figure 3.3.5C). These data strongly suggest that α Syn is important in regulating the DDR in a way that facilitates DSB repair and that its loss-of-function leads to higher levels of DNA damage that melanoma cells are slower to repair.

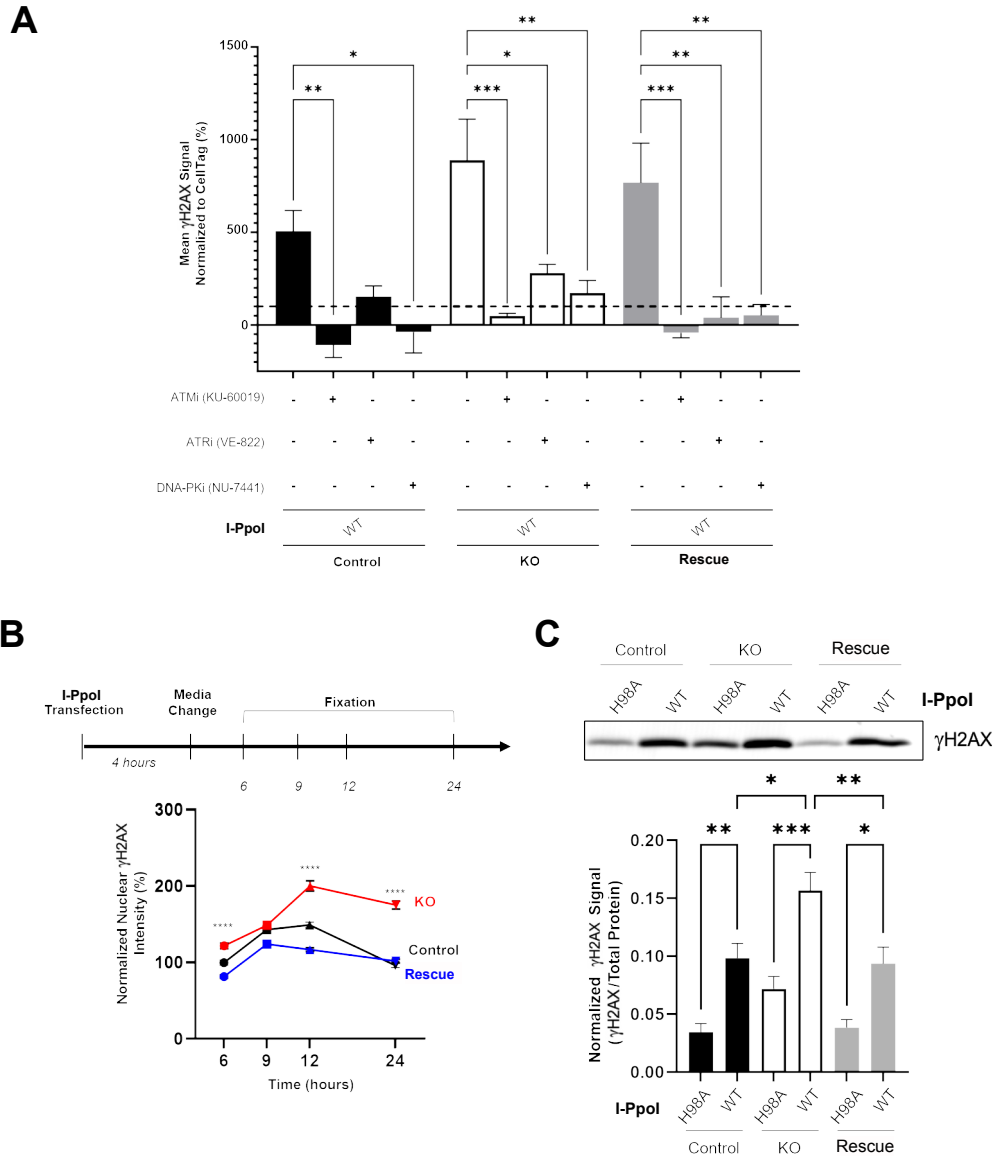


Figure 3.3.5. Alpha-synuclein knockout significantly impairs recovery of rDNA damage downstream of ATM signaling. A) SK-Mel28 cells were seeded in a black-welled PDL-coated 96 well plate and treated with DMSO, KU-60019 (10 μ M), VE-822 (0.1 μ M), or NU-7441 (1 μ M) for 24 hours. Cells were then treated with WT and H98A I-Ppol mRNA for 6 hours in the presence of the inhibitors. Cells were processed according to the In-Cell Western manufacturer instructions and stained for γ H2AX (800) and CellTag (700). Plates were imaged on the Licor CLx. * $p < 0.05$, ** $p < 0.01$, *** $p < 0.001$ by ANOVA. Error bars denote SEM. Quantification from 6 biological replicates (with 3 technical replicates per biological replicate). Normalization to control cells transfected with I-Ppol H98A and treated with DMSO. B) SK-Mel28 cells (control/KO/rescue) were seeded on PLL-coated coverslips and then transfected with WT and H98A I-Ppol mRNA. At the indicated time point post transfection, cells were fixed and stained for Syn1, γ H2AX, nucleostemin, and DAPI. Cells were imaged on the Zeiss 980 confocal microscope and

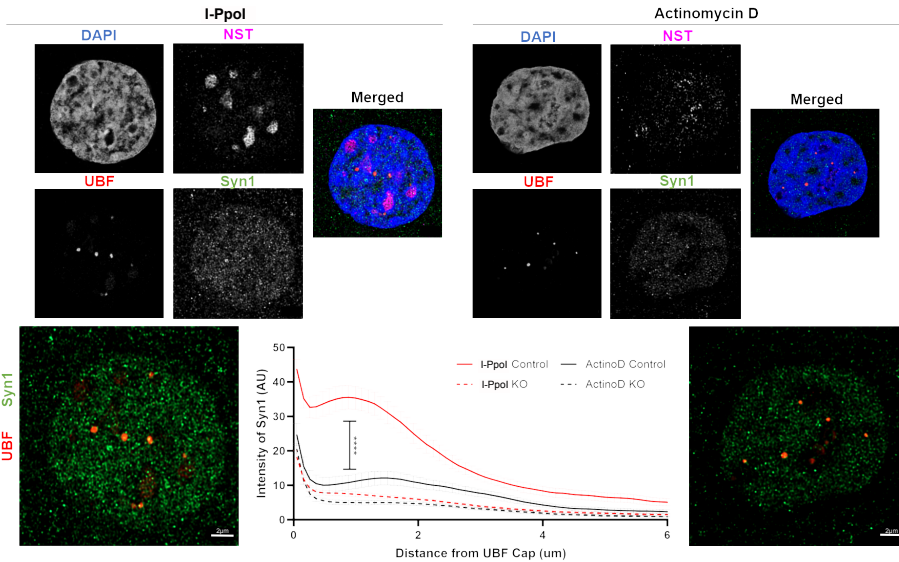
data was analyzed using FIJI. Quantification from 3 biological replicates (total n=1909-3194 nuclei per condition). Statistical labeling denotes significance between control and KO cell lines, ****p<0.0001 by ANOVA. C) SK-Mel28 cells (control/KO/rescue) were transfected with WT and H98A I-Ppol mRNA. After 24 hours, cells were lysed and a nuclear fractionation was performed. Nuclear protein was run out on SDS-PAGE and probed for γ H2AX and total protein. Quantification from 5 biological replicates. *p<0.05, **p<0.01, ***p<0.001, by ANOVA. Error bars denote SEM.

Alpha-Synuclein is Recruited near Nucleolar Caps and Regulates the Rate of DSB Repair

I-Ppol-treated SK-Mel28 cells were studied to understand the spatial distribution of α Syn after rDNA DSB induction and nucleolar cap formation. Discrete α Syn foci were found directly adjacent to the nucleolar cap (Figure 3.3.6A), similar to previous reports for 53BP1 and BRCA1 after rDNA DSB formation (569, 570, 625), with the most α Syn signal within 2 microns of the nucleolar cap. Actinomycin D-mediated RNA Pol I inhibition, which also induces nucleolar caps by a mechanism independent of DNA damage, did not show the same α Syn localization to the juxta-nucleolar cap region (Figure 3.3.6A). To better understand how α Syn regulates DSB repair and nucleolar cap kinetics, we next utilized longitudinal live-cell imaging techniques. GFP-tagged treacle-expressing control, α Syn KO, and α Syn rescue cells were transfected with I-Ppol mRNA to induce rDNA DSBs and nucleolar dynamics were visualized over a ~12-hour period (~5-18 hours after I-Ppol transfection). No significant differences in percentage of cells with nucleolar caps or the time to cap formation were detected (Figure 3.3.6B). Interestingly, however, the rate at which nucleolar caps reorganized back to normal nucleoli was slower in α Syn KO cells compared to control or α Syn rescue cells (Figure 3.3.6B). Similar to our γ H2AX time

course experiments (Figure 3.3.5A-B), this live-cell imaging data also strongly suggests that α Syn is important in regulating the rate at which DSBs in rDNA are repaired.

A



B

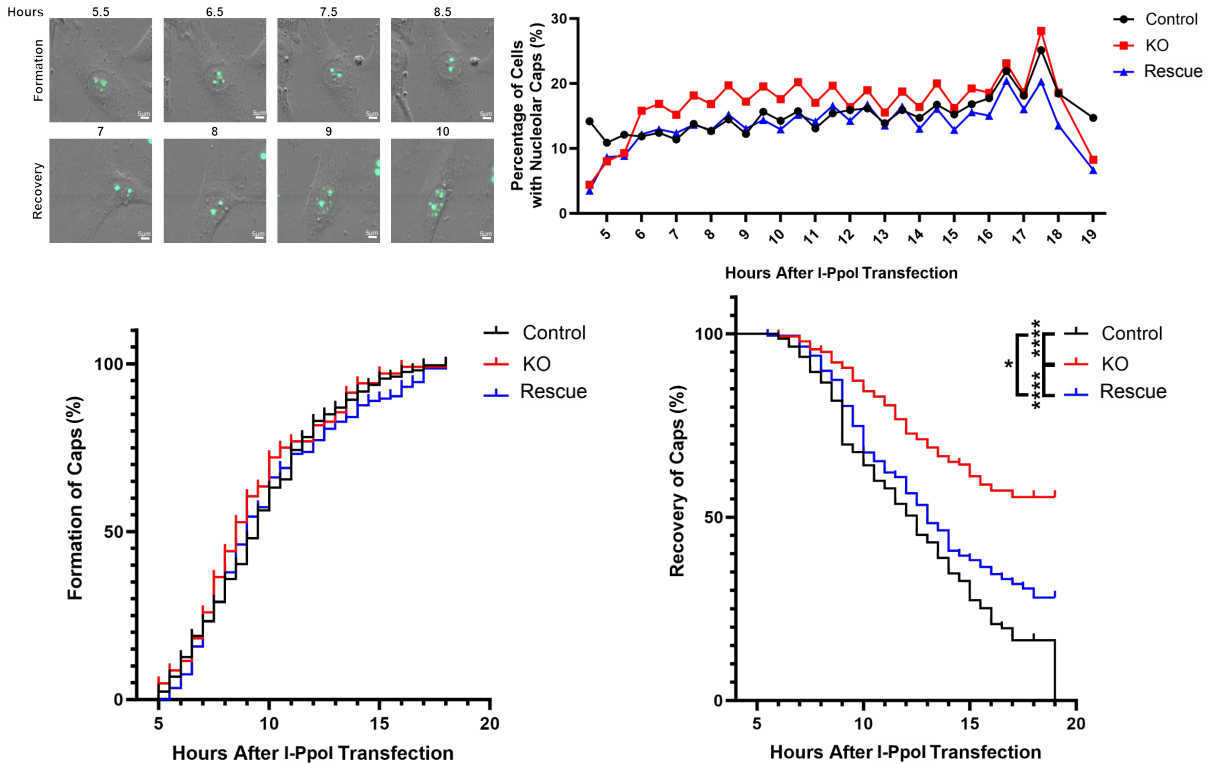


Figure 3.3.6. Alpha-synuclein localizes to DSB-induced nucleolar caps and is important for nucleolar cap recovery. A) SK-Mel28 cells were seeded on PLL-coated

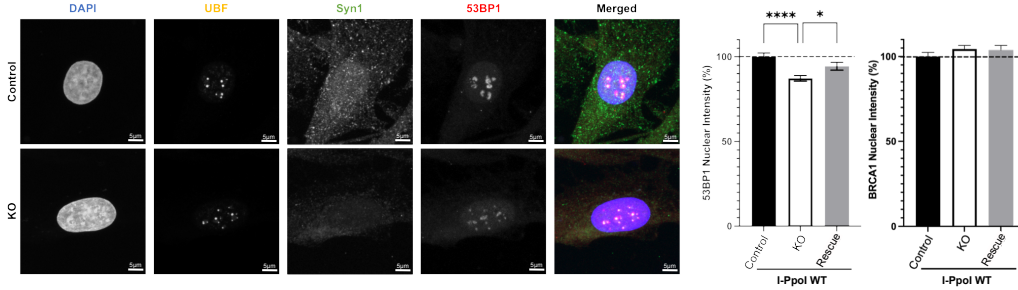
coverslips and then treated with WT I-Ppol mRNA for 6 hours or 100ng/ml Actinomycin D for 1 hour prior to fixation. Cells were stained for Syn1, nucleolar caps marker (UBF), nucleostemin, and DAPI. Cells were imaged on the Zeiss 980 confocal microscope with Airyscan oversampling and Joint Deconvolution and Channel Alignment post-processing. 3D renderings and distance from cap analysis were produced using Imaris software. Quantification from 5 biological replicates. Error bars denote SEM. Statistical significance was calculated via nonlinear regression (99% confidence interval). B) SK-Mel28 cells (control/KO/rescue) were seeded on PDL-coated 8-well Ibidi plates. Cells were transfected with 800ng GFP-Treacle using Lipofectamine 3000. Twenty-four hours post-transfection, cells were treated with WT I-Ppol mRNA. Four hours after treatment, live-cell imaging was performed using the Zeiss Celldiscoverer 7 and imaged for 15 hours. Quantification from 5 biological replicates (>200 cells analyzed per genotype per experiment). * $p < 0.05$, **** $p < 0.0001$ by two-way ANOVA or Mantel-Cox test. Data acquisition and formal analysis of Figure 3.3.6B performed by Somarr Elliott.

Alpha-Synuclein Knockout Impairs MDC1-Mediated 53BP1 Recruitment to Nucleolar Caps and Leads to Micronuclei Formation and Growth Dysregulation

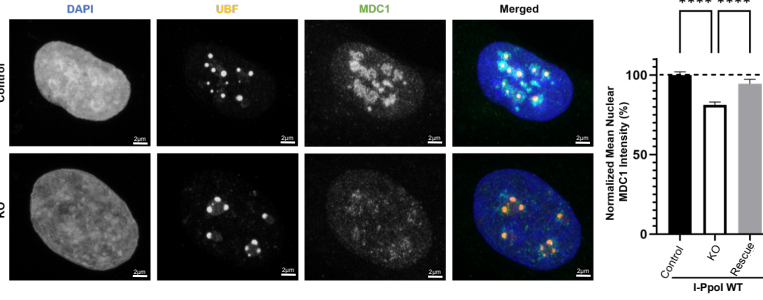
Given our data suggesting that γ H2AX levels are persistently elevated after DSB formation in the α Syn loss-of-function condition (Figures 3.3.3-5), we next tested whether this could be due to a deficiency in a step downstream of γ H2AX during DDR signaling. 53BP1 has been previously shown to be recruited near nucleolar caps after specific rDNA DSBs induction (569, 570, 625) and downstream of H2AX phosphorylation. 53BP1 is important for DSB repair pathway choice, generally promoting non-homologous end joining (NHEJ) and limiting homologous recombination (HR) (626). However, DSB repair in heterochromatin by HR also requires 53BP1, suggesting that the role of 53BP1 may vary dependent on the context (627). We found a decrease in 53BP1 near the nucleolar cap in α Syn KO cells compared to control or α Syn rescue cells after I-Ppol transfection (Figure 3.3.7A), suggesting that α Syn is important for 53BP1 recruitment to DSBs downstream of γ H2AX in nucleolar DDR signaling. In contrast, there was no significant difference in the recruitment of BRCA1 to the nucleolar cap in α Syn KO cells compared to control or α Syn rescue cells after I-Ppol transfection (Figure 3.3.7A, Figure 3.8.7).

Although several pathways have previously been implicated in 53BP1 recruitment, the best understood one involves MDC1 binding to γ H2AX followed by multiple histone modification events that ultimately lead to 53BP1 localization at DSBs. We found that α Syn-mediated 53BP1 recruitment involves this MDC1 signaling cascade. Specifically, there was a significant decrease in MDC1 recruitment to the nucleolar cap in α Syn KO cells compared to control or α Syn rescue cells after I-Ppol transfection (Figure 3.3.7B). We next tested for possible downstream cellular consequences of delayed DSB repair in α Syn KO cells. Importantly, previous work suggests that progressing through mitosis with damaged rDNA leads to abnormal nuclear morphology in cells, like micronuclei (565), and that 53BP1 dysregulation may influence micronuclei formation (628, 629). We measured an increase in the percentage of cells with micronuclei at baseline in the α Syn KO condition, that was also present 6- and 24-hours post rDNA DSB induction with I-Ppol (Figure 3.3.7C). We also measured proliferation, migration, and invasion to determine the contributions of α Syn function to these downstream cellular phenotypes, since previous studies have found dysregulation of various growth measurements in α Syn KO cells (478, 480), and dysregulated DDR is linked to cancer proliferation and metastatic phenotypes (630). SK-Mel28 α Syn KO cells also exhibited impaired proliferation, migration, and invasion capabilities compared to control and α Syn rescue cells (Figure 3.3.7D), suggesting that α Syn-mediated rDNA DSB repair is important for these forms of cell survival and growth. α Syn's role in metastasis will be discussed later in Appendix A.2.

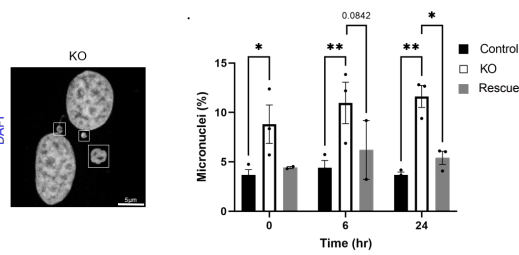
A



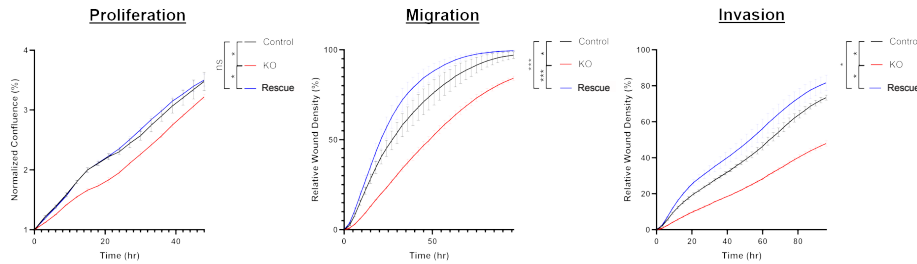
B



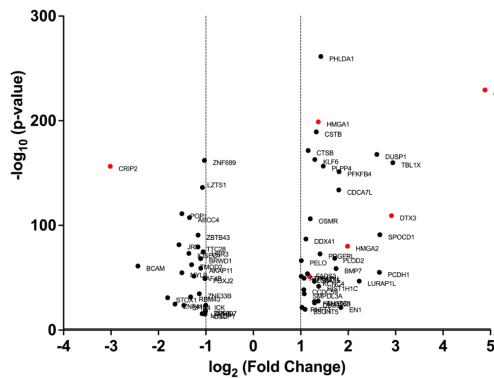
C



D



E



F

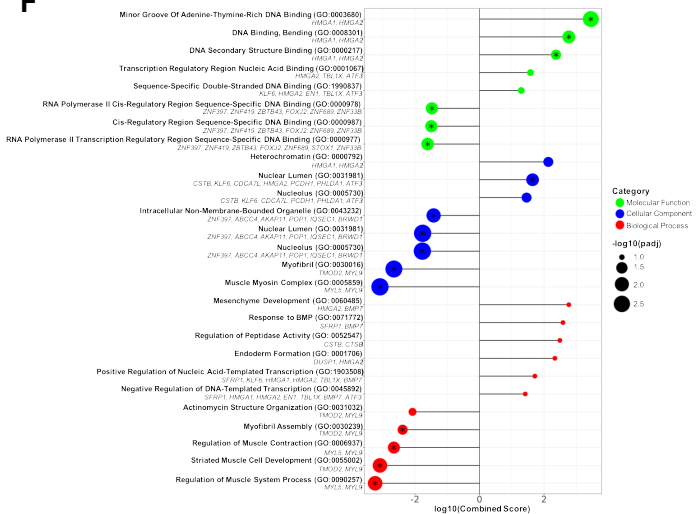


Figure 3.3.7. Alpha-synuclein knockout leads to reduced recruitment of MDC1 and 53BP1 to nucleolar caps and is associated with impaired cellular growth and dysregulated expression of transcripts associated with DNA repair pathways. A, B, C) SK-Mel28 cells were transfected with WT I-Ppol mRNA. 0-, 6-, or 24-hours post transfection, cells were stained for Syn1, UBF, 53BP1, and DAPI or Syn1, Treacle, BRCA1, and DAPI or UBF, MDC1 and DAPI. Data was analyzed using FIJI. Micronuclei were hand counted with the experimenter blinded to cell condition. Quantification from 3-4 biological replicates (total n=84-956 nuclei or cells per condition). * p<0.05, **p<0.01, ****p<0.0001 by ANOVA. Error bars denote SEM. D) SK-Mel28 cells were plated on Matrigel coated ImageLock plates. Graphs represent temporal progression of total confluence (proliferation), or wound closure using Relative Wound Density as the metric to measure migration or invasion. Data represents time-course of means of each cell line among 3 biological replicates (with 16 technical replicates per experiment). *95%CI, ***99%CI by nonlinear regression (migration) or simple linear regression (proliferation and invasion) analysis. E) Total RNA was extracted from SK-Mel28 control and KO cells and sent for RNA-sequencing (n=3 biological replicates per condition). Differentially expressed gene transcripts in KO cells compared to control were identified. These were cross-referenced to over 500 nucleolar-specific genes. 64 genes were identified and plotted on a volcano plot using p-value and fold change. All transcripts, greater than 1 standard deviation and less than -1 standard deviation are plotted. Red labeling indicates RT-PCR validated genes. F) All significant upregulated and downregulated transcripts underwent gene ontology analysis. Gene sets found to be significant after Benjamini-Hochberg multiple testing correction (P adj. < 0.05) are marked with an asterisk. Data acquisition of Figure 3.3.7E performed by Sahar Shekoohi. Figure assembly of Figure 3.3.7F performed by Dillon Brownell.

Transcriptomic Analysis Reveals Alpha-Synuclein Involvement in Nucleolar DNA Binding Regulation and Damage Repair Pathways

Previous work has shown that rDNA DSB induction leads to transcriptional silencing of rDNA via an ATM-dependent process important for nucleolar cap formation (563, 565, 568, 571, 625, 631), and other work has implicated α Syn in transcriptional regulation, both in the nucleolus (576, 577) and in the context of neurodegeneration (632). Therefore, we next tested for a potential role of α Syn in rDNA transcriptional silencing after DSB induction. Measurements of transcription using 5-EU (5-Ethynyl Uridine) incorporation in SK-Mel28 cells treated with gRNAs targeting rDNA or Actinomycin D (Act D) were compared between control, α Syn KO, and α Syn rescue backgrounds. Our results

suggest that α Syn plays no detectable role in the specific silencing of rDNA transcription that occurs after DSB induction, but that it may have effects on general rDNA transcription, since this was increased in the α Syn KO condition at baseline (Figure 3.8.8A, B).

In order to better understand these possible changes in baseline rDNA transcription in the α Syn KO cells and what cellular processes might be altered, whole-cell RNA extraction and bulk sequencing (RNAseq) analysis was performed in SK-Mel28 control and α Syn KO cells. Differentially expressed transcripts were identified and assigned p-values and false discovery rates (FDR) (633). A gene set was selected that included all immunofluorescence-validated nucleolar genes (543) and cross-referenced to our RNAseq differential gene expression list. 64 nucleolar-associated genes were identified to be significantly up- or down-regulated in the α Syn KO line compared to the control cells (Table 3.8.1). We identified 37 upregulated (\log_2 -fold change 2.01 to 29.53) and 27 downregulated (\log_2 -fold change -2.00 to -8.07, Figure 3.3.7D) nucleolar-associated gene transcripts. Six of the transcripts exhibiting the largest changes were validated by qRT-PCR and all showed changes in the expected direction (Figure 3.3.7E, Table 3.8.2), with *ATF3*, *DTX3*, and *HMGGA2* significantly upregulated and *CRIP2* downregulated (Figure 3.8.8C). *ATF3* (Activating Transcription Factor 3), which showed the largest upregulation in α Syn KO cells both by RNAseq and qRT-PCR, has been previously implicated in cellular responses to a variety of stresses (634) and to be important for regulating DSB repair (635, 636). Further gene ontology analysis revealed upregulated transcripts associated with DNA binding (*HMGGA1*, *HMGGA2*) and transcription (*SFRP1*, *HMGGA1*, *HMGGA2*, *EN1*, *TBL1X*, *BMP7*, *ATF3*) and downregulated gene

populations associated with RNA polymerase DNA binding (*ZNF397*, *ZNF419*, *FOXJ2*, *ZBTB43*, *ZNF689*, *ZNF33B*, *STOX1*) (Figure 3.3.7F).

3.4 Discussion

In this study, we have expanded our knowledge of the nuclear functions of the neurodegeneration and cancer-associated protein, α Syn, by showing its particular importance in facilitating nucleolar DDR pathways in melanoma. Our data suggest that α Syn is preferentially enriched within the nucleolar granular component, where it colocalized with the marker of DSB repair γ H2AX. α Syn loss-of-function by genetic deletion increased γ H2AX levels in the nucleolus via an ATR- and ATM-dependent pathway. Pan-nuclear DNA damage induction via bleomycin treatment increased global nuclear α Syn, while α Syn KO exacerbated the increase in γ H2AX throughout the nucleolus and nucleoplasm. Selective rDNA DSB induction within the nucleolus via I-Ppol- or CRISPR/Cas9-based approaches both increased nuclear α Syn and γ H2AX, and in α Syn KO cells this γ H2AX increase was even greater and mediated in large part by ATM. Our DI-PLA analysis showed that α Syn is present within close proximity (~40nm) of these rDNA DSB ends and to γ H2AX. Kinetic studies of the γ H2AX response after selective rDNA DSB induction also revealed a significant delay in γ H2AX resolution in α Syn KO cells, which was also associated with impaired resolution of nucleolar caps. α Syn KO led to a reduction in important DDR effectors downstream of γ H2AX, including MDC1 and 53BP1 recruitment to the nucleolar caps, after inducing rDNA DSBs, while leaving BRCA1 recruitment unaffected. These abnormalities in nucleolar DSB repair were

associated with multiple downstream cellular effects, including increased micronuclei formation, impaired proliferation, migration, and invasion. Lastly, transcriptomic analysis of α Syn KO cells reinforced our finding that α Syn loss-of-function leads to dysregulated DSB repair. Altogether, these findings illuminate a role for α Syn in the nucleolar DDR. It acts directly downstream of ATM-mediated H2AX phosphorylation to help facilitate MDC1 recruitment and α Syn loss-of-function leads to delayed DSB repair with specific cellular consequences.

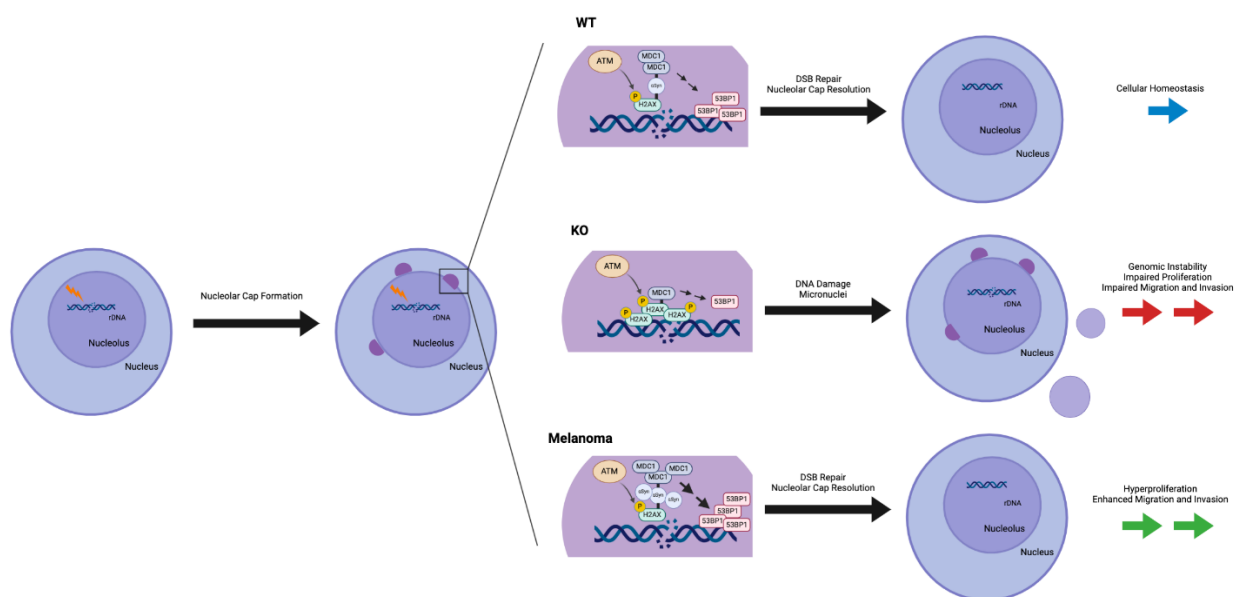


Figure 3.4.1. Potential molecular mechanism by which α Syn facilitates nucleolar DDR and the downstream cellular consequences.

Our findings strongly suggest that α Syn acts downstream of H2AX phosphorylation to enable proper MDC1 recruitment to DSBs and that this has subsequent effects on downstream events in the DDR pathway. Previous work has shown that ATM phosphorylation leads to the creation of the γ H2AX histone mark and MDC1 directly binds to this γ H2AX (637-640). MDC1 binding then continues the cascade that involves H2AX K13-K15 ubiquitination by the RING-type E3 ubiquitin ligases RNF8 and RNF168 (641-

644), and histone H4 K20 methylation (645, 646), ultimately leading to 53BP1 recruitment to DSBs. Our data demonstrate an increase in γ H2AX, but a decrease in MDC1 and 53BP1, after inducing DSBs selectively in rDNA in an α Syn KO environment. BRCA1 recruitment appears to be unaffected. This pattern strongly suggests that α Syn is directly involved in the recruitment and/or stabilization of MDC1 bound to γ H2AX. Previous work showing that MDC1 directly binds γ H2AX (638-640) and our PLA data showing close proximity between α Syn and γ H2AX leads us to propose a model where α Syn may physically interact with both components to facilitate this γ H2AX-MDC1 interaction (Figure 3.4.1). Recent work shows that both α Syn and MDC1 are intrinsically disordered proteins that can undergo liquid-liquid phase separation (LLPS) under specific conditions (647-651), so it will be interesting in future work to test if α Syn's ability to undergo LLPS may be important in facilitating MDC1's interaction with γ H2AX. Other molecular mechanisms by which α Syn could promote 53BP1 recruitment may also be important. Protein methylation is another post-translation modification important for 53BP1 recruitment during the DDR and very recent work identified PRMT5 (Protein Arginine Methyltransferase 5) as an α Syn interactor through proteomic analysis (652). PRMT5 can directly methylate 53BP1 in its GAR domain to facilitate docking of 53BP1 to DSB sites (653, 654). It will be important to test in future studies whether α Syn regulates the histone post-translational modification cascade mediated by RNF8/168, PRMT5 mediated 53BP1 methylation, and/or other pathways to directly facilitate 53BP1 binding to DSBs, in addition to its effects on γ H2AX-MDC1 binding. Interestingly, expression of the PD-associated A53T α Syn point mutation has recently been shown to cause delayed repair and abnormal RNF8 retention at DSB repair foci after ionizing radiation treatment

(499), which is similar to our results with α Syn KO cells which show persistently elevated γ H2AX levels after selective rDNA DSB induction.

Our RNA-seq analysis identified 64 nucleolar-associated transcripts that were up or down regulated in α Syn KO cells, many of which have direct links to the DDR. Gene ontology analysis also showed enrichment of DNA binding and transcriptional regulation pathways (Figure 3.3.7E). ATF3, which had the largest change of any identified transcript (~30-fold increase in α Syn KO cells) is particularly interesting, since it is activated upon DNA damage in a p53-dependent manner and its overexpression moderately suppresses cell growth (655-657) and it facilitates DSB repair (635, 636). HMGA1 and HMGA2 are small non-histone proteins that can bind to DNA and modify chromatin state and were also upregulated in our dataset 2.5- and 4-fold, respectively. Both have been implicated in the DDR and are direct ATM/ATR kinase targets (658-661). HMGA2 is associated with suppression of NHEJ via hyperphosphorylation of DNA-PKcs (662), and interestingly, our data suggests α Syn KO reduces both MDC1 and 53BP1 recruitment. These RNA-seq data are consistent with the concept that α Syn is important in melanoma cells for determining the mechanism of DSB repair, which will also be important to test further in future studies (discussed in Chapter 5.2).

Our data also fits into a larger landscape of links between the nucleolus, genomic instability, and cancer. Due to their highly proliferative nature, cancers are vulnerable to replicative exhaustion and subsequent genome instability. The nucleolus is especially prone to this due to its extremely high levels of transcriptional activity of repetitive rDNA sequences. Estimates suggest that up to 60% of all transcription within a normal mammalian cell occurs at rDNA(557), and faithful ribosome biogenesis is even more

important in malignant cells to sustain their increased levels of cell division and growth (558, 559). In melanoma specifically, substantial evidence suggests that there is upregulation of DSB repair pathways to promote increased DSB repair capacity critical for survival (523, 524). Evidence for this includes melanoma's relative resistance to ionizing radiation (525, 526) and that DSB repair inhibitors are particularly effective in many treatment models (527, 528). For example, melanoma has been shown to upregulate NHEJ protein, DNA-PK (663), which has been an effective drug target in cancer therapeutics using small molecule inhibitors (527). Another study, using DNA strand break bait (Dbait) molecules, which mimic DSBs and trap DNA repair proteins, thereby inhibiting DNA DSB repair, have been shown to be effective in pre-clinical trial models of melanoma (528) and a phase I clinical trial study is currently ongoing. Our findings that α Syn modulates nucleolar DSB repair and its loss-of-function negatively impacts cellular growth suggest that upregulation of α Syn levels in melanoma may also be part of a similar mechanism to improve DSB repair, allowing these cells to evade the programmed cell death and senescence pathways that would normally be triggered by high DSB levels. In contrast to what is seen in neurons, the high overexpression of α Syn by melanoma cells does not lead to frank aggregation or the formation of detectible Lewy pathology within these cancer cells. The reasons for this are unclear, but could involve melanoma-specific factors that act to limit this protein's aggregation and allow it to remain soluble, even when it is at high concentration within the cell. Alternatively, if melanoma cells were to form Lewy pathology and then die quickly, they would also be hard to detect in a melanoma sample at any one given point in time. It will be interesting to explore in future work which of these or other mechanisms might be operative, especially since

specific anti-aggregation factors expressed by melanoma cells could reveal strategies to limit aggregation and keep α Syn soluble in a neurodegenerative disease context.

It is well-established that PD patients and their first-degree relatives are at increased risk of melanoma, and symmetrically that melanoma patients are at increased risk of PD (2, 5-23). Our previous work suggests that genetic or environmental factors that cause increased α Syn expression within certain individuals would predispose their post-mitotic neurons to accumulate cytoplasmic Lewy pathology and this, counterintuitively, triggers a loss of soluble, functional α Syn from the nucleus. This could lead to deficient DSB repair that contributes to programmed cell death (427, 442). Our current data suggest these same individuals could also be predisposed to develop melanoma via a gain-of-function mechanism where increased α Syn levels improve DSB repair capacity within the nucleolus, which limits the senescence and programmed cell death pathways that are triggered by excessive DSBs associated with oncogenesis. This provides a framework for understanding the link between PD and melanoma and offers potential therapeutic targets in melanoma that are focused on reducing α Syn-mediated nucleolar DSB repair.

3.5 Methods

Cell lines

The SK-Mel28 cell line were produced by Dr. Stephan Witt (Louisiana State University), after being purchased from ATCC and authenticated at the University of Arizona Genetics Core via their STR Profiling Cell Authentication service. Per Shekoohi

et al. 2021, α Syn knockout cells were created through CRISPR/Cas9 genome editing targeting *SNCA* (478). In addition, re-expression of α Syn in the *SNCA* KO clone was established using lentivirus transduction of human α Syn under the CMV promoter. All SK-Mel28, A375, and PIG1 cell lines were cultured in appropriate medium suggested by ATCC. Primary melanocytes were isolated from male patient foreskin samples provided by Oregon Health and Science University. Isolation protocol followed the steps outlined in (664). All cells were maintained in a humidified chamber with constant supply of 5% CO₂ and 95% O₂ at 37C.

Patient biopsy and immunohistochemistry and immunofluorescence staining

For immunohistochemistry staining (Figure 3.3.1A), IRB 1623 (Brain Bank, deceased anonymized subjects) and IRB 3493 (Pathology Department, postdiagnostic tissue) of Oregon Health and Science University gave ethical approval for this work. Human pathological analysis was done using standard hematoxylin methods. Standard IHC methods were used to evaluate alpha-synuclein. In brief, formalin-fixed, paraffin-embedded sections of primary cutaneous or metastatic brain melanoma were incubated with antibody LB509 (1:3000; Thermo Scientific), developed with diaminobenzidine chromagen, and counterstained with hematoxylin, as previously described (665).

For immunofluorescence staining (Figure 3.3.1B), eIRB STUDY00024716 of Oregon Health and Science University gave ethical approval for this work. Archival samples were formalin-fixed, paraffin-embedded (FFPE) and 7 micron sections were cut onto slides. Tissue sections were deparaffinized and an antigen retrieval was performed overnight at 56C (10 mM Tris base, 1 mM EDTA solution, 0.05% Tween 20, pH 9.0).

Samples were washed in 1X PBS, permeabilized in 0.25% Triton X-100 in PBS for 10 minutes, and blocked for 2 hours at room temperature (RT) (2% FBS, 1% BSA in PBS). Primary antibody incubation occurred overnight at 4C in blocking buffer. The next day, tissue samples were washed in 1X PBS and incubated with secondary antibody at 37C for 1 hour in blocking buffer. After additional 1X PBS washes, samples were stained with DAPI and mounted using CFM2 antifade reagent and sealed with BioGrip. All immunofluorescence images were taken on a Zeiss Laser-Scanning Confocal Microscope 980 with Airyscan.

Immunocytochemistry staining

SK-Mel28 cells were seeded onto poly-l-lysine treated glass coverslips and treated as indicated in the figure legends. Cells were then washed with 1x PBS and fixed using 4% paraformaldehyde for 15 minutes. After one wash in 1x PBS, cells were permeabilized in 0.25% Triton X-100 in PBS for 5 minutes. Coverslips were blocked in 10% goat serum/0.1% Triton X-100 in PBS for 30 minutes and then placed in the primary antibody overnight at RT. The next morning, cells were washed three times in 1x PBS and placed in secondary antibody overnight at RT. The following day, coverslips were washed 4 times in 1x PBS. The third wash contained DAPI (2.5µg/ml) for 20min. Coverslips were mounted using CFM2 antifade reagent and sealed with BioGrip. All immunofluorescence images were taken on a Zeiss Laser-Scanning Confocal Microscope 980 with Airyscan and analyzed with FIJI (2D analysis using custom made macro available on GitHub) or Imaris (3D analysis). Mean intensity was measured after imposing DAPI, RNA Polymerase II, or Nucleostemin masks over each cell. All cells within a 63x image were analyzed and

numbers of n are provided in each figure legend. Statistical significance was assigned using one-way ANOVA with multiple comparisons.

Colocalization analysis was performed using Imaris 3D colocalization function following masking of either DAPI or NST. Thresholds were set using the automatic threshold function and Pearson's coefficients were calculated. To produce the randomization scramble for statistical significance testing, the Syn1 channel (Alexa Fluor 488) was moved 20 voxels in the x and y planes prior to Pearson's coefficient reanalysis.

Ultra-resolution imaging samples were processed as described above and imaged on Zeiss Laser-Scanning Confocal Microscope 980 with Airyscan oversampling parameters. These images underwent Airyscan Joint Deconvolution and Channel Alignment post-processing steps, prior to Imaris 3D analysis.

Antibody specifics were as follows: LB509 (Abcam #27766, RRID:AB_727020, 1:500), RPA32 (Bethyl #A300-245A, RRID:AB_210547, 1:1000), Syn1 (BD Biosciences #610786, RRID:AB_398107, 1:500), Nucleophosmin (Abcam #52644, RRID:AB_881735, 1:100), Nucleostemin (Santa Cruz #166430, RRID:AB_2110097, 1:500), Treacle (Millipore Sigma #HPA038237, RRID:AB_10670660, 1:200), Fibrillarin (Abcam #5821, RRID:AB_2105785, 1:100), RPA194 (Santa Cruz #48385, RRID:AB_675814, 1:200), γ H2AX (Cell Signaling #9718, RRID:AB_2118009, 1:500), Treacle (Sigma-Aldrich #GW22821, RRID:AB_1857861, 1:10,000), RNA Pol II (Santa Cruz #47701, RRID:AB_677353, 1: 500), UBF (Millipore Sigma #HPA006385, RRID:AB_1080447, 1:10,000), 53BP1 (BD Biosciences #612522, RRID:AB_2206766, 1:1000), BRCA1 (Sigma-Aldrich #07-434, 1:1000), MDC1 (Sigma-Aldrich #05-1572, 1:500).

DNA Damage In Situ Ligation followed Proximity Ligation Assay (DI-PLA)

This protocol is adapted from Galbiati et al (624). SK-Mel28 cells were grown on 13mm poly-d-lysine treated coverslips and fixed in 4% PFA for 15 minutes at RT followed by two washes with 1x PBS.

DI-PLA: Blunting

Coverslips were washed twice for 5 minutes with NEB2 buffer (50mM NaCl, 10mM Tris-HCl pH 8, 10mM MgCl₂, 1mM DTT, 0.1% Triton X-100) and twice for 5 minutes with Blunting buffer (50mM NaCl, 10mM Tris-HCl pH 7.5, 10mM MgCl₂, 5mM DTT, 0.025% Triton X-100). Coverslips were then inverted onto a 35µL drop on parafilm of NEB Blunting Reaction (NEB, E1201): (1mM dNTPs, 1X Blunting Buffer, 0.2mg/mL BSA, 1X Blunting Enzyme). Coverslips were incubated in a dark humidity chamber for 1 hour at RT.

DI-PLA: Ligation

Coverslips were washed twice for 5 minutes with NEB2 buffer (50mM NaCl, 10mM Tris-HCl pH 8, 10mM MgCl₂, 1mM DTT, 0.1% Triton X-100), then twice for 5 minutes with ligation buffer (50mM Tris-HCl pH 7.5, 10mM MgCl₂, 10mM DTT, 1mM ATP). Coverslips were then inverted onto a 50µL drop on parafilm of Ligation Reaction (0.1µM DI-PLA Linker, 1X T4 Ligation Buffer (NEB, B0202), 1mM ATP, 0.2 mg/mL BSA, 1X T4 Ligase (NEB, M0202)) overnight at 4°C in dark humidity chamber followed by proximity ligation assay between biotin and protein of interest.

DI-PLA Linker: 5'-TACTACCTCGAGAGTTACGCTAGGGATAACAGGGTAATATAGTTT [BtdT] TTTCTATATTACCCTGTTATCCCTAGCGTAACTCTCGAGGTAGTA -3'.

Proximity Ligation Assay

Proximity Ligation Assay was performed without deviation from manufacturer's instructions (DUO92008). Coverslips were washed in a 0.5mL volume and reactions were performed by inverting the coverslip onto a 35 μ L drop on parafilm. Following the proximity ligation reaction, cells were stained with DAPI (0.2 μ g/mL) for 3 minutes followed by one wash in PBS and one water wash. The cells were then inverted and mounted on glass coverslips with 15 μ L of prolong gold mounting media (LifeTech, P36934) & were cured overnight in the dark at RT.

All immunofluorescence images were taken on a Zeiss Laser-Scanning Confocal Microscope 980 and analyzed with CellProfiler. All cells within a 63x image was analyzed (~30cells/condition/biological replicate). Statistical significance was assigned using t-test or one-way ANOVA with multiple comparisons.

Transmission electron microscopy

SK-Mel28 control and KO cell pellets were fixed with 0.1M sodium cacodylate buffer (pH 7.2) containing 0.05% glutaraldehyde, 4% paraformaldehyde, and 0.1% picric acid for 2 hours at RT. The pellet was then processed for immuno-gold electron microscopy, using a microwave tissue processor (Pelco Biowave, Ted Pella, Inc, Redding, CA) as previously reported (666). The pellet was gently removed from the tube and transferred to specimen dishes (Ted Pella, Inc). Briefly, the pellet was exposed to 1% osmium tetroxide/1.5% potassium ferricyanide in the Biowave, washed in water, then followed by 0.5% aqueous uranyl acetate, dehydrated in alcohol/propylene oxide, and embedded in Epon/Spurr resin. The pellet was thin sectioned (60 nm) on an

ultramicrotome (Leica EM UC7, Buffalo Grove, IL), using a diamond knife (Diatome, Hatfield, PA). The sections were placed on 75 mesh grids, then incubated overnight using an antibody against alpha-synuclein (abcam, Boston, MA, #AB138501, RRID:AB_2537217, rabbit polyclonal, 1:75) in TBST (tris buffered saline triton, pH 7.6) blocking solution (0.05% normal goat serum). The sections were then incubated in a secondary antibody (goat anti-rabbit, 1:50, in TBST 8.2, Jackson ImmunoResearch, West Grove, PA) tagged with a 12 nm gold particle for 90 minutes at RT. The sections were then viewed on a JEOL electron microscope (1400 TEM, JEOL, Peabody, MA). Photographs (digital camera, AMT, Danvers, MA) were taken of immuno-gold labeling of the nucleolus. The density of gold labeling was quantified as $\#/\mu\text{m}^2$ of nucleolar area.

Western blot analysis

SK-Mel28 cells were seeded on 10cm plates to be ~80% confluent the day of treatment. Cells were treated with bleomycin (100 $\mu\text{g}/\text{ml}$) for 1hour or I-Ppol WT or H98A mRNA (7 μg) as detailed below. After treatment, media was removed and cells were washed 1x with ice cold PBS. Cells were harvested by trypsinization, collected into 15ml conical tubes, and pelleted for 5min 200rc. Liquid was aspirated, pellets were resuspended in 2ml PBS and transferred to 2ml microcentrifuge tubes. Proteins were extracted into cytosolic and nuclear fraction using the NE-PER extraction kit (Thermo-Fisher, cat 78833) according to the manufacturer's recommendations with the addition of a brief sonication (10 seconds, 10 kHz) after the first nuclear resuspension step. Protein preps were stored at -80C until Western blot analysis. 10-30 μg protein was run on a 10-20% Tris-Glycine 1.0 mm gradient gel (Invitrogen) and transferred onto an immobilon-FL

PVDF membrane (Millipore) at 30V for 2 hours on ice in 0.5% TBE using the Novex XCell II Blotting System (Invitrogen). If completing Syn1 staining, membranes are fixed in 4% paraformaldehyde/0.01% glutaraldehyde in PBS for 10 minutes at RT. Membranes were blocked overnight in Odyssey PBS Blocking Buffer (Li-Cor) and stained for 2 hours at RT with Syn1 (BD Biosciences #610786, RRID:AB_398107, 1:1,000;), γ H2AX (Cell Signaling #9718, RRID:AB_2118009, 1:1,000), or H2AX (Santa Cruz #sc-517336, 1:500) and 1 hour at RT with IRDye 680CW Goat anti-mouse (1:10,000; Li-Cor) or IRDye 800CW Goat anti-rabbit (1:5,000; Li-Cor). All staining was normalized to total protein (Revert 700 Total Protein Stain, Licor). Images were acquired using Li-Cor Odyssey CLx Imaging System.

In-cell western

SK-Mel28 cells were seeded on poly-d-lysine treated 96-well plates to be ~80% confluent the day of treatment. Cells were treated as indicated in the figure legends. After treatment, media was removed and cells were fixed using 4% paraformaldehyde for 15 minutes. After one wash in 1x PBS, cells were permeabilized in 0.25% Triton X-100 in PBS for 5 minutes and blocked in 10% goat serum/0.1% Triton X-100 in PBS for 30 minutes and then placed in the primary antibody overnight at RT (γ H2AX, Cell Signaling #9718, RRID:AB_2118009, 1:500). The next morning, cells were washed three times in 1x PBS and placed in secondary antibody at RT for 2 hours (IRDye 800CW Goat Anti-Rabbit, Licor, 1:800). Cells were then washed 2 times in 1x PBS and then stained with CellTag (CellTag 700, Licor, 1:500) for 1 hour at RT. After a final wash in 1x PBS, the 96-well plate was dried and images were acquired using Li-Cor Odyssey CLx Imaging System.

Ionizing radiation

Ionizing radiation was delivered by an x-ray generator (Rad Source RS-2000 X-ray Irradiator; 160 kV; 25mA; 2.0 Gy/min dose rate). Cells were treated with a total of 5 Gy of irradiation, followed by a 20-minute recovery period. Following the recovery period, cells were fixed and processed for immunocytochemistry as described above.

I-Ppol mRNA production and transfection

I-Ppol WT and H98A plasmids were generously gifted from Dr. Brian McStay (NUI Galway) and previously characterized (569). Plasmids were linearized at a NotI site positioned in the polylinker downstream from the I-Ppol ORF and transcribed using MEGAscript T7 kit (Invitrogen) according to the manufacturer's instructions. I-Ppol mRNA was subsequently polyadenylated using a Poly(A) tailing kit (Invitrogen) according to the manufacturer's instructions and then precipitated using lithium chloride. SK-Mel28 cells were seeded on poly-L-lysine treated glass coverslips at least 36 hours prior to transfection with the *in vitro* transcribed mRNA using the TransMessenger transfection reagent (Qiagen). One microgram of I-Ppol mRNA and 2 μ l of Enhancer R were diluted in buffer EC-R to a final volume of 100 μ l and incubated for 5 minutes at RT. Two microliters of TransMessenger transfection reagent was added and further incubated for 10min at RT. After addition of 900 μ l of serum-free medium, the transfection cocktail was added to cells. Following 4 h of incubation, the transfection medium was replaced by full medium, and cells were grown for an additional 2 hours or 24 hours prior to further processing.

RNP transfection

SK-Mel28 cells were grown on coverslips and transiently transfected with ribonucleoprotein complexes consisting of purified recombinant Cas9 protein (Truecut Cas9 Protein v2, Invitrogen, #36499) and synthetic guide RNAs (Invitrogen TrueGuide Synthetic sgRNA #35514 or Negative Control, non-targeting 1 #A35526) using Lipofectamine CRISPRMAX Cas9 Transfection Reagent (Invitrogen) according to the manufacturer's specifications unless otherwise stated. Cells were collected 24 hours post-transfection. The gRNA oligos targeted sequences in the 28S rDNA sequence or a human non-targeting control (Invitrogen, #CMAX00015). Unless otherwise stated, the two rDNA gRNA oligos were pooled in a ratio of 1:1 for each transfection. rDNA guide 1: CGAGAGAACAGCAGGCCCGC; rDNA guide 3: GATTTCCAGGGACGGCGCCT. Cells were collected 24 hours post-transfection. When applicable, Actinomycin D (Act D) was used as a positive control with cells treated at a final concentration of 100ng/ml for 1 hour.

Laser-induced damage

SK-Mel28 control cells were seeded onto poly-l-lysine treated live-cell imaging glass-bottom 4-well plates at 60,000 cells per well. Cells were then transfected with 800ng Synuclein-GFP or Empty Vector-GFP using Lipofectamine 3000 transfection reagent. Twenty-four hours post-transfection, cells underwent laser-induced damage (LID) using a Zeiss 880 LSM multiphoton microscope outfitted with dual channel BiG (binary GaAsP) detectors and a Coherent Technologies Chameleon titanium-sapphire femtosecond pulsed laser source (for imaging Synuclein-GFP). The Bleaching function in Zen was used to illuminate small, submicron-sized regions within the nucleolus with Chameleon laser

tuned to ~730 nm for 65 or 130 μ s. There is a ~4 second time delay required to switch the laser to and from the LID (~730nm) wavelength. Transmitted light was used to localize the LID pulse to the nucleolus. LID images were analyzed with ImageJ where regions of interest (ROIs) were selected to obtain mean fluorescence values in LID and control ROIs within the nucleolus. The ratio of the signal at each time point from the LID versus the control ROIs was used to calculate the Enrichment Ratio.

Live-cell nucleolar cap imaging

SK-Mel28 cells were seeded onto poly-l-lysine treated live-cell imaging glass-bottom 4-well plates at 60,000 cells per well. Cells were then transfected with 800ng GFP-Treacle (pcDNA 4TO-Strep-HA-AcGFP-Treacle) using Lipofectamine 3000 transfection reagent. Twenty-four hours post-transfection, cells were transfected with 1 μ g l-Ppol WT mRNA in serum free media. Four hours after transfected, cells were washed and media was replaced with DMEM Fluorobrite + 10% FBS. Live cell imaging was performed using the Zeiss Celldiscoverer 7 equipped with a 40x oil objective at 37C with 5% CO₂. Cells were imaged every hour over 15 hours as z-stacks. Images were processed in FIJI and nucleolar caps were hand-counted by investigators blinded to condition.

IncuCyte proliferation, migration, and invasion assay

SK-Mel28 cells were seeded onto Matrigel treated (80 μ g/ml) 96-well plates (IncuCyte ImageLock) at 6,000 cells per well. Five hours after seeding, the cells were placed in the IncuCyte for 48 hours for proliferation analysis. At 48 hours, cells were taken out of the IncuCyte and placed in a standard incubator for 72 additional hours to obtain

100% confluence. After 120 hours post-seeding, the confluent cell layer was scratched with an IncuCyte 96-pin wound making tool. An additional 50 μ l of media (migration) or 50 μ l of 0.3mg/ml Matrigel (invasion) was added to the wells with scratches. The subsequent movement of cells into the wound was observed and documented with the IncuCyte ZOOM software every 3 hours for 96 hours. The data were exported as the width of the cell-free area. For calculation of the cell migration/invasion distance, the equation the Relative Wound Density was used, where it is a measure (%) of the density of the wound region relative to the density of the cell region:

$$\%RWD(t) = 100 \cdot \frac{w(t) - w(0)}{c(t) - w(0)}$$

$w(t)$ = Density of wound region at time, t

$c(t)$ = Density of cell region at time, t

5-EU labeling and immunofluorescence

For 5-EU labeling, the RNP transfection reagents was performed using double the manufacturer's specifications. 30 minutes prior to fixing cells were incubated with 1 μ M 5-Ethynyl Uridine (EU) (Invitrogen #E10345), except for the unlabeled control. Cells were fixed with 4% paraformaldehyde at RT for 10 minutes and subsequently permeabilized with 0.5% Triton X-100 for 10 minutes at RT. Click-iT reaction cocktail (100 Mm Tris-buffered saline, 4 mM CuSO₄, 100 mM ascorbic acid and 4 μ M Alexa Fluor™ 488 azide (Invitrogen #A10266) was used for detecting EU. Subsequently, samples were incubated at RT with primary antibodies (RNA Polymerase II, rabbit polyclonal, 1:1000, Abcam, ab5131, RRID:AB_449369; Treacle, mouse monoclonal, 1:500, Santa Cruz, sc-374536, RRID:AB_10987865) for 1 hour, 30 minutes with secondary antibody and 5 mg/ml DAPI

(Invitrogen #D1206) in a dark humid chamber. Cells were washed three times in PBS between incubation steps, rinsed with water, mounted with Fluoromount-G™ mounting medium (Invitrogen #00-4958-02), and sealed with nail polish. Qualitative image analysis of fluorescence was done using the confocal microscope LSM800 (Zeiss), using the 40x oil immersion objective and ZEN Software (Zeiss). Quantitative analysis was done using CellProfiler™ cell image analysis software. The analysis pipeline first segmented nuclei through the DAPI staining, and subsequently identified nucleoli through an inverted mask of the RNA Polymerase II staining. The nucleolar mask could then be used to measure nucleolar EU intensity per nuclei. For cells treated with Act D or gRNA, cells without nucleolar caps were manually removed for the data analysis. Experiments were repeated three times and at least 100 cells were quantified for each condition per repeat.

Bulk RNA-sequencing

RNA-sequencing was carried out as previously described (633) and is publicly available on GEO. Differential expression results were cross-referenced with antibody-validated nucleolar transcripts previously identified (543). Nucleolar differentially expressed transcripts were submitted to the Enrichr online gene set enrichment platform (667-669), and results were visualized with ggplot2. All results were filtered for significance ($P < 0.05$) and ordered by combined score (\log of p value * zscore of deviation from expected rank). Gene sets found to be significant after Benjamini-Hochberg multiple testing correction ($P_{\text{adj}} < 0.05$) were marked with an asterisk.

Quantitative RT-PCR

Total RNA was extracted from SK-Mel28 cells (control/KO) using the Qiagen RNeasy Mini Kit (#74104) following the manufacturer's instructions. RNase-Free DNase Set (Qiagen) was used to remove genomic DNA contaminants. Total RNA was eluted with nuclease-free water. cDNA was synthesized from 500ng RNA with TaqMan Reverse Transcription Reagents Kit (Applied Biosystems). Relative quantification with qRT-PCR was performed by using TaqMan Gene Expression Master Mix (Applied Biosystems) and TaqMan assay reagents (Table 3.8.2) on the QuantStudio 3 (Applied Biosystems). Gene expression was normalized to GAPDH expression. SNCA gene expression was used as a positive internal assay control.

Statistical analysis

Beyond individualized analysis within each assay methodology, all data was processed using GraphPad Prism version 9.0. Data was analyzed using one-way ANOVA, unless stated otherwise, and considered statistically significant if $p < 0.05$. All data was presented as a mean +/- standard error of the mean (SEM).

3.6 Acknowledgements

All imaging experiments could not have been possible without help from Stefanie Kaech Petrie and Felice Kelly in the OHSU Advanced Light Microscopy Core (RRID:SCR_009961). Patient biopsies for immunofluorescence staining were graciously provided by Dr. Gregory Scott at OHSU. I-Ppol plasmids were graciously gifted by Dr. Brian McStay (NUI Galway). We thank Dr. Pamela Cassidy for the isolation and culturing of primary melanocytes and PIG1 cells and for the invaluable discussions. Thank you to Dr. Rosie Sears (OHSU) for providing PLA reagents. We thank the Bioimaging Core Facility headed by Dr. Chris Dinant at the Danish Cancer Institute for support. Lastly, many thanks to Unni Lab members who helped with the revision process: Valerie Osterberg, Dr. Sydney Boutros, Dr. Carlos Soto Faguas, Elizabeth Rose, Anna Bowman, Elias Wisdom, and Jessica Keating.

Funding

The work was supported by:

National Institute on Aging of the National Institutes of Health F30AG082406
National Institute of Health R01NS102227
National Institute of Health P30NS061800
National Institute of Health P30CA065823
Danish Cancer Institute, Danish Cancer Society R302-A17506
Melanoma Research Alliance
Michael J Fox Foundation
Kuni Foundation
Melanoma Research Foundation Medical Student Research Award
OHSU Knight Cancer Institute PhD Scholar COVID-relief Award

3.7 Author Contributions

Conceptualization: MRA, CKM, DHL, VKU

Data Curation: MRA, CKM, VKU

Formal Analysis: MRA, SNE, DB, CKM, DHL, VKU

Funding Acquisition: MRA, RCS, DHL, VKU

Investigation: MRA, KCO, GMC, SNE, CM, AMZ, CKM, SNW, RLW

Methodology: MRA, GMC, SNE, AMZ, RCS, CKM, SNW, DHL, RLW, VKU

Project Administration: MRA, DHL, VKU

Resources: MRA, GMC, RCS, CKM, SNW, DHL, RLW, VKU

Software: MRA, GMC, SNE, PVL, VKU

Supervision: MRA, CKM, DHL, VKU

Validation: MRA, GMC, SNE, CKM, VKU

Visualization: MRA, SNE, CKM, VKU

Writing- original draft: MRA, CKM, VKU

Writing- review & editing: MRA

3.8 Supplemental Material

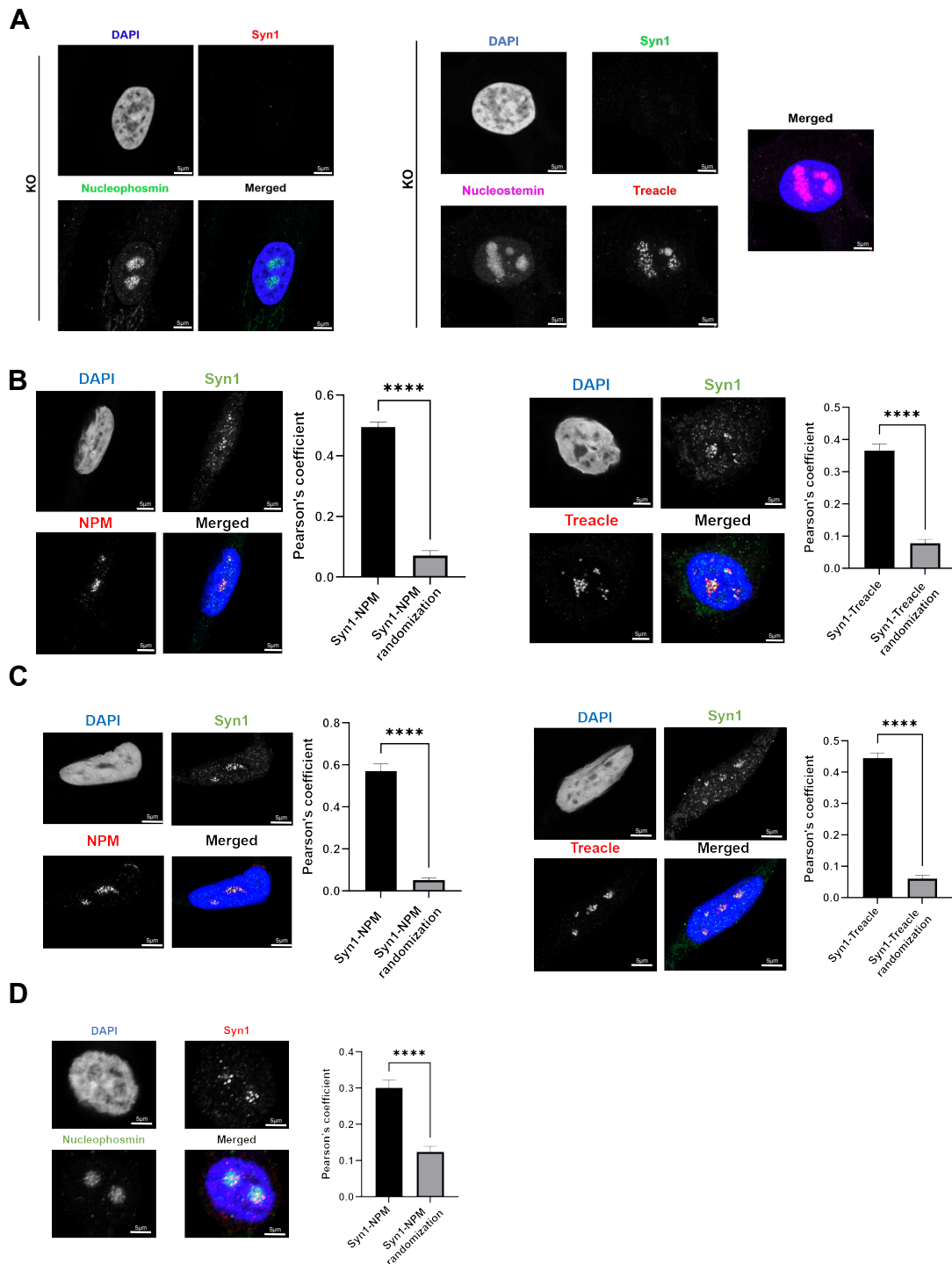


Figure 3.8.1. Alpha-synuclein localizes to nucleolar markers in melanoma cells and primary melanocytes. A, B, C, D) SK-Mel28 KO (A), primary melanocytes (B), PIG1 (C), and A375 (D) cells were seeded on PDL-coated coverslips and then fixed and stained for alpha-synuclein (Syn1), nucleolar markers (nucleophosmin, treacle), and DAPI. Cells were imaged on the Zeiss 980 confocal microscope with Airyscan and colocalization was

analyzed in Imaris software. Error bars represent Standard Error of the Mean (SEM) with quantification from 1 biological replicate (total n=12-15 nuclei per condition). ****p<0.0001 by T-test.

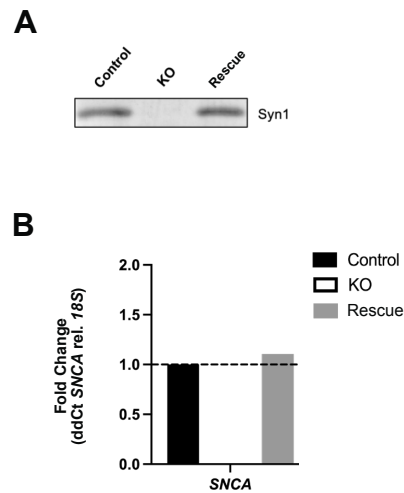


Figure 3.8.2. Knockout and reintroduction validation of alpha-synuclein in SK-Mel28 cells. A) SK-Mel28 cells (control/KO/rescue) were lysed using RIPA buffer and run out on SDS-PAGE and probed for Syn1 and total protein. Representative image of western blot. B) Total RNA was isolated from SK-Mel28 cells (control/KO/rescue). Using *SNCA* TaqMan primers, qRT-PCR amplification was determined when normalized to 18S internal control. Data is from 1 representative biological replicate with 2 technical replicates.

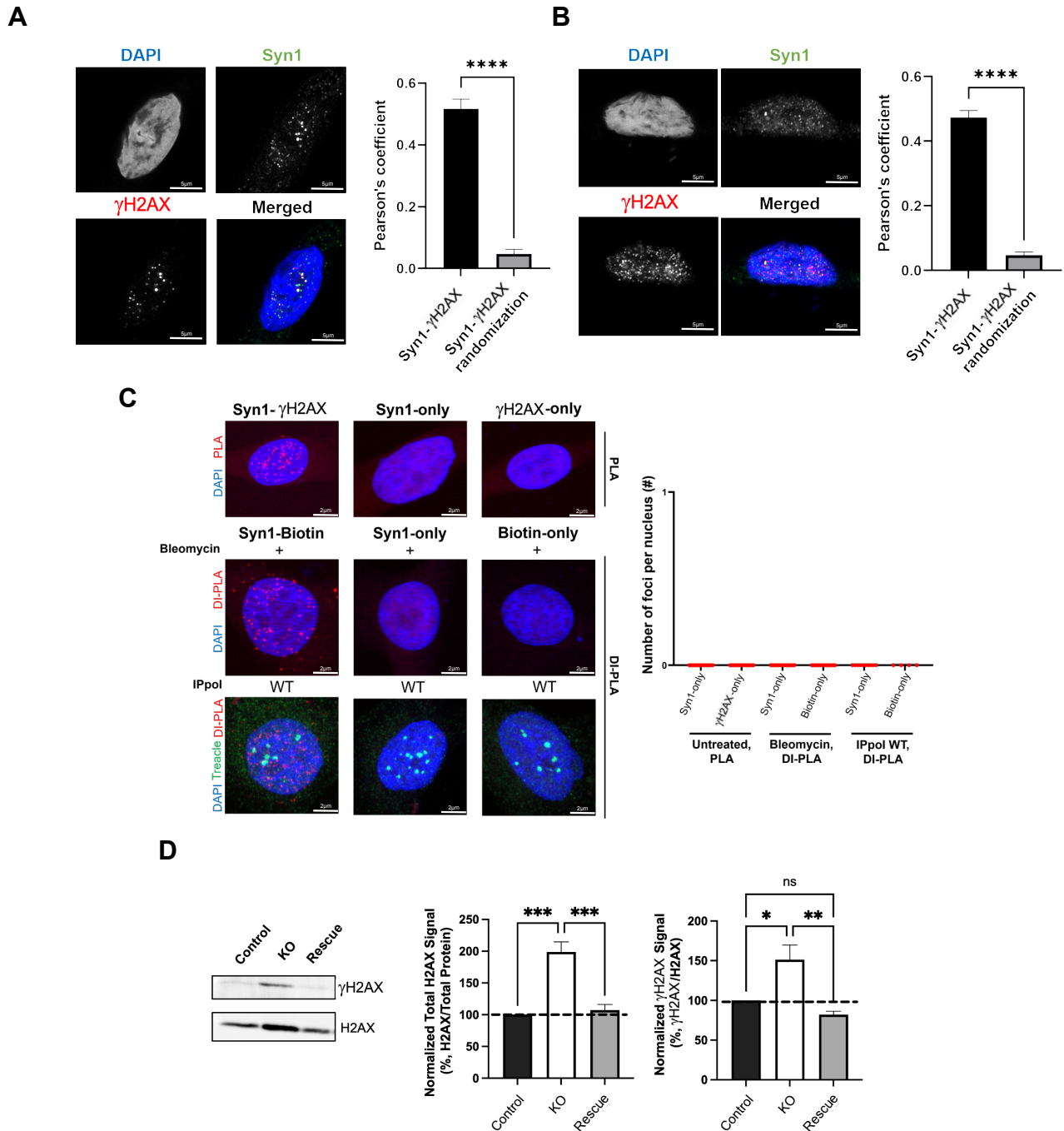


Figure 3.8.3. Alpha-synuclein localizes with γ H2AX in melanoma cells & primary melanocytes and γ H2AX increases in alpha-synuclein knockout cells. A, B) Primary melanocytes (A) and PIG1 (B) cells were seeded on PDL-coated coverslips and then fixed and stained for alpha-synuclein (Syn1), DSB marker (γ H2AX), and DAPI. Cells were imaged on the Zeiss 980 confocal microscope with Airyscan and colocalization was analyzed in Imaris software. Error bars represent Standard Error of the Mean (SEM) with quantification from 1 biological replicate (total $n=15$ nuclei per condition). **** $p<0.0001$ by T-test. C) SK-Mel28 control and KO cells were seeded on PDL-coated coverslips and

then fixed in 4% paraformaldehyde. Proximity Ligation Assay (PLA) or DNA Damage In Situ Ligation Followed by Proximity Ligation Assay (DI-PLA, Duolink) was completed using antibodies against Syn1, γ H2AX, or biotin. Cells were imaged on the Zeiss 980 confocal microscope and number of foci per nucleus was measured using CellProfiler while masking for the nucleus using DAPI. Each figure shows representative images and quantification from 2 technical replicates (total n=10-30 nuclei per condition). D) SK-Mel28 cells (control/KO/rescue) were lysed and a nuclear fractionation was performed. Nuclear protein was run out on SDS-PAGE and probed for γ H2AX, total H2AX, and total protein. Western blots were imaged on Licor CLx imager. * $p < 0.05$, ** $p < 0.01$, **** $p < 0.0001$ by ANOVA. Error bars denote SEM. Quantification from 4 biological replicates. Staining of Figure 3.8.3C performed by Gabe Cohn.

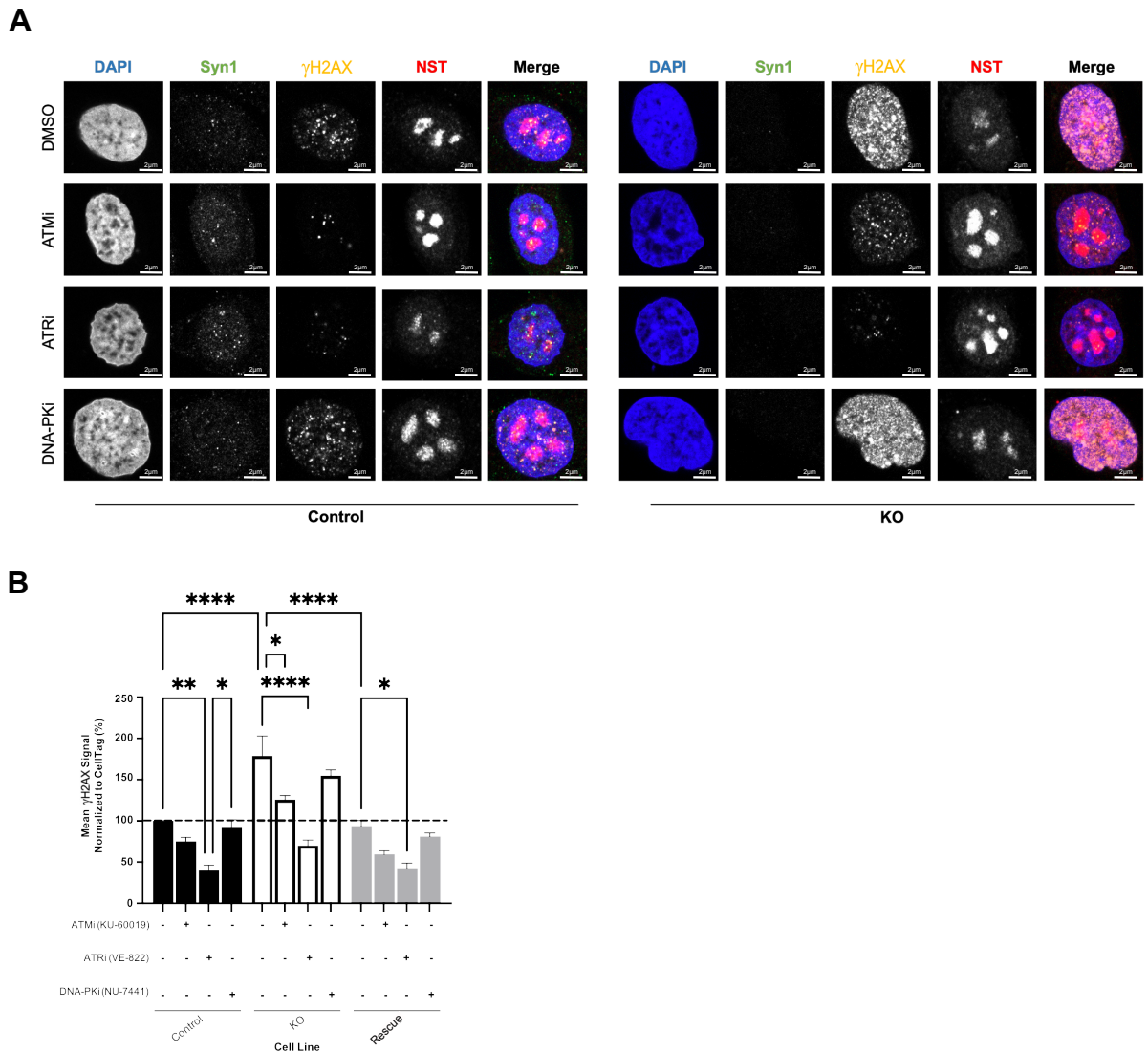
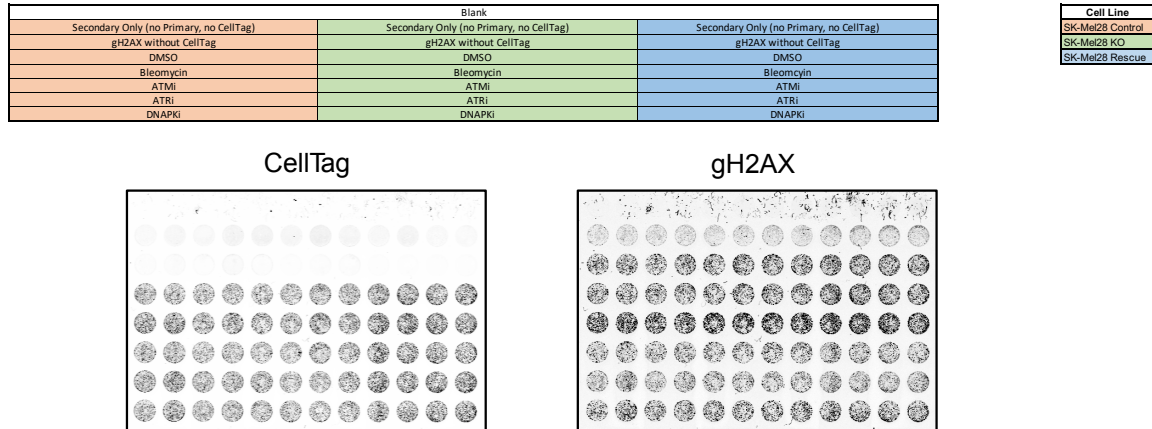


Figure 3.8.4. γ H2AX increase is driven by ATM and ATR in alpha-synuclein knockout cells. A) SK-Mel28 cells were seeded on PLL-coated coverslips and treated with DMSO, KU-60019 (10 μ M), VE-822 (0.1 μ M), or NU-7441 (1 μ M) for 24 hours. Cells were fixed and stained for Syn1, γ H2AX, nucleostemin and DAPI. Representative images

are shown above. Quantification from 3 biological replicates is found in Figure 2E-F. B) SK-Mel28 cells were seeded in a black-welled PDL-coated 96 well plate and treated with DMSO, KU-60019 (10 μ M), VE-822 (0.1 μ M), or NU-7441 (1 μ M) for 24 hours. Cells were processed according to the In-Cell Western manufacturer instructions and stained for γ H2AX (800) and CellTag (700). Plates were imaged on the Licor CLx. * $p < 0.05$, ** $p < 0.01$, **** $p < 0.0001$ by ANOVA. Error bars denote SEM. Quantification from 3 biological replicates (with 4 technical replicates per experiment). Same γ H2AX quantification from DMSO condition as Figure 3C as samples were run on the same plate.

A



B

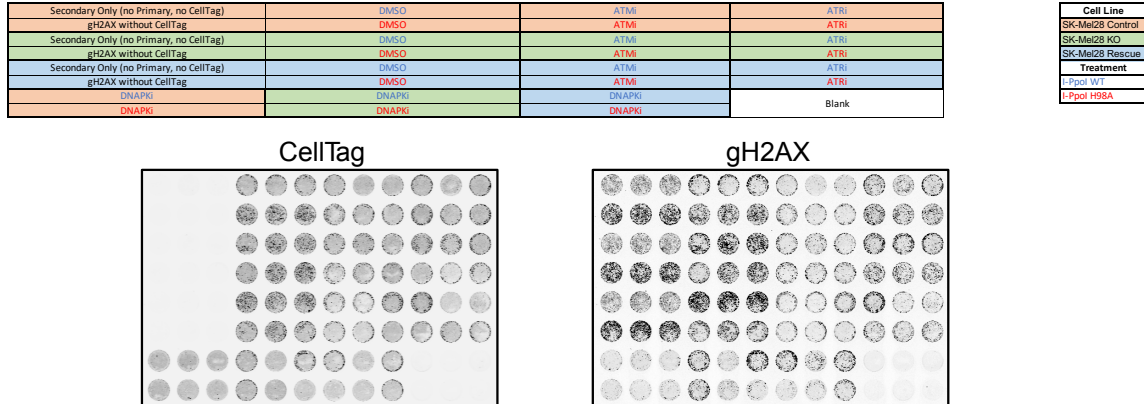


Figure 3.8.5. Representative Images of ICW plates. A, B) SK-Mel28 cells were seeded in a black-welled PDL-coated 96 well plate and treated with indicated treatments. Cells were processed according to the In-Cell Western manufacturer instructions and stained for γ H2AX (800) and CellTag (700). Plates were imaged on the Licor CLx. Quantification from 3-5 biological replicates are in Figures 3C, 5A and Supplemental Figure 4B.

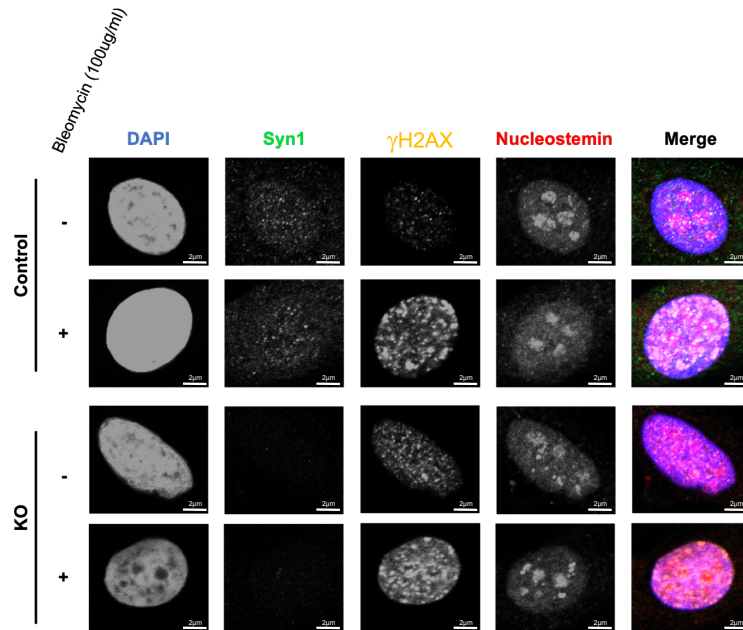
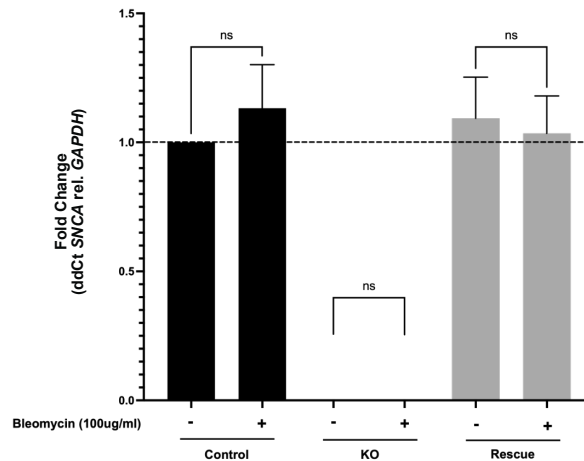
A**B**

Figure 3.8.6. Increase in alpha-synuclein following bleomycin treatment is not due to transcriptional regulation. A) SK-Mel28 cells (control/KO/rescue) were seeded on PLL-coated coverslips and treated with DMSO or 100 µg/ml bleomycin for 1 hour. Cells were fixed and stained for Syn1, γ H2AX, nucleostemin, and DAPI. Representative figures shown above. Quantification from 3 biological replicates is shown in Figure 3D. B) Total RNA from SK-Mel28 cells (control/KO/rescue) was isolated and cDNA was prepared using Invitrogen TaqMan Reverse Transcriptase Reagents. Quantitative RT-PCR was performed using TaqMan assay reagents (Table 2) and gene expression levels were normalized to GAPDH. Quantification from 4 biological replicates (with 2 technical replicates per experiment). Significance calculated by one-way ANOVA. Error bars denote SEM.

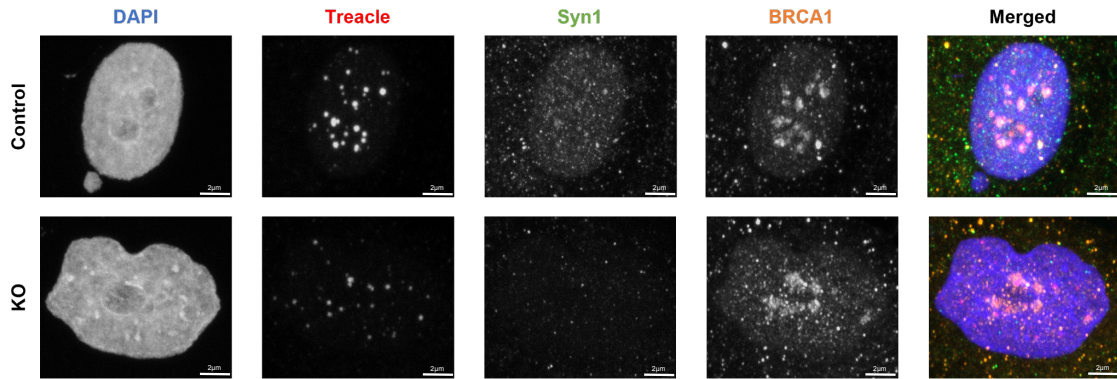


Figure 3.8.7. Representative images of BRCA1 staining. SK-Mel28 cells (control/KO/rescue) were seeded on PLL-coated coverslips and then transfected with WT I-Ppol mRNA. 6-hours post transfection, cells were fixed and stained for Syn1, Treacle, BRCA1, and DAPI. Cells were imaged on the Zeiss 980 confocal microscope and data was analyzed using FIJI. Quantification from 3 biological replicates is shown in Figure 7A.

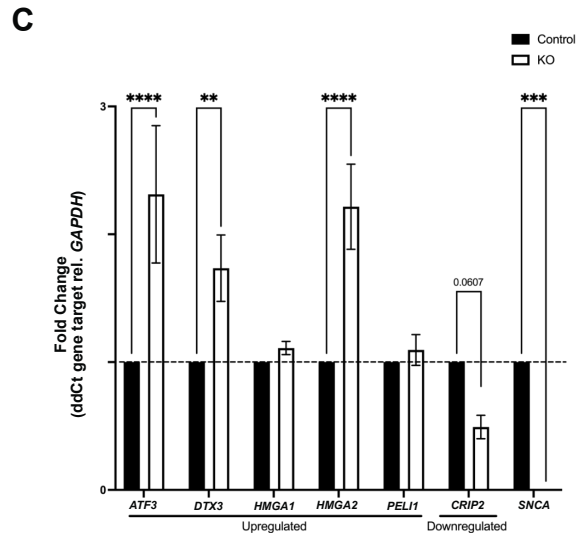
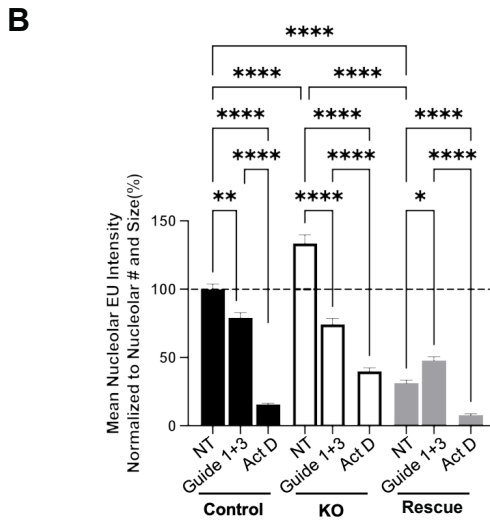
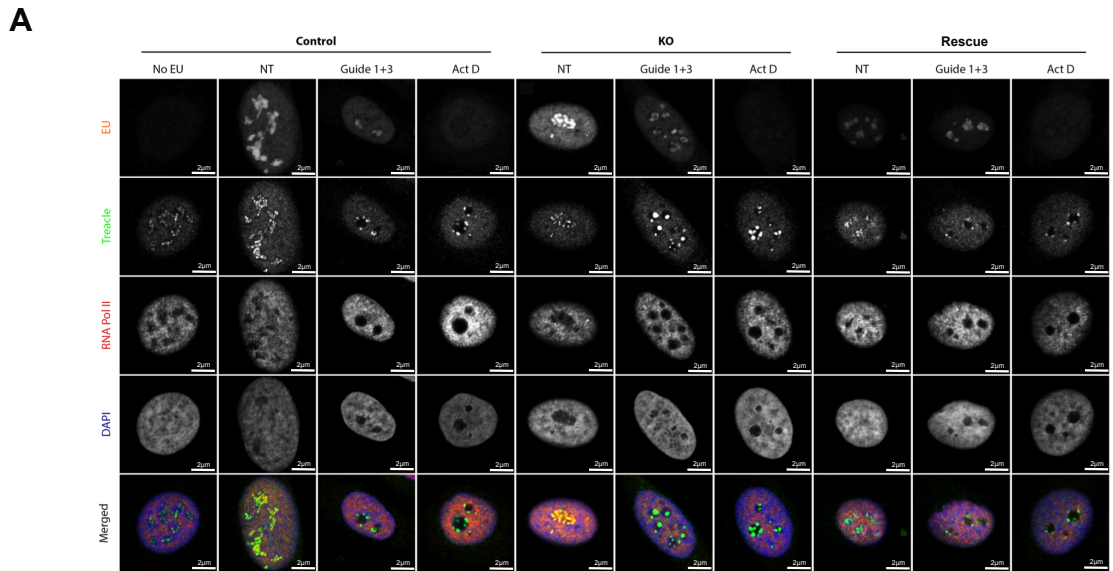


Figure 3.8.8. Alpha-synuclein is not involved in nucleolar DDR-mediated transcriptional silencing. A, B) SK-Mel28 cells (control/KO/rescue) were seeded on coverslips and then transfected with Cas9 (TrueCut Cas9 Protein v2, Invitrogen) and guide RNAs that target portions of the 28S unit of rDNA or non-targeting control (NT vs. Guide 1+3). Twenty-four hours after transfection, cells were treated with 5-Ethynyl Uridine before fixing and performing Click-iT reaction to detect EU. Additional staining for treacle, RNA polymerase II, and DAPI were completed. Cells were imaged on the Zeiss LSM800 confocal microscope and analyzed using RNA polymerase II anti-masking. 5EU intensity was measured and normalized to nucleolar pixel number and size. Quantification from 3 biological replicates (total n=519-737 nuclei per condition). * p<0.05, ** p<0.01, ****p<0.0001 by ANOVA. Error bars denote SEM. C) Total RNA from SK-Mel28 cells (control/KO) was isolated and cDNA was prepared using Invitrogen TaqMan Reverse Transcriptase Reagents. Quantitative RT-PCR was performed using TaqMan assay

reagents (Table 2) and gene expression levels were normalized to GAPDH. Quantification from 5 biological replicates (with 3 technical replicates per experiment). ** $p < 0.01$, *** $p < 0.001$, **** $p < 0.0001$ by two-way ANOVA. Error bars denote SEM. Data acquisition and formal analysis of Figure 3.8.8A-B performed by Kezia Catharina Oxe.

Gene Name	Nucleolar Location	Fold Change	log2(Fold Change)	PValue	FDR
ATF3	Nucleoli	29.52536727	4.8838831	1.91E-227	2.98E-225
SFRP1	Nucleoli	16.07883589	4.007091054	0	0
TBL1X	Nucleoli	7.685113901	2.942066642	6.34E-158	5.55E-156
DTX3	Nucleoli	7.540997575	2.914755386	2.6E-107	1.27E-105
SPOCD1	Nucleoli	6.350004811	2.666757685	4.22E-89	1.62E-87
PCDH1	Nucleoli	6.316758918	2.659184512	4.18E-53	7.86E-52
DUSP1	Nucleoli	6.078912815	2.603813327	8.99E-166	8.96E-164
LURAP1L	Nucleoli	4.698106043	2.232079277	1.09E-44	1.66E-43
HMG2	Nucleoli rim	3.958533749	1.984966151	3.57E-78	1.19E-76
EN1	Nucleoli rim	3.593823411	1.845519521	1.37E-19	8.43E-19
PFKFB4	Nucleoli	3.501787008	1.808091336	2.55E-149	2.04E-147
CDC47L	Nucleoli	3.485427803	1.801335744	7.4E-132	5.22E-130
BMP7	Nucleoli	3.351598842	1.744849481	9.51E-57	1.94E-55
PLOD2	Nucleoli	3.283596221	1.715276732	1.28E-66	3.33E-65
PLPP4	Nucleoli rim	2.781738245	1.475986672	9.86E-155	8.22E-153
PHLDA1	Nucleoli rim	2.685250597	1.425056732	2.34E-259	4.23E-257
PDGFRL	Nucleoli	2.652722178	1.407473589	7.97E-71	2.26E-69
HIST1H1C	Nucleoli rim	2.601212023	1.379183997	9.35E-40	1.24E-38
HMG1	Nucleoli	2.58668238	1.371102916	6.88E-197	9.19E-195
SH3TC1	Nucleoli rim	2.582615378	1.368832803	9.98E-26	8.1E-25
CSTB	Nucleoli	2.51382743	1.329885615	2.49E-187	3.06E-185
KLF6	Fibrillar center	2.460415276	1.298901838	5.08E-161	4.75E-159
DLG3	Nucleoli	2.448057714	1.291637571	5.95E-24	4.5E-23
FAM198B	Fibrillar center	2.445531037	1.290147775	3.04E-25	2.41E-24
KCNC4	Nucleoli	2.439896714	1.286820077	1.73E-44	2.62E-43
OSMR	Nucleoli	2.300357658	1.201858188	2.26E-104	1.05E-102
PEL1	Nucleoli	2.272113094	1.184034646	4.11E-49	7.03E-48
CTSB	Nucleoli	2.23062657	1.157449012	1.78E-169	1.84E-167
FADS3	Fibrillar center	2.20816123	1.142845515	7.9E-52	1.46E-50
DDX41	Nucleoli	2.156596089	1.108755998	6E-85	2.19E-83
B3GNT5	Nucleoli	2.131456723	1.091839763	9.73E-18	5.46E-17
SMPDL3A	Nucleoli	2.108575404	1.076268615	1.06E-32	1.12E-31
SLC6A15	Nucleoli	2.100790212	1.070932099	1.73E-47	2.85E-46
CCDC59	Nucleoli rim	2.091777836	1.064729633	1.24E-36	1.49E-35
RNFT1	Nucleoli	2.03805413	1.027192369	1.14E-19	7.04E-19
PELO	Fibrillar center	2.016925559	1.012157837	2.25E-64	5.49E-63
ATP6AP1L	Nucleoli	2.013390254	1.009626836	2.55E-49	4.4E-48
ICK	Fibrillar center	-2.000231199	-1.000166765	1.08E-21	7.34E-21
DPH6	Nucleoli rim	-2.005977839	-1.004305668	3.59E-16	1.85E-15
ZNF397	Nucleoli	-2.013859384	-1.009962952	5.51E-16	2.82E-15
OSCP1	Nucleoli	-2.024484901	-1.017554883	3.04E-13	1.32E-12
FOXJ2	Fibrillar center	-2.027796062	-1.019912566	3.27E-47	5.35E-46
ZNF689	Fibrillar center	-2.040976132	-1.029259311	3.71E-160	3.4E-158
UBR3	Nucleoli	-2.079282131	-1.056085526	8.36E-73	2.47E-71
LZTS1	Nucleoli	-2.100734509	-1.070893846	3.34E-134	2.42E-132
MYL5	Nucleoli	-2.112441599	-1.078911457	1.02E-13	4.56E-13
AKAP11	Nucleoli	-2.154422695	-1.107301332	4.51E-57	9.27E-56
BRWD1	Nucleoli	-2.158029608	-1.109714658	2.45E-66	6.31E-65
ZNF33B	Fibrillar center	-2.198838417	-1.136741591	8.08E-33	8.57E-32
ZBTB43	Nucleoli	-2.239812724	-1.16337811	1.03E-88	3.96E-87
TTC28	Nucleoli	-2.242272354	-1.164961523	1.65E-77	5.44E-76
TAF4B	Fibrillar center	-2.378460438	-1.250028029	1.66E-49	2.91E-48
TMOD2	Fibrillar center	-2.463846408	-1.300912323	1.59E-60	3.5E-59
RBM43	Nucleoli	-2.499687886	-1.321747969	1.03E-29	9.78E-29
ABCC4	Nucleoli	-2.539678916	-1.344646113	1.9E-105	8.93E-104
IQSEC1	Nucleoli rim	-2.559626688	-1.355933414	3.08E-71	8.81E-70
SPIN4	Nucleoli	-2.76010701	-1.464724201	1.39E-21	9.41E-21
MYL9	Fibrillar center	-2.840665986	-1.506229205	9.12E-53	1.7E-51
POP1	Nucleoli	-2.840967431	-1.506382293	3.57E-109	1.79E-107
JRK	Nucleoli	-2.960246116	-1.565717127	1.26E-79	4.24E-78
ZNF419	Fibrillar center	-3.137808254	-1.649757194	7.28E-23	5.24E-22
STOX1	Fibrillar center	-3.498043645	-1.80654829	5.71E-29	5.27E-28
BCAM	Fibrillar center	-5.401784718	-2.433436144	3.55E-59	7.67E-58
CRIP2	Nucleoli	-8.074263539	-3.013330676	1.58E-154	1.31E-152

Table 3.8.1. Differentially expressed nucleolar transcripts in alpha-synuclein knockout cells. Total RNA was extracted from SK-Mel28 control and KO cells and sent for RNA-sequencing analysis at Indiana University. Differentially expressed gene transcripts in KO cells compared to control were identified. These were cross-referenced to over 500 nucleolar-specific genes. 64 genes were identified. Data acquisition of Table 3.8.1 performed by Sahar Shekoohi.

Gene of Interest	TaqMan Assay
ATF3	Hs00231069_m1
DTX3	Hs01595350_m1
HMGA1	Hs00852949_g1
HMGA2	Hs04397751_m1
PELI1	Hs00900505_m1
CRIP2	Hs00373842_g1
SNCA	Hs00240906_m1
GAPDH	Hs02786624_g1
18S	Hs99999901_s1

Table 3.8.2. TaqMan assay probes

[Jump Back to Table of Contents](#)

**Chapter 4:
Alpha-synuclein knockout impairs melanoma development and alters
DNA damage repair in the TG3 mouse model in a sex-dependent
manner**

Moriah R. Arnold^{1,2}, Suzie Chen³, Vivek K. Unni^{*2,4}

¹Medical Scientist Training Program, Oregon Health and Science University, Portland, OR, USA., arnoldmo@ohsu.edu

²Department of Neurology and Jungers Center for Neurosciences Research, Oregon Health and Science University, Portland, OR, USA.

³Departments of Chemical Biology, Ernest Mario School of Pharmacy, Rutgers University, NJ, USA., suziec@pharmacy.rutgers.edu

⁴OHSU Parkinson Center, Oregon Health and Science University, Portland, OR, USA., unni@ohsu.edu

Published on bioRxiv December 5th, 2024

In Press at *Frontiers in Oncology*

4.1 Abstract

Strong evidence suggests links between Parkinson's Disease (PD) and melanoma, as studies have found that people with PD are at an increased risk of developing melanoma and those with melanoma are at increased risk of developing PD. Although these clinical associations are well-established, the cellular and molecular pathways linking these diseases are poorly understood. Recent studies have found a previously unrecognized role for the neurodegeneration-associated protein alpha-synuclein (α Syn) in melanoma; the overexpression of α Syn promotes melanoma cell proliferation and metastasis. However, to our knowledge, no studies have investigated the role of α Syn in *in vivo* melanoma models outside of a xenograft paradigm. Our study created and characterized *Snca* knockout in the spontaneously developing melanoma TG3 mouse line, TG3^{+/+}*Snca*^{-/-}. We show that α Syn loss-of-function significantly delays melanoma onset and slows tumor growth *in vivo*. Furthermore, decreased tumor volume is correlated with a decreased DNA damage signature and increased apoptotic markers, indicating a role for α Syn in modulating the DNA damage response (DDR) pathway. Overall, our study provides evidence that targeting α Syn and its role in modulating the DDR and melanomagenesis could serve as a promising new therapeutic target.

4.2 Introduction

The association between Parkinson's Disease (PD) and melanoma has been well established. Many epidemiological studies have found a significant increase in the risk of melanoma among individuals with PD compared to healthy individuals, ranging from 1.4-20-fold (2, 5-20). Likewise, there is also an increased risk for PD in melanoma patients, ranging from 1.7-4.2 fold (12, 15, 21-23). Altogether, it is clear that common environmental, genetic, and/or molecular mechanisms are at play to influence this clinical association, yet the underlying mechanism is still poorly understood.

One potentially promising avenue of investigation is the biological function of the neurodegeneration-associated protein, alpha-synuclein (α Syn). Misfolded and aggregated forms of α Syn are found in cytoplasmic inclusions called Lewy bodies, which are neuropathological hallmarks in PD and other Lewy body disorders (614, 615). Lewy bodies are found primarily in the central nervous system, where their presence in dopaminergic neurons in the midbrain is associated with the degeneration of these cells in PD (616). α Syn is not only found in the central nervous system, but can also be found in the periphery, including in melanocytes (617, 618) and therefore could be a key molecular link between these disease pathologies. In primary and metastatic melanoma, ~85% of biopsies show high expression of α Syn (5, 395-397, 592). Since this initial characterization, there have been several studies investigating the role of α Syn in melanoma growth and metastasis; the majority of these being *in vitro* studies. Overall, these studies using human and mouse melanoma cell lines have found that α Syn expression is important in cell proliferation (398, 478, 479, 592), motility (480), and protects against cell death (398, 504), through multiple potential mechanisms, such as

altering the inflammatory response (506, 633, 670), autophagy pathways (398, 504), and DNA damage repair (592).

Fewer studies have investigated the role of α Syn in *in vivo* melanoma mouse models and all this previous *in vivo* work, to our knowledge, has used a xenograft paradigm. In general, these xenograft studies corroborate previous *in vitro* work and find that α Syn is important in melanoma tumor growth and metastasis. Specifically, α Syn knockout (KO) human/mouse melanoma cells implanted as xenografts in mice exhibited slower growth and increased apoptosis (478), and reduced tumor-induced mechanical allodynia (481). Furthermore, WT melanoma cells in α Syn overexpressing mice show increased metastasis (479). Lastly, human melanoma xenografts implanted in mice and treated with an α Syn aggregation inhibitor (anle138b) led to increased cell death (398) and upregulation of anti-melanoma immune responses (506). Despite this substantial data linking α Syn to melanoma tumor growth *in vivo*, whether α Syn expression within melanocytes influences tumorigenesis is still not understood. In our current study, we aimed to create and characterize a new TG3 *Snc*^{-/-} mouse line to better understand the function of α Syn in melanomagenesis, tumor growth, and metastasis in a spontaneous melanoma-forming mouse line. TG3 mice display melanin-pigmented lesions after a short latency and with complete penetrance (671-674). This model is driven by multiple tandem insertions of a transgene into intron 3 of *Grm1* (metabotropic glutamate receptor 1) with concomitant deletion of an intronic sequence that increases expression of *Grm1*. Homozygous TG3 mice form primary melanoma tumors on pinna and perianal regions, in addition to metastatic tumors in lymph nodes, lung, and liver (671-674). The TG3 line

also has the advantage of being mono-allelic, therefore making breeding to other genetically modified mice practical.

Our previous work has shown α Syn's role in modulating nuclear DNA damage response (DDR) pathways in human melanoma cells (592) and other cell types (442, 443). Specifically, we found a novel function of α Syn in DNA double-strand break (DSB) repair, where α Syn colocalizes with DSB repair components and its knockout leads to increased DSBs and their slowed repair (442, 592). In this study, we aimed to investigate whether similar mechanisms are important for melanomagenesis and growth using the TG3^{+/+} *Snca*^{-/-} mouse model to test whether α Syn loss-of-function dysregulated DNA damage pathways and led to downstream cell death phenotypes.

4.3 Results

Loss of Alpha-Synuclein Delays Melanoma Onset and Decreases Tumor Growth in vivo

To study the role of α Syn in melanoma tumorigenesis *in vivo*, TG3 mice (671) were crossed with *Snca*-knockout mice. The generated TG3^{+/+} *Snca*^{+/+} (“wildtype”) and TG3^{+/+} *Snca*^{-/-} (“homozygous KO”) mice were then analyzed for tumor growth from P30 to P100, at which point the mice were sacrificed and dissected for tissue processing (Figure 4.3.1A). There was no significant difference in weight of the mice between wildtype and homozygous KO genotypes (Figure 4.8.1). Melanoma tumor onset was evaluated, and homozygous KO mice developed melanoma significantly later compared to the wildtype control group (Figure 4.3.1B). Wildtype mice on average exhibited tumors at P43, whereas melanoma onset was observed on average at P50 for homozygous KO mice.

This difference is driven primarily by male mice, since when stratified by sex there was no significant difference between genotypes in female mice but there was in male mice (Figure 4.3.1B). Further, the progression of melanoma growth on pinna and perianal regions were followed for ~70 days. Here, a graded scoring system from minimal (0) to extreme tumor growth (5) was used to quantify melanoma progression on pinna as previously described (675) (Figure 4.8.2) and quantitative size measurement was used to quantify melanoma progression in perianal regions. This analysis revealed no significant differences in tumor progression of the pinna between wildtype and homozygous KO genotypes, even when stratified by sex (Figure 4.3.1B). However, homozygous KO mice display decreased perianal tumor growth compared to wildtype mice, which becomes significant at later time points (Figure 4.3.1C). Again, this difference is driven primarily by male mice when stratified by sex (Figure 4.3.1C).

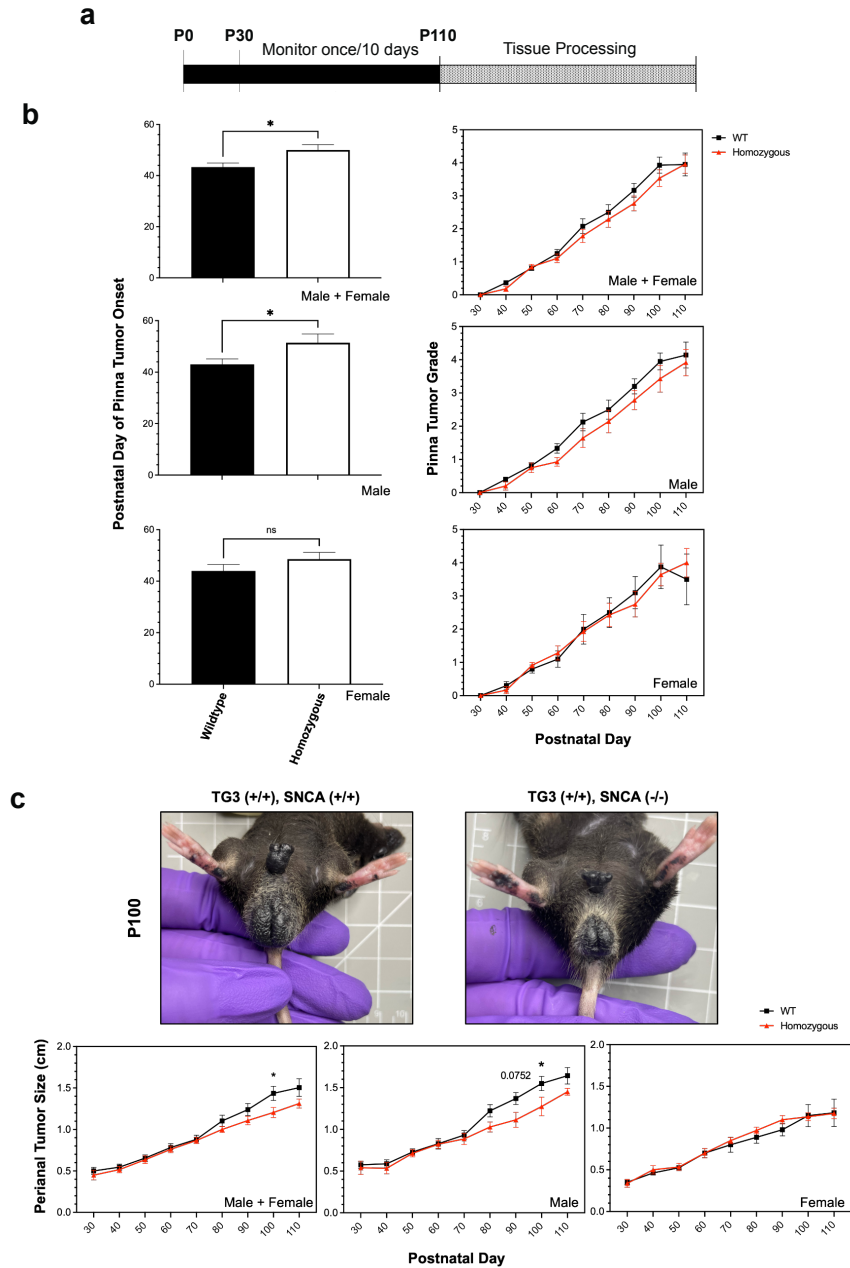


Figure 4.3.1. Alpha-synuclein knockout significantly delays tumor onset and slows tumor progression. a) Schematic representing experimental timeline. b,c) Pinna melanoma onset in TG3^{+/+}Snca^{+/+} (n=15) and TG3^{+/+}Snca^{-/-} (n=14). Pinna and perianal tumor progression of the TG3^{+/+}Snca^{-/-} compared to the TG3^{+/+}Snca^{+/+} after tumor onset. The grading system to evaluate the progression of tumor growth at the pinna region until endpoint at P110 is further described in Figure S2. Analysis was further stratified by sex with TG3^{+/+}Snca^{+/+} male (n=10), TG3^{+/+}Snca^{+/+} female (n=5), TG3^{+/+}Snca^{-/-} male (n=7), and TG3^{+/+}Snca^{-/-} female (n=7). Error bars represent Standard Error of the Mean (SEM). *p<0.05 by unpaired T-test for tumor onset or Two-way ANOVA for tumor progression.

Experimental Genotypes Display Similar Pigment Formation and Grm1 Expression

We next wanted to confirm the presence of melanoma-like cells in the primary tumors of these mice through histopathological analysis. Hematoxylin and eosin (H+E) staining revealed significant levels of pigmented cell growth in the primary pinna and perianal tumors of both wildtype and homozygous KO mice compared to control C57BL/6 wildtype mice without tumors (Figure 4.3.2A). qRT-PCR analyses revealed comparable *Grm1* mRNA expression levels between the wildtype and homozygous KO pinna and perianal primary tumors. This suggests that mice express the *Grm1* transgene at similar levels regardless of *Snca* expression (Figure 4.3.2B). These levels were compared to positive control cerebellum tissue where *Grm1* mRNA expression is known to be high.

Additionally, H+E staining confirmed the presence of pigmented melanoma cells in the lymph nodes of both wildtype and homozygous KO mice, indicating lymph node metastasis had occurred in both genotypes (Figure 4.3.2A). The *Grm1* mRNA expression in lymph node tissues of wildtype and homozygous KO mice was analyzed as a marker for melanoma cell dissemination. Here a less, although not significant, *Grm1* expression was observed in lymph nodes of the homozygous KO mice compared to wildtype mice (Figure 4.3.2B), suggesting that α Syn loss-of function may decrease metastatic potential but that larger cohorts would be needed to detect this possible difference given inter-animal variability.

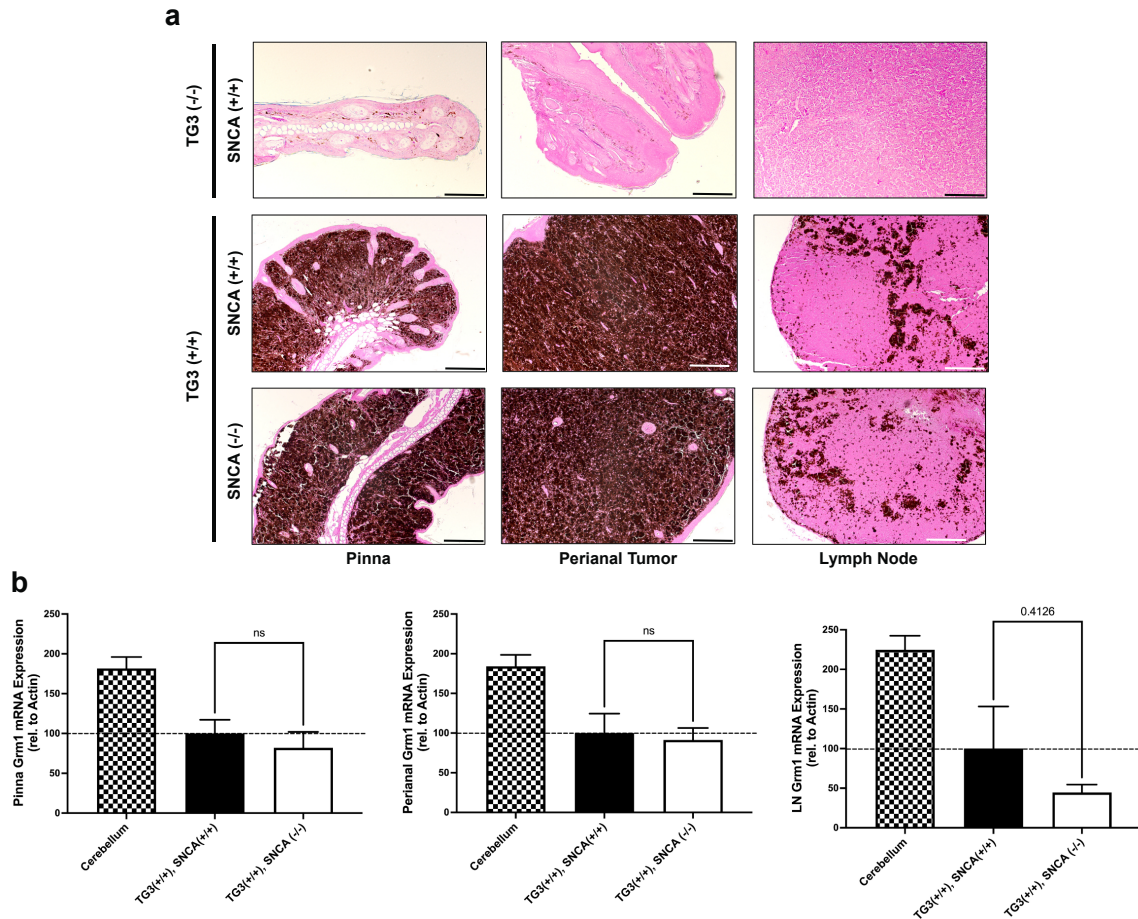


Figure 4.3.2. Alpha-synuclein knockout does not interfere with *Grm1* expression and results in possible decrease in lymph node metastasis. a) Formalin-fixed paraffin-embedded pinna and perianal primary tumors and lymph nodes were stained for hematoxylin and eosin in TG3^{-/-}*Snca*^{+/+}, TG3^{+/+}*Snca*^{+/+}, or TG3^{+/+}*Snca*^{-/-} mice. Stained samples were imaged on the Zeiss ApoTome2 microscope. Scale bar=100μm, except for TG3^{-/-}*Snca*^{+/+} perianal scale bar=200μm and lymph node scale bar=50μm. b) Total RNA was isolated from pinna and perianal primary tumors and lymph nodes from TG3^{+/+}*Snca*^{+/+} or TG3^{+/+}*Snca*^{-/-} mice. Using primers against the *Grm1* gene, qRT-PCR amplification was determined when normalized to *beta-actin*. For pinna and perianal analysis, TG3^{+/+}*Snca*^{+/+} (n=5) and TG3^{+/+}*Snca*^{-/-} (n=6). For lymph node analysis, TG3^{+/+}*Snca*^{+/+} (n=12) and TG3^{+/+}*Snca*^{-/-} (n=9). Cerebellum samples (n=3). Each sample was run with 2 technical replicates. Statistical analysis via unpaired T-test.

Loss of Alpha-Synuclein Decreases DNA Damage Signatures in the Melanoma Tumor

αSyn has been previously linked to DNA DSB repair, since knocking out αSyn significantly increases DNA damage levels in SK-Mel28 cells (592), Hap1 cells (442, 443),

and mouse brain (442) due to less efficient DNA DSB repair. We wanted to investigate whether there were differences in DNA damage burden and repair mechanisms between TG3^{+/+} *Snca*^{+/+} (“wildtype”) and *Snca*^{-/-} (“homozygous KO”) mice. Formalin-fixed paraffin-embedded perianal primary tumor samples from wildtype and homozygous KO mice underwent immunofluorescence (IF) staining. Genotypes were first validated via IF when stained using an α Syn antibody, LB509, where homozygous KO tissue showed significantly reduced levels of staining compared to wildtype mice (Figure 4.3.3A). In addition, when analyzing the localization of α Syn labelling in the wildtype samples, discrete nuclear foci were seen in the melanoma tumor cells, similar to our previous studies where these foci are implicated in DNA damage repair processes (442, 443, 592). Given these findings and previous data, these samples were next stained for DNA damage and damage repair markers: γ H2AX, RPA32, and 53BP1.

γ H2AX, a phosphorylated form of histone H2AX, is involved in the early stages of DNA DSB detection and is a sensitive marker for DNA damage burden. IF staining for γ H2AX revealed a significant decrease in mean intensity of γ H2AX signal, number of nuclear γ H2AX foci, and density of nuclear γ H2AX foci in the homozygous KO group compared to the wildtype group (Figure 4.3.3B). These trends remained similar when stratified by sex. RPA32, replication protein A2, binds and stabilizes single-stranded DNA intermediates that form during DNA repair and is important in homologous recombination (HR) DSB repair. IF staining for RPA32 revealed no significant differences in the mean nuclear intensity, number of nuclear RPA32 foci and their density in the homozygous KO group compared to the wildtype group (Figure 4.3.3C). Interestingly when stratified by sex, there were significant, but opposite, differences in mean nuclear intensity of RPA32

between the wildtype and homozygous KO group, despite no significant differences when combined. Male homozygous KO mice exhibited a significant increase in mean nuclear RPA32 intensity compared to wildtype mice, whereas female homozygous KO mice exhibited a significant decrease in mean nuclear RPA32 intensity compared to wildtype mice (Figure 4.3.3C). Lastly, 53BP1, p53-binding protein 1, is an important regulator of DNA DSB repair and promotes non-homologous end-joining (NHEJ) DSB repair. IF staining for 53BP1 revealed a significant increase in mean nuclear 53BP1 intensity in homozygous KO mice compared to wildtype mice, driven by both male and female mice (Figure 4.3.3D). Homozygous KO female mice showed a significant increase in number and density of 53BP1 foci compared to wildtype mice, but male mice showed no genotype differences.

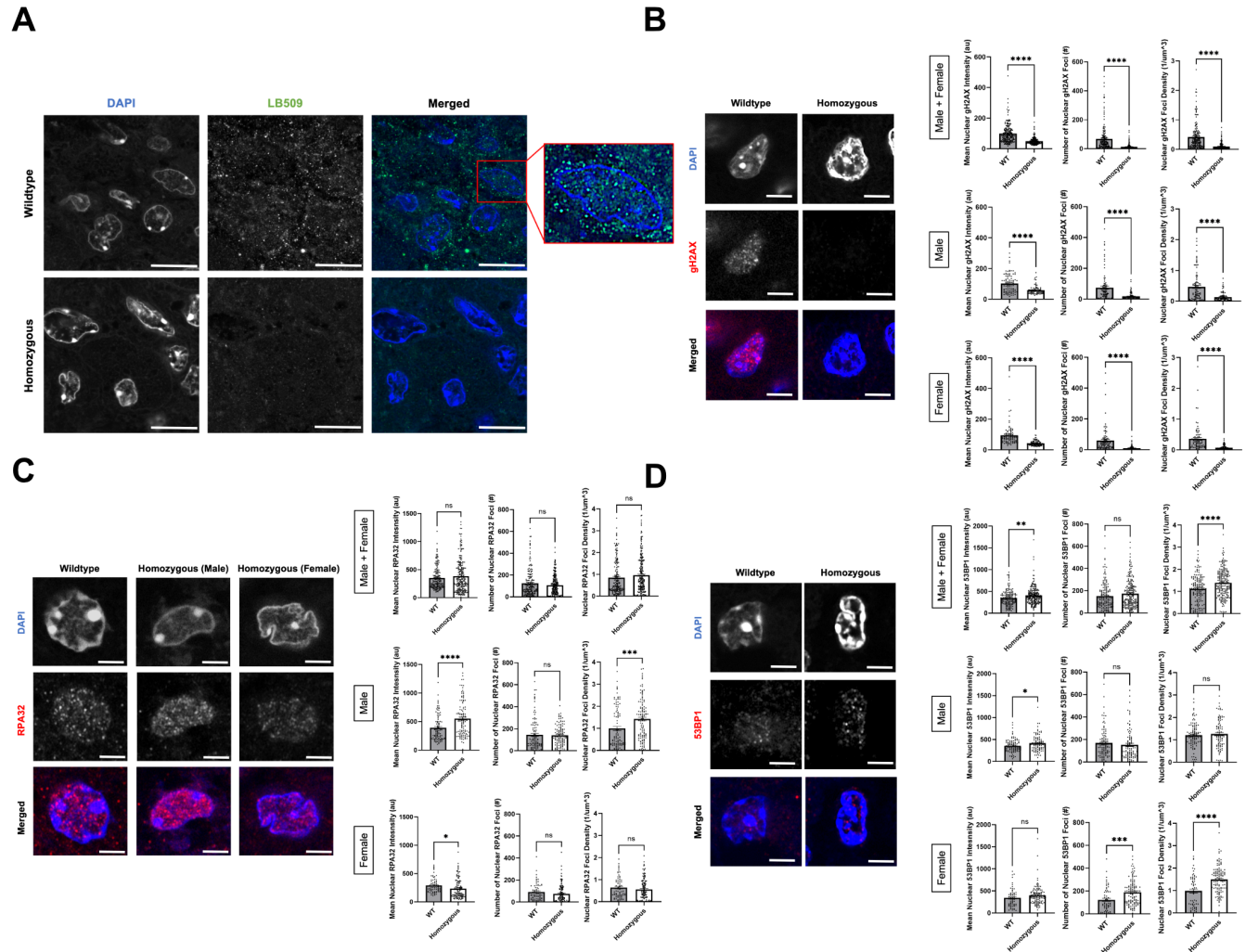


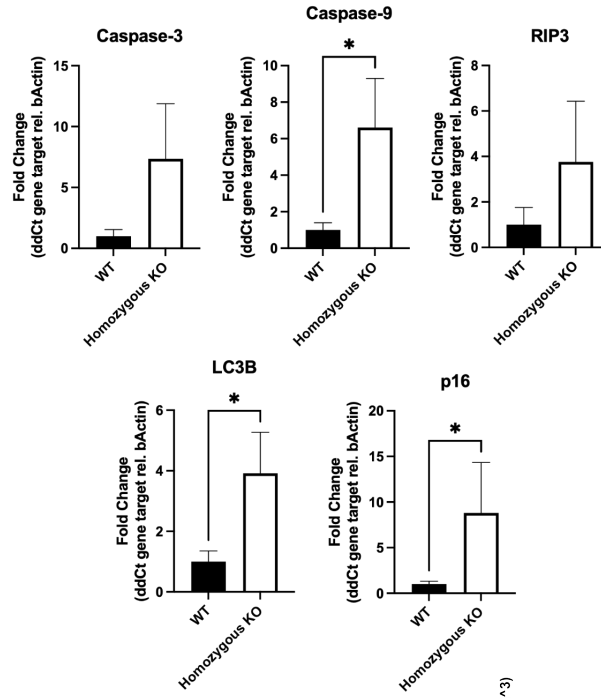
Figure 4.3.3. Alpha-synuclein loss-of-function leads to lower DNA damage signature in P110 perianal tumors. a, b, c, d) Formalin-fixed paraffin-embedded perianal primary tumors from TG3^{+/+}*Snca*^{+/+} (n=5) and TG3^{+/+}*Snca*^{-/-} (n=5) were stained for LB509, γH2AX, RPA32, 53BP1, or DAPI. Stained samples were imaged on the Zeiss 990 confocal microscope with Airyscan processing. Mean intensity, number of foci, and density of foci within DAPI masks were analyzed using Arivis. * p<0.05, ** p<0.01, *** p<0.001, **** p<0.0001 by unpaired T-test. Error bars denote SEM. Scale bar=5μm (a) or 2μm (b,c,d). Quantification from 5 biological replicates (separate animals) per group were performed (n=163-249 nuclei analyzed per condition).

DNA Damage Signature Correlates to Cell Death Phenotypes

To further understand the downstream cellular consequences of altered DNA damage repair mechanisms in αSyn homozygous KO mice, we assayed various cell

death markers via qRT-PCR. These included markers for apoptosis (*Caspase-3*, *Caspase-9*), necroptosis (*RIP3*), autophagic cell death (*LC3B*), and senescence (*Cdkn2a-p16*). We found that perianal tumors of homozygous KO mice exhibited significantly higher gene expression levels of *Caspase-9*, *LC3B*, and *p16* compared to wildtype tumors (Figure 4.3.4A). Furthermore, to directly correlate the DNA damage signatures seen with immunofluorescence (Figure 4.3.3) with *Caspase-9*, *LC3B*, and *p16*, we ran linear regression analyses. Average nuclear mean intensity, foci number, and foci density of γ H2AX and 53BP1 showed no significant associations with these cell death markers (data not shown). However, RPA32 nuclear mean intensity and foci density significantly correlated with the levels of *p16*, with mean foci number close to significance, but did not correlate with *Caspase-9* or *LC3B* levels (Figure 4.3.4B). This indicates that mice with higher RPA32 levels also showed higher *p16* mRNA levels, and this trend was statistically significant. This data suggests that α Syn loss-of-function and the subsequent dysregulation of the DDR this causes leads to a senescence-like phenotype, potentially driving the impaired tumor growth we measured *in vivo*.

a



b

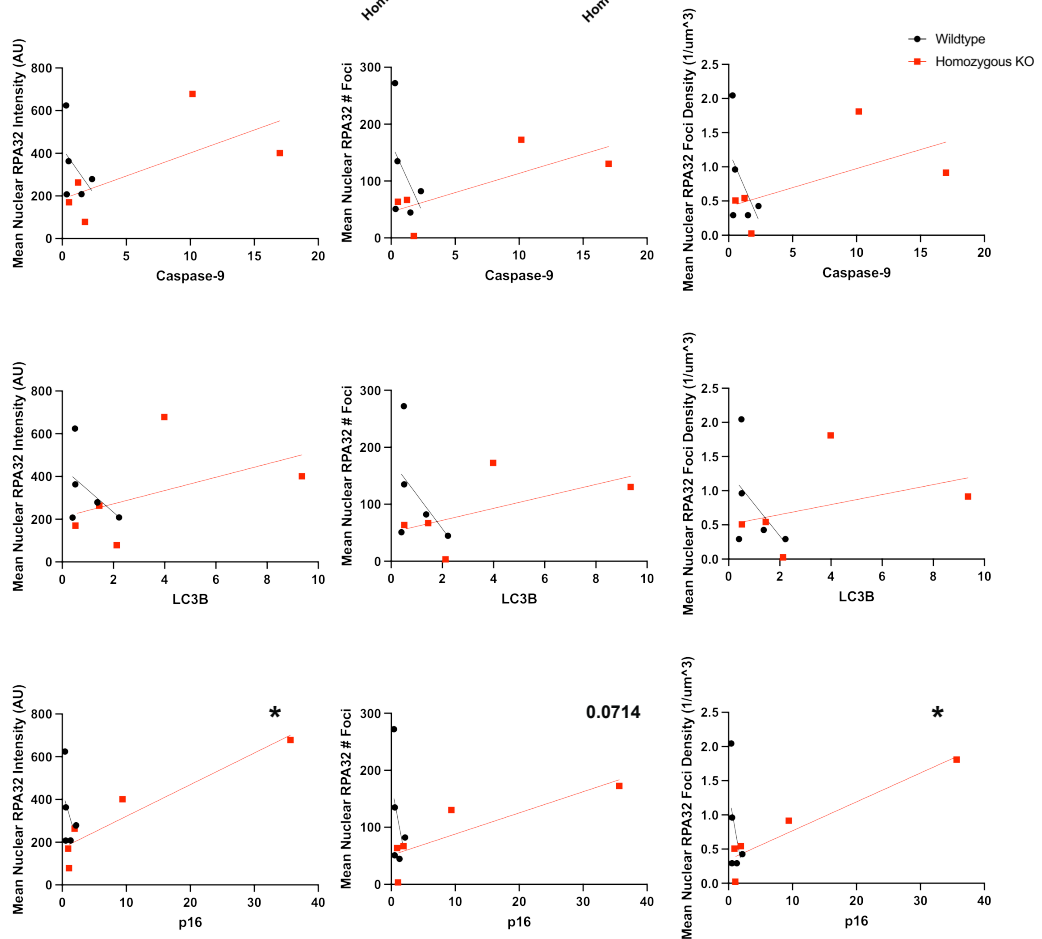


Figure 4.3.4. Alpha-synuclein knockout increases apoptosis, autophagy, and senescence marker expression. a) Total RNA was isolated from perianal primary tumors from TG3^{+/+}*Snca*^{+/+} or TG3^{+/+}*Snca*^{-/-} mice. Using primers against the various genes described in Table S1, qRT-PCR amplification was determined when normalized to *beta-actin* internal control. For analysis, TG3^{+/+}*Snca*^{+/+} (n=5) and TG3^{+/+}*Snca*^{-/-} (n=6). Each sample was run with 2 technical replicates. * p<0.05 by unpaired Mann-Whitney T-test. b) Simple linear regression analysis of mean nuclear intensity, number of foci, and density of foci of RPA32 immunofluorescence (Figure 3) compared to gene expression of *Caspase-9*, *LC3B*, and *p16*. Each point represents a single animal, with TG3^{+/+}*Snca*^{+/+} (n=5, same animals from Figure 3) and TG3^{+/+}*Snca*^{-/-} (n=5, same animals from Figure 3). * p<0.05 by simple linear regression with 95% confidence intervals.

4.4 Discussion

In this study, we extend our knowledge of the molecular connection between PD and melanoma, by uncovering roles for the neurodegeneration-associated protein, α Syn, in melanoma formation and growth. We developed a model to investigate α Syn deficiency on melanomagenesis and metastasis *in vivo* in TG3 mice (671-674). Our data suggest that α Syn loss-of-function significantly delayed melanoma tumor onset in primary pinna tumors and growth of primary perianal tumors. Furthermore, there was a non-significant, but trending, decrease in the metastasis to lymph nodes as measured by *Grm1* mRNA expression. Immunofluorescence staining of the primary perianal tumors revealed a significantly decreased DNA damage signature in *Snca* KO mice, as measured by quantifying nuclear γ H2AX. Interestingly, there were sex-dependent differences in nuclear 53BP1 and RPA32 levels in homozygous KO mice compared to wildtype. Lastly, cell death marker analysis revealed that homozygous KO perianal tumors exhibited significantly higher levels of the apoptosis marker *Caspase-9*, autophagic marker *LC3B*, and senescence marker *p16*. In homozygous KO tumors, RPA32 immunofluorescence

significantly correlated with *p16* mRNA levels, suggesting a potential senescence-like phenotype partly controlled by dysregulated RPA32-dependent DDR.

These results fit into a larger landscape of links between cancer growth, genomic instability, and DDR. Due to their highly proliferative nature, cancers are especially vulnerable to replication-induced DNA damage and genome instability. Inherently, this leads to the high DNA damage signatures seen in many cancer types (676) and melanoma cells upregulate DSB repair pathway proteins (523, 524) to increase metastatic potential (677). Our findings suggest that when α Syn is present (“wildtype” mice), DSB repair pathways remain intact, allowing for cell survival and tumor growth. However, DNA damage from hyperproliferation creates large DNA damage signatures in late-stage tumors (Figure 4.4.1). In contrast, when α Syn is not present (“homozygous KO” mice), there is impaired DSB repair due to a decrease in DSB repair machinery (592). Accumulation of unrepaired DSBs ultimately leads to cell death and senescence phenotypes, with data suggesting that RPA32 levels synergize with senescence marker *p16* upregulation. This could result in the impaired tumor growth and a decreased DNA damage signature (γ H2AX) we detect, since the cells with a high DNA damage signature die and are removed from late-stage tumors (Figure 4.4.1). As a consequence of this unrepaired DNA damage and subsequent cell death, remaining cells may upregulate DDR pathways components 53BP1 and RPA32 and this may be sex dependent (discussed later in this chapter). Overall, our findings suggest that α Syn upregulation in melanoma may be part of a mechanism to improve DSB repair, allowing cells to evade the programmed cell death that would normally be triggered by high DSB levels, similar to what is seen with the upregulation of other DSB repair pathway proteins (523, 524).

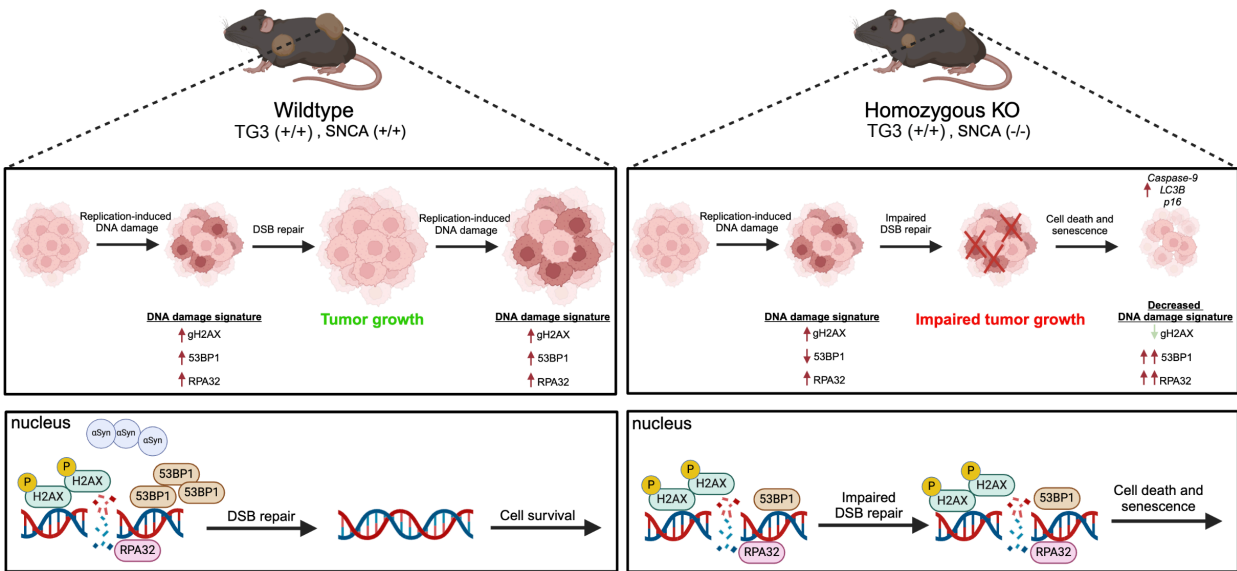


Figure 4.4.1. Schematic summary of proposed mechanism.

Loss of α Syn resulted in upregulation of various cell death and senescence markers, likely downstream of dysregulated DDR and resulting in the decreased tumor growth *in vivo*. Caspase-9 is an initiator caspase in the intrinsic apoptosis pathway that is activated when cytochrome c is released from mitochondria in response to death signals (678). LC3B, microtubule-associated protein 1 light chain-3B, is an autophagic protein that plays a role in cell death and autophagy. Autophagic cell death, also known as type 2 cell death, is characterized by large-scale autophagic vacuolization of the cytoplasm (679, 680). In general, autophagy can protect cells from stresses like nutrient depletion or starvation, but excessive autophagy can lead to cell death. Furthermore, LC3B can also promote apoptosis through interactions with the extrinsic apoptotic factor Fas (681). Lastly, p16(INK4a) is a cyclin-dependent kinase inhibitor that is often expressed in senescent cells, which have stopped growing due to stress (682). This tumor suppressor gene is commonly mutated in human tumors, allowing precancerous lesions to bypass

senescence (683). These processes have all been associated with DNA damage accumulation and implicated in melanoma, where suppression of Caspase-9 and p16 and over-stimulation of LCB3 have been linked to melanomagenesis, contributing to disease progression and resistance to therapy (684-693). Targeted therapy of some of these modulators is currently being explored as potential therapeutic strategies for melanoma (687, 694). Interestingly, our data suggesting a significant synergistic effect of RPA32 protein levels and *p16* expression coincides with previous reports of “RPA exhaustion”. This is a phenomenon by which persistent DNA damage can lead to replication catastrophe and cells then acquire senescent traits and is associated with various age-related pathologies (695, 696). It is plausible that α Syn loss-of-function can induce such a pattern, however further investigation is necessary to elucidate mechanistic insight.

The mechanism of how α Syn regulates DNA DSB repair is still an area for investigation. Our previous work uncovered a novel role for α Syn in the recruitment of 53BP1 to ribosomal DNA DSBs, downstream of γ H2AX signaling and upstream of MDC1 activity, in the SK-Mel28 melanoma cell line (592). Furthermore, α Syn has been implicated in regulating DSB repair through a DNA-PK-dependent manner in Hap1 cells (443). These data suggest that α Syn may modulate the NHEJ repair pathway, where both 53BP1 and DNA-PK are important. However, the choice between NHEJ and HR is particularly interesting and at the intersection of neurodegeneration and cancer. NHEJ is thought to be the primary DSB repair pathway in post-mitotic cells, like neurons, since it does not require a sister chromatid to act as a template, yet is more error prone (537). In contrast, there is growing evidence that different cancers rely primarily on the error-free HR to counteract the genomic instability associated with replicative stress (697). Studies

have shown that a high frequency of melanoma patients harbor mutations in HR-associated genes (698-700), making these tumors vulnerable to immunotherapies and treatments that target HR (698, 699, 701). Yet, the choice between HR and NHEJ is a growing topic in the field (536). In our data, α Syn loss-of-function resulted in decreased γ H2AX intensity and foci, sex-dependent differences in RPA32 intensity (increased in males, decreased in females), and an increase in nuclear 53BP1 (more robust response in females). This potentially suggests that α Syn upregulation in the TG3 melanoma mouse line is important for functional DDR in a sex dependent way and that when α Syn is no longer present and there is a buildup of unrepaired DNA breaks, male mice can better upregulate HR machinery (RPA32) in the surviving cells, while female mice can better upregulate NHEJ machinery (53BP1) in the surviving cells to try to compensate. Further investigation is necessary to uncover the specific mechanism of how α Syn is influencing the DDR as a function of melanomagenesis and sex *in vivo*.

The sex differences we detect (in tumor onset, growth, and DDR components) are interesting since male sex is a recognized risk factor to the prevalence and outcome of both PD and melanoma. In PD, the prevalence is twice as high in males compared to females and is frequently associated with earlier disease onset (32, 702); men may develop a postural instability-dominant phenotype, which includes freezing of gait and falling (32, 33); and men experience more sleep and cognitive issues associated with the disease, such as REM sleep behavior disorder (33) and mild cognitive impairment with a more rapid progression to dementias (34, 35). In melanoma, men have a higher risk of developing melanoma over the age of 50 and ethnicities (240); men exhibit a higher risk of melanoma progression and metastasis than females (240, 703), with a greater risk of

mortality (239, 703, 704); and pathologically, thicker and more ulcerated tumors were observed in men (238). In both diseases, there have been many hypotheses as to what is driving these sex differences, including the involvement of sex hormones, the immune system response, and potential environmental exposures. However, in the context of our study, it is interesting to note previously reported sex disparities in DDR pathways. Others have found a greater accumulation of somatic mutations in male cells compared to female cells (705), suggesting decreased DNA damage repair. Females have an increased capacity to repair DNA damage by base excision repair (BER) compared to males in mice (706). Additionally, analysis of molecular difference in 13 cancers from The Cancer Genome Atlas database revealed that DNA repair genes are expressed at higher levels in female patients (707). Furthermore, steroid hormones can regulate DSB repair, both NHEJ and HR (708). Specifically, androgen receptors stimulate the activity and expression of DNA-PK in the NHEJ pathway (709), estrogens positively regulate the expression of NBS1 (710), and steroid hormones can regulate HR (711, 712). Our tumor growth and immunofluorescence data suggest that α Syn plays a role in modulating DSB repair pathways in a sex-dependent manner. Females may be better at upregulating compensatory mechanisms to counteract the unrepaired DNA damage (53BP1 upregulation), and therefore are more resistant to negative effects of α Syn loss-of-function in tumor onset and growth phenotypes. Males may be more vulnerable to DNA damage dysregulation as a consequence of α Syn loss-of function and serve as a more appropriate candidate for therapeutics that target α Syn in melanoma treatment regimens. For example, our data showed a direct relationship between RPA32 increase and *p16* mRNA senescence marker upregulation in male mice and our *in vitro* data, in the male

human melanoma cell line, SK-Mel28, α Syn KO significantly impaired growth phenotypes (592).

In summary, the newly generated mouse model, TG3^{+/+}*Snca*^{-/-}, allows for the investigation of the function of α Syn in malignant melanoma. It is possible that individuals with upregulated expression of α Syn may predispose them to Lewy body aggregation in neurons (427, 442), but also melanocytic transformation and melanoma progression. The resulting loss-of-function due to α Syn aggregation (in PD) or gain-of-function of α Syn by increased expression without aggregation (in melanoma) would have differential effects on DNA damage repair pathways, potentially contributing to either neuronal cell death or melanoma cell growth, respectively. Our findings demonstrate the impact of α Syn on melanoma onset, progression, and metastasis in a sex-dependent manner and provide novel therapeutic targets focused on reducing α Syn-mediated DNA repair in melanoma.

4.5 Methods

Mice

The transgenic TG3 mice (671-674), were established at the Department of Chemical Biology, Rutgers University, Piscataway, USA and provided by Dr. Suzie Chen. Alpha-synuclein KO mice (C57BL/6N-*Sncatm1Mjff/J*) were obtained from Jackson Laboratories (strain #016123, RRID:IMSR_JAX:016123). Homozygous alpha-synuclein KO mice were crossed with TG3 heterozygous mice and double heterozygote F1 mice were crossed to each other to generate F2 mice for analysis. Genotyping of mice was carried out by Transnetyx Inc. and primer sequences and protocols are available upon

request. For all analyses, homozygous transgenic TG3 *Snca*^{+/+} and TG3 *Snca*^{-/-} animals (litter mates) were used. Mice were housed in OHSU's Department of Comparative Medicine (DCM) facilities in a light-dark cycle vivarium. Animals were maintained under *ad libitum* food and water diet. All animal protocols were approved by OHSU IACUC, and all experiments were performed with every effort to reduce animal lives and animal suffering, according to the US National Research Council's Guide for the Care and Use of Laboratory Animals, the US Public Health Service's Policy on Humane Care and Use of Laboratory Animals, and Guide for the Care and Use of Laboratory Animals.

Tumor growth analysis

Starting at P30, mice underwent isoflurane anesthesia every 10 days to assess weight and tumor growth. Researchers were blinded to condition. To quantitate the severity of melanoma progression, detailed observation and photodocumentation was used to assign numerical scores of 0 to 5 to the thickness of pinna tumors (see Figure 4.8.2 for detailed description) or quantitative measurements for thickness of perianal tumors. For pinna tumors, 0=tumor not palpable or visible; 1=individual small, clearly recognizable nodes or elevations in skin; 2=small, numerous recognizable nodes or elevations; 3=significantly thickened ears, clearly nodular tumors; 4=severely thickened ears or coarse tumors; 5=extreme tumor growth with risk of ulceration. Tumor onset was designated as time when tumor changed from 0 to 1. For perianal tumors, a ruler was used to manually measure the length of the perianal tumor in centimeters.

Immunofluorescence staining

For immunofluorescence staining of perianal tumors, 5µm sections of formalin-fixed and paraffin-embedded tissue blocks were deparaffinized and bleached in a H₂O₂ solution for 1 hour at RT (1% dipotassium phosphate, 0.5% potassium hydroxide, 3% hydrogen peroxide). Tissue underwent antigen retrieval overnight at 56C (10 mM Tris base, 1mM EDTA solution, 0.05% Tween 20, pH 9.0). Samples were permeabilized in 0.25% Triton X-100 in PBS for 10 minutes and blocked in 2% FBS/1% BSA in PBS for 2 hours and then placed in the primary antibody overnight at 4C. The next morning, samples were washed in 1x PBS and placed in secondary antibody for 1 hour at 37C. Samples were washed 4 times in 1x PBS. The third wash contained DAPI (2.5µg/ml) for 20min. Coverslips were mounted using CFM2 antifade reagent and sealed with BioGrip. All immunofluorescence images were taken on a Zeiss Laser-Scanning Confocal Microscope 980 with Airyscan and analyzed in Arivis Software. Mean intensity was measured after imposing DAPI masks over each nucleus. All cells within a 63x image were analyzed and numbers of n are provided in each figure legend. Statistical significance was assigned using T-test.

Antibody specifics were as follows: LB509 (Abcam #27766, RRID:AB_727020, 1:500), RPA32 (Bethyl #A300-245A, RRID:AB_210547, 1:1000), γH2AX (Cell Signaling #9718, RRID:AB_2118009, 1:500), 53BP1 (BD Biosciences #612522, RRID:AB_2206766, 1:1000).

Quantitative RT-PCR

Pinna tumors, perianal tumors, and lymph nodes were homogenized in RNeasy mini kit buffer (Qiagen) using a hand-held tissue homogenizer followed by Qias shredder centrifugation (Qiagen). Total RNA was isolated using the RNeasy mini kit (Qiagen) according to the manufacturer's instructions. RNA concentration was measured with a NanoDrop spectrophotometer and cDNA was synthesized from 500ng RNA with M-MLV reverse transcriptase (Promega). Analysis of mRNA expression was performed using quantitative Real-Time PCR on the QuantStudio 3 (Applied Biosystems). A volume of 1 μ l cDNA template, 1 μ l of forward and reverse primers (each 10 μ M) and 10 μ l of SYBR Green I (Roche) were combined to a total volume of 20 μ l. Primers used are described in Table 4.8.1. Each sample was analyzed in duplicates. The target cDNA was normalized to β -Actin levels. Statistical significance was assigned using T-test.

Statistical analysis

Beyond individualized analysis within each assay methodology, all data was processed using GraphPad Prism version 9.0 (RRID:SCR_002798). Data was analyzed using T-test, unless stated otherwise, and considered statistically significant if $p < 0.05$. All data was presented as a mean +/- standard error of the mean (SEM).

4.6 Acknowledgements

All immunofluorescence imaging could not have been possible without help from Stefanie Kaech Petrie, Felice Kelly, and Hannah Bronstein in the OHSU Advanced Light Microscopy Core (RRID:SCR_009961). We thank Dr. Pamela Cassidy (OHSU) for the invaluable discussions. Thank you to Dr. Suzie Chen (Rutgers University) for providing the TG3 mouse line and help with genotyping protocols. We thank Dr. Sebastian Staebler and Dr. Anja Bosserhoff (Friedrich-Alexander University of Erlangen-Nurnberg) for the invaluable advice and help with TG3 mouse line management, qRT-PCR protocols, and IF protocols. Lastly, many thanks to Unni Lab members who helped with the revision process: Dr. Carlos Soto Faguas, Dr. Elizabeth Rose, Anna Bowman, Elias Wisdom, Jessica Keating, and Samuel Kim.

Funding

The work was supported by:

National Institute on Aging of the National Institutes of Health F30AG082406
National Institute of Health R01NS102227
National Institute of Health P30NS061800
National Institute of Health P30CA065823
Melanoma Research Alliance
Michael J Fox Foundation
Kuni Foundation
Melanoma Research Foundation Medical Student Research Award
Oregon Partnership for Alzheimer's Research

4.7 Author Contributions

Conceptualization: MRA, VKU

Data Curation: MRA, VKU

Formal Analysis: MRA, VKU

Funding Acquisition: MRA, VKU

Investigation: MRA

Methodology: MRA, VKU

Project Administration: MRA, VKU

Resources: MRA, SC, VKU

Software: MRA, VKU

Supervision: MRA, VKU

Validation: MRA, VKU

Visualization: MRA

Writing- original draft: MRA, VKU

Writing- review & editing: MRA, SC, VKU

4.8 Supplemental Material

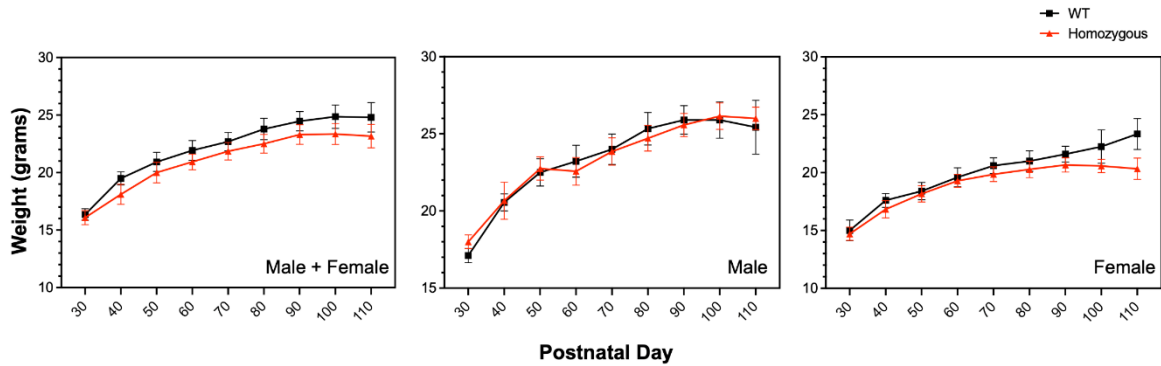
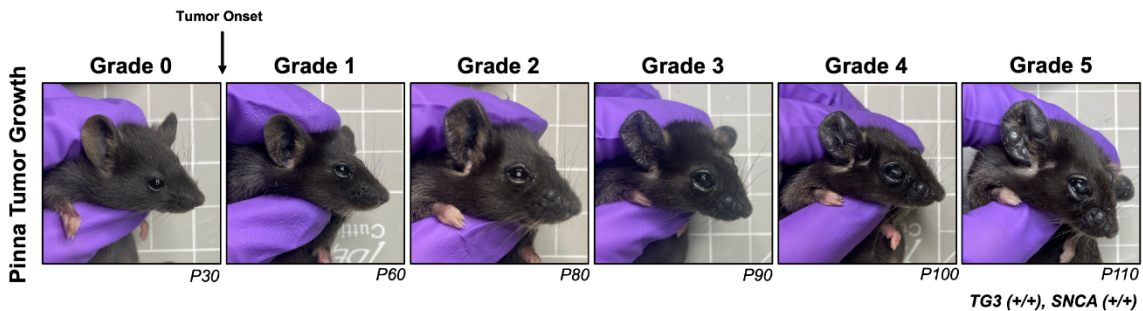


Figure 4.8.1. Alpha-synuclein knockout does not affect mouse weight.

Weight of TG3^{+/+}*Snca*^{+/+} (n=15) and TG3^{+/+}*Snca*^{-/-} (n=14) from P30 to P110 (endpoint). Analysis was further stratified by sex with TG3^{+/+}*Snca*^{+/+} male (n=10), TG3^{+/+}*Snca*^{+/+} female (n=5), TG3^{+/+}*Snca*^{-/-} male (n=7), and TG3^{+/+}*Snca*^{-/-} female (n=7). Error bars represent Standard Error of the Mean (SEM). Statistical testing by two-way ANOVA. Weight is represented in grams.



Grade	Description
0	Tumor not palpable or visible
1	Individual small, clearly recognizable nodes or elevations in skin
2	Small, numerous recognizable nodes or elevations
3	Significantly thickened ears, clearly nodular tumors
4	Severely thickened ears or coarse tumors
5	Extreme tumor growth with risk of ulceration

Figure 4.8.2. Representative images and description of pinna tumor grading scale.

Primer	Forward (5'-3')	Reverse (5'-3')
β -Actin	TGGAATCCTGTGGCATCCATGAAAC	TAAAACGCAGCTCAGTAACAGTCCG
Grm1	GGGCAGGGAACGCCAATTCT	TGGAAGGGCTGCTGGGAGGG
Caspase-3	AGCAGCTTTGTGTGTGTGATTCTAA	AGTTTCGGCTTTCCAGTCAGAC
Caspase-9	TCCTGGTACATCGAGACCTTG	AAGTCCCTTTCGCAGAAACAG
RIP3	AAGTGCAGATTGGGAACTACAACCTC	AGAATGTTGTGAGCTTCAGGAAGTG
LC3B	CCCCACCAAGATCCCAGT	CGCTCATGTTACGTGGT
Cdkn2a (p16)	CCCAACGCCCCGAACCT	GCAGAAGAGCTGCTACGTGAA

Table 4.8.1. Primers used in qRT-PCRs.

[Jump Back to Table of Contents](#)

Chapter 5: Discussion

5.1 Summary

The studies presented herein further demonstrate the robust connection between PD and melanoma through human epidemiological, human cell *in vitro*, and murine *in vivo* methodology. Utilizing both human and mouse models, the translational implications for this research are robust. In Chapter 2, I have leveraged large human datasets to characterize melanoma pathophysiology in pPD populations. In addition, I have uncovered novel synergistic relationships between melanocytic lesions, non-melanocytic skins disorders, and other pPD disorders to provide clinical criteria for the development of PD in melanoma populations. I have explored the mechanistic cellular and molecular connections between PD and melanoma, by investigating the role of α Syn in the DDR pathway in Chapters 3 and 4. I have uncovered a novel role for α Syn in the nucleolus and in nucleolar DNA DSB repair, via 53BP1 recruitment, utilizing an *in vitro* human melanoma cell line. Furthermore, α Syn's function in the DDR was confirmed in translational studies in an *in vivo* TG3 melanoma mouse model. Together, these data suggest that melanoma may upregulate the expression of α Syn to facilitate the DDR, and this has significant downstream cellular consequences, such as increased proliferation, migration, and invasion, while inhibiting senescence pathways. This underlying mechanism may connect these two diseases clinically and contribute to the increased incidence of PD in melanoma patients. It is plausible that individuals with high α Syn expression are predisposed to both LB aggregation (PD) and melanocytic transformation (melanoma), which could be leveraged for diagnostic and therapeutic purposes.

5.2 DNA Damage Repair Pathways

Mechanistic Insight

In Chapter 3, I uncovered a role for α Syn downstream of ATM-mediated phosphorylation of H2AX and upstream of MDC1-mediated recruitment of 53BP1 to rDNA DSB at the nucleolar cap. In Chapter 4, I further validated the role of α Syn in 53BP1 recruitment and RPA32-mediated downstream cellular phenotypes. More specific investigation into the α Syn-mediated recruitment of 53BP1 and how this influences repair pathway choice would be a useful future direction. Recent publications have suggested that the recruitment of 53BP1 to damaged sites requires γ H2AX-MDC1 binding, followed by ubiquitination of K13-K15 on H2AX by the RING-type E3 ubiquitin ligases RNF8 and RNF168 (641-644) and methylation of histone H4 on lysine 20 (645, 646). It is possible that α Syn works within this post-translational modification cascade in conjunction with RNF8 and/or RNF168 (Figure 5.2.1). It is also plausible that α Syn acts in the “docking” of 53BP1 to the DNA damage sites (Figure 5.2.1), considering previous evidence that α Syn can directly bind to DNA (515, 516, 713) and is present at the DSB site (Figure 3.3.4). Interestingly, a recent study identified PRMT5 (Protein Arginine Methyltransferase 5) as a protein interactor of α Syn through proteomic analysis (652). PRMT5 is important in the docking of 53BP1 to DSB sites through methylation and stabilization (653, 654). Given α Syn’s well-studied role in SNARE-dependent vesicle docking at the presynaptic terminus (405-407), it is interesting to consider whether similar molecular characteristics play a role in MDC1, PRMT5, and/or 53BP1 docking. Once 53BP1 docking occurs, it is phosphorylated further by ATM, leading to recruitment of 53BP1 effector proteins RIF1 and PTIP, both of which protect the DSB ends from hyper-resection, ultimately inhibiting

HR and promoting NHEJ. However, it has been shown that DSB repair in heterochromatin by HR also requires 53BP1, suggesting that the role of 53BP1 may vary dependent on the context (627). How nucleolar α Syn-mediated 53BP1 recruitment fits into these dichotomous pathways needs to be explored.

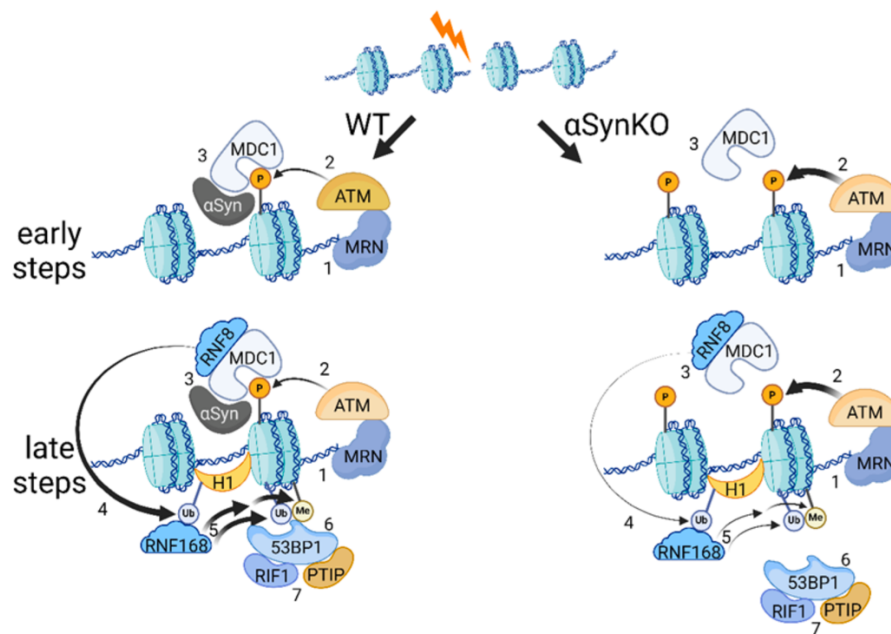


Figure 5.2.1. Proposed model for how α -syn regulates 53BP1 recruitment to sites of DSBs. *Left side:* WT condition. *Right side:* α -syn KO condition. DSB signaling begins with early events, including recognition of the break site by the MRN complex (1) and subsequent recruitment and activation of ATM, which phosphorylates H2AX, creating gH2AX (2). MDC1 directly binds γ H2AX, and my data suggest that α Syn facilitates this interaction (3). Later events include recruitment of ubiquitin ligases RNF8 & UBC13 (UBC13 not shown), which ubiquitinates Histone 1 (4) and L3MBTL2 (not shown), leading to recruitment of a second ubiquitin ligase, RNF168, which is responsible for H2AK13/15, L3MBTL1 and JMJD2A ubiquitination, exposing a ubiquitinous H4K20 methylation mark (5). The combination of H2AK13/15 ubiquitination and exposed H4K20 methylation recruits 53BP1 to DSBs (6). Once 53BP1 is recruited, it is phosphorylated further by ATM (not shown), leading to recruitment of 53BP1 effector proteins RIF1 and PTIP (7). RIF1 and PTIP both act to protect DSB ends from hyper-resection, inhibiting HR and promoting NHEJ. In the α -syn KO condition, my preliminary data suggest that H2AX phosphorylation is increased (2), while MDC1 (3) and 53BP1 (6, NHEJ component) recruitment are both decreased, and recruitment of BRCA1 (HR component) is unaffected (not shown). Aim 1

will test at which steps in this DNA damage response signaling pathway α -syn regulates DSB repair.

Additionally, a recent publication has suggested that tumor suppressor RASSF1A acts as a scaffold during initial nucleolar DNA damage response and promotes local ATM signal amplification within the damaged repetitive heterochromatic elements, which then leads to H2BS14 phosphorylation to silence RNA polymerase I at the nucleolar interior (714). Furthermore, Tsaridou et al. proposed that RASSF1A subsequently translocates to the nucleolar cap with the rDNA DSBs to facilitate the recruitment of 53BP1. RASSF1A is commonly silenced during malignant transformation, which is linked to early cancer onset and worse disease outcome (715). It is plausible that in the context of a cancerous state like melanoma, where RASSF1A silencing leads to impaired rDNA DDR and increased genomic instability, melanoma cells upregulate compensatory machinery, like α Syn, that help facilitate 53BP1 recruitment in the absence of RASSF1A. Testing whether α Syn is involved in this nucleolar-specific mechanism could indicate a complex multi-protein system adapted to prevent genomic instability.

One way to test these hypotheses is through ICC approaches. After I-Ppol treatment, WT and α Syn KO SK-Mel28 cells could be assayed for levels of each factor and their respective epitope enrichment (MDC1, RNF8, Histone 1, L3MBTL2, RNF168, H2AK15ub, H4K20me2, 53BP1, pSer25/29-53BP1, RIF1, PTIP, RASSF1A). The use of other pharmacological inhibitors could aid in the discovery of α Syn's mechanistic role in the DDR pathways, including inhibitors more selective for NHEJ (Ku60/70, DNA ligase IV) or HR (RAD51, DNA ligase I). Although effective, pharmacological inhibitors also possess experimental limitations as well, including insufficient inhibition of target if high enough concentrations aren't used and off target inhibition leading to adverse

downstream effects. Other methods could be utilized *in vitro*, as well. Performing a co-immunoprecipitation assay or proximity ligation assay between α Syn and MDC1, PRMT5, 53BP1, and/or other DDR proteins could reveal whether α Syn is directly binding to these repair factors or rather indirectly affecting DSB repair pathway choice. These techniques have been previously successful for nucleolar-specific DDR questions (716). Furthermore, chromatin immunoprecipitation could be utilized to validate the diminished recruitment of various DDR factors to the rDNA DSB in α Syn KO cells to better understand where in the pathway α Syn is functioning, as previously described (524, 717-719). Lastly, live-cell fluorescence imaging experiments could be completed to investigate the kinetics of recruitment of each factor using a set of GFP-tagged constructs.

Although Chapter 3 provides mechanistic insight into the role of α Syn in the nucleolar DSB DDR *in vitro*, Chapter 4 provides only an initial analysis *in vivo*. One major limitation in Chapter 4 was the lack of temporal data in tissue analyses (Figure 4.3.3. and Figure 4.3.4.). Due to animal breeding constraints, the experimental cohort of mice were all sacrificed at P110, for consistent analysis. Therefore, my proposed mechanism of α Syn's involvement in the DDR at prior timepoints (Figure 4.4.1) is speculative and based on my previous data from Chapter 3. Immunofluorescence optimization obstacles limited my ability to stain for nucleolar-specific markers, which could validate my *in vitro* studies and determine whether the dysregulation in γ H2AX, RPA32, and 53BP1 in α Syn KO mice were specific to the nucleolus. Overall, these *in vivo* limitations hinder my ability to address the translatability of my Chapter 3 findings, and further investigation is warranted to elucidate the role of α Syn in nucleolar DDR *in vivo*. Melanoma mouse model choice will be discussed further in Chapter 5.6.

Lastly, the dysregulation of γ H2AX seen as a function of α Syn knockout in both Chapter 3 *in vitro* and Chapter 4 *in vivo* models raises mechanistic questions. For example, is the γ H2AX elevation, seen in Chapter 3 and hypothetically proposed at earlier time points of tumor development in Chapter 4, mediated by increased activation of one or more of the three PI3K kinase family members that are known to phosphorylate H2AX, including ATM, ATR, or DNA-PK (720, 721)? My results suggest that both ATM and ATR facilitate the elevated γ H2AX levels in α Syn KO cells at baseline (Figure 3.3.2) and that ATM facilitates the elevated γ H2AX levels in α Syn KO cells after I-Ppol treatment, although ATR and DNA-PK had moderate effects (Figure 3.3.5). It is also possible that there is reduced activity of γ H2AX phosphatase, PP2A, whose inhibition has been shown to lead to persistent γ H2AX foci (722) and whose activity is regulated by α Syn and its aggregation (369, 723). There are additional γ H2AX phosphatases as well to consider, like PP2C and PP4 (724-726). Future comparison of levels of phospho-proteins known to be targets of ATM, ATR, and DNA-PK phosphorylation, as well as those that are dephosphorylated by PP2A, PP2C, and PP4 could provide valuable insight into whether alterations in activity of one or more of these kinases/phosphatases causes the increase in γ H2AX in my results. Furthermore, distinct functions for ATM and ATR have been previously established in the nucleolar DDR cascade (574); how α Syn fits into these DDR kinase signaling pathways is worth further investigation. These phospho-proteomics studies could be performed in WT and α Syn KO cells at baseline (see Appendix A.2 for preliminary data), during I-Ppol or CRISPR/Cas9 treatment when rDNA DSBs are occurring, or during various stages of melanomagenesis and tumor growth in an α Syn KO *in vivo* mouse line. Further validation in the SK-Mel28 system is important to

determine the enriched target relevance to α Syn-regulated DSB repair, via kinase inhibitors that target the modifications discovered.

Other Forms of DNA DSB Repair

It is possible that α Syn may facilitate other forms of DNA repair, like alternative NHEJ (aNHEJ) or replication stress-induced damage. aNHEJ, also known as microhomology-mediated end joining (MMEJ), was first discovered in NHEJ-deficient cells, yet were still able to perform end-joining (727). aNHEJ uses microhomology regions near the break site on each end to ligate the two ends together (540). Similar to HR, aNHEJ uses poly ADP-ribose polymerase 1 (PARP1), CtIP, and the MRN complex at the early stages of repair. However, this pathway then diverges and uses Pol θ to synthesize new DNA (728). Compared to NHEJ, aNHEJ incorporates much larger deletions into the repaired product and therefore operates with slower kinetics (729). However, a recent study found that α Syn facilitates DSB repair through a DNA-PK dependent manner, shunting cells away from aNHEJ and towards NHEJ (443). Blocking aNHEJ with a Pol θ inhibitor showed no significant differences in α Syn KO cells compared to WT (443). However, these experiments were not done in melanoma models. There is evidence that metastasis suppressor, NME1, modulates DSB repair pathway choice by enhancing aNHEJ and inhibiting NHEJ and HR in melanoma (524). Further investigation for the role of α Syn in aNHEJ within a melanoma context through the usage of pharmacological inhibitors or pathway specific repair plasmids is warranted.

α Syn has also been previously implicated in replication stress-induced DNA damage in yeast (510). While cancerous hyperproliferation can indirectly cause replication stress, it can also cause DNA damage from ROS, incomplete DNA repair, and telomere shortening, all of which can subsequently lead to DSBs. Although the downstream DSB repair pathways are similar between replication stress-induced DSBs and the other types of DSBs, the initiation and recognition of the DNA damage is distinct (730). When replication stress occurs, stalled replication forks will form due to various factors, including DNA lesions, nucleotide depletion, or protein-DNA crosslinks. Tension at these forks because of continued DNA unwinding to downstream DNA eventually cause fork collapse, which in turn prompts endonucleases to process the exposed single-stranded DNA into a DSB. This type of DSB is unique in that they are recognized predominantly by ATR at the single-stranded DNA stage to initiate the DDR (731-733). To test whether α Syn could protect against replication stress-induced DNA damage, as was previously shown to occur in yeast (510), I treated SK-Mel28 cells with hydroxyurea, a compound known to induce ATR-dependent replication stress-induced DSBs. I did not find evidence in this one experiment that α Syn was important for repairing DNA damage induced by hydroxyurea (data not shown). However, more investigation is warranted, as this type of DNA DSB is more biologically relevant to a hyperproliferative cancerous state, like melanoma, and current research is uncovering ways to leverage this type of DDR in cancer therapy (734). In addition, UV irradiation has been shown to induce replication stress DNA DSB formation through an ATR-dependent mechanism (735). Taken together, this type of ATR-dependent DSB mechanism may be important in melanoma pathogenesis and therefore the role of α Syn in this process should be explored, especially

within the context of rDNA and the nucleolus. It is important to note that in Chapter 3, ATR inhibition did not completely attenuate the phenotype seen in I-Ppol-treated α Syn KO cells (Figure 3.3.5), yet the methods for initiating these rDNA DSBs do not fully recapitulate an ATR-dependent replication stress mechanism. Future experiments utilizing UV irradiation or other replication stress chemical inductors, like camptothecin, etoposide, cisplatin, or aphidicolin could be used (736) (see Appendix A.2 for preliminary data).

DSB Inducer Limitations

As just mentioned, inducing DSBs both *in vitro* and *in vivo* is challenging, with each technique possessing strengths and weaknesses. In this section, I will be highlighting the ones used throughout the chapters of this dissertation and alternative approaches.

There are many techniques to induce DNA DSBs in global non-predictive genomic positions, including chemical agents, UVR, and IR treatments. In Chapter 3, bleomycin was used as a drug-induced technique in SK-Mel28 cells. Bleomycin causes DSBs in DNA by binding to specific DNA sequences, particularly guanine-rich regions, and then generating free radicals through a reaction with iron (Fe^{2+}) and oxygen, which ultimately leads to the cleavage of the DNA backbone (737, 738). Even more efficient than bleomycin at inducing DSBs are the bicyclic enediynes. These molecules, which include neocarzinostatin, form a highly reactive para-benzyne diradical that can abstract hydrogens from the C-1', C-4' and C-5' positions of deoxyribose moieties in both DNA strands, and subsequently cause DSBs (739). Another major class of drugs that induce

DSBs are topoisomerase II inhibitors, which include etoposide, doxorubicin, mitoxantrone, and others. These drugs primarily work by trapping the topoisomerase II enzyme in a complex with cleaved DNA, preventing re-ligation, and leading to DSBs through a replication stress-dependent mechanism (740, 741). IR damages DNA through direct interactions or indirectly by generating hydroxyl radicals ($\bullet\text{OH}$) through radiolysis of water. This leads to oxidative base modifications, SSBs with altered chemical ends, and clustered damage, which can escalate into DSBs when both strands are affected. UVR on the other hand, induces damage by forming covalent bonds between adjacent pyrimidine bases, creating bulky distortions such as cyclobutane pyrimidine dimers and pyrimidine photoproducts. UV-A radiation differs from UV-B and UV-C because it primarily causes DNA damage through photooxidation reactions, leading to the formation of oxidative lesions and direct strand breakages. UV-induced lesions interfere with replication and transcription, sometimes leading to SSBs and DSBs. Cells rely on nucleotide excision repair (NER) and other pathways to correct UV-induced damage, but if left unrepaired, these lesions contribute to genomic instability and mutations (739, 742, 743).

It is important to note that the way in which the DSB is produced will result in preferential choice of repair pathway, either HR or NHEJ. Evidence suggests that HR and aNHEJ is recruited in the repair of breaks with more complex multiple damaged ends during late S and G2 phases of the cell cycle. In one study, where HeLa cells were treated with either bleomycin or IR, researchers found that cells treated with bleomycin preferentially employed NHEJ repair processes due to less complex breaks (744). Conversely, IR-induced DSBs usually contain overhanging 3' and 5' ends and are

surrounded by additional forms of DNA damage, termed complex or clustered lesions (745). Therefore, IR-induced DSBs may preferentially induce HR-mediated repair. Despite seeing similar effects of α Syn KO between both bleomycin and IR in Chapter 3, it would be worth using other global DSB-inducing methods that specifically target HR preference, like topoisomerase II inhibitors that rely on DNA replication machinery. If no effects of α Syn KO are seen, I can be more confident in α Syn's involvement in NHEJ repair. In addition, active euchromatin is more vulnerable to IR than heterochromatin (739, 746-748), therefore the α Syn KO effects seen in SK-Mel28 treated with IR may be more reflective of DSBs in euchromatin regions, like the nucleolus.

As one can imagine from the mechanisms of action described above, these techniques to induce global DSBs are “dirty”, in the sense that they cause both SSBs and DSBs in non-discriminatory regions of the genome. For example, bleomycin treatment has been shown to produce one DSB for every ten SSBs (749, 750), topoisomerase class I inhibitors, like camptothecins, generate transient SSBs (751, 752), and UV and IR methods have also been shown to create various types of DNA lesions (743). Alternatively, endonuclease-derived techniques can be used to induce DSBs in a more selective manner, which can be useful in targeting rDNA regions in the nucleolus. Used in Chapter 3, I-Ppol is an intron-encoded endonuclease that targets a specific 15-base pair sequence found in the gene encoding for the ribosomal 28S subunit and creates defined 4 base 3'-overhangs (753, 754). Alternatively, AsiSI is an endonuclease that targets an 8-base pair recognition site in the 47S RNA coding region, but evidence suggests that AsiSI most likely cleaves only active repeats that are demethylated. Both methodologies have the advantage of providing the opportunity to study the kinetics of

repair via microscopic techniques, and fusion to the estrogen receptor has allowed researchers to follow inducible DSBs in real-time (755, 756). Although site-specific, these homing endonucleases also target regions outside of rDNA. For example, I-PpoI additionally targets 13 other genomic sites, the majority of which belong to 28S rRNA pseudogenes (717) and AsiSI induces lesions in 174 other sites of the human genome (757). In addition, I-PpoI does not efficiently cut every genomic region harboring the cut site due to either recognition sequence degeneration or inaccessibility caused by heterochromatinization (717, 758, 759).

For these reasons, CRISPR/Cas9 technology provides a highly efficient means to introduce DSBs in rDNA in a targeted manner. Cas proteins can help guide CRISPR RNA, to DNA targets, unwind the foreign DNA, and cleave it to create DNA DSBs with blunt ends, 5'-, or 3'-overhangs (760). The CRISPR/Cas9 system used in Chapter 3 utilizes the adopted CRISPR-Cas9 ribonucleoprotein (RNP) complex, comprised of Cas9 protein and a single guide RNA (sgRNA) that recognizes a specific sequence of DNA. This RNP delivery method has become popular because 1) of its transient genome editing, 2) it avoids plasmid DNA integration, and 3) it results in faster gene editing.

Like the global DSB-inducers, these targeted methods also exhibit repair pathway preferences. Cas9, specifically, produces blunt ends (761) and it has also been suggested that Cas9 remains tied on the substrate DNA after break induction, restraining the recognition of the break by DDR proteins and impeding repair (762, 763). This means that CRISPR/Cas9 generally favors NHEJ over HR(764). In addition, I-PpoI generally favors HR due to the nature of the clean breaks it creates (569), although there are suggestions that the “clean cuts” produced by endonucleases may aid in rapid accurate

repair by NHEJ prior to the formation of the nucleolar cap (566). Finally, both endonuclease and CRISPR/Cas9 systems can lead to cycles of break and repair, where the prompt rejoining after the first induction will lead to immediate re-cutting by the still present enzyme, also coined “chronic DSBs”. Such a scenario may influence check-point activation and repair pathway selection. Alternative inducible and tunable expression systems or transcription activator-like effector nucleases (TALENs), that generate “frayed” ends could alleviate this chronic DSB cycle and be utilized in the future for the study of α Syn in nucleolar DDR.

Lastly, limitations also exist in these site-specific modalities in the ability to induce DSBs in only a sub-set of cells. Despite many optimization efforts, nucleolar caps were only produced in about 50% of I-Ppol-treated SK-Mel28 cells and 25-30% of CRISPR/Cas9-treated SK-Mel28 cells. This limitation restricted us from multiple large-scale methodologies, including chromatin immunoprecipitation (ChIP), qRT-PCR, bulk-RNA sequencing, and phospho-proteomics under rDNA DSB induction. Unless a large quantity of starting material is used to compensate for “dilution” of the DDR cells, these methods require more global DNA damage treatments and/or other cell lines with higher induction efficiencies.

5.3 Forms of Synuclein

The experiments presented in Chapters 3 and 4 and Appendix A focus on WT, unmodified, monomeric α Syn. Additional forms of α Syn may be biologically relevant to the mechanism proposed and therefore should be considered for future investigation.

Phosphorylated Alpha-Synuclein

The phosphorylation at serine 129 (S129) in the C-terminus is the most common post-translational modification for α Syn. Although there are other phosphorylation sites within α Syn (Figure 1.4.1), S129 phosphorylated α Syn (pSyn) is a form of great interest due to its correlation with PD neuropathology progression. Over 90% of the α Syn found in LBs is S129 phosphorylated compared to only 4% of α Syn in the healthy brain (765). pSyn levels are associated with PD disease severity in CSF (766, 767), plasma (768, 769), and nerves in the skin (459, 460, 467). In addition, numerous murine and drosophila PD models report increased pSyn levels and aggregation (770-773). Although pSyn can be used as a biomarker for PD, how phosphorylation at S129 drives pathology progression is still an area of investigation, yet some studies have found that S129 phosphorylation alters α Syn function in various biological contexts. For example, S129 phosphorylation increases the ability of α Syn to bind to membranes (774, 775) and cytoskeletal and vesicle-trafficking presynaptic proteins (776).

The role of α Syn phosphorylation in DDR is unknown. S129 phosphorylation regulates the translocation of α Syn from the nucleus to the cytoplasm and drives the malignant transformation of melanocytes (473). pSyn also alters how α Syn interacts with DNA, where pSyn has a lower binding propensity to linear DNA and minimal binding propensity to circular DNA (515). These data suggest that while soluble un-phosphorylated α Syn in the nucleus facilitates the DDR, S129 phosphorylation can modulate how α Syn interacts with DNA and its function in DDR in melanoma. It would be interesting to investigate these questions using *in vitro* phospho-mimic (S129D) and phospho-deficient (S129A) approaches. Additionally, pharmacological manipulation of

endogenous kinases that have been identified to phosphorylate α Syn (G-protein-coupled receptor kinases, Casein Kinase II, Polo-like Kinase) could be fruitful.

PD-Associated Mutations

As described in Chapter 1.4, six point mutations leading to autosomal dominant genetic forms of PD have been found within the N-terminal domain of the *SNCA* gene (A30P, E46K, H50Q, G51D, A53E, A53T) (Figure 1.4.1) (73, 445, 446, 777-781). Although *SNCA* mutations are found in a very small percentage of PD patients, they are associated with more aggressive forms of the disease, potentially due to faster rates of fibril amplification and lipid-induced aggregation (782). These mutations have been found to possess differing biological functions that may underly propensity for disease progression compared to WT α Syn. In a recent publication, researchers found that PD-associated mutants will differentially affect DNA binding *in vitro*. Specifically, two of the disease-causing point mutations, A53T and A30P, were less efficient at binding DNA than WT, while mutation E46K was more efficient at binding DNA. Interestingly, a deletion of the central non-amyloid-beta component (NAC) domain, which is important for aggregation of the protein, also showed higher DNA binding (515). Furthermore, mutations seen in familial PD have been shown to alter rDNA biogenesis (783, 784). Together, these data suggest that PD-associated mutations may regulate α Syn's ability to facilitate DDR and prompts further consideration. Stable reintroduction of α Syn WT, A53T, A30P, E46K, and Δ NAC into the α Syn KO SK-Mel28 cell line via lentiviral transduction would be an obvious next step in experimentation. This would test whether PD-associated mutations alter nucleolar DSB repair efficiency, as seen in Chapter 3, and

give further mechanistic insight into their differing capabilities in DNA binding. However, it is possible that some of these constructs are toxic when stably expressed, and therefore will not produce viable cell lines. In that case, an alternative approach would be transient transfection of these constructs at low levels on the α Syn KO background.

Conformational Strains

Conformational strains of α Syn refer to different structural variations of the misfolded α Syn protein that can aggregate into distinct amyloid fibrils. This ultimately has been shown to lead to diverse pathological features, which can explain the heterogeneity observed in PD symptoms (785, 786). Studies have found that these different strains of α Syn aggregates can have varying levels of toxicity, propagation rates, and tissue distribution within PD, as well as other synucleinopathies (787-789). One study found that different conformations of α Syn pathology correspond to different stages of maturity for LB pathology, suggesting a temporal component to conformational differences (789). Furthermore, injection of different conformational strains into the olfactory bulb of mice, yielded distinct propagation patterns to other regions of the brain (787), suggesting that conformational strains of α Syn may underscore the heterogeneity among PD patients not only in clinical symptoms, but also neuropathologically on autopsy as described in Chapter 1.1.

Although the biological mechanisms proposed in this dissertation work pertain to monomeric and soluble forms of α Syn within melanoma cells, it is possible that oligomeric forms of α Syn are relevant to the association between PD and melanoma. A handful of

studies have found aggregated forms of α Syn in the skin of PD patients (474) and that these aggregates are resistant to protease degradation, a hallmark of α Syn amyloids (469). In addition, inhibiting α Syn aggregation with anle138b significantly hinders melanoma cell proliferation *in vitro* and the growth of xenograft melanoma tumors(398) and also upregulates anti-melanoma immune responses (506). Whether or not polymerized forms of α Syn are important in melanomagenesis and tumor growth is still understudied. However, it is intriguing to consider the pPD period as a time when melanocytes interact with early α Syn pathology and are vulnerable to melanomagenesis.

Our data in Chapter 2 suggest that there is a common mechanism at play years before clinical symptoms of PD. There have been reports that LB pathology in PD develops in peripheral autonomic neurons and certain brain regions prior to the onset of motor symptoms (790) and that PD patients will also harbor Lewy pathology in skin cells (394, 395). Therefore, it is plausible that melanoma progression may interact with these aggregates, whereby pPD α Syn aggregation and/or even its dysregulation in the DDR pathway may be an unbeknownst “hit” in the multi-hit melanoma model (256). However, it is important to note that melanoma staging was less advanced in the prodromal-PD group (Table 2.3.1), indicating that while melanoma may increase the risk of developing PD, there may be a somewhat protective effect of early PD-pathology on melanoma progression. Conversely, dysregulation of α Syn in melanoma cells may increase the likelihood to aggregate, which could then spread and seed in the brain, similar to theories that α Syn pathology starts in the gut and travels peripherally to centrally via the vagus nerve (425). There is also evidence that erythrocyte-derived extracellular vesicles, that contain pathological α Syn, can originate in the periphery of the body and traverse the

blood-brain barrier under certain conditions to “seed” into the brain (791-794). It is possible that melanoma cells can also release such extracellular vesicles, like melanosomes, exosomes, microvesicles, and extracellular particles containing aggregated forms of α Syn (795). These are just a few hypotheses to explain the increased incidence of PD in previously diagnosed melanoma patients, as seen in Chapter 2. Further investigation is warranted.

Beta- and Gamma-Synuclein

Lastly, there is abundant evidence that other synuclein family members play a role in cancer pathogenesis and may underly the connection between PD and melanoma. The synuclein family is comprised of three members: alpha-, beta-, and gamma-synuclein (α Syn, β Syn, and γ Syn, respectively). All three synucleins share sequence homology at the N-terminal region, while their C-terminus is specific for each family member. In the brain, it is suggested that β Syn modulates cell survival, metal levels, and dopamine uptake, and decreases α Syn aggregation (796-798), while γ Syn is proposed to influence neurofilament network integrity and chaperone in retinal photoreceptor cells (799, 800). Both β Syn and γ Syn have been shown to be linked to multiple types of cancers (801). β Syn has been implicated in the progression of breast (802), ovarian (802), glial (803), medulloblastoma (803), colon (804), and leukemia (805). Whereas, γ Syn has been linked to many other cancers, including, breast (802, 806, 807), ovarian (802, 808), retinoblastoma (809), esophageal (810), pancreatic (811), gastric (812), bladder (813), prostate (814), cervical (814), colon (804, 814, 815), lung (814), uterine carcinoma (816),

endometrium (817), squamous cell carcinoma (818), and biliary tract (819). The underlying molecular functions of β Syn and γ Syn in these various cancers are controversial depending on cancer type and study, where some describe an overexpression and others reduced expression. These disparities may reflect differing stabilizations of these proteins, including post-translational modifications and conformational propensities. Although no direct evidence shows a role for β Syn and γ Syn in melanoma progression and reports suggest a much lower expression of these proteins in melanocytes compared to α Syn (477), it should be explored further, and more specifically in the context of DDR pathways. Simple colocalization of β Syn and γ Syn with nucleolar DDR proteins should be investigated in addition to β Syn and γ Syn knockout melanoma models.

5.4 Liquid-Liquid Phase Separation

The implication that α Syn is involved in nucleolar DDR is intriguing within the context of the known biology of liquid-liquid phase separation (LLPS). LLPS was initially discovered through observations of the nucleolus and cytoplasmic P granules, which led Hyman and colleagues to propose a set of criteria to define LLPS in cells: 1) maintenance of spherical shape, 2) fusion after touching, and 3) contain mobile molecules that undergo internal rearrangement and external exchange (820). The nucleolus is a dynamic membrane-less compartment and utilizes phase separation not only as a way to delineate from the nucleoplasm, but also in the formation of the nucleolar cap after transcriptional silencing or rDNA DSBs (631, 821, 822). It has also been shown that LLPS is important

in the condensation and dissolution of DNA repair factors during DSB repair, in order for proper DSB sensing and DDR signal transduction to initiate both HR and NHEJ (823).

Interestingly, LLPS is a highly discussed topic in the neurodegeneration field, as α Syn is commonly described as an intrinsically disordered protein (IDP) (824). IDPs are characterized by containing few hydrophobic residues, a high net charge, low sequence complexity, and structure breaking residues (like proline) that facilitate disorder (825, 826). Because of these features, they are prone to aggregate. Misfolded aggregates of α Syn will undergo phase separation during the formation of LBs in the context of synucleinopathies (647, 822, 827), potentially through an RNA G-quadruplex-mediated manner (828). It is believed that the liquid-like α Syn droplets will gradually undergo an irreversible liquid-to-solid phase transition into amyloid-like hydrogel entrapping oligomers and fibrils, which may underlie the cellular toxicity associated with PD (827). In addition, studies have suggested that PD-associated mutations, E46K and A53T, and the S129 phospho-mimic, S129E, greatly increases α Syn's ability to undergo LLPS in purified systems (647, 829). Considering these findings and ours illuminating a role for α Syn in the nucleolar DDR (Chapter 3), it is plausible that α Syn may be modulating this process in a way that is beneficial for DSB repair in the nucleolus to promote genomic stability and thus melanoma cell survival.

One plausible mechanism that fits within the findings of this dissertation is the role of 53BP1 in LLPS. A recent study found that 53BP1 undergoes LLPS with the heterochromatin protein HP1 α to maintain heterochromatin integrity and genome stability (830). The role of α Syn in this mechanism is unclear, yet my findings showing that α Syn regulates 53BP1 recruitment could have downstream effects on LLPS-mediated genomic

stability pathways. Studies investigating presynaptic terminals show that α Syn modulates the phase separation of synapsin and changes its ability to cluster synaptic vesicles (831, 832). It is possible that α Syn may be modulating LLPS of other proteins, like 53BP1, within repair foci to regulate their function in a way that is conceptually parallel to its role in presynaptic terminals.

Another plausible mechanism is that the structural changes associated with nucleolar cap formation involves the merging of the fibrillar center and the dense fibrillar component of the nucleoli. Many studies have proposed that nucleolar segregation, which is LLPS driven, is dependent on ATM-mediated transcriptional inhibition (562, 563, 569, 570). However, a recent finding suggested that nucleolar segregation may be transcription-independent, involving forces arising from nuclear envelope invaginations and the actin network (567). Although I found that α Syn loss-of-function does not regulate rDNA transcriptional inhibition after rDNA DSB induction (Figure 3.8.8), it is possible that α Syn facilitates DSB-induced nucleolar segregation via actin networking, which has previously been implicated in LLPS-driven systems (833-835). Additionally, evidence suggests that α Syn regulates actin polymerization by sequestering actin monomers, while in pathological states, its misfolding and aggregation can disrupt cytoskeleton dynamics, contributing to neurodegeneration associated with PD (836, 837).

The experimental identification of LLPS is challenging in that no one criterion is sufficient to demonstrate phase separation of a protein. However, high mobility, which can be measured by fluorescence recovery after photobleaching (FRAP), is one indicator. Our previous work in mouse cortical neurons *in vivo* (442), in primary culture (442), and SK-Mel28 cells (Figure 3.3.4) shows that α Syn tagged to GFP is rapidly recruited to DNA

induced by high intensity laser illumination of subnuclear regions. This LID technique could be exploited to measure the kinetics and mobility of Syn-GFP or other GFP-tagged DDR proteins within DSB repair foci. Furthermore, LLPS status can be confirmed by the loss of phase separation with exposure to the compound 1,6 hexanediol that inhibits LLPS, but not with 2,5 hexanediol, which is chemically similar but preserves LLPS. Under this FRAP LID technique, it would be critical to test the sensitivity of Syn-GFP recruitment after 1,6 hexanediol treatment.

5.5 Downstream Cellular Phenotypes

The growth phenotypes associated with α Syn KO both *in vitro* (Chapter 3) and *in vivo* (Chapter 4) are interesting to examine in the context of downstream pathways associated with DSB DDR. These pathways, like apoptosis, senescence, and autophagy, are of particular interest because of both previously reported studies, my own data in mouse melanoma tissue (Figure 4.3.4), and unpublished data (Appendix A.2). There are additional cell death pathways that have been implicated in both PD and melanoma, like ferroptosis, necroptosis, and pyroptosis, but my preliminary data did not show a significant role for α Syn in these alternative pathways (Appendix A.2).

Apoptosis

Apoptosis refers to a regulated process of cell death which is marked by distinct alterations in cellular morphology, such as cellular shrinkage, nuclear condensation, and DNA degradation. There are two main pathways that can initiate apoptosis: 1) the

extrinsic pathway and 2) the intrinsic pathway (838). The extrinsic pathway begins outside of the cell when conditions in the extracellular environment indicate that a cell should die. T cells generate a surface receptor called Fas, which increases production during an infection. When Fas binds to its ligands, apoptosis is triggered. The intrinsic pathway begins when a cell senses stress due to an injury within the cell and cytochrome c is released from the mitochondria. Both pathways converge on the execution pathway, which is initiated by the activation of caspase-3.

Apoptosis can be initiated in response to unresolved DSBs, partly as a way to prevent the propagation of severely damaged genetic material in proliferating cells. The DDR pathway will activate pro-apoptotic proteins like Bax, which can then lead to mitochondrial dysfunction and release of factors that trigger the caspase cascade, ultimately causing cell death (839-841). The tumor suppressor protein p53 also plays a critical role in the apoptotic response to DSBs, as it can be activated by the DDR via ATM and ATR phosphorylation cascades and induce the expression of pro-apoptotic genes. Specifically, p53 induces BIM, PUMA, and NOXA, which inhibit pro-survival BCL2 family members and leads to activation of Bax and downstream mitochondrial dysfunction. One study found that I-Ppol-induced rDNA DSBs were sufficient to induce p53-dependent apoptosis (842). Further discussion regarding the important role of p53 in senescence, melanomagenesis and tumor proliferation will be discussed later in this section and in Chapter 5.6.

In PD, apoptotic cell death has been documented in postmortem tissue, animal models, and *in vitro* cultures, with the characteristic morphological changes and DNA fragmentation (843). Studies have found that oxidative stress, imbalance of calcium

homeostasis, and mitochondrial dysregulation are important factors in the apoptosis of dopaminergic neurons within the substantia nigra (844, 845). It is plausible that α Syn-mediated DDR dysregulation can also lend to a pro-apoptotic phenotype in this vulnerable cell population. One study found that α Syn KO xenografts implanted into WT mice showed significantly increased apoptosis, as measured by the DNA fragmentation-measuring TUNEL assay (478). Furthermore, my data suggests that α Syn loss-of-function leads to an increased apoptosis response *in vitro* with the increase in micronuclei formation (Figure 3.3.7), a common indicator for DDR-induced apoptosis (846). In addition, *in vivo* experiments showed elevated levels of caspase-9 gene expression in α Syn KO mice melanoma tumors compared to WT mice (Figure 4.3.4). This result highlights the possibility for DSB-induced apoptosis, as caspase-9 is specifically involved in the intrinsic apoptosis cascade. Although caspase-3 levels were not significantly different between α Syn KO and WT tumors (Figure 4.3.4), the difference was trending toward significance ($p=0.0628$) and the potentially functional extrinsic apoptosis factor could be “diluting out” the changes seen in the intrinsic pathway as these two cascades converge at caspase-3. While gene expression of these pro-apoptotic factors is an important measurement, their total protein levels and activated byproducts are critical in understanding the downstream apoptotic phenotype as a result of α Syn loss-of-function. This would be a key next step in investigation (see Appendix A.2 for preliminary data).

Senescence

Genome instability has long been implicated as an important factor in cellular aging (578). Dividing cells are constantly exposed to various sources of DNA damage, with an

accumulation of such damage sufficient to cause the phenotypic changes associated with aging, like senescence. Cellular senescence is defined as a stable cell cycle arrest that can be triggered by various intrinsic and extrinsic stimuli and is characterized by cell swelling and the secretion of the senescence-associated secretory phenotype (SASP). DDR-induced senescence is thought to arise through p53-dependent or p53-independent pathways. The p53-dependent pathway entails ATM and ATR kinase signaling cascades resulting in CHK1/2 activation upstream of p53. This signaling then activates p21, which in turn inhibits the CDK's inhibitory effect on RB1, ultimately leading to senescence. Alternatively, DNA damage can directly activate a p16 cascade independent of p53, resulting in CDK and RB1 activation. Traditionally, senescence has been viewed as an irreversible process that is a consequence of anti-proliferation; however, recent advances have extended its known role to complex biological processes, such as neurodegenerative disease and cancer.

In the context of neurodegeneration, post-mitotic cells, like neurons, are especially vulnerable to cellular senescence. The continuous activation of DNA damage repair pathways associated with aging produces senescence in neurons (847) and is linked with the pathogenesis of several neurodegenerative disorders (848). Patients with PD show enhanced levels of SA- β -gal in their CSF (849) and brain tissue (850), with the level of α Syn aggregation directly correlating with level of senescence (851). One study found direct evidence that the accumulation of DNA DSBs and cellular senescence are intermediaries of α Syn-induced pathogenesis in a PD mouse model (620). A loss-of-function of α Syn in the nucleus could account for these observations.

In the cancer field, there has been substantial focus on senescence, as oncogene-induced senescence (OIS) is a tumor-suppressive mechanism that prevents cells from becoming malignant. OIS is initiated from an activating mutation of an oncogene and is a defense mechanism by the cell that when is escaped, leads to carcinogenesis. In melanoma, this mechanism becomes particularly salient in the context of the multi-hit model (Chapter 1.2). Initial *BRAF* V600E and *NRAS* Q61R mutations in melanocytes will promote benign nevus formation, at which point these cells will initiate OIS to prevent dysplastic nevus transformation. However, upon the loss of tumor-suppressor genes (the “second hit”), many of which are involved in the OIS pathway like p53, pRB, and p16, OIS escape leads to melanomagenesis. Alternatively, cells that fail to undergo senescence can also lead to malignant transformation in the absence of the acquisition of additional mutations (852).

My data detecting an upregulation of α Syn in SK-Mel28 cells and its potential DSB repair function fits into senescent characteristics of cancer pathogenesis as well. Persistent DSBs can drive cancer cells into senescence in a p53-dependent or p53-independent manner (696, 853-855), as described above. This phenomena can be reversed by improving DSB repair fidelity (856, 857), and there is evidence that melanoma cells upregulate DSB repair components critical for survival (523, 524). Furthermore, studies have found that α Syn overexpression can inhibit cellular senescence (858). Given that increased nucleolar DSB repair capacity contributes to senescence escape and previous findings that α Syn modulates DSB repair, it is possible that α Syn gain-of-function due to overexpression of soluble α Syn in melanoma reduces senescence. Not only do α Syn KO SK-Mel28 cells show slower proliferation rates (Figure

3.3. 7) and α Syn KO mice show slower tumor growth (Figure 4.3.1), but on observation, nuclei of these cell populations are larger than in WT conditions, a key morphological characteristic of a senescent cell (859). In addition, micronuclei formation (Figure 3.3.7) can also be an indicator of cell senescence (860), which can trigger SASP via leakage of DNA into the cytoplasm (861, 862). More directly, my data shows that α Syn loss-of-function leads to an increase in p16 levels, which are significantly correlated to RPA32 signal in melanoma tumors *in vivo* (Figure 4.3.4). This data, as it stands, fits both the p53-dependent and p53-independent pathways.

Studies suggest that p53 and RPA interact to form a complex that dissociates as a part of DNA damage signaling (863) and phosphorylation of RPA by DNA-PK and phosphorylation of p53 by ATM and ATR promote HR repair pathways during transcriptional stress-induced DNA damage (864, 865). It is possible that α Syn is involved in the RPA-p53 dissociation mechanism, so that when during replicative stress in highly proliferating melanoma cells, RPA and p53 are freed to mediate DNA damage repair, ultimately leading to lower levels of senescence (and lower p16). Interestingly, higher p16 levels have been shown to impair HR in head and neck squamous cell carcinomas (866), suggesting that α Syn KO-induced increases in p16 could be promoting conversion to NHEJ repair, which has been seen in a senescence-phenotype mouse model of PD (620). Further investigation into senescent phenotypes is warranted, although multiple techniques have been tested through the course of this dissertation, including Western blotting for p16 and immunocytochemical staining for senescence-associated β -galactosidase. Ultimately, these techniques did not work in the SK-Mel28 cell lines. An ELISA to detect a panel of proteins in conditioned media for SASP (IL-6, IL-8, GRO α)

would be a valid next step to confirm the senescence phenotype inferred by increased p16 gene expression. Additionally, further studies elucidating the role of α Syn in the relationship between RPA, p53, p16 and DDR-induced senescence are justified (and proposed in Chapter 5.6).

Autophagy

The autophagy pathway is a cellular process that breaks down cytoplasmic material and delivers it to the lysosome for degradation. In response to DSBs, autophagy is often activated to help repair the injury by degrading damaged proteins and organelles, providing building blocks for repair, and facilitating the overall DDR through selective degradation of damaged components (867-869). Specifically, there are many pathways that lead to autophagy activation after DNA damage, but one to highlight is the ATM/CHK2-mediated nuclear exclusion of autophagic protein, FOXK (870). Furthermore, nucleophagy is a subtype of autophagy that targets nuclear material for degradation and helps cells respond to cell cycle perturbations and nuclear insults (871). This process, like apoptosis and senescence, involves the formation of micronuclei that contain genetic material, which allows for the identification and clearance of micronuclei with CGAS-mediated nucleophagy (872). Ultimately, autophagy is integral in many disease pathologies, including neurodegeneration and cancer (873, 874).

In PD, disruptions in the autophagy pathway can result in the buildup of proteins and the formation of LBs. Autophagy is thought to play a role in the breakdown of α Syn fibrils, involving both the autophagy-lysosomal and ubiquitin-proteasomal pathways.

Furthermore, certain PD-associated genes also contribute to autophagy regulation (875). For example, mutated *LRRK2* leads to axonal shortening and the formation of autophagic vacuoles (876). Additionally, *PARKIN* and *PINK1* (autosomal recessive PD genes) can cause mitochondrial damage and promote autophagy (877). Currently, treatment modalities that influence autophagic and lysosomal activity to reduce LB accumulation are being explored in the PD field.

Autophagy is equally as important in melanoma pathogenesis, yet has a more sequential and complex role (878, 879). In the early stages of melanomagenesis, autophagy can act as a tumor suppressor, removing damaged organelles and protein aggregates to prevent the buildup of harmful material. However, in advanced stages of the disease, autophagy promotes tumor growth and resistance to therapy by reducing stress from drugs and metabolism and aiding in growth and metastasis (880). Melanomas that harbor *BRAF* mutations are often associated with increased autophagic activation, making these types of melanomas more resistant to targeted therapies (687).

Autophagic cell death is a type of programmed cell death that occurs when autophagy is excessive or dysregulated, leading to the accumulation of autophagosomes, which eventually engulf critical cellular components, causing the cell to self-destruct. Current development of therapeutic targets is underway to exploit this pathway (881). In my data, α Syn KO led to significantly elevated levels of autophagic marker, LC3B, potentially indicating activation of autophagic cell death leading to diminished tumor growth (Figure 4.3.4). Furthermore, studies have found that α Syn overexpression can protect primary and metastatic melanoma cells from autophagic cell death (398, 504). This again fits the general picture that α Syn gain-of-function is critical

in melanoma growth by protecting against autophagic cell death and requires further investigation, such as immunocytochemistry, western blot, and electron microscopy techniques to quantify the formation of autophagosomes in α Syn KO cells.

5.6 Melanoma Models

Limitations (in vitro)

In Chapter 3, multiple *in vitro* cell models were utilized, including SK-Mel28, A375, PIG1, and primary melanocytes. However, SK-Mel28 cells were chosen as the primary cell model to study the role of α Syn in nucleolar DDR for various reasons, including the previous development of α Syn KO and KI clones (478) and the high levels of endogenous expression of α Syn in this particular melanoma cell line (397, 401). Like any immortalized cell line, there are drawbacks influencing translatability of the model to conclusions about the human disease. For example, human melanomas are associated with a variety of oncogenic and tumor suppressor gene mutations (multi-hit model, Chapter 1.2). SK-Mel28 cells are WT *RAS* and *CDKN2A*, yet are mutated in *PTEN* (T167A), *BRAF* (V599E), *CDK4* (R24C), and *p53* (L145R) (882). Therefore, reproducing these experiments in alternative human melanoma cell lines, with differing genetic backgrounds, becomes crucial in understanding α Syn's role in the nucleolar DDR.

The *BRAF* (oncogenic first-hit) and *PTEN* (tumor suppressor second-hit) mutations in SK-Mel28 cells are common in human melanomas and critical for melanomagenesis. However, the mutated isotype of p53 could potentially affect whether α Syn modulates downstream phenotypes through a p53-dependent or -independent pathway (as

suggested in Chapter 5.5). There is a discrepancy in the literature as to whether mutated forms of p53 are functionally deficient or not in SK-Mel28 cells(883-886). Of note, one study found no significant differences in downstream target gene activation between p53 WT and mutant melanoma cell lines (887). Furthermore, another study found that both WT and mutant p53 proteins show kinetics of aggregation and fibrillar morphology that resemble those of classical amyloidogenic proteins, such as α Syn (888, 889), suggesting that p53-mutant cancers may be a class of protein aggregation diseases. Similar to α Syn, p53 was described to be transmitted between cells in a prion-like mechanistic fashion (890). Experiments utilizing a p53 inhibitor, like Pifithrin- α as previously described(883), could test whether downstream cellular phenotypes, like apoptosis, senescence, and autophagic cell death as a function of α Syn KO are p53-dependent or p53-independent.

Furthermore, the pigmentation status of the cell line may influence its susceptibility to DNA damage and how α Syn interacts with the DDR. One study analyzing patient pigmented melanoma tissue found that cells with increased amounts of α Syn had little to no pigmentation (397), later supported by another study (395). This observation is seen in SK-Mel28 cells, where high expression of α Syn correlates to hypopigmentation and knocking down *SNCA* expression increases overall melanin production (367). Conversely, overexpressing α Syn in pigmented A375 cells decreases melanin production. This becomes important in the context of DDR-induced carcinogenesis, as melanin serves to absorb UV radiation (891), so varying pigmented cell lines could also have evolutionarily diverged in their capacity for efficient DDR. Therefore, α Syn expression in SK-Mel28 cells, which disrupts melanin production, could be an evolved mechanism by which amelanotic melanomas evade early detection. Data showing that

patients with higher levels of *SNCA* expression had worse survival outcomes supports this hypothesis (478), although whether or not these cases are enriched by amelanotic melanomas is unclear. I did not find any synergistic patterns between amelanotic lesions and PD incidence in Chapter 2, yet further investigation is warranted to determine whether this hypothesis and the downstream DNA damage sensitivity, could be contributing to the PD-melanoma association. Utilizing other pigmented cell lines could help answer these questions and preliminary studies utilizing pigmented primary melanocytes is presented in Appendix A.1.

Lastly, one limitation to the SK-Mel28 lines that were utilized in Chapter 3 is the way in which the KI/Rescue line was created. The re-expression of α Syn in the α Syn KO background was achieved through transduction of a lentivirus expressing human α Syn under the CMV promoter with puromycin for colony selection and expansion (478). As a result, WT α Syn becomes randomly inserted into the genome and not at the endogenous locus. This means that 1) the expression of the “rescue” α Syn is not controlled by the endogenous promoter and 2) the system lacks α Syn splice isoforms. Both of these discrepancies to the WT cell line could ultimately influence how the cell is responding to DNA damage and how the “rescued” α Syn is facilitating the DDR. In the future, re-engineering a gene-targeted KI line using CRISPR/Cas9 could be beneficial.

Limitations (in vivo)

The TG3 mouse line was carefully chosen in Chapter 4 from one of several possibilities. The TG3 mouse is a model that produces tumors within a short timeframe

(~2-3 months) at 100% penetrance (671-674). Due to this reason, any impaired growth due to α Syn KO could be more easily measurable. In addition, the TG3 is a single allelic model, which is advantageous for crossing with an additional α Syn KO allele. Although the most common genetic mutation associated with human melanoma, *BRAF*, as well as other mutations in *KRAS*, *HRAS*, and *NRAS* are options for mouse models, most are not spontaneous and are double- or triple-allelic (892). Lastly, *Braf* is located close to *Snca* on chromosome 6, which makes breeding both alleles challenging.

Despite these advantages, the TG3 mouse line, like other genetically engineered melanoma mouse lines, have limitations. First, human and mouse skin morphology is different (892). Human melanocytes are distributed along the basal layer of the epidermis. In contrast, mouse melanocytes are located primarily in the bulb regions of the hair follicles. Therefore, most genetically engineered models initiate in the dermis and share limited histological similarities with human melanoma that have a predominantly epidermal and dermoepidermal junctional component. There has been advancement in the melanoma field that when mice constitutively express the hepatocyte growth factor/scatter factor transgene, melanocyte distribution is modified to be present more at the dermoepidermal junction, which in turn allows this model to share more histopathological features with their human counterparts (893, 894). Additionally, the promoter which is driving transgene expression is important to consider in genetically engineered models. For example, the most commonly used tissue-specific promoter in melanoma models is derived from the *Tyr* gene, which is also expressed in other cells of similar embryological origin, not just melanocytes (895, 896). Therefore, using promoters from genes that are expressed at later stages of melanocyte differentiation is critical to

consider for the most specificity. The transgene associated with the TG3 line is not expressed under the control of a melanocyte-specific promoter and is an additional limitation to the experiments in Chapter 4.

Another important factor when choosing a melanoma mouse model is whether external carcinogenic agents are necessary for melanomagenesis and how relevant these processes are to human disease. For the most part, melanoma mouse models are either 1) double transgenic (oncogenic activation and tumor suppressor inactivation) and will spontaneously form melanoma at low penetrance, 2) double transgenic (oncogenic activation and tumor suppressor inactivation) inducible system with high penetrance, or 3) single transgenic (oncogenic activation or tumor suppressor inactivation) with the addition of a carcinogenic agent, like UV radiation, with variable penetrance (892). The TG3 mouse line falls into neither of these categories and is a rare model by which a single allelic transgene spontaneously induced melanomagenesis with 100% penetrance. Systems that require carcinogenic agents are the most biologically relevant as UV radiation is the main environmental risk factor for melanoma in humans. However, the strain background of mouse makes a large impact on UV radiation sensitivity due to variations in skin pigmentation and hair amount (248, 893). It would be translationally beneficial to study the role of α Syn in melanomagenesis through the use of UV-induced models. There are several questions that my results prompt: Would α Syn overexpression lead mice to be more susceptible to UV-induced melanoma initiation and growth? Could the therapeutic target of α Syn result in higher resistance to UV-induced models? Preliminary studies investigating α Syn in UV-treated primary melanocytes is presented in

Appendix A.1. Overall, mouse models can play a vital role in advancing our understanding of the molecular underpinnings of the process of melanomagenesis and α Syn's role in it.

Alternative Disease Models

In order to fully translate the findings of this dissertation to the PD-melanoma association, it is important to test whether α Syn facilitates nucleolar biology in neurons, as I observed in melanoma. The substantial evidence suggesting the importance for nucleolar DDR in PD and other neurodegenerative disease pathogenesis raises the question of whether α Syn is regulating such processes. This is not an unconventional transition, however. One previous study investigating α Syn modifier, amino-terminal acetyltransferase B, did exploratory genome-wide CRISPR screening in SK-Mel30 cells followed by more targeted CRISPRi screening in a neuronal cell population, showing shared screening hits (897), suggesting that melanoma cell lines that highly express α Syn can be representative models for neurons. Previous work from the Unni Lab in mouse cortex shows that α Syn colocalizes with markers of DSB repair, like γ H2AX and PAR, in neurons similar to SK-Mel28 cells (442). In addition, α Syn KO increases levels of DSBs, and re-expression of WT human α Syn in specific cortical neurons within the mouse α Syn KO background reduced γ H2AX and PAR levels (442). Future experiments would entail culturing E18 primary cortical neurons, as previously described (443), and visualizing α Syn nucleolar colocalization via ICC at baseline and after I-Ppol treatment. In addition, comparing WT and α Syn KO mice will allow us to implement similar techniques as to the ones optimized in Chapter 3. One advantage to these proposed future experiments is that increased transfection efficiency is seen for mRNA transfection over DNA plasmid

transfection in primary cell culture, including primary cortical neuronal cultures (898, 899). However, neurons do not have the same nucleolar prominence as other cell types and would require more dedicated staining experiments. Alternatively, other immortalized neuronal models in cell culture could be utilized and aid in ease of experimental optimization, including PC12, N2a, SH-SY5Y, and NT2 cells. Lastly, induced pluripotent stem cells (IPSCs) are becoming an increasingly common research tool to study highly translatable questions. Patient IPSCs from individuals with PD, melanoma, and/or both diseases could be differentiated into both neuronal and melanoma cell populations to investigate the role of α Syn in the DDR in a variety of genetic backgrounds.

5.7 Clinical Implications

The findings presented in Chapters 2, 3, and 4 of this dissertation collectively emphasize the intricate relationship between PD, melanoma, and α Syn's role in DNA damage repair pathways. These insights have profound clinical implications, spanning early diagnoses, risk managements, therapeutics, interventions, and the broader approaches to patient care.

Chapter 2 established a compelling link between melanoma, its precursor lesions, and pPD. The unique clinical characteristics of melanoma in pPD patients highlight a bidirectional relationship that could inform both neurological and oncological screening practices. Integrating dermatological evaluations with neurological assessments for individuals presenting with atypical melanocytic lesions or a family history of PD may enable earlier identification of at-risk individuals. Such approaches could incorporate the

use of predictive algorithms that integrate genetic, clinical, and molecular markers to stratify patient risk profiles more effectively (such as the proposed PD THRESHOLD mnemonic). Returning to the overarching hypothesis posed in Chapter 1.6, it is plausible that in the general population, individuals with high expression of α Syn are 1) more predisposed to LB formation in PD and 2) more predisposed to melanocytic transformation in melanoma (Figure 1.5.1). Therefore, screening efforts to measure baseline α Syn expression levels, may be fruitful in a clinical setting as an additional risk factor. Furthermore, these findings call for enhanced patient and physician awareness of the PD-melanoma connection. Educational initiatives aimed at primary care providers, neurologists, and dermatologists could ensure that subtle prodromal symptoms of PD or unusual dermatological findings are not overlooked. These overlapping pathologies also call for a holistic, interdisciplinary approach to patient care. Collaborative care teams could provide comprehensive care plans that address shared molecular pathways and environmental risk factors, ensuring optimal outcomes for patients with either or both diseases.

Chapters 3 and 4 reveal that α Syn's involvement in DNA DSB repair pathways has significant implications for both neurodegeneration and tumor progression. α Syn's modulation of 53BP1 recruitment and its role in maintaining genomic stability underscore its dualistic nature: the detrimental loss of α Syn's nuclear function in PD and protective gain of α Syn's nuclear function in melanoma. This nuanced role opens the door to targeted therapeutic interventions.

In PD, therapeutic strategies that preserve α Syn's nuclear function could be transformative, especially because existing therapeutic approaches focus largely on

symptom management. This may involve developing small molecules or gene therapies that enhance its DNA repair capabilities while minimizing its cytoplasmic aggregation tendencies. Enoxacin is an FDA-approved fluoroquinolone antibiotic that has recently been shown to promote recruitment of MDC1 and 53BP1 to DSBs by stimulating production of short non-coding RNAs (sncRNAs) associated with the DNA damage response (900). Enoxacin has also been used successfully in rodent models to improve brain function after systemic administration (901). It would be beneficial to test whether increasing 53BP1 recruitment to sites of damage with the small molecule enoxacin rescues DSB repair deficiencies and downstream growth phenotypes caused by α Syn KO in SK-Mel28 cells. In addition, *in vivo* multiphoton imaging of mice treated with PFFs and then subsequently given enoxacin would test whether pharmacologically increasing 53BP1 recruitment to DSBs influences the formation of LB-like pathology and/or increases the lifetime of neurons in which LB-like inclusions have formed. A positive result would not only have broad ramifications in terms of validating my hypothesis, but would immediately provide the field with an unexpected, FDA-approved agent that could be tested in people for efficacy in PD and other synucleinopathies.

Conversely, in melanoma, strategies to downregulate α Syn in tumor cells or disrupt its interactions with DNA repair machinery could sensitize tumors to other genotoxic therapies, especially when resistance mechanisms remain a significant hurdle. Many therapies are currently being tested to reduce the aggregation of α Syn in neurodegenerative disease models (902, 903), yet whether these disease-modifying therapies can be translated to decreasing soluble (non-aggregated) α Syn in melanoma is unknown. Alternatively, targeting parts of the nucleolar DDR that α Syn facilitates would

be a valid therapeutic option. Ultimately, these insights also raise the possibility of dual-benefit therapies for patients with comorbid PD and melanoma. Targeted modulation of α Syn could simultaneously mitigate neurodegeneration and limit melanoma progression, representing a paradigm shift in personalized medicine. Moreover, the sex-dependent effects observed in Chapter 4's *in vivo* studies suggest that therapies targeting α Syn may need to be tailored based on sex to maximize efficacy and minimize off-target effects. Precision medicine approaches that consider patient-specific genetic, molecular, and demographic factors will be critical in the development of these therapies.

Lastly, the clinical implications of this work extend beyond PD and melanoma, shedding light on the broader relationships between neurodegeneration, cancer, and genomic instability. For example, micro- and macro-nucleoli have been reported in brain tissue samples of patients with not only PD, but also AD (904), amyotrophic lateral sclerosis (ALS) (905, 906), and Huntington's disease (HD) (907), indicating nucleolar stress. One major limitation of the findings in Chapter 2 is the lack of neuropathological confirmation of clinical PD diagnosis, where it is possible that individuals diagnosed with "PD" may have had other neurodegenerative diseases, both clinically and pathologically. As mentioned previously in Chapter 1.1, many neurodegenerative diseases share clinical symptoms, yet neuropathological analysis of individuals with other neurodegenerative clinical diagnoses will also show α Syn pathology. LBs laden with α Syn are detected in the brains of about 50-60% of sporadic Alzheimer's disease (AD) cases (908-912), 96% of familial *PSEN1* cases (913), and in 10-20% of elderly individuals with no neurodegenerative disorders (914, 915). The clinical implications for this co-pathology are still not fully characterized, but the molecular mechanisms underlying this observation

is even less understood. Exploring these connections could yield additional therapeutic targets and diagnostic biomarkers, which will be evaluated further in Appendix B.

5.8 Conclusions

This dissertation bridges two seemingly disparate diseases, PD and melanoma, by unveiling shared molecular mechanisms mediated by α Syn. The clinical findings from Chapter 2 provide compelling evidence of a bidirectional relationship between PD and melanoma, underscoring the potential for improved diagnostic frameworks that integrate dermatological and neurological markers. The experimental insights from Chapters 3 and 4 further reveal the dualistic nature of α Syn: while its aggregation in the CNS accelerates neurodegeneration, its upregulation in peripheral tissues like melanoma may enhance DNA repair and cell survival, facilitating tumorigenesis.

These results have far-reaching implications. They emphasize the importance of α Syn as a biomarker and therapeutic target, inspiring novel treatment strategies that transcend traditional disease boundaries. In conclusion, this work not only advances our understanding of the molecular interplay between neurodegeneration and cancer but also highlights the transformative potential of interdisciplinary research in developing innovative diagnostics and therapeutics. Future investigations should aim to refine these insights, exploring targeted therapies and personalized approaches to improve outcomes for patients navigating these challenging diseases.

[Jump Back to Table of Contents](#)

Appendix A (unpublished)

A.1 Primary Melanocytes

Introduction

As mentioned in Chapter 5.6, UV radiation-based models are more biologically relevant systems, as UV radiation is the main environmental risk factor for melanoma in humans. Both *in vitro* and *in vivo* models can utilize UV radiation to induce melanomagenesis, however primary melanocyte cell culture has multiple advantages, such as shortened timing of experiments and downstream analysis. There are two independent pathogenic pathways for UV-induced melanomagenesis that have been postulated (briefly mentioned in Chapter 1.2): 1) a melanin-independent pathways associated with UVB-induced DNA damage and 2) a UVA-initiated melanin-dependent pathway associated with indirect oxidative DNA damage (248, 249). Both pathways will not only create cyclobutane pyrimidine dimers in DNA (250) but will also upregulate molecules like α MSH and MCR1, which are linked to *BRAF*-mediated proliferation and pigmentation. Whether or not α Syn is involved in these UV-associated melanomagenesis pathways is unknown and a clear area for translationally relevant investigation.

Results

To investigate α Syn's role in UV-induced DNA DSB repair, optimization of γ H2AX response after UV radiation was performed on primary melanocytes. Primary melanocytes were cultured on coverslips and stimulated with UV radiation (5 minutes for total of 1,429 mJ/cm²) followed by various incubations times. Cells were then fixed and

stained for γ H2AX. Compared to no UVR, there was a significant stepwise increase in γ H2AX after UVR with increasing incubation times, with 60 minutes of incubation time resulting in the highest increase (Figure A.1.1). This condition was used for the remainder of the experiments. Next, primary melanocytes treated with UV for 5 minutes and incubated for 60 minutes were stained for α Syn (Syn1). Analysis revealed that UVR not only increased γ H2AX levels, but also significantly increased α Syn compared to untreated controls (Figure A.1.2). Additionally, the colocalization of nuclear foci of γ H2AX and α Syn was significantly increased under UV conditions compared to untreated conditions (Figure A.1.2). Lastly, to investigate which UV-induced melanomagenesis pathway α Syn may be involved in, primary melanocytes were cultured in growth medium lacking α MSH. Immunocytochemistry analysis revealed no significant differences in γ H2AX increased response between α MSH+ and α MSH- conditions, yet a significant decrease in α Syn levels under α MSH- conditions that attenuated the UV-induced response (Figure A.1.3). No significant differences were seen in colocalization of γ H2AX and α Syn between α MSH+ and α MSH- conditions.

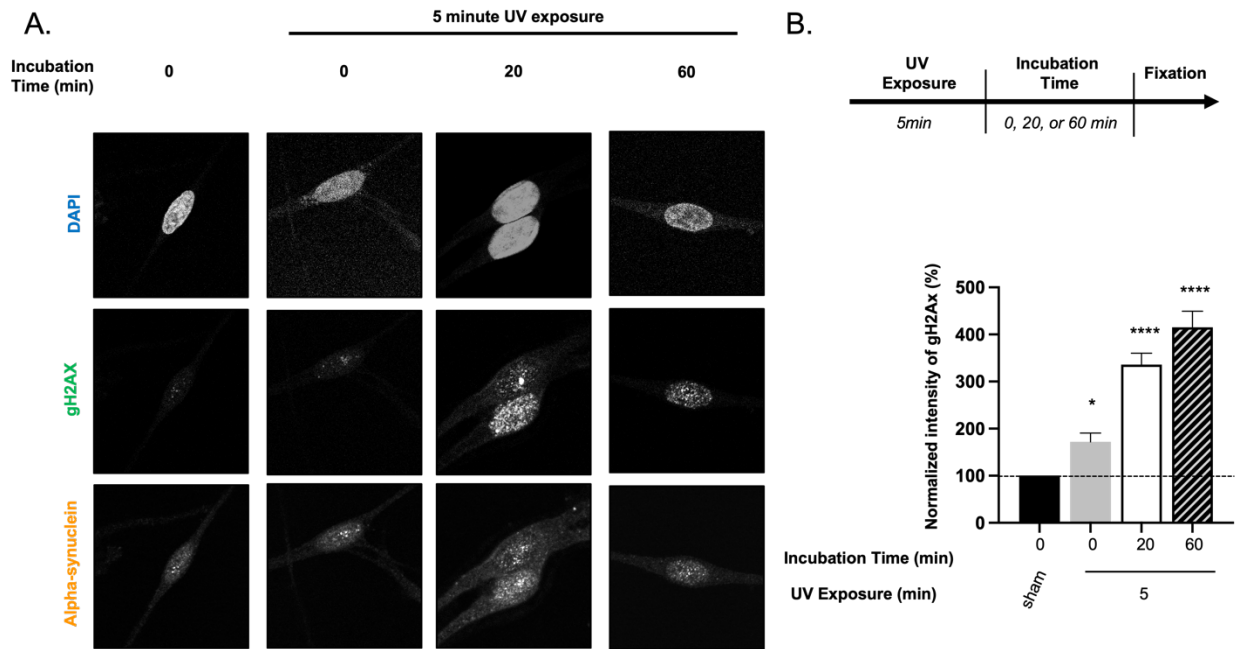


Figure A.1.1 Response of γH2AX after UV radiation. A, B) Primary melanocytes were treated with UVR for 5 minutes, and incubated for various time points indicated, followed by staining for Syn1, γH2AX, and DAPI. Mean intensity of γH2AX signal within DAPI were analyzed using FIJI. * $p < 0.05$, **** $p < 0.0001$ by one-way ANOVA. Error bars denote SEM. Quantification from 1 biological replicate (total $n = 39-46$ nuclei per condition). Melanocyte culturing and UV exposure of Figure A.1.1 performed by Gail Kent and Pam Cassidy.

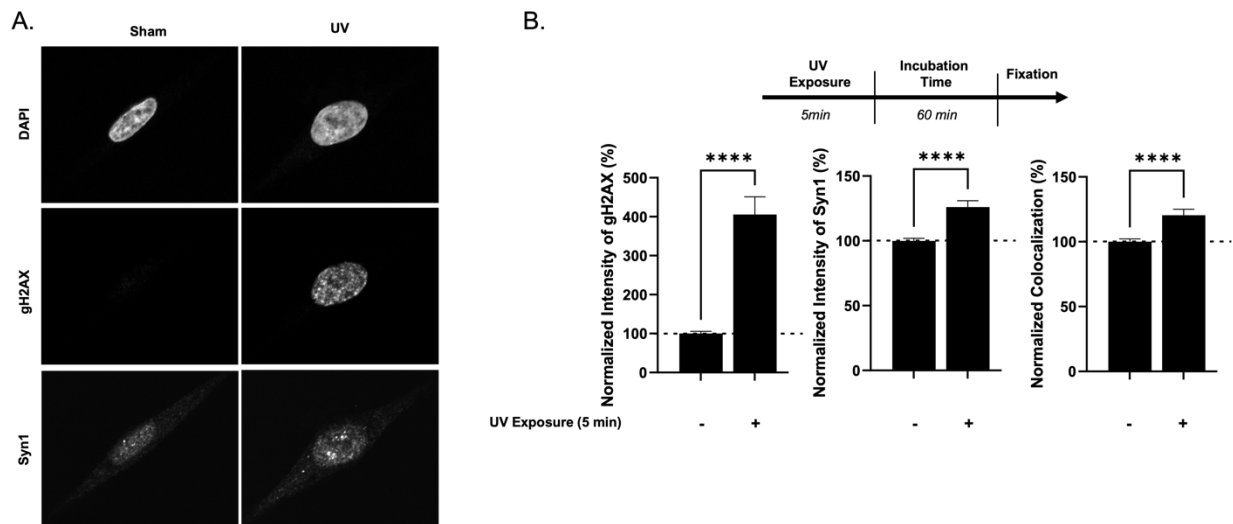


Figure A.1.2. Alpha-synuclein is important in bleomycin and IR-induced DNA damage response pathways. A, B) Primary melanocytes were treated with UVR for 5 minutes, incubated for 60 minutes, and stained for Syn1, γH2AX, and DAPI. Mean intensity of γH2AX and Syn1 signal within DAPI and colocalization between γH2AX and

Syn1 foci were analyzed using FIJI. **** $p < 0.0001$ by unpaired t test. Error bars denote SEM. Quantification from 3 biological replicates (total $n = 66-270$ nuclei per condition). Melanocyte culturing of Figure A.1.2 performed by Gail Kent and Pam Cassidy.

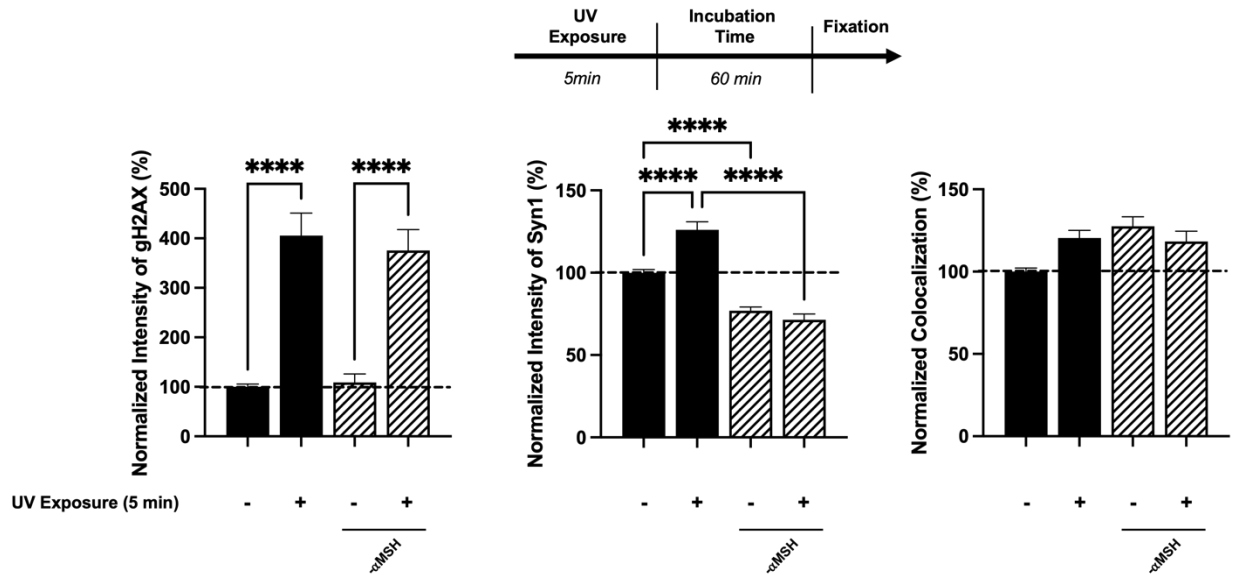


Figure A.1.3. Alpha-MSH removal significantly diminished alpha-synuclein levels and its response to UV radiation. A, B) Primary melanocytes were cultured in complete media or media without α MSH and treated with UVR for 5 minutes, incubated for 60 minutes, and stained for Syn1, γ H2AX, and DAPI. Mean intensity of γ H2AX and Syn1 signal within DAPI and colocalization between γ H2AX and Syn1 foci were analyzed using FIJI. **** $p < 0.0001$ by one-way ANOVA. Error bars denote SEM. Quantification from 3 biological replicates (total $n = 41-270$ nuclei per condition). Melanocyte culturing of Figure A.1.3 performed by Gail Kent and Pam Cassidy.

Discussion

These results further emphasize α Syn's role in DNA DSB DDR, in accordance with data presented in Chapter 3. Like bleomycin and I-Ppol treatment, UVR also led to a significant increase in α Syn levels, suggesting that upregulation of this protein may help facilitate the DDR at the DSB (increased α Syn colocalization with γ H2AX). This data also implies that the results found in Chapter 3 are translatable to other cell types that are

pigmented (discussed in Chapter 5.6) and other DNA damage inducing paradigms (discussed in Chapter 5.2), further strengthening the developed hypothesis and highlighting the therapeutic potential in targeting α Syn in melanoma treatment.

Furthermore, the results in Figure A.1.3 are intriguing in that they open many possibilities for future investigation of the role of α Syn in α MSH and MCR1 biology. MC1R is the major genetic determinant of hair color. Binding of its ligand α MSH to MC1R in melanocytes activates the cAMP pathway and facilitates eumelanin synthesis (916, 917). MC1R is not only present in melanocytes but also has been found in dopaminergic neurons in the mouse substantia nigra (350) and these receptor levels are reduced in the substantia nigra of PD patients (352), with elevated α MSH seen in the CSF of patients with PD and MSA (918, 919). Evidence suggests that MC1R interacts with α Syn, however studies are contradicting. One study found that MC1R prevents α Syn oligomerization through Nrf2 activation (352), while another study found that α MSH treatment induced α Syn aggregation in a melanized human dopaminergic cell model and led to parkinsonism symptoms in mice (920). How α MSH and MCR1 are involved in PD pathogenesis is still unclear, but these preliminary results (Figure A.1.3) offer an interesting perspective of the role of α MSH and MCR1 in α Syn-mediated DSB repair in melanocytes.

Recent studies have identified a crucial role of MC1R in regulating DNA repair within melanocytes following UV exposure, which can be pigmentation-dependent or -independent (921, 922). One study found that pre-treatment of melanocytes with α MSH reduced UV-induced generation of oxidative DNA damage and increased protein levels of antioxidants, catalase and ferritin, as a defense response (923). It was also reported that pre-treatment of melanocytes with α MSH augmented their DDR by increasing

phosphorylation of ATR and ATM and enhancing formation of γ H2AX at nuclear sites of repair (924), which have downstream effects on nucleotide excision repair (NER) (925). It is possible that α MSH also initiates the upregulation of α Syn in melanocytes as a defense mechanism for UV-induced DNA damage, since the absence of α MSH leads to a significant reduction in α Syn protein levels in primary melanocytes both prior to and following UV radiation (Figure A.1.3). It is also possible that diminished ATR and ATM phosphorylation in the absence of α MSH, has downstream consequences on the expression of α Syn and/or may interact directly with nuclear α Syn. Further investigation is warranted to uncover mechanistic insight into the convergence of α Syn-mediated DDR and the MCR1/ α MSH pathway in melanomagenesis and melanoma growth phenotypes.

Methods

Cell lines

Primary melanocytes were isolated from male patient foreskin samples provided by Oregon Health and Science University. Isolation protocol followed the steps outlined in (664). Cells were maintained in a humidified chamber with constant supply of 5% CO₂ and 95% O₂ at 37C.

Ultraviolet radiation

One day prior, 30,000 primary melanocytes were seeded onto PDL coated coverslips in 35mm plates in complete melanocyte medium. At the time of UVR treatment, complete medium was replaced with PBS and UVR was delivered by a simulated solar radiation generator (Oriel 1600 W solar simulator; 21 seconds = 100 mJ/cm² thermally-

weighted solar radiation or 1SED) for 5 minutes. Cells were put in complete medium followed by a 60-minute recovery period. Following the recovery period, cells were fixed and processed for immunocytochemistry as described below.

Immunocytochemistry staining

After UVR treatment and fixation in formalin for 15 minutes, cells were washed in 1x PBS and permeabilized in 0.25% Triton X-100 in PBS for 5 minutes. Coverslips were blocked in 10% goat serum/0.1% Triton X-100 in PBS for 30 minutes and then placed in the primary antibody overnight at RT. The next morning, cells were washed three times in 1x PBS and placed in secondary antibody overnight at RT. The following day, coverslips were washed 4 times in 1x PBS. The third wash contained DAPI (2.5µg/ml) for 20min. Coverslips were mounted using CFM2 antifade reagent and sealed with BioGrip. All immunofluorescence images were taken on a Zeiss ApoTome2 Microscope or Zeiss Laser-Scanning Confocal Microscope 980 and analyzed with FIJI (2D analysis using custom made macro available on GitHub). Mean intensity and Pearson's coefficient colocalization analysis was measured after imposing DAPI masks over each cell. All cells within a 63x image were analyzed and numbers of n are provided in each figure legend. Statistical significance was assigned using one-way ANOVA with multiple comparisons or unpaired t test.

Antibody specifics were as follows: Syn1 (BD Biosciences #610786, RRID:AB_398107, 1:500), γH2AX (Cell Signaling #9718, RRID:AB_2118009, 1:500).

A.2 SK-Mel28 Cells

Introduction

Additional experiments were performed utilizing the SK-Mel28 cell line to investigate the role of α Syn in global DDR and specifically the nucleolar DDR prior to and in continuation of the data presented in Chapter 3. These results were not included in publication due to non-significant findings and/or complicated mechanistic outcomes. Each experiment is outlined under its respective subheading.

Results

Neutral Comet Assay: DNA DSB Levels (Figure A.2.1)

In order to further test whether the DDR may be compromised in α Syn KO cells following induced DNA damage, the neutral comet assay was performed to measure DSBs, as previously described (442). SK-Mel28 α Syn Control and KO cells were treated with bleomycin (100 μ g/ml) or vehicle for 1 hour followed by neutral comet assay. Results show a significant increase in olive moment, tail moment, and % DNA in tail after bleomycin treatment compared to vehicle (Figure A.2.1). However, α Syn loss-of-function did not alter the response to bleomycin treatment, and in some measurements (olive moment and % DNA in tail), actually had a diminished response to bleomycin compared to Control and Rescue cells (Figure A.2.1).

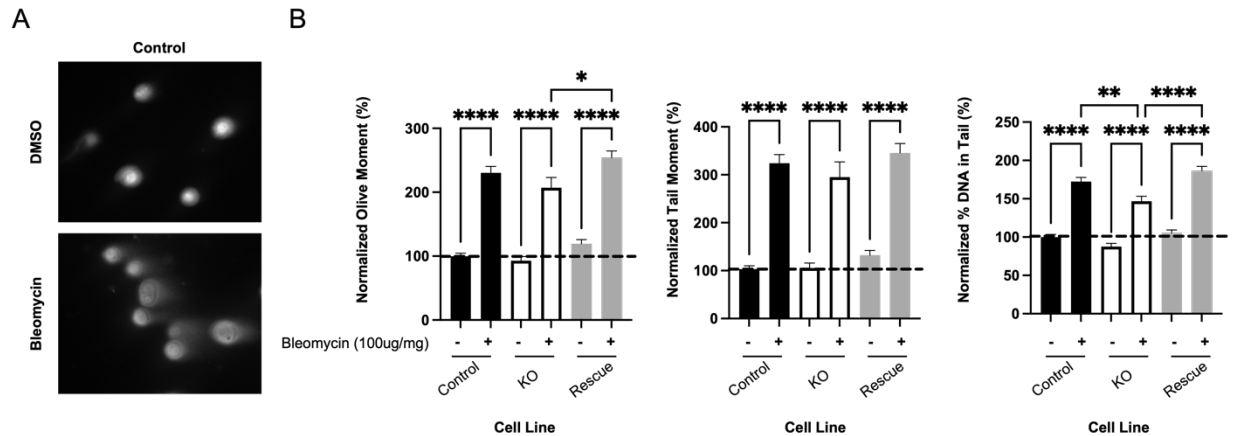


Figure A.2.1. Alpha-synuclein KO does not affect DNA DSB levels as measured by neutral comet assay. A) Representative images of control SK-Mel28 cells treated with DMSO or 100 μ g/ml Bleomycin. Comet assay proceeded using Neutral Comet Assay protocol (Trevigen). Cells were stained with SYBR Green and imaged at 10x. B) Quantification of images collected from Neutral Comet Assay. Values are normalized to the average DMSO control within each replicate. Error bars indicate SEM (n= 2 biological replicates, total of 359-430 cells). Statistical significance calculated via one-way ANOVA with Tukey's multiple comparisons tests, * p<0.05, ** p<0.01, **** p<0.0001.

HR and NHEJ Repair Pathways (Figure A.2.2)

Results from Chapters 3 and 4 clearly indicate the important role of α Syn in facilitating DNA DSB repair through 53BP1-specific pathways. 53BP1 is important for DSB repair pathway choice, generally promoting NHEJ and limiting HR (626). However, DSB repair in heterochromatin by HR also requires 53BP1, suggesting that the role of 53BP1 may vary dependent on the context (627). To further elucidate which repair pathway α Syn may be involved in, HR and NHEJ plasmid reporters were utilized in the SK-Mel28 cell lines, as previously reported (443). This system involves two different plasmids that can be linearized and transfected into cells: one plasmid is sensitive to HR repair and the other plasmid is sensitive to NHEJ, both of which will produce fluorescent GFP expression when re-circularized (926). After transfection of these linearized

plasmids into SK-Mel28 cells, GFP expression and RFP expression (transfection control) were measured using flow cytometry. Results show that at 72 hours post-transfection, α Syn loss-of-function does not influence HR or NHEJ plasmid repair efficiency compared to Control and Rescue lines (Figure A.2.2).

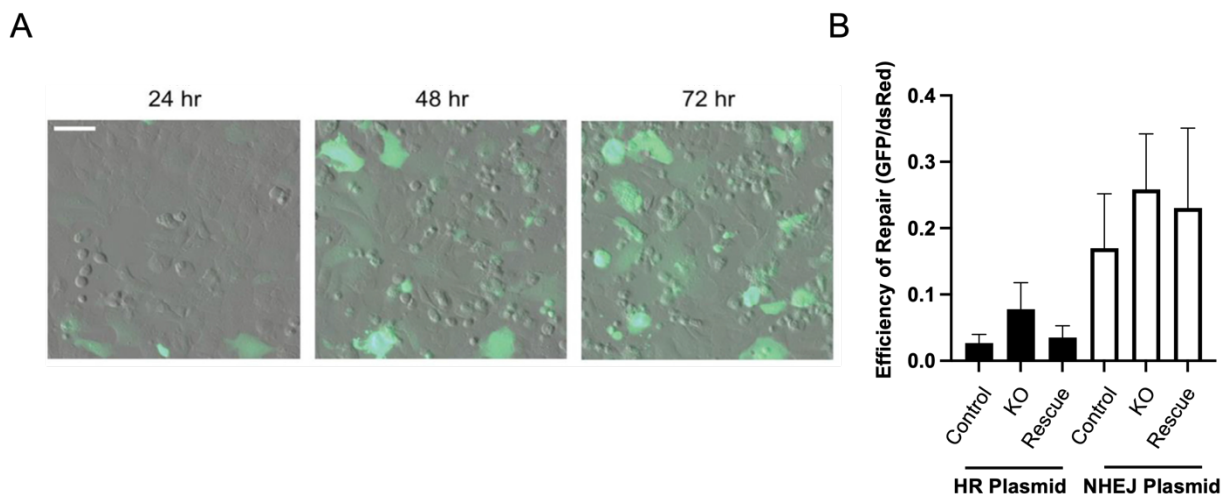


Figure A.2.2. Alpha-synuclein KO does not affect HR or NHEJ reporter plasmid repair efficiency. A) A representative image sequence of NHEJ reporting green fluorescing HAP1 cells after repair events at 24, 48, and 72 h post transfection (Scale bar = 50 μ m). Images taken from Rose et al. (443). B) Quantification from 72 h timepoint. Efficacy of DSB repair was quantified by taking the ratio of cells with repaired events (green cells) over the transfection control (red cells). Error bars indicate SEM (n=140,149-642000 cells counted per replicate, 2 biological replicates). Statistical significance calculated via one-way ANOVA with Tukey's multiple comparisons tests.

Localization and Interaction with Nucleolar Proteins (Figure A.2.3)

Despite the aforementioned non-significant data investigating the role of α Syn in global DDR (Figures A.2.1 and A.2.2), localization data from Chapter 3 (Figure 3.3.1), clearly shows an enrichment of α Syn in the granular compartment of the nucleolus. While investigation moved on to induced rDNA damage paradigms (Chapter 3), it is important to confirm the baseline enrichment of α Syn in the nucleolus, not only through

immunocytochemistry and electron microscopy techniques (Figure 3.3.1), but also through protein-protein interaction methodology. Proximity ligation assay (PLA) approaches also confirmed colocalization of α Syn with the nucleolar proteins, UBF, treacle, fibrillarin, and nucleophosmin (Figure A.2.3). Taken together, these data strongly suggest that α Syn localizes to the nucleolus in melanoma cells.

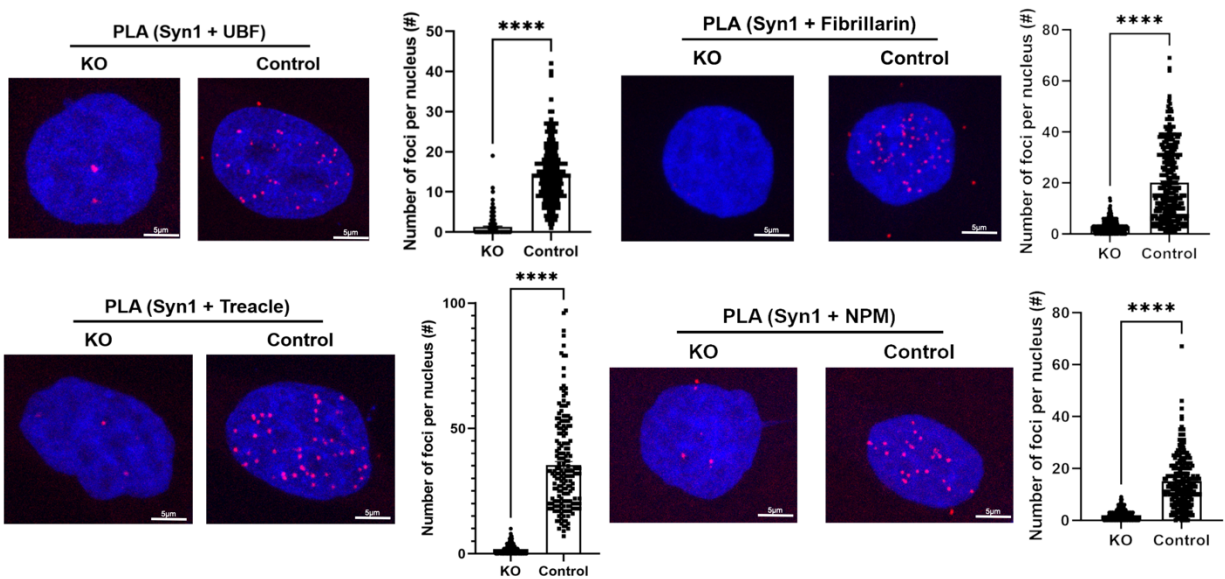


Figure A.2.3. Alpha-synuclein interacts with multiple nucleolar proteins. SK-Mel28 control and KO cells were seeded on PDL-coated coverslips and then fixed in 4% paraformaldehyde. Proximity Ligation Assay (Duolink) was completed using antibodies against Syn1 and UBF, Fibrillarin, Treacle, and Nucleophosmin. Cells were imaged on the Zeiss 980 confocal microscope and number of foci per nucleus was measured using CellProfiler while masking for the nucleus using DAPI. Each figure shows representative images and quantification from 3 biological replicates. **** $p < 0.0001$ by T-test. Error bars denote SEM. Staining of Figure A.2.3 performed by Gabe Cohn.

53BP1 Recruitment and Western Blot Analysis (Figure A.2.4)

To confirm the mechanistic findings in Chapter 3 regarding the impairment of 53BP1 recruitment to the nucleolar cap in α Syn KO cells, additional western blot verification was performed. Unlike the data from immunocytochemistry (Figure 3.3.7),

treatment of cells with I-Ppol did not lead to a significant increase in 53BP1 protein levels and α Syn loss-of-function did not impair 53BP1 response to rDNA damage, although a small non-significant trend could be seen (Figure A.2.4).

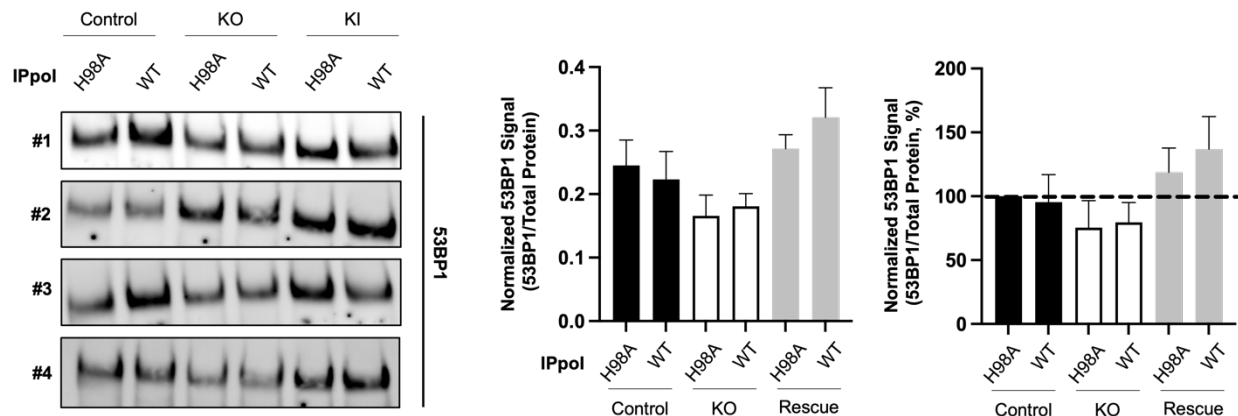


Figure A.2.4. Alpha-synuclein KO does not affect 53BP1 total protein expression as measured by western blot. The same cell lysates from Figure 3.3.4B were used in this experiment. SK-Mel28 cells were transfected with WT and H98A I-Ppol mRNA for 6 hours, cells were lysed and nuclear fractionation was performed. Protein was run out on 3-8% Tris-Acetate gel and transferred onto PVDF and probed for 53BP1 and total protein. Quantification from 4 biological replicates. Statistical analysis by ANOVA. Error bars denote SEM.

Kinase Dysregulation in DDR Pathways (Figures A.2.5 and A.2.6)

The dysregulation in 53BP1 recruitment seen in Figure 3.3.7 and the mechanism proposed in Chapter 3 (Figure 3.4.1) both highlight the DDR kinase-phosphorylation cascades upstream of 53BP1 recruitment and α Syn recruitment to the rDNA DSB. Future experiments proposed in Chapter 5.2 included phospho-proteomic analysis to investigate potential alterations in multiple DDR kinase signaling pathways that occur with α Syn loss-of-function. Using advanced mass spectrometry proteomics and the established TMT/IMAC bottom-up LC-MS/MS proteomics pipeline (927), we directly measured the

relative levels of phospho-targets in Control, α Syn KO and Rescue SK-MEL28 cells at baseline. Differentially abundant phosphosites were identified between Control and KO cells and validated through KO versus Rescue comparisons and hyperactivated/deactivated kinase signaling was inferred based on differential abundance of phosphosites using the kinase/substrate enrichment approach (KSEA R package (928)). Intriguingly, this data set identified 41 kinases that were upregulated or downregulated in α Syn KO compared to Control and Rescue cells (Figure A.2.5). Of these 41, 4 downregulated kinases were identified with a greater than 1-fold-change and have been previously implicated in DDR pathways using gene ontology analysis (Figure A.2.5, red annotation), including PLK1, PRKCD, PLK3, and MTOR. Their respective phosphosite heatmaps are represented in Figure A.2.6.

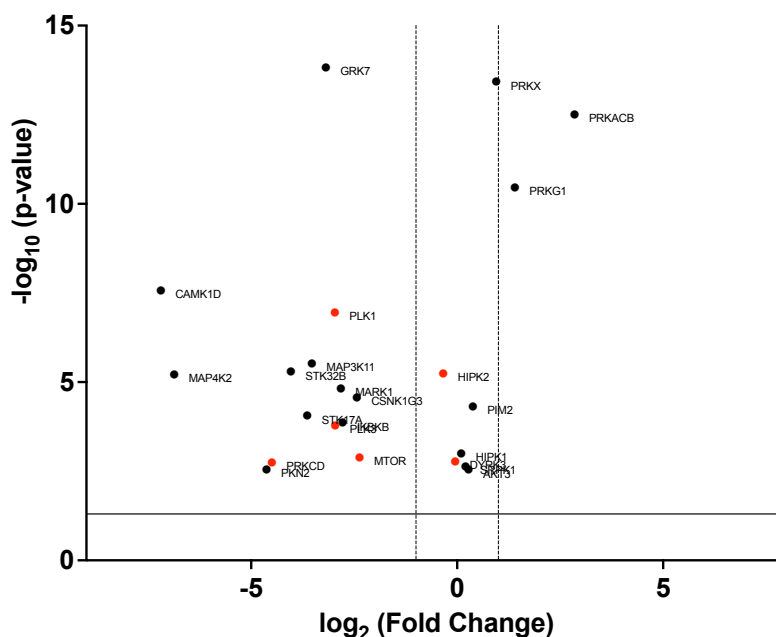


Figure A.2.5. Volcano plot of dysregulated kinases after alpha-synuclein loss-of-function. Total protein was extracted from SK-Mel28 control, KO and rescue cells and sent for TMT/IMAC bottom-up LC-MS/MS proteomics (n=5 biological replicates per condition). Hyperactivated/deactivated kinase signaling was inferred based on differential abundance of phosphosites using the kinase/substrate enrichment approach (KSEA R

package. 41 kinases were identified and plotted on a volcano plot using p-value and fold change. Red labeling indicates kinases of interest. Formal analysis of Figure A.2.5 performed by Vladislav Petyuk.

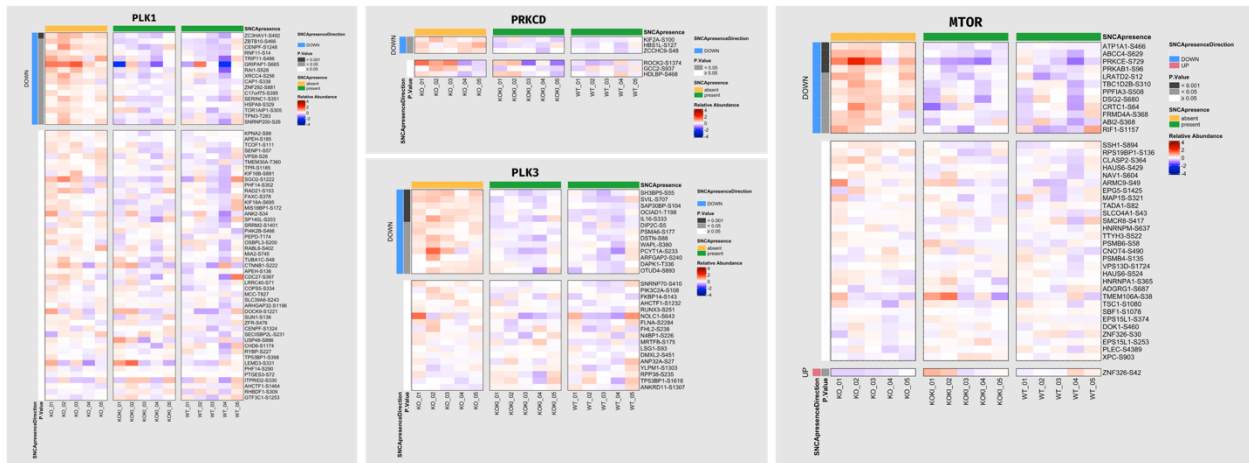


Figure A.2.6. Heat maps of the identified phosphosites from 4 kinases of interest (Figure A.2.5). The heat map represents the significantly different phosphorylation sites identified between α -syn Control and KO SK-Mel28 cells. The phosphosites with increased intensities are marked in red, and phosphosites with lower intensities are marked in blue. Formal analysis of Figure A.2.6 performed by Vladislav Petyuk.

rDNA Copy Number and Ribosome Biogenesis (Figure A.2.7)

In addition to the proposed role of α Syn in the nucleolar DDR (Figure 3.4.1), it is possible that α Syn is involved in other processes within the nucleolus. As mentioned in Chapter 1.5, NORs contain around 300 rDNA repeats and due to recombinogenic instability of the rDNA repeats, there is a 10-fold variation in copy numbers among humans (929, 930). However, during malignant transformation, replication stress can lead to copy number alterations within the rDNA repeats, and this has been proposed to serve as a biomarker in disease severity (548, 719, 931, 932). Furthermore, perturbations in DDR pathways can alter rDNA copy number (933, 934). These changes in rDNA copy number can ultimately have downstream effects on ribosome biogenesis. Ribosome

biogenesis is a complicated set of steps that start with the transcription of pre-rRNAs, their subsequent cleavage, and processing into the 28S, 5S, 5.8S, and 18S mature rRNAs, which along with an additional ~80 proteins are folded and organized to form the 40S and 60S subunits. Several groups have documented nucleolar abnormalities in PD patient substantia nigra neurons (501, 555, 575), that monogenic forms of PD alter ribosomal function (783, 784), and that α Syn overexpression in the nucleus leads to altered rRNA processing and ribosome biogenesis (577). Whether α Syn loss-of-function leads to abnormalities in rDNA copy number or ribosome biogenesis as a consequence or not of nucleolar DDR dysregulation is unknown.

To investigate whether α Syn KO influences rDNA copy number and therefore rRNA biogenesis, qPCR analysis was completed using isolated gDNA from SK-Mel28 Control, KO, and Rescue cell lines probing for 18S, 28S, 5S, and tRNA^{Met} (internal control), as previously described (549). Results show no significant differences in 5S, 18S, or 28S copy numbers between Control, KO, and Rescue cell lines (Figure A.2.7). To induce genomic instability and reveal perhaps more subtle differences in the α Syn KO line, cells were passaged greater than 35 times. Cells that are repeatedly divided in a lab setting over many passages accumulate DNA damage in addition to telomere shortening, leading to a state of senescence and a higher likelihood of genetic mutations, potentially impacting the cell's function and behavior. At this high passage number, there was a significant decrease in 28S copy number in the α Syn KO line, however this result was not rescued when α Syn was reintroduced (Figure A.2.7).

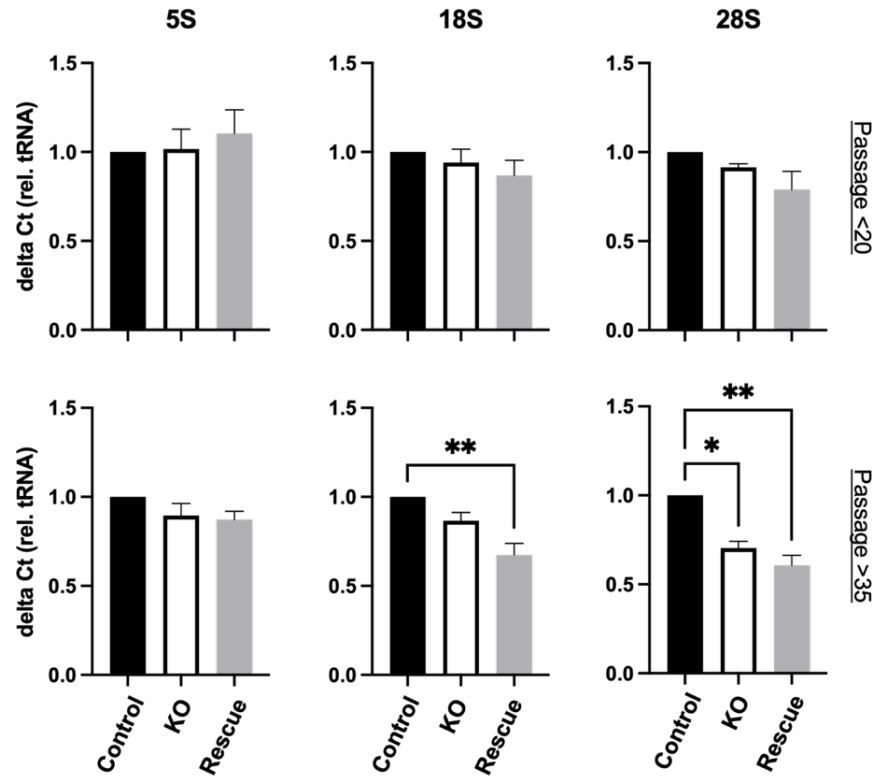


Figure A.2.7. Alpha-synuclein KO does not affect rDNA copy number. Genomic DNA was isolated from SK-Mel28 Control, KO, and Rescue cells at various passage numbers. Using primers against the various targets described in Table A.2.1, qPCR amplification was determined when normalized to tRNA^{Met} internal control. Each sample was run with 2 technical replicates across 3 biological replicates. * p<0.05, **p<0.01 by one-way ANOVA.

Ferroptosis and Lipid Peroxidation (Figure A.2.8)

The cellular growth pathways explored in Chapter 5.5 are in response to data presented in Chapters 3 and 4 regarding apoptosis, senescence, and autophagy. However, the dysregulation of multiple other cell growth pathways has been implicated in both PD and melanoma pathogenesis, including ferroptosis, necroptosis, and pyroptosis. Therefore, α Syn loss-of-function and dysregulation of the DDR could be leading to other downstream cellular growth abnormalities as well. Investigation into ferroptosis was completed using the compound, BODIPY (935). BODIPY™ 581/591 C11 is a sensitive

fluorescent probe that senses lipid peroxidation and localizes to membranes in live cells. Lipid peroxidation is involved in apoptosis and one of the main contributors to ferroptosis, an iron-dependent, non-apoptotic form of cell death. Oxidation of the polyunsaturated butadienyl portion of this fatty acid analog in live cells results in a shift of the fluorescence emission peak from red (~590 nm) to green (~510 nm), allowing ratiometric analysis of lipid peroxidation using flow cytometry. SK-Mel28 Control, KO, and Rescue cells were treated with 1 μ M RSL3 for 24 hours to induce ferroptosis followed by a 20-minute treatment with BODIPY-C11 and FACS analysis. Results show that α Syn KO did not significantly change ferroptosis levels as measured by increased shift in BODIPY-488 oxidation signal from DMSO to RSL3, however reached a near-significant increase compared to Control and Rescue cells (Figure A.2.8).

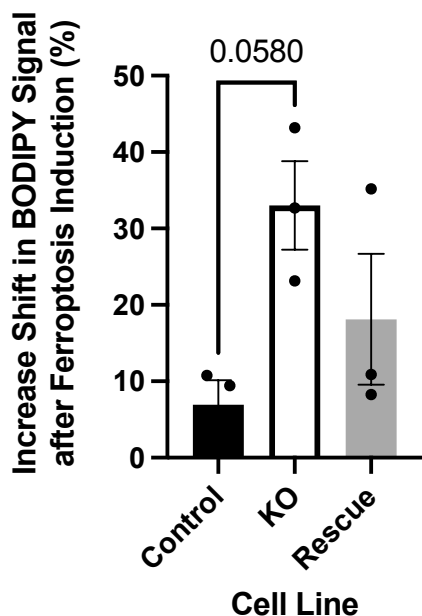


Figure A.2.8. Alpha-synuclein KO does not affect ferroptosis levels. SK-Mel28 cells were treated with DMSO or 10 μ M RSL3 for 24 hours. After a 20-minute treatment with BODIPY-C11, cells were prepared for FACS. Ferroptosis was quantified by taking the

percent increase in geometric mean 488 signal between DMSO and RSL3 treated cells in each condition. Error bars indicate SEM (n=6,833-18,514 cells counted per replicate across 3 biological replicates). Statistical significance calculated via one-way ANOVA with Tukey's multiple comparisons tests.

EMT and Metastatic Potential (Figure A.2.9)

DSB repair is also linked to cellular processes with important implications for metastasis, including the epithelial-mesenchymal transition (EMT). The EMT is important for melanoma progression since the transition to a mesenchymal phenotype produces motile and invasive properties that promote the initial steps of metastasis. Interestingly, the opposite mesenchymal-epithelial transition (MET) is also important once malignant cells reach their target organ, in order to adopt an epithelial phenotype again and integrate successfully into the distant metastatic site. DSB repair can regulate the EMT, since loss-of-function of the DSB repair factor γ H2AX promotes the EMT by regulating the transcription factors Slug, Twist1 and ZEB1 in a colon carcinoma (936) and non-malignant (937) cell lines. Suppressing DSB repair via a Growth Hormone-dependent mechanism promotes the EMT and metastasis in an *in vivo* mouse model of colon carcinoma (938). Conversely, enhancement of HR in an ATM-dependent process inhibits the EMT (favoring MET) in breast carcinoma (939). Importantly, recent work in renal proximal tubule epithelial cells strongly suggests that α Syn promotes an epithelial nature and α Syn knockout promotes the EMT and renal fibrosis (940). This suggests that α Syn may play similar roles in melanoma and it is therefore important to test if α Syn regulates the EMT and the ability of malignant melanoma cells to metastasize. Consistent with the results

from renal proximal tubule epithelial cells (940), western blot analysis revealed that α Syn loss-of-function upregulates mesenchymal marker, vimentin (Figure A.2.9).

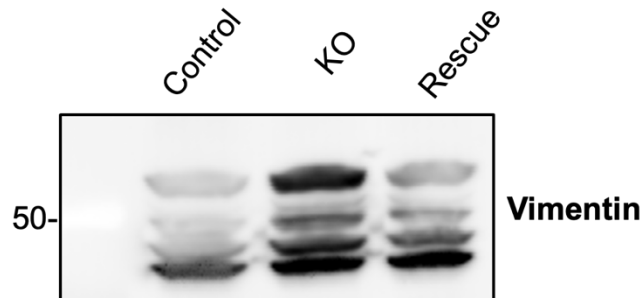


Figure A.2.9. Alpha-synuclein KO increases mesenchymal marker, vimentin. SK-Mel28 cells were lysed and protein was run out SDS-PAGE and probed for vimentin and total protein. Expected band size for vimentin = 57kDa.

Replication Stress and Caspase-3 Activity (Figure A.2.10)

Lastly, as alluded to in Chapter 5.2, α Syn may be involved in other DDR processes, not just ATM-mediated DSB repair. For example, α Syn has been previously implicated in replication stress-induced DNA damage in yeast (510). This type of DSB is unique in that it is recognized predominantly by ATR at the single-stranded DNA stage to initiate the DDR (731-733). To test whether α Syn could protect against replication stress-induced DNA damage and downstream apoptotic phenotypes, SK-Mel28 cells were treated with etoposide, a compound known to induce ATR-dependent replication stress-induced DSBs, and measured Caspase-3 activity. Interestingly, I found a significant decrease in caspase-3 activity in α Syn KO cells compared to Control and Rescue cells when treated with etoposide (Figure A.2.10).

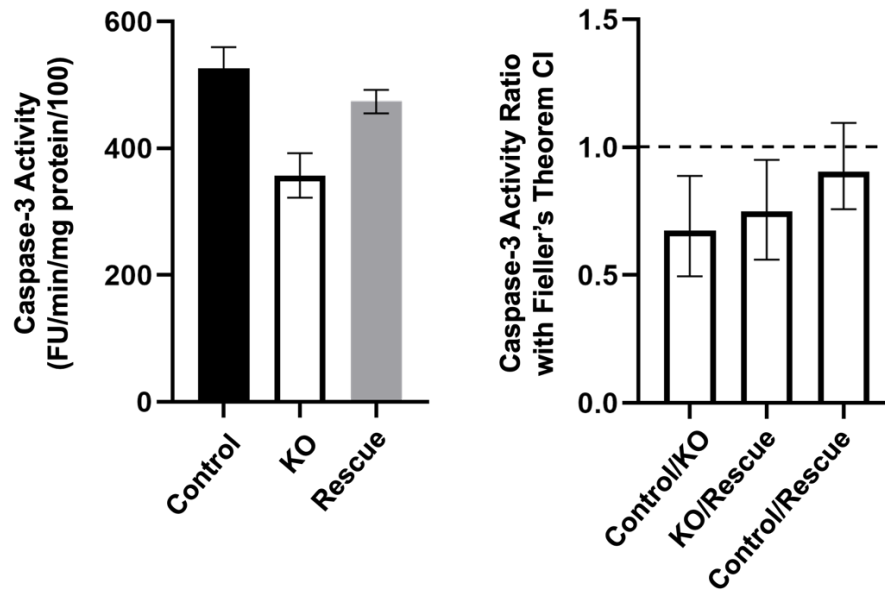


Figure A.2.10. Alpha-synuclein KO decreases Caspase-3 activity after etoposide treatment. SK-Mel28 Control, KO, and Rescue cells were treated with 25 μ M etoposide for 72 hours. Cells and floating cells in the medium were lysed and Caspase-3 activity assay was performed. Each sample was run with 3 technical replicates across 3 biological replicates. Statistical significance by Fieller's Theorem Confidence Intervals. Data acquisition and formal analysis of Figure A.2.10 performed by Pam Cassidy.

Discussion

The results presented in this Appendix A.2 provide valuable insights into the role of α Syn in the DDR and nucleolar biology, even though some findings were inconclusive or context dependent. Each experimental figure highlights specific aspects of α Syn's involvement (or lack thereof) in various cellular processes. Below, I provide a detailed discussion of these findings, organized by the corresponding figure.

Neutral Comet Assay: DNA DSB Levels (Figure A.2.1)

The neutral comet assay revealed that bleomycin treatment significantly increased DNA damage in SK-Mel28 cells, as evidenced by elevated olive moment, tail moment, and % DNA in the tail. However, α Syn KO did not amplify this response. Surprisingly, certain metrics, such as the olive moment and % DNA in the tail, exhibited a diminished response in KO cells compared to controls. These results suggest that while bleomycin effectively induces DSBs, α Syn loss-of-function may not exacerbate or mitigate the DDR in this context. One potential explanation for these findings is the compensatory activity of alternative DDR pathways or proteins, masking any α Syn-specific effects. Furthermore, while the comet assay is widely used in the field to measure DSBs, the neutral comet assay has notable limitations and controversies (941). First, although it measures DNA breaks, its specificity in distinguishing SSBs from DSBs is debated, as relaxation of supercoiling can occur under both neutral and alkaline conditions, potentially leading to misinterpretations. Second, the assay's dynamic range is limited, saturating when a significant portion of DNA migrates to the comet tail, which may underestimate extensive damage. Lastly, the neutral comet assay may not be sensitive at detecting apoptotic DNA fragments (or DSBs found in micronuclei, Figure 3.3.7), as these fragments tend to diffuse away or are too small to be retained before electrophoresis. Taken together, while the results in Figure A.2.1 were non-significant, it is possible that this assay is not well-suited for detecting changes in the DSB burden under α Syn loss-of-function. Other techniques that were utilized in Chapter 3 are more sensitive and specific.

HR and NHEJ Repair Pathways (Figure A.2.2)

Contrary to expectations, α Syn KO in SK-Mel28 cells did not alter the efficiency of HR or NHEJ in plasmid repair assays, as seen in HAP1 cells (443). Despite this result, these findings are similar to other studies in that the efficiency of NHEJ repair \gg efficiency of HR repair. In human fibroblasts, NHEJ efficiency is typically 0.6-1.3 and HR efficiency is 0.05-0.3 (942). However, since DSB efficiency is measured as a ratio of GFP+/DsRed+ cells, variations in the mixture of I-SceI and DsRed plasmids may affect the result. This confound becomes important because each cell in the experiment contains only one copy of the integrated reporter construct, thus successful repair events will reconstitute the GFP gene in a fraction of the cells. Furthermore, the DSB repair efficiency is affected by cell type, cell cycle phase, and chromosomal location of the integrated constructs. Based on the high percentage of DsRed+ cells compared to GFP+ in my experiments in Figure A.2.2, it seems that SK-Mel28 cells may uptake and/or express the DsRed empty vector plasmids more proficiently than the DSB repair reporter plasmids, resulting in much smaller efficiency values of HR and NHEJ compared to previous reports. Lastly, the repair of extrachromosomal DNA transfected into cells, as described above, is likely to involve different processes than those that occur in the context of genomic DSBs. Other factors like DNA methylation, histone modifications, and higher order chromatin organization are absent in this paradigm. Given the complexity of DDR and the influence of cellular context, future studies using different cell lines or stress paradigms might elucidate α Syn's nuanced roles in repair pathway dynamics.

Localization and Interaction with Nucleolar Proteins (Figure A.2.3)

The PLA demonstrated robust colocalization of α Syn with key nucleolar proteins, including UBF, treacle, fibrillarin, and nucleophosmin. This enrichment underscores α Syn's potential involvement in nucleolar functions, such as ribosome biogenesis and/or nucleolar DDR. The consistent localization across methods (immunocytochemistry, electron microscopy, and PLA) strengthens the conclusion that α Syn's presence in the nucleolus is functionally significant. However, it is important to note that nucleolar masking is required to confirm these protein-protein interactions within the nucleolus. As it stands, the PLA signal presented in Figure A.2.3 is spatially non-discriminatory within the nucleus. Future work should address whether these interactions influence nucleolar processes or contribute to disease phenotypes in melanoma or PD.

For example, other proximity-labelling techniques could be utilized, like the Biotinylation by Antibody-Recognition (BAR) method (943), to validate PLA findings and investigate functional properties of α Syn in nucleolar DSB repair. In this method, the Syn1 primary antibody would be used to label endogenous α Syn in fixed SK-Mel28 cells and a second antibody conjugated to HRP would be bound to the primary antibody. Biotin-XX Tyramide reagent in conjunction with hydrogen peroxide reaction would label nearby proteins with biotin. Streptavidin Dynabeads would pull out biotinylated proteins to be submitted to LC-MS for identification. This experiment could be useful both at baseline and when the nucleolar DDR is initiated via rDNA DSB induction. In addition, preliminary data from Eli Wisdom (graduate student in the Unni Lab), utilizing an α Syn-TurboID LC-MS pipeline in HEK293T cells, showed that treacle, nucleophosmin, and nucleolin

proteins interact with α Syn-TurboID at baseline (data not shown). These preliminary results further emphasize the functional significance of α Syn in the nucleolus and provide rationale for future experimentation.

53BP1 Recruitment and Western Blot Analysis (Figure A.2.4)

Despite earlier findings in Chapter 3 showing impaired 53BP1 recruitment to nucleolar caps in α Syn KO cells (Figure 3.3.7), western blot data failed to demonstrate significant changes in 53BP1 protein levels following I-Ppol treatment. The discrepancy between immunocytochemistry analysis in Figure 3.3.7 utilized a masking feature of the nucleolar cap to measure 53BP1 signal directly surrounding the cap. Second, transfection efficiency for I-Ppol mRNA in SK-Mel28 cells is ~40-50%; during the immunocytochemistry pipeline, only cells with nucleolar caps were imaged and analyzed. Taken together, cell lysate-based western blotting may not have the spatial sensitivity or transfection efficiency required to detect the dysregulation of recruitment of 53BP1 to the nucleolar cap. Additional experiments utilizing global DNA damage inducers could provide clarity using this technique, however would have other significant drawbacks (explained in Chapter 5.2).

Kinase Dysregulation in DDR Pathways (Figures A.2.5 and A.2.6)

Proteomic analysis identified 41 dysregulated kinases in α Syn KO cells, with four (PLK1, PRKCD, PLK3, and MTOR) implicated in DDR pathways by gene ontology

analysis. The kinase/substrate enrichment analysis suggests that α Syn loss-of-function alters upstream signaling cascades, potentially affecting repair pathway activation. These findings provide a foundation for targeted studies on how specific kinases mediate α Syn-dependent DDR mechanisms. The downregulation of MTOR, a known regulator of cellular growth and stress responses, is particularly intriguing given its implications in cancer and neurodegeneration. In addition, PLK1 and PLK3 are of particular interest. Of the kinases that phosphorylate α Syn, the Polo-like Kinase (PLK) family is suggested to be the main kinase responsible for α Syn S129 phosphorylation (discussed in Chapter 5.3) (944-946). Two of the five PLK family members, PLK2 and PLK3 have been shown to promote α Syn shuttling from the nucleus to the cytoplasm (947) and PLK2 can regulate the clearance of α Syn via autophagy. Furthermore, one study found that α Syn inclusions from PLK2 KO mice survived at a higher rate than those from WT mice, yet there was no difference in S129 phosphorylation of Lewy pathology after genetic deletion of PLK2 (948). A follow-up study found that pan-inhibition of the PLKs with the compound BI 2536, led to a significant increase in survival of neurons bearing LB inclusions *in vivo* (949). These previous findings in conjunction with the downregulation of PLK1 and PLK3 in SK-Mel28 α Syn KO cells (Figures A.2.5, A.2.6) suggests that phosphorylation of α Syn may modulate its ability to facilitate the DDR, which in turn influences neurodegeneration and melanomagenesis properties, an interesting area for future investigation (proposed in Chapter 5.3). Lastly, the discovery nature of this omics data can be leveraged by further investigating the top-enriched kinases, regardless of their currently known role in DSB repair, via kinase inhibitors that target the modifications discovered.

rDNA Copy Number and Ribosome Biogenesis (Figure A.2.7)

Quantitative PCR revealed no significant differences in rDNA copy number across Control, KO, and Rescue cell lines under baseline conditions. However, after extensive cell passaging, a reduction in 28S rDNA copy number was observed in α Syn KO cells. This result suggests that α Syn might influence rDNA stability under conditions of replicative stress. The lack of rescue upon α Syn reintroduction implies that these changes may be irreversible or involve additional factors beyond α Syn's immediate role. Additionally, limitations in the Rescue line creation (discussed in Chapter 5.6) may account for the lack of complete rescue. Furthermore, it is interesting to consider the implications of DSB repair pathway choice in the findings of 28S copy number loss at high passage number. It has been shown that HR-mediated repair is a driver of rDNA copy number loss (719). The findings in Figure A.2.7 fit into this discovery by the potential hypothesis that α Syn KO, which seems to preferentially affect NHEJ repair process more than HR (443), leads to impairment of NHEJ, compensatory increase of HR, and therefore an increase in copy number loss. The 28S rDNA region may be more vulnerable than the other regions to this type of stressor. Future implementation of DSB inducers followed by rDNA copy number measurement may exacerbate these findings and increase the sensitivity for measuring α Syn KO-mediated changes in the other rDNA regions.

Further experiments to determine whether these significant changes in 28S copy number influence ribosome biogenesis is warranted. Using established approaches, ribosome biogenesis could be measured via 47S pre-rRNA levels by qRT-PCR (950), specific probes that measure all major pre-rRNA intermediated by Northern blot (951), or

the newly-described technique “Riboprobing” (952). These future experiments could be performed in SK-Mel28 cells and mouse primary cortical neurons at baseline and after I-Ppol mRNA transfection to test whether deficiencies in ribosome biogenesis occur in the α Syn KO context after DSB repair has been compromised by α Syn loss-of-function compared to WT cells.

Ferroptosis and Lipid Peroxidation (Figure A.2.8)

Although α Syn KO did not significantly increase ferroptosis levels, a near-significant trend was noted. This result aligns with the hypothesis that α Syn mediates the DDR, which may have downstream cellular phenotypes, including ferroptosis. Previous findings have shown that α Syn KO in SK-Mel28 cells dysregulate iron metabolism by TfR1 and FPN1 deficiency and ferric iron and ferritin accumulation (478). Furthermore, an isoform of GPX4, a molecule important in the lipid peroxidation pathway and the selective target of RSL3 treatment to induce ferroptosis, plays a role in nucleoli-damaged cell death (953). Whether or not α Syn regulates ferroptosis cell death pathways through its function in nucleolar DDR is unknown, but future investigation is warranted given these preliminary results (Figure A.2.8). Variability between flow cytometry experiments is a limitation of these findings and other methods to measure ferroptosis should be employed, like qRT-PCR of ferroptosis markers, *CHAC1* and *PTGS2*.

EMT and Metastatic Potential (Figure A.2.9)

Consistent with findings in renal epithelial cells (940), α Syn KO in melanoma cells upregulated the mesenchymal marker, vimentin. These data suggest that α Syn may suppress the epithelial-to-mesenchymal transition (EMT) but upregulate the mesenchymal-to-epithelial transition (MET), a key process in distant metastasis. Unfortunately, due to breeding and institutional animal regulation restraints, the experimental TG3 mouse cohort from Chapter 4, which has previously demonstrated solid organ metastasis at later time points (673), could not be analyzed for genotype-specific differences in solid-organ metastasis. However, it is important to note that data from Chapter 4 showed an un-significant yet trending impairment in metastasis to lymph nodes in α Syn KO TG3 mice (Figure 4.3.2), potentially due to impairment of the MET.

Potential future experiments include western blot analysis and immunocytochemistry for established markers of epithelial (E-cadherin) versus mesenchymal (N-cadherin) phenotypes. Additionally, *in vivo* metastasis paradigms could be fruitful in exploring α Syn's role in cancer pathogenesis and metastatic potential. An athymic (*rnu/rnu*) rat *in vivo* brain metastasis model has been previously developed and validated for several melanoma lines (954). In this methodology, rats would undergo intracardiac cell infusion under ultrasound guidance of SK-Mel28 Control, KO, and Rescue lines. Animals would be euthanized on day 21 and brains analyzed with primary antibody staining for melanoma markers. I would predict that α Syn KO will decrease metastasis since cells will not be able to undergo MET to reincorporate at the distant site. Furthermore, it would be translationally beneficial to perform studies in human tissue from

patients with primary and metastatic melanoma to test whether levels of α Syn are correlated with melanoma cells expressing more epithelial markers. Understanding how α Syn modulates EMT/MET transcription factors or signaling pathways could reveal novel targets for melanoma therapy.

Replication Stress and Caspase-3 Activity (Figure A.2.10)

Etoposide-induced replication stress led to decreased caspase-3 activity in α Syn KO cells, suggesting that α Syn plays a role in regulating the apoptotic response to replication stress-induced DNA damage. While α Syn's role in replication stress was not supported by earlier hydroxyurea-induced damage experiments (Chapter 5.2), the significant alteration in caspase-3 activity with etoposide treatment underscores the need for further exploration of α Syn's function in ATR-mediated pathways. Given the distinct initiation and recognition of replication stress-induced DSBs compared to other types, these findings may reflect a context-dependent role for α Syn that is specific to certain types of DDR stimuli. This is particularly relevant in melanoma pathogenesis, where replication stress-induced DSBs are biologically significant due to the hyperproliferative nature of cancer cells.

The potential implications of α Syn loss-of-function extend to the interplay between replication stress, genomic instability, and apoptosis (Chapter 5.5). As replication stress is a critical driver of genomic instability in cancer, the observed reduction in caspase-3 activity may suggest a mechanism by which α Syn modulates cell survival under such stress. Future experiments using additional ATR-dependent inducers, such as UV

irradiation, camptothecin, or aphidicolin, will be essential to dissect the mechanistic underpinnings of these findings and to validate the broader role of α Syn in apoptosis downstream of replication stress responses. Moreover, investigating the interaction between α Syn and key apoptotic regulators, including p53 and pro-apoptotic BCL2 family members, could provide insights into how α Syn influences the apoptotic threshold in cancer cells, especially because these findings are in opposition to the increase in caspase-9 levels in α Syn KO mouse tumors (Figure 4.3.4).

Overall, this Appendix A.2 highlights the multifaceted roles of α Syn in cellular processes related to DDR, nucleolar biology, cell death phenotypes, and stress responses. While some results were inconclusive or context dependent, the data collectively emphasize the complexity of α Syn's functions in the SK-Mel28 cells line. Future studies employing advanced methodologies and diverse model systems will be crucial in unraveling these intricate mechanisms.

Methods

Cell lines

The SK-Mel28 cell line were produced by Dr. Stephan Witt (Louisiana State University), after being purchased from ATCC and authenticated at the University of Arizona Genetics Core via their STR Profiling Cell Authentication service. Per Shekoohi et al. 2021, α Syn knockout cells were created through CRISPR/Cas9 genome editing targeting *SNCA* (478). In addition, re-expression of α Syn in the *SNCA* KO clone was established using lentivirus transduction of human α Syn under the CMV promoter. SK-

Mel28 cell lines were cultured in appropriate medium suggested by ATCC. Primary melanocytes were isolated from male patient foreskin samples provided by Oregon Health and Science University. Isolation protocol followed the steps outlined in (664). All cells were maintained in a humidified chamber with constant supply of 5% CO₂ and 95% O₂ at 37C.

Neutral Comet Assay

SK-Mel28 cells were treated overnight with DMSO or 100µg/ml Bleomycin for 1 hour. Cells were washed with 1x PBS, trypsinized, resuspended in a 1000,000 cells/ml 1x PBS solution, and mixed with molten agarose 1:2. The agarose mixture was placed onto CometSlides and the comet assay was completed following the manufacturer instructions (Trevigen, 4250-050-K). DNA was stained using SYBR Green and slides were imaged on a Zeiss ApoTome2 on AxioImager using a 10x objective (>100 cells/condition). Olive Moment, Tail Moment, and % DNA in tail was analyzed using CometScore software and statistical significance calculated via one-way ANOVA with Tukey's multiple comparisons tests.

Plasmid NHEJ and HR Reporters and Flow Cytometry

SK-Mel28 cells were seeded for ~75 % confluency and transfected with NHEJ and HR plasmid reporters linearized at the I_{sc}e-I_{sc}e site (926) using Lipofectamine 3000 Transfection Reagent (2µlDNA:5µlreagent) in OptiMEM (Gibco #31985062). Empty vector dsRed was also transfected concurrently as transfection control used for

normalization in FACS analysis. Images were taken on a Zeiss Axio Observer.D1 outfitted with an Excelitas X-Cite 120 LED GFP light at 24, 48, 72 hours. After 72 hours, cells were trypsinized with 0.5 % trypsin (Gibco #25300062) to transfer cells to an 0.6 mL tube. Cells were incubated in trypsin for 10 min on ice. Cells were spun down and resuspended in PBS. Cells were spun down and resuspended in FACS Buffer (PBS +1 % FBS). Cells were strained and submitted to OHSU's Flow Cytometry for GFP expression analysis. Cells were first gated on a forward side scatter to exclude debris and next gated on forward side scatter height x forward side scatter area for doublet discrimination. GFP efficiency was measured by taking GFP positive singlets over the total amount of single cells.

Proximity Ligation Assay

SK-Mel28 cells were grown on 13mm poly-d-lysine treated coverslips and fixed in 4% PFA for 15 minutes at RT followed by two washes with 1x PBS. Proximity Ligation Assay was performed without deviation from manufacturer's instructions (DUO92008). Coverslips were washed in a 0.5mL volume and reactions were performed by inverting the coverslip onto a 35 μ L drop on parafilm. Following the proximity ligation reaction, cells were stained with DAPI (0.2 μ g/mL) for 3 minutes followed by one wash in PBS and one water wash. The cells were then inverted and mounted on glass coverslips with 15 μ L of prolong gold mounting media (LifeTech, P36934) & were cured overnight in the dark at RT. All immunofluorescence images were taken on a Zeiss Laser-Scanning Confocal Microscope 980 and analyzed with CellProfiler. All cells within a 63x image were analyzed (~30cells/condition/biological replicate). Statistical significance was assigned using t-test.

Antibody specifics were as follows: Syn1 (BD Biosciences #610786, RRID:AB_398107, 1:500), Nucleophosmin (Abcam #52644, RRID:AB_881735, 1:100), Treacle (Millipore Sigma #HPA038237, RRID:AB_10670660, 1:200), Fibrillarin (Abcam #5821, RRID:AB_2105785, 1:100), UBF (Millipore Sigma #HPA006385, RRID:AB_1080447, 1:10,000).

I-Ppol mRNA production and transfection

I-Ppol WT and H98A plasmids were generously gifted from Dr. Brian McStay (NUI Galway) and previously characterized (569). Plasmids were linearized at a NotI site positioned in the polylinker downstream from the I-Ppol ORF and transcribed using MEGAscript T7 kit (Invitrogen) according to the manufacturer's instructions. I-Ppol mRNA was subsequently polyadenylated using a Poly(A) tailing kit (Invitrogen) according to the manufacturer's instructions and then precipitated using lithium chloride. SK-Mel28 cells were seeded on poly-L-lysine treated glass coverslips at least 36 hours prior to transfection with the *in vitro* transcribed mRNA using the TransMessenger transfection reagent (Qiagen). One microgram of I-Ppol mRNA and 2 μ l of Enhancer R were diluted in buffer EC-R to a final volume of 100 μ l and incubated for 5 minutes at RT. Two microliters of TransMessenger transfection reagent was added and further incubated for 10min at RT. After addition of 900 μ l of serum-free medium, the transfection cocktail was added to cells. Following 4 h of incubation, the transfection medium was replaced by full medium, and cells were grown for an additional 2h prior to further processing.

Western Blot Analysis

SK-Mel28 cells were seeded on 10cm plates to be ~80% confluent the day of treatment. Cells were treated with I-Ppol WT or H98A mRNA (7µg) as detailed above. After treatment, media was removed and cells were washed 1x with ice cold PBS. Cells were harvested by trypsinization, collected into 15ml conical tubes, and pelleted for 5min 200rc. Liquid was aspirated, pellets were resuspended in 2ml PBS and transferred to 2ml microcentrifuge tubes.

For 53BP1 western blots, proteins were extracted into cytosolic and nuclear fraction using the NE-PER extraction kit (Thermo-Fisher, cat 78833) according to the manufacturer's recommendations with the addition of a brief sonication (10 seconds, 10 kHz) after the first nuclear resuspension step. Protein preps were stored at -80C until Western blot analysis. 15µg protein was run on a 3-8% Tris-Acetate gradient gel (Invitrogen) with 500ul Antioxidant Reagent and transferred onto an immobilon-FL PVDF membrane (Millipore) at 30V for 1 hour on ice in NuPAGE Transfer Buffer using the Novex XCell II Blotting System (Invitrogen). Membranes were blocked overnight in Odyssey PBS Blocking Buffer (Li-Cor) and stained for 2 hours at RT with 53BP1 (BD Biosciences #612522, RRID:AB_2206766, 1:1000) and 1 hour at RT with IRDye 800CW Goat anti-mouse (1:10,000; Li-Cor). All staining was normalized to total protein (Revert 700 Total Protein Stain, Licor). Images were acquired using Li-Cor Odyssey CLx Imaging System.

For EMT marker western blots, cells were lysed in RIPA buffer (50 mM Tris-HCl [pH 8.0], 150 mM NaCl, 0.1% SDS, 1% Triton X- 100, 1x cOmplete protease inhibitors (Roche), Phosphatase inhibitors, and 1M Veliparib) and were stored at -80C until Western blot analysis. 10-30µg protein was run on a 10-20% Tris-Glycine 1.0 mm gradient gel

(Invitrogen) and transferred onto an immobilon-FL PVDF membrane (Millipore) at 30V for 2 hours on ice in 0.5% TBE using the Novex XCell II Blotting System (Invitrogen). Membranes were blocked overnight in Odyssey PBS Blocking Buffer (Li-Cor) and stained for 2 hours at RT with Vimentin (Abcam #92547, RRID:AB_10562134, 1:1,000) and 1 hour at RT with IRDye 680CW Goat anti-mouse (1:10,000; Li-Cor) or IRDye 800CW Goat anti-rabbit (1:5,000; Li-Cor). All staining was normalized to total protein (Revert 700 Total Protein Stain, Licor). Images were acquired using Li-Cor Odyssey CLx Imaging System.

Phospho-proteomics

SK-Mel28 cells were grown in 10cm dishes, trypsinized, and spun down (n=5 biological replicates). Cell pellets were frozen until further processing was completed. The phosphoproteome of the three cell lines were quantitatively analyzed using an established TMT/IMAC bottom-up LC-MS/MS proteomics pipeline (927). The data was processed with in-house developed PlexedPiper R pipeline or FragPipe tools (955). The quantitative data was compiled at the individual phospho-site level and the discovered differentially abundant phosphosites will be validated in KO vs KO/KI comparison. This data was cross-referenced with the PhosphoSitePlus database (956) containing determined kinase/substrate relationships. The hyperactivated/deactivated kinases was inferred based on differentially abundance phosphosites using kinase/substrate enrichment approach (KSEA R package (928)).

Copy Number Quantitative PCR

Genomic DNA was isolated from SK-Mel28 Control, KO, and Rescue cells using the DNeasy kit (Qiagen) according to the manufacturer's instructions. DNA concentration was measured with a NanoDrop spectrophotometer. Analysis of 5S, 18S, and 28S rDNA copy number was performed using quantitative Real-Time PCR on the QuantStudio 3 (Applied Biosystems). A volume of 1µl gDNA template(10ng), 1µl of forward and reverse primers (each 500nm) and 6µl of SYBR Green I (Roche) were combined to a total volume of 12µl. Primers used are described in Table A.2.1. Cycling specifics: 95C for 10min, 40 cycles (95C for 3sec, 60C for 30sec). Each sample was analyzed with 2 technical replicates across 3 biological replicates. The target gDNA was normalized to tRNA^{Met} levels. Statistical significance was assigned using one-way ANOVA.

Primer	Forward (5'-3')	Reverse (5'-3')
18S	CGATCAGATACCGTCGTAGTTC	GGTCATGGGAATAACGCCGC
28S	GAAGCGCGGGTAAACGGC	TGACGAGGCATTTGGCTACC
5S	CATACCACCCTGAACGCGCC	CCGACCCTGCTTAGCTTCCG
tRNA ^{Met}	GAGTGGCGCAGCGGAAGCGTGCTGG	GCAGAGGATGGTTTCGATCCATCG

Table A.2.1. Primers used in qRT-PCRs.

BODIPY-C11 and Flow Cytometry Analysis

SK-Mel28 cells were treated with DMSO or 10µM RSL3 for 24 hours. Cells were then treated with 1.5µM BODIPY-C11 for 20 minutes. To prepare cells for FACS, cells were washed with HBSS, trypsinized, and spun down at 500g for 4 minutes. Cell pellets were resuspended in HBSS and immediately submitted to OHSU's Flow Cytometry for

analysis. Cells were first gated on a forward side scatter to exclude debris and next gated on forward side scatter height x forward side scatter area for doublet discrimination. Ferroptosis was quantified by taking the percent increase in geometric mean 488 signal between DMSO and RSL3 treated cells in each condition. Statistical significance calculated via one-way ANOVA with Tukey's multiple comparisons tests.

Caspase-3 Activity Assay

SK-Mel28 cells were seeded at 1×10^5 cells per 35mm plate. Cells were treated with DMSO or 25 μ M etoposide. After 72 hours of treatment, medium and cells were removed and pelleted at 500g for 5 minutes at 4C followed by washing with cold PBS. Supernatant was removed and cells were lysed in 160 μ l Caspase-3 Assay Buffer (25mM HEPES pH7.5, 5mM EDTA, 0.1% 3-[3-cholamidopropyl]dimethylamino]-1-propanesulfonate, 2mM dithiothreitol) with sonication. 45 μ l supernatant and 135 μ l Caspase-3 Assay Buffer was used per well of a 96-well plate and 20 μ l Caspase-3 Assay Substrate (Ac-DEVD-MCA, Acetyl-L-Aspartyl-L-Glutamyl-L-Valyl-L-Aspartic Acid α -(4-Methyl-Coumaryl-7-Amide, 0.5mM) was added. The plate was covered and incubated at 37C for 2 hours. Fluorescence was then measured at 360nm excitation and 460nm emission. Protein concentrations were measured separately via Bradford Assay to normalize to caspase-3 activity.

A.3 In Vivo Class Switch Recombination

Introduction

The role of α Syn in adaptive immune modulation has recently gained more attention in the PD research community. Patients with PD have significantly higher levels of immunoglobulin G (IgG) binding to dopaminergic neurons, whereas IgM binding was not increased (957). In addition, PD patient blood samples were found to contain antibodies (958) and T cells (959) autoreactive to α Syn epitopes. In this context, interesting work from the Maitta Lab investigated potential abnormalities in the development of T (960) and B cells (961), in α Syn WT and KO mice. Their work on B cell maturation reports a reduction in total serum IgG in α Syn KO mice compared to WT mice, but no abnormality in IgM. When α Syn KO mice were challenged with a specific antigen, there was decreased production of antigen-specific IgG1 and IgG2b, but no change in antigen-specific IgM compared to WT mice (961).

Although this preliminary data indicates a potential critical role for α Syn in B cell lymphopoiesis, the specific mechanism underlying the differences in immunoglobulin levels remains unknown, especially in an environment independent of secondary adaptive immune factors. In conjunction with the findings of this dissertation and other reports, demonstrating the critical role of α Syn in NHEJ-mediated DSB repair (443), I hypothesize that α Syn may be involved in immunoglobulin class switch recombination (CSR), a process that is critically dependent on NHEJ to produce immunoglobulin isotypes other than IgM (e.g. IgG, IgA, IgE). CSR is initiated by the introduction of DSBs by activation-induced cytidine deaminase (AID) in the S regions of the IgM gene and a looping out-deletion-recombination process ensues, where the constant region gene of the μ heavy

chain ($C\mu$) is replaced by a downstream constant region ($C\gamma$, $C\alpha$, or $C\epsilon$) (Figure A.3.1). NHEJ is considered to be the principal mechanism used in CSR (962, 963). These set of experiments aim to elucidate whether α Syn is critical for CSR through an NHEJ-dependent mechanism.

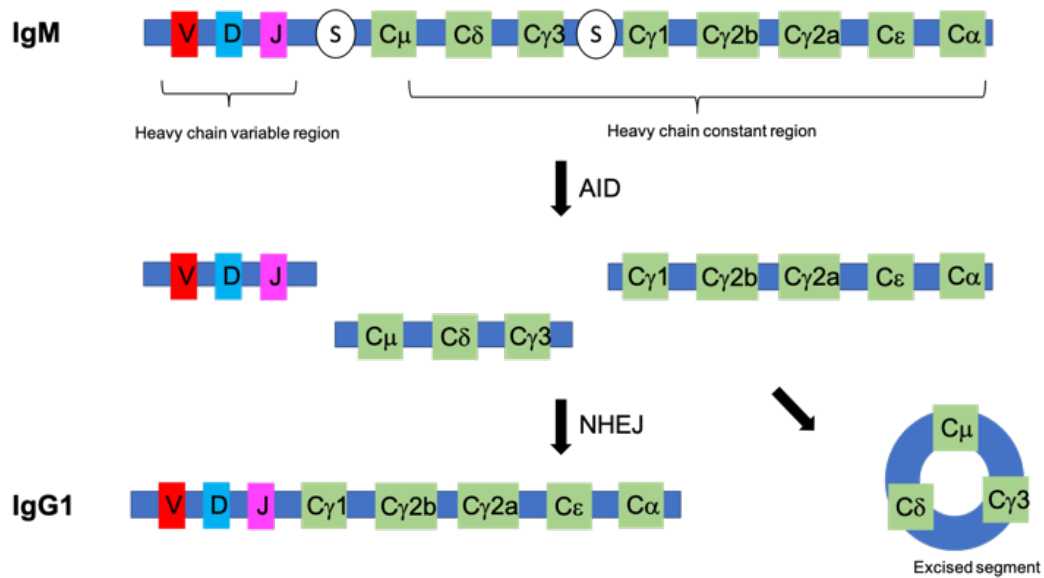


Figure A.3.1. A model of immunoglobulin class switch recombination.

Results

Primary B lymphocytes were cultured *ex vivo* from splenic tissue of α Syn WT and KO mice via negative selection magnetic enrichment (964). Cells then underwent LPS-induced proliferation and class switching (Figure A.3.2A). Staining of cells for IgG2b and subsequent flow cytometric analysis revealed no significant differences in % increase of IgG2b between α Syn WT and KO mice (Figure A.3.2B).

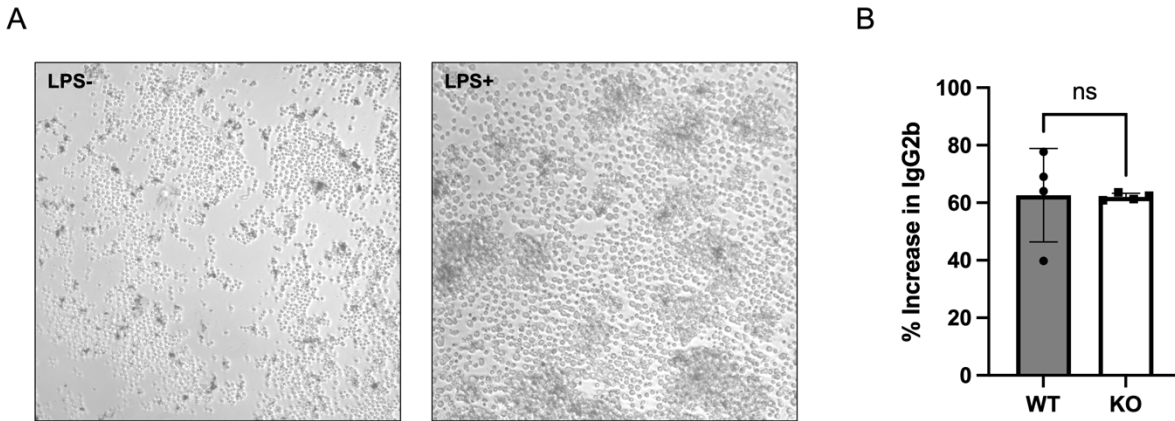


Figure A.3.2. Alpha-synuclein loss-of-function does not influence IgG2b class switch recombination. A) Magnetically enriched splenic B cells before LPS stimulation and 48 hours after stimulation with 25 μ g/ml of LPS. Proliferating cells are seen as clusters in a background of blasting and apoptotic cells. B) LPS stimulated cells after 96 hours in culture were stained for CFSE and IgG2b showing the emergence of an IgG2b positive population following several rounds of cells division. Statistical analysis between α Syn WT (n=4) and KO mice (n=4) using unpaired t-test.

Discussion

This preliminary experiment aimed to investigate whether α Syn loss-of-function impairs IgG2b CSR in murine B lymphocytes. My data suggests that there is no significant difference in % increase of IgG2b CSR after LPS stimulation compared to unstimulated cells. Despite these results, multiple future directions for investigation are possible. In the previously reported finding of decreased IgG2b in α Syn KO mice compared to WT mice (961), a different α Syn KO mouse model was utilized compared to the one used in this preliminary experiment. It is possible that different genetic backgrounds of mice influence CSR processes. Furthermore, this study found a decreased production of antigen-specific IgG1 in α Syn KO mouse compared to WT mice. IgG1 CSR can be achieved within my experimental design by adding 10ng/ml IL-4 to the stimulation cocktail, which could have led to significant differences between animal groups. Additionally, the ELISA technique

could be utilized to assay multiple isotypes concurrently. Lastly, while IgG2b isotype global levels were not significantly different, it is unclear whether α Syn loss-of-function affected NHEJ-specific CSR repair. Further sequencing analysis at the NHEJ repair junction (Figure A.4.1) would be useful to determine the frequency of additional insertions and deletions. Additional experiments could also include measuring the activity of key enzymes specific to NHEJ after LPS stimulation of B lymphocytes, like DNA-PK, via ELISA and western blot or implementing chemical inhibitors of repair enzymes specific to the NHEJ pathway, Ku70 or 80, Dnl4, 53BP, and DNA-PK during LPS stimulation of primary B lymphocytes.

Methods

B Lymphocyte Isolation and Class Switch Recombination Stimulation

Mice aged 8-12 weeks old were euthanized via cervical dislocation. Spleens were surgically removed and placed in a 70 μ m sterile strainer to homogenize the tissue. Cells were spun down at 350g for 5 minutes and resuspended in PBS. A 2ml suspension of 1×10^8 cells/ml was prepared followed by the addition of 100 μ l of normal rat serum. 100 μ l of EasySep Negative Selection Mouse B Isolation Cocktail was added to each sample and incubated at RT for 10 minutes. 150 μ l EasySep Magnetic RapidSpheres were subsequently added to each sample and supernatants were taken after magnetic separation. Cells within the supernatant were isolated after 350g centrifugation for 5 minutes and resuspended in warm 2ml PBS with 0.1% BSA. A 7ml suspension of 1×10^6 cells/ml was prepared and incubated with 14 μ l of CFSE for 10 minutes in the dark. CFSE

staining was quenched with equal volume of bovine calf serum. Cells were washed 2 times in culture medium (RPMI 1640, 10% FBS, 50 μ M BME) and resuspended in 500 μ l culture media. 125 μ l of cells at a final concentration of 3.2x10⁶ cells/ml was added to a single well of a 96-well plate in addition to 125 μ l of culture media or stimulation media (culture media, 25 μ g/ml LPS). Cells were imaged on a brightfield microscope at 48 hours.

IgG2b Staining and FACS

96 hours after seeding and LPS stimulation, cells were washed with 1ml staining buffer (PBS, 2% Bovine Calf Serum). Cells were spun down at 350g for 5 minutes and incubated in 100 μ l Fcblock buffer (staining buffer, 5% normal mouse serum, 2 μ l 0.5mg/ml Fcblock) per sample for 15 minutes on ice. Anti-mouse IgG2b antibody (2 μ l 0.5mg/ml) was then added for an additional incubation of 30 minutes on ice. Cells were washed twice in staining buffer followed by secondary incubation of 100 μ l of APC-Streptavidin (1:100) for 30 minutes on ice. Cells were washed twice in staining buffer and fixed in 50 μ l 4% PFA for 10 minutes at RT in the dark. Samples were washed and stored at 4C in the dark for 12 hours followed by FACS analysis. CFSE was excited at 492 nm by an argon-ion laser and emits at 517nm. The emission spectrum of APC-streptavidin is a fluorescence emission maximum of 660 nanometers (nm) when excited by 600–635 nm laser light. FACS data was gated and analyzed by FlowJo.

[Jump Back to Table of Contents](#)

Appendix B:
 **α -synuclein seed amplification in CSF and brain from patients with
different brain distributions of pathological α -synuclein in the context
of co-pathology and non-LBD diagnoses**

Moriah R. Arnold, BA¹, David G. Coughlin, MD, MTR², Barbara H. Brumbach, PhD³,
Denis S. Smirnov, PhD², Luis Concha-Marambio, PhD⁴, Carly M. Farris, MS⁴, Yihua Ma,
MS⁴, Amprion Inc.⁴, Yongya Kim², Edward N. Wilson, PhD⁵, Jeffrey A. Kaye, MD⁶,
Annie Hiniker, MD, PhD⁷, Randy L. Woltjer, MD, PhD⁸, Doug R. Galasko, MD², Joseph
F. Quinn, MD^{6,9}

¹ Medical Scientist Training Program, Oregon Health and Science University

² Department of Neurosciences, University of California San Diego

³ Biostatistics and Design Program, Oregon Health and Science University

⁴ Amprion Inc.

⁵ Department of Neurology & Neurological Sciences, Stanford University

⁶ Department of Neurology, Oregon Health and Science University

⁷ Department of Pathology, University of California San Diego

⁸ Department of Pathology, Oregon Health and Science University

⁹ Portland VA Medical Center, Parkinson's Disease Research Education and Clinical
Care Center (PADRECC)

Published in medRxiv March 2nd, 2022

Published in *Annals of Neurology* July 9th, 2022

B.1 Abstract

Objective: To determine the sensitivity and specificity of α -synuclein seed amplification assay (α Syn-SAA) in antemortem and postmortem CSF of autopsy-confirmed patients with different distributions of pathological α Syn, co-pathologies, and clinical diagnoses.

Methods: α Syn-SAA was used to test antemortem CSF samples from 119 subjects with a variety of clinical syndromes and standardized neuropathological examinations from OHSU and UCSD (56 additional postmortem CSF samples available). The α Syn-SAA was also applied to frontal cortex and amygdala homogenates. Sensitivity and specificity were compared across distributions of α Syn-pathology. Clinical data and co-pathologies were compared across α Syn-SAA positive and negative groups.

Results: Fifty-three individuals without and 66 with α Syn-pathology (neocortical (n=38), limbic (n=7), and amygdala-predominant (n=21)) were included. There was a sensitivity of 97.8% and specificity of 98.1% of the α Syn-SAA to identify patients with limbic/neocortical pathology from antemortem CSF. Sensitivity to detect amygdala-predominant pathology was only 14.3%. Postmortem CSF and brain tissue α Syn-SAA analyses also showed higher assay positivity in samples from limbic/neocortical cases.

Interpretation: CSF α Syn-SAA reliably identifies α Syn seeds in patients with diffuse α Syn-pathology in the context of co-pathology and non-LBD diagnoses. The analysis of brain homogenates suggests that pathological α Syn in amygdala might differ from pathological α Syn in frontal cortex. α Syn-SAA might facilitate the differential diagnosis of dementias with mixed pathologies.

B.2 Introduction

Aggregated α -synuclein (α Syn) is the main component of cytoplasmic inclusions called Lewy bodies (LB) and Lewy neurites, which are the defining pathological features of Lewy body diseases (LBD), including Parkinson's disease (PD) and dementia with Lewy bodies (DLB) (614, 615). In addition, α Syn-laden LBs are found in the brains of as many as 50-60% of sporadic Alzheimer's disease (AD) cases (908-912), 96% in familial *PSEN1* cases (913), and in 10-20% of normal elders (914, 915). AD cases with α Syn-pathology (sometimes called AD Lewy Body variant, AD-LBV) present relevant clinical differences compared to AD without α Syn-pathology, such as lower age of onset, lower age of death, more severe delusions, hallucinations, aberrant motor function, and sleep disorders (912, 965). Similarly, co-incidental AD pathology in DLB may lower the likelihood of patients manifesting certain core features like visual hallucinations (966). α Syn-pathology in AD cases affects amygdala, limbic and can affect neocortical areas with sparing of the brainstem and recent neuropathological studies in AD cases with amygdala-predominant α Syn-pathology found different α Syn truncations and modifications compared to limbic and neocortical α Syn-pathology found in PD or DLB (789, 967, 968).

To date, neuropathological assessment at autopsy remains the gold standard to diagnose LBDs and *in vivo* α Syn biomarkers have been an unmet need. Recently, α Syn Seed Amplification Assays (α Syn-SAAs) (also known as protein misfolding cyclic amplification (PMCA) and real time quaking induced conversion (RT-QuIC)), have been adapted to detect misfolded α Syn aggregates (α Syn seeds) in CSF and peripheral tissues with remarkable diagnostic accuracy (603, 969-973). α Syn-SAA in CSF of clinically and

in some cases pathologically confirmed PD and DLB cases has shown impressive results, with several independent groups reporting sensitivities and specificities near or above 90% (969-971, 974-981). However, α Syn-SAA performance in neuropathologically validated cohorts with varying distribution of α Syn pathologies, co-pathologies, and non-LBD diagnoses has not been evaluated. Thus, it remains unknown if different types of α Syn-pathology distributions produce differences in seeding activity. A few studies have reported detection of α Syn seeds in CSF from clinically diagnosed AD patients (5/14 or 36% in one report (970) and 0/16 in another (971)) and from patients clinically diagnosed with AD who were pathologically confirmed to have DLB (11/17 or 65%) or incidental Lewy bodies (2/13 or 15%) (969). Despite the low number of cases, these results suggest that current assays may have different sensitivities, which may depend on α Syn-pathology distribution, co-pathologies, and/or pathological α Syn species.

In this multi-center study, we evaluated the capability of α Syn-SAA to detect α Syn seeds in antemortem and postmortem CSF samples as well as brain tissue of patients who underwent autopsy and neuropathological analyses. We compared the α Syn-SAA results to clinical and neuropathological data to determine sensitivity, specificity, clinical, and pathological correlations of this assay across different distributions of α Syn-pathology in the context of co-pathology and non-LBD diagnoses.

B.3 Results

Neuropathological α Syn Analysis and Comparison

The neuropathological analysis of the 119 subjects revealed α Syn-pathology in the brains of 66 (55%) cases. Of the 66 patients with α Syn-pathology, 38 showed neocortical

stage α Syn-pathology, 7 showed limbic stage α Syn-pathology, and 21 showed amygdala-predominant α Syn-pathology. Rates of AD pathology was high across the cohort. 40/53 (75%) of cases without α Syn-pathology had intermediate or high degrees of AD neuropathological change, as did 19/21 (90%) cases with amygdala predominant α Syn-pathology and 39/45 (87%) cases limbic or neocortical disease (Table B.3.1). These rates were not statistically significant across the α Syn driven categories ($\chi^2=3.3$, $p=0.2$). The cases that did not have significant AD neuropathological change composed a variety of tauopathies, TDP-43-opathies, and vascular disease (Table B.3.1, Table B.8.1). No significant difference in A β 40, A β 42, A β 42/40 ratio, t-tau, and p-tau in antemortem CSF were observed between the α Syn-pathology groups within institution (Table B.8.2).

Pathology	n	αSyn Pathology	αS-SAA positivity							
			Antemortem		Postmortem		Frontal		Amygdala	
AD	26	Negative	4%	1/26	20%	3/14	-	-	-	-
AD + VD	5	Negative	0%	0/5	0%	0/3	-	-	-	-
AD + VD + HS	2	Negative	0%	0/2	0%	0/2	-	-	-	-
AD + VD + AA	1	Negative	0%	0/1	-	-	-	-	-	-
AD + AA	3	Negative	0%	0/3	0%	0/1	0%	0/1	0%	0/1
AD + HS	1	Negative	0%	0/1	0%	0/1	-	-	-	-
AD + HS + LMN Encephalitis	1	Negative	0%	0/1	-	-	-	-	-	-
AD + Pick's disease	1	Negative	0%	0/1	-	-	-	-	-	-
AD + PART	1	Negative	0%	0/1	-	-	-	-	-	-
AD + PART + METS	1	Negative	0%	0/1	0%	0/1	-	-	-	-
AD + VD + AA + ARTAG	1	Negative	0%	0/1	0%	0/1	0%	0/1	0%	0/1
CBD + VD + AA	1	Negative	0%	0/1	-	-	100%*	1/1	0%	0/1
PSP	2	Negative	0%	0/2	-	-	-	-	-	-
CBD	1	Negative	0%	0/1	0%	0/1	-	-	-	-
FTLD-TDP43	1	Negative	0%	0/1	0%	0/1	-	-	-	-
FTLD-Tau	1	Negative	0%	0/1	-	-	-	-	-	-
VD	2	Negative	0%	0/2	-	-	0%	0/1	0%	0/1
Normal	2	Negative	0%	0/2	0%	0/1	-	-	-	-
AD + αSyn-Path	26	Neocortical/ Limbic	100%	26/26	91%	10/11	100%	4/4	100%	4/4
AD + αSyn-Path	7	Amygdala- predominant	14%	1/7	-	-	50%	1/2	100%	1/1
AD + VD + αSyn-Path	6	Neocortical/ Limbic	83%	5/6	75%	3/4	100%	1/1	100%	1/1
AD + VD + αSyn-Path	4	Amygdala- predominant	0%	0/4	100%	4/4	100%*	1/1	100%	1/1
AD + AA + αSyn-Path	2	Neocortical	100%	2/2	100%	2/2	100%	1/1	100%	1/1
AD + AA + αSyn-Path	3	Amygdala- predominant	0%	0/3	50%	1/2	0%	0/2	50%	1/2
AD + AA + FTLD-TDP43 + αSyn-Path	2	Neocortical/ Limbic	100%	2/2	100%	1/1	100%	1/1	100%	1/1
AD + AA + FTLD-TDP43 + αSyn-Path	3	Amygdala- predominant	0%	0/3	33%	1/3	0%	0/3	33%	1/3
AD + HS + αSyn-Path	4	Neocortical/ Limbic	100%	4/4	100%	1/1	-	-	-	-
AD + Pick's disease + αSyn-Path	1	Amygdala- predominant	0%	0/1	-	-	-	-	-	-
AD + ARTAG + αSyn-Path	1	Neocortical	100%	1/1	100%	1/1	100%	1/1	100%	1/1
AD + VD + PSP + αSyn-Path	1	Amygdala- predominant	100%	1/1	-	-	0%	0/1	100%*	1/1
AD + Infarcts + αSyn-Path	1	Amygdala- predominant	100%	1/1	-	-	-	-	-	-
PSP + CBD + HS + αSyn-Path	1	Neocortical	100%	1/1	-	-	-	-	-	-
FTLD-TDP43 + αSyn-Path	1	Amygdala- predominant	0%	0/1	0%	0/1	0%	0/1	0%	0/1
αSyn-Path	3	Neocortical	100%	3/3	-	-	-	-	-	-

Table B.3.1. α S-SAA positivity as a function of pathology diagnosis. AD:Alzheimer's disease, VD: Vascular disease, HS: hippocampal sclerosis, AA: Includes amyloid angiopathy, leptomenigeal congophilic angiopathy, and lepto/parenchymal congophilic angiopathy, LMN Encephalitis: Limbic Microglial Nodular Encephalitis, PART: Primary-Age Related Tauopathy, METS: Micrometastases, ARTAG: Aging-related tau astroglipathy, CBD: corticobasal degeneration, PSP: progressive supranuclear palsy, FTLD-TDP43: Frontotemporal lobe degeneration with TDP43 pathology, and α Syn-Path: Includes neocortical, limbic, and amygdala predominant α Syn pathology. *2/3 wells were positive. SAA for Table B.3.1 was performed by Amprion Inc. Neuropathology analysis was performed by Randy Woltjer and UCSD pathology.

Using a Kruskal-Wallis test, we compared patients within α Syn distribution groups (none, amygdala-predominant, limbic/neocortical) on several standardized clinical and pathological variables to determine if there were important group differences. UPDRS part III scores were significantly different between α Syn groups at lumbar puncture ($X^2=21.59$, $p<0.0001$, Table B.8.2) and at last visit prior to death ($X^2=14.93$, $p=0.0006$, Table B.8.2). Post-hoc analyses showed that the limbic/neocortical group had higher UPDRS part III scores at lumbar puncture than those without α Syn-pathology and the amygdala-predominant α Syn group (Wilcoxon $z=-3.71$, $p=0.0006$ and Wilcoxon $z=-3.44$, $p=0.002$ respectively). The limbic/neocortical group also had higher UPDRS III scores at last visit prior to death compared to the amygdala-predominant group (Wilcoxon $z=-3.70$, $p=0.0007$). The majority of patients diagnosed with DLB (8/9) and PD (4/4) showed limbic/neocortical α Syn while 16/21 patients with amygdala predominant α Syn had a clinical diagnosis of AD ($X^2=28$, $p=0.002$, Table B.8.2, Table B.8.1). Lastly, male sex was over-represented across the three α Syn distribution groups ($X^2=6.94$, $p=0.03$, Table B.8.2).

Sensitivity and Specificity of the α Syn-SAA using CSF Samples

A total of 119 antemortem CSF samples were analyzed with the clinical α Syn-SAA. All but 1 of the 53 patients without α Syn-pathology were negative by the clinical α Syn-SAA and thus, the specificity for the clinical assay in this cohort was 98.1% (95% CI 90.1% to 99.9%) (Table B.3.2). Of the 66 individuals with α Syn-pathology, 47 were found positive by the clinical α Syn-SAA; Neuropathological analysis is the gold standard to which α Syn-SAA results were compared to. Thus, samples with positive α Syn-SAA results from patients with pathological α Syn found at autopsy were called true-positives, while samples with negative α Syn-SAA results from patients without α Syn-pathology were called true-negatives. The overall sensitivity of the assay to detect α Syn-pathology in any form was 71.2% (95% CI 59.4% to 80.7%). However, significant differences were observed when stratifying sensitivity analysis by pathological α Syn distribution. α Syn-SAA had sensitivity of 97.8% (95% CI 88.4% to 99.9%) in detecting α Syn seeds in limbic/neocortical pathology, but only 14.3% (95% CI 5.0% to 34.6%) in detecting amygdala-predominant α Syn-pathology (Table B.3.2).

Fifty six of the 119 patients had postmortem CSF for clinical α Syn-SAA analysis, 26 had no α Syn-pathology and 30 had α Syn-pathology at autopsy (limbic/neocortical n=20, amygdala-predominant n=10). Of the 26 patients without α Syn-pathology, 23 were found negative by the α Syn-SAA, for an estimated specificity of 88.5% (95% CI 71.0% to 96.0%) (Table B.8.2). Of the 30 individuals with α Syn-pathology, 24 were found positive by α Syn-SAA; thus, the sensitivity for the combined cohort was 80% (95% CI 62.7% to 90.5%). Similarly, when stratified by α Syn distribution, the clinical α Syn-SAA in postmortem CSF had sensitivity of 90% (95% CI 69.9% to 98.2%) to detect individuals

with limbic or neocortical α Syn, but sensitivity of only 60% (95% CI 31.3% to 83.2%), to detect amygdala-predominant α Syn (Table B.3.2). Despite a decrease in sensitivity of the α Syn-SAA between antemortem and postmortem CSF samples, there was no significant difference in postmortem interval between patients that tested positive or negative using postmortem CSF in both limbic/neocortical ($p=0.45$) and amygdala-predominant groups ($p=0.12$).

ANTEMORTEM (n=119)

Variable	Value, % (95% CI)
Sensitivity	71.2 (59.4-80.7)
<i>Limbic/Neocortical</i>	97.8 (88.4-99.9)
<i>Amygdala</i>	14.3 (5.0-34.6)
Specificity	98.1 (90.1-99.9)
Positive predictive value	97.9 (89.1-99.9)
Negative predictive value	73.2 (62.0-82.2)

POSTMORTEM (n=56)

Variable	Value, % (95% CI)
Sensitivity	80.0 (62.7-90.5)
<i>Limbic/Neocortical</i>	90.0 (69.9-98.2)
<i>Amygdala</i>	60.0 (31.3-83.2)
Specificity	88.5 (71.0-96.0)
Positive predictive value	88.9 (71.9-96.2)
Negative predictive value	79.3 (61.6-90.2)

Table B.3.2. Sensitivity, specificity, and predictive values for antemortem and postmortem CSF α Syn-SAA against α Syn-pathology. SAA for Table B.3.2 was performed by Amprion Inc.

Of the 56 individuals with both antemortem and postmortem CSF, 46 (82.1%) showed concordant α Syn-SAA results, 9 (16.1%) changed from negative results antemortem to positive results on the postmortem assay, and 1 (1.8%) changed from positive to negative. Interestingly, changes between antemortem and postmortem CSF

α Syn-SAA results was significantly higher in amygdala-predominant cases (6/10, all negative to positive) than in limbic/neocortical cases (1/20) ($\chi^2=28.49$, $p<0.0001$).

116 antemortem (51 no α Syn-pathology, 44 limbic/neocortical α Syn-pathology, 21 amygdala-predominant α Syn-pathology) and 33 postmortem (11 no α Syn-pathology, 15 limbic/neocortical α Syn-pathology, 7 amygdala-predominant α Syn-pathology) CSF samples were also analyzed by a research kinetic α Syn-SAA to accurately estimate kinetic parameters and further characterize seeding activity in these samples. Fewer samples were run using this assay because some samples had been exhausted in the previous analysis. The kinetic assay provides a diagnostic output based on a probabilistic algorithm, which deems samples as “negative”, “positive”, or “inconclusive. The kinetic α Syn-SAA “negative” and “positive” determinations were consistent with the CLIA-regulated version of the assay for the antemortem and postmortem analyzed in parallel (data not shown). F_{\max} was analyzed between groups, with no α Syn-pathology ($p<0.0001$, $q=20.42$, $DF=113$) and amygdala-predominant α Syn-pathology ($p<0.0001$, $q=14.07$, $DF=113$) groups having significantly lower F_{\max} than individuals with neocortical or limbic α Syn-pathology on antemortem CSF, most likely caused by the abundance of “negative” samples (Figure B.3.1A). Representative raw kinetic graphs are shown in Figure B.3.1B. There were kinetic differences in the seed amplification of amygdala-predominant cases compared to neocortical/limbic cases (TTT ($p=0.0007$) and T_{50} ($p=0.0002$)) where amygdala-predominant cases had slower seeding activity. However, the small number of amygdala-predominant α Syn-SAA positive cases ($n=3$) precludes reliable conclusions. There were no significant differences in kinetic parameters between α Syn-pathology groups using postmortem CSF in the kinetic α Syn-SAA (data not shown).

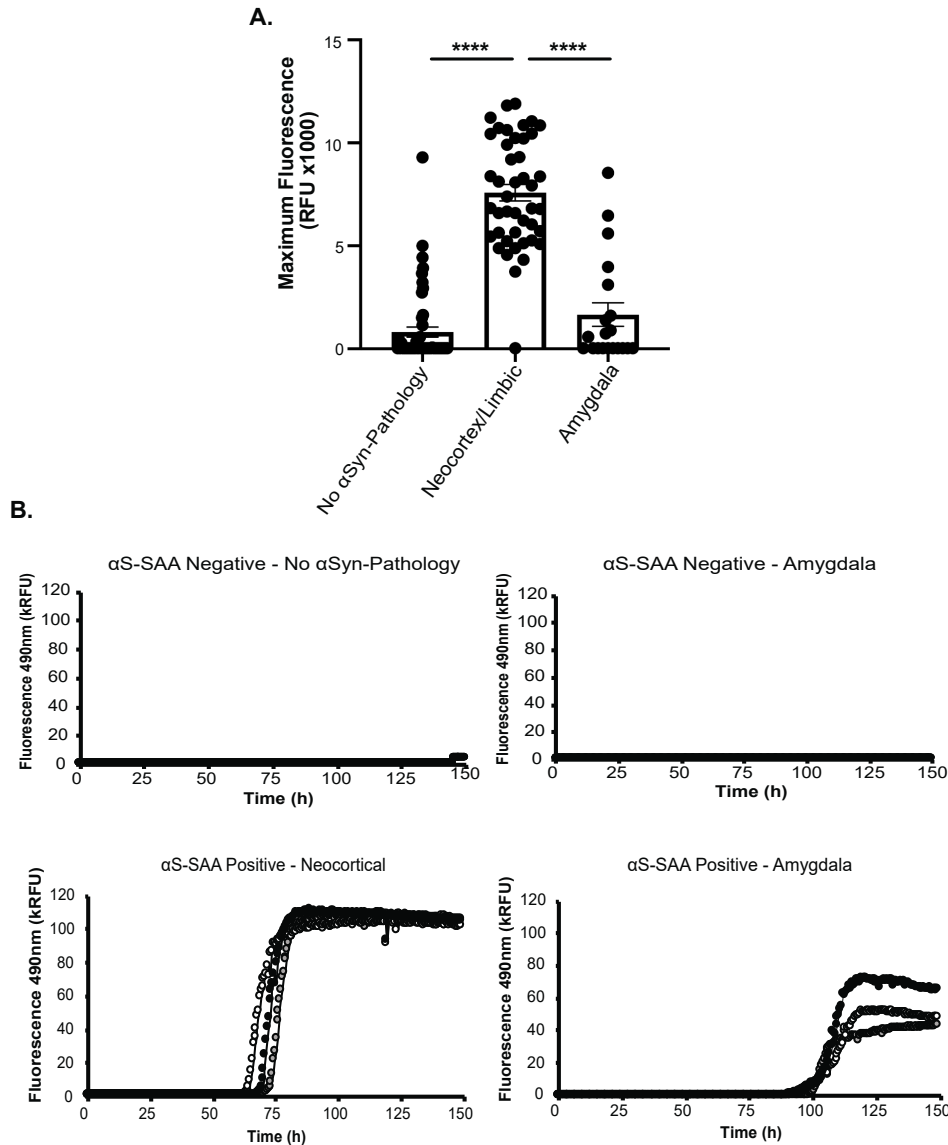


Figure B.3.1. Kinetic parameters of Research SAA stratified by alpha-synuclein distribution. A) Maximum Fluorescence Signal from R/D α Syn-SAA using antemortem CSF between no α Syn-pathology (n=51), Neocortex/Limbic (n=44), and Amygdala-predominant (n=21) groups. B) Representative figures of raw kinetic data from the Research SAA using antemortem CSF. Included are “negative” samples that are from no α Syn-pathology and amygdala-predominant individuals, and “positive” samples that are from neocortical and amygdala-predominant individuals. Statistical analysis using one-way ANOVA with Tukey’s multiple comparisons post hoc (A). Error bars represent Standard Error of the Mean (SEM). SAA for Figure B.3.1 was performed by Amprion Inc.

To investigate the potential effects of AD co-pathology on likelihood of α Syn-SAA seeding activity, we compared antemortem CSF α Syn-SAA results to CERAD scores

(C0/C1 v C2/C3), Braak tau stage (B0/B1 v B2/B3) and Amyloid- β Thal Phase (A0/A1 v A2/A3) for cases with pathological α Syn (Figure B.3.2). There were no significant associations between the likelihood of α Syn-SAA positivity and CERAD score ($p=0.7$), Thal phase ($p>0.9$), and by Braak tau stage ($p>0.9$) (Figure B.3.2). We also evaluated the effect of proteins associated to AD biomarkers in CSF as they could interfere with the amplification process in the assay. No significant differences were found in levels of A β 40, A β 42, A β 42/40 ratio, t-tau, and p-tau, between limbic/neocortical cases and amygdala-predominant cases as a function of α Syn-SAA result within institution (data not shown). Overall, α Syn-SAA positivity or lack thereof is not associated with the presence of AD co-pathology or commonly used AD CSF biomarkers.

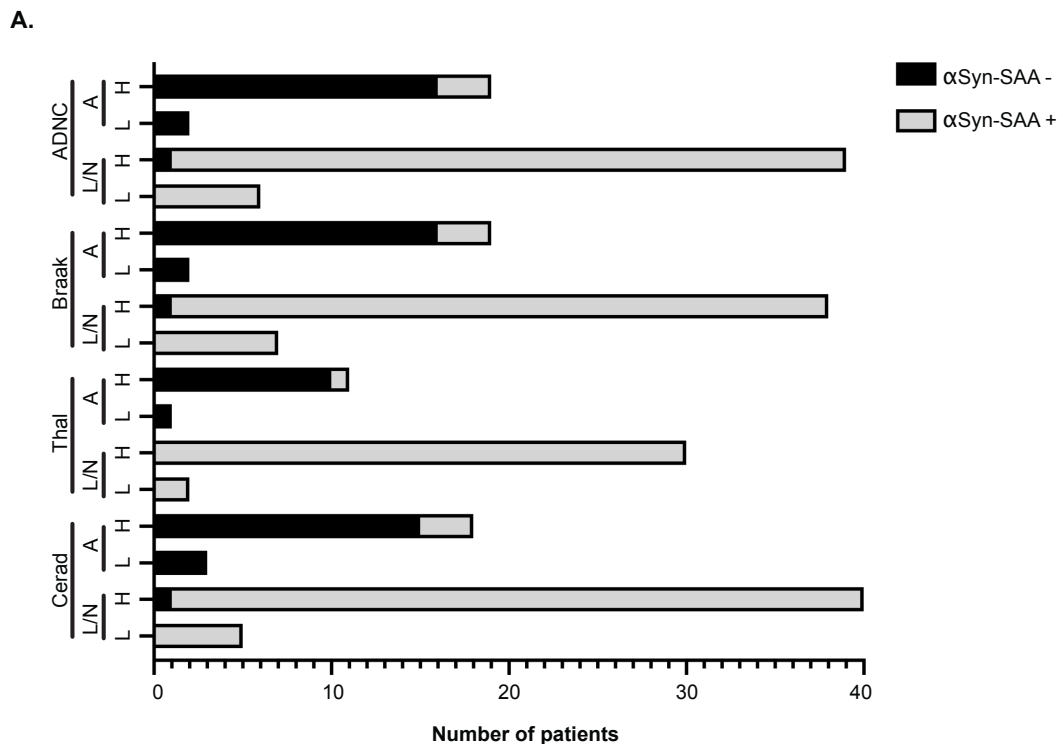


Figure B.3.2. Differences in neuropathology scores between synuclein-pathology groups as a function of SAA result. Bars represent the distribution of SAA positive or SAA negative within high (“H”) or low (“L”) categorization of ADNC, Braak, Thal, and Cerad neuropathological staging. Patients are further classified by limbic/neocortical (“L/N”) or amygdala-predominant (“A”) groups. Statistical analysis using Fisher’s exact

test within synuclein-pathology group. SAA for Figure B.3.2 was performed by Amprion Inc. Neuropathology analysis was performed by Randy Woltjer and UCSD pathology.

Comparisons of Subjects with Positive vs Negative CSF α Syn-SAA Results

UPDRS part III scores at the time of lumbar puncture were significantly lower in the antemortem false negative group compared to the true positive group ($Z=-3.12$, $p=0.002$), considering pathological analysis as gold standard. The interval between lumbar puncture and death was significantly different between true positive and false negative groups, with the false negative group having on average a longer interval than the true positive group ($Z=2.09$, $p=0.04$, Figure B.3.3A). The two groups also differed in the distribution of α Syn-pathology ($X^2=48.69$, $p<0.0001$); 94.7% of the false negatives fell into the amygdala-predominant group, while 93.6% of the true positives fell into the limbic/neocortical group. Similarly, in postmortem CSF, 66.7% of false negatives were in the amygdala-predominant group and 75% of true positives were in the limbic/neocortical α Syn group ($X^2=3.75$, $p=0.05$) (Figure B.3.3B).

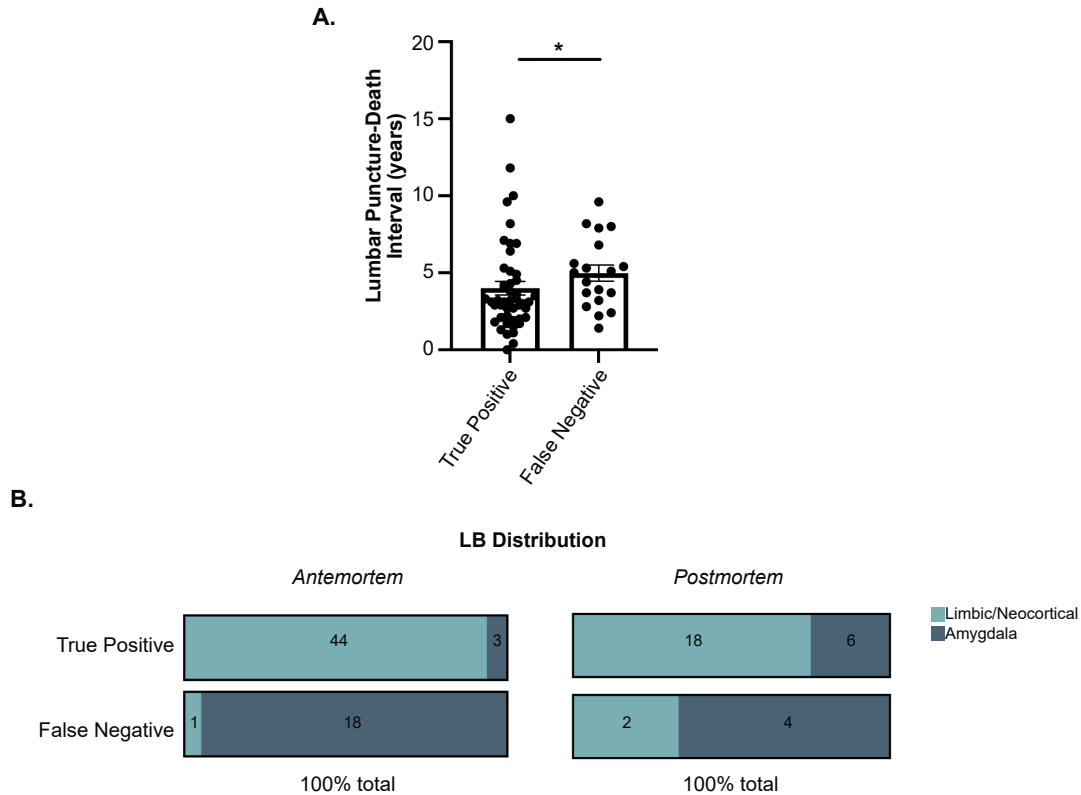


Figure B.3.3. Clinical and pathological differences between True Positive and False Negative. A) Interval in years from lumbar puncture to death between True Positives (n=47) and False Negative (n=19) groups. B) Distribution of Neocortex/Limbic and Amygdala-predominant LRP in True Positive and False Negative groups for antemortem and postmortem CSF analysis. Number of patients in each category is indicated on the bar. Statistical analysis using Wilcoxon rank-sum test with post hoc pairwise comparisons from Dwass, Steel, Critchlow-Fligner method (A) or chi-square (B). Error bars represent Standard Error of the Mean (SEM).

Clinical Significance of Incidental Synuclein Pathology

Lastly, we explored how clinical diagnosis related to clinical α Syn-SAA performance, in order to better understand whether subtle clinical predictors were present among patients without a diagnosis of a synucleinopathy whose antemortem CSF tested positive by α Syn-SAA. In this analysis, we examined all patients who were clinically diagnosed with AD, without concomitant PD or DLB, and whose antemortem CSF α Syn-SAA results were positive versus negative. There was a significant difference in patient

biological sex, where α Syn-SAA-positive patients had a significantly greater proportion of males (23/29, 79.3%) compared to α Syn-SAA-negative patients (25/46, 54.3%) ($X^2=7.84$, $p=0.005$). Clinically diagnosed AD patients with positive α Syn-SAA CSF had higher UPDRS part III scores (6.71 +/- 8.6) than those with negative α Syn-SAA CSF (1.82 +/- 4.92) at most recent visit prior to death ($Z=2.53$, $p=0.01$).

Detection of α Syn Seeds from Frontal Cortex and amygdala brain samples

We next analyzed a subset of patients ($n=22$) from the UCSD-ADRC cohort who had frozen brain tissue available for analysis, including 4 no α Syn-pathology, 10 amygdala-predominant, and 8 limbic/neocortical cases. In both brain regions, the 4 patients without α Syn-pathology were negative by the α Syn-SAA, consistent with the results for antemortem CSF in both kinetic and clinical assays (Table B.3.3). In agreement with the high sensitivity in CSF for limbic/neocortical cases, seeding activity was detected in both frontal cortex and amygdala of all 8 analyzed cases. However, there was a significant decrease in seeding activity in both frontal cortex and amygdala of the amygdala-predominant cases. Of the 10 amygdala-predominant cases, 4 cases showed no seeding activity in both frontal cortex and amygdala. There were 2 cases with seeding activity detected in the amygdala, with one of them showing 2/3 wells positive in frontal cortex.

Within no α Syn-pathology and limbic/neocortical groups, there was 100% concordance between brain homogenate results and CSF results. Of the 5 patients with amygdala-predominant α Syn-pathology that also tested positive on the α Syn-SAA using amygdala brain tissue, 3 also had some seeding activity on the α Syn-SAA using either

antemortem or postmortem CSF (Table B.3.3). Overall, the assay detected higher seeding activity in amygdala tissue in amygdala-predominant cases, while neocortical cases presented high levels of seeding activity in both brain regions.

Case	Sex	Age at onset	Age at death	Case Information						Brain Tissue		AM CSF	PM CSF	
				Primary Pathology	Thal Phase	CERAD Stage	Braak Stage	ADNC	LRP Classification	Frontal Cortex	Amygdala	LP to death (y)	Result	Result
1	Male	NA	84	Normal	A0	C0	I	Not	None	-	-	1.8	-	-
2	Male	65	71	CBD	A3	C1	I	Low	None	2/3	-	2.9	-	-
3	Female	65	76	AD	A3	C3	VI	High	None	-	-	4.7	-	-
4	Female	58	66	AD	A3	C3	VI	High	None	-	-	3.0	-	-
5	Female	72	84	AD	A3	C2	VI	High	Amygdala	-	-	2.7	-	-
6	Female	83	90	AD + PSP	A3	C2	VI	High	Amygdala	-	2/3	0.9	+	-
7	Female	84	91	AD	A3	C3	VI	High	Amygdala	2/3	+	4.6	-	-
8	Male	75	84	AD	A3	C2	VI	High	Amygdala	2/3	+	4.9	-	+
9	Female	56	66	FTLD TDP-43	A0	C0	I	Not	Amygdala	-	-	3.8	-	-
10	Male	69	76	AD	A3	C3	VI	High	Amygdala	-	-	5.5	-	-
11	Male	55	73	AD	A3	C3	V	High	Amygdala	-	-	1.9	-	-
12	Male	77	86	AD	A3	C3	V	High	Amygdala	-	+	5.3	-	+
13	Female	79	87	AD	A3	C3	IV	Intermediate	Amygdala	-	+	5.3	-	+
14	Female	90	100	AD	A3	C3	V	High	Amygdala	-	-	8.0	-	-
15	Male	54	67	LBD	A1	C2	I	Low	Limbic/Neocortical	+	+	8.1	+	-
16	Male	72	81	LBD	A3	C2	V	High	Limbic/Neocortical	+	+	3.7	+	-
17	Male	59	71	LBD	A3	C2	IV	Intermediate	Limbic/Neocortical	+	+	3.5	+	-
18	Male	63	71	LBD	A3	C2	III	Intermediate	Limbic/Neocortical	+	+	1.2	+	-
19	Male	66	71	LBD	A3	C3	VI	High	Limbic/Neocortical	+	+	1.7	+	+
20	Male	62	73	LBD	A3	C1	II	Low	Limbic/Neocortical	+	+	6.8	+	+
21	Male	52	72	LBD	A2	C2	V	Intermediate	Limbic/Neocortical	+	+	9.3	+	+
22	Female	51	59	LBD	A3	C3	VI	High	Limbic/Neocortical	+	+	2.7	+	+

Table B.3.3. Patient categorization from brain homogenate samples. Abbreviations: AM: Antemortem, PM: Postmortem, ADNC: Alzheimer’s disease neuropathological change NA: not applicable. LRP: Lewy Related Pathology, CSF: cerebrospinal fluid. CBD: corticobasal degeneration, AD: Alzheimer’s disease, PSP: progressive supranuclear Palsy, FTLTDP-43: frontotemporal lobar degeneration TAR DNA-binding protein 43, LBD: Lewy-body disease. Inconclusive cases have 2/3 replicate wells that were positive. Brain tissue samples were analyzed at 10⁻⁸ dilution. Positive results indicate 3/3 replicates were positive and negative results indicate 0/3 replicates were positive. Amygdala tissue could not be obtained for case 5. SAA for Table B.3.3 was performed by Amprion Inc.

B.4 Discussion

Although there have been large strides in the understanding of the molecular basis of synucleinopathies, *in vivo* methods for detecting α Syn are still limited. Misfolded α Syn aggregation likely begins years to decades before the onset of symptoms, allowing for the potential ability to identify patients in the earliest stages of their diseases. The development of a sensitive and specific diagnostic tool for synucleinopathies would allow for early diagnosis of patients where often there is the highest level of clinical uncertainty and when disease modifying therapies are of the greatest potential use (982). Thus, α Syn-related biomarkers remain a crucial need to the field. Several publications have shown promising results for α Syn-SAAs performed in academic laboratories (970, 976), but the performance of the assay within a regulated CLIA environment, and against pathology-confirmed samples, has been a gap. Moreover, the knowledge of whether current generations of α Syn-SAAs can detect pathological α Syn in patients with other pathologies and with clinical diagnoses other than PD or DLB, is crucial to understanding the range of their diagnostic utility. α Syn-SAA offers the ability to identify α Syn seeds in living patients and studies have focused largely on cases with clinical DLB, PD, and MSA and where performed, autopsy was used as a validation of the clinical diagnosis. However, these assays offer the potential ability to identify patients with α Syn-pathology who may not exhibit a 'synucleinopathy phenotype'. One factor that can complicate diagnosis is the presence of AD co-pathology which affect clinical expression particularly in PD and DLB(966, 983-988). Furthermore, in AD, α Syn-pathology in AD-LBV is common and also associated with worse prognosis and specific clinical features (912, 965). The use of α Syn-SAA assays to help characterize patients in terms of their α Syn-

pathology is immediately clinically applicable and potentially valuable in clinical trials to recruit homogenous populations; but detailed studies in well-characterized pathologically validated cohorts has been needed to understand how the current α Syn-SAA assay can be applied. We used pathologically driven categories of α Syn pathology, independent of clinical diagnosis, in a cohort of patients with high degrees of co-pathology to assess the performance of the α Syn-SAA assay. In these cases, the use of such a biomarker could prove useful in identifying α Syn pathology that was not necessarily suspected.

Our results add to the previous reports that α Syn-SAAs can robustly detect α Syn seeds in limbic/neocortical stage α Syn-pathology, but also show decreased sensitivity in detecting α Syn seeds in amygdala-predominant cases. An additional unique feature to this study is the number of subjects with postmortem CSF, providing a proximal time point to the autopsy assessment. Classification using postmortem CSF showed a sensitivity of 80% and specificity of 88.5%, however when stratified by pathology distribution, again the assay performed significantly better in detecting limbic/neocortical than amygdala-predominant α Syn-pathology. Lastly, we also observed decreased seeding activity from amygdala-predominant cases when assaying frozen brain tissue from frontal cortex and amygdala.

The lower sensitivity of CSF α Syn-SAA to detect α Syn seeds in amygdala-predominant pathology may represent assay dependence on degree of brain α Syn “burden”. Alternatively, negative α Syn-SAA CSF samples in the amygdala-predominant group could be explained by localized brain pathology that does not enter the CSF. However, direct analysis of amygdala homogenate from amygdala-predominant cases showed low detection, suggesting less seeding activity by these particular α Syn species.

Recent studies have found that α Syn species in amygdala-predominant pathology found in AD may have different immunohistochemical properties than PD or DLB patients with limbic and neocortical α Syn-pathology (789, 967, 968). It is plausible that these amygdala-predominant α Syn seeds have lower rates of amplification due to unique conformation or post-translational modifications of these α Syn species. Currently, there is no method to quantify α Syn seeds in a sample, thus, it is not possible to determine if α Syn seeds were extracted with similar efficiencies from amygdala and frontal lobe tissues. Lower concentrations in the amygdala homogenates could explain negative results. However, we found positivity in dilutions up to 10^{-9} in some cases which is higher than previously shown in the literature (not shown), suggesting the homogenization protocol did not artificially decrease the amount of α Syn seeds. The small number of amygdala-predominant cases who had seeding activity had slower time-to-threshold and T50 values than limbic/neocortical cases (TTT ($p=0.0007$) and T_{50} ($p=0.0002$)). This is potentially of interest given that *in vitro* models have shown that lower levels of synthetic α Syn seeds take longer to amplify in α Syn-SAA (970, 971). However, future studies of larger cohorts will be needed to confirm these preliminary observations.

Since α Syn-pathology commonly coexists in AD and may be associated with faster clinical progression (989), identifying this pathology with a biomarker would improve clinical monitoring and create options for clinical trials targeting α Syn in these patients. If amygdala-predominant type α Syn-pathology is an early stage or precursor of more widespread concomitant LB pathology in AD, then detecting its presence through biomarkers such as α Syn-SAA would be useful. However, the effect of amygdala-predominant α Syn-pathology in AD appears to have less clinical impact in some cases or

may take years to convert to a more widespread seeding. Further work is needed to determine why the seeding potential of amygdala-predominant α Syn-pathology is lower in some cases, or whether different types of α Syn-SAAs could provide detection of this pathology. We also report for the first time that α Syn seeds can be amplified from postmortem CSF samples. This is relevant because it could offer some insights when antemortem CSF samples are negative but there is detectable brain pathological α Syn upon neuropathological analysis. In these cases, positive postmortem CSF results could indicate that the α Syn pathological process started after antemortem CSF collection or that the disease process was too early at the time of antemortem CSF collection. However, we observed a reduction in sensitivity when testing postmortem CSF from neocortical/limbic cases, driven by 2 samples that were negative. Since we observed an increase in sensitivity when analyzing amygdala-predominant postmortem CSF, α Syn seed degradation or overall CSF instability is unlikely to explain the difference. Preliminary observations suggest that brain debris or cellular breakdown products could contaminate the sample during postmortem CSF collection, which effects could be minimized at least partially by centrifugation. Nevertheless, the instability of α Syn seeds and other CSF components in postmortem CSF and their potential effects on α Syn-SAA have not been systematically studied and require further exploration.

The assay's ability to identify clinically unexpected synuclein pathology is an area of great potential. Our results indicate that 27/75 (36%) of the clinically diagnosed AD patients had α Syn aggregates in their antemortem CSF and were later autopsy-confirmed to have limbic/neocortical LB disease. DLB can be misdiagnosed as AD during life, and the presence of moderate to severe AD-related tau pathology is associated with a lower

likelihood of visual hallucinations and cognitive fluctuations, and worse performance on tests of episodic memory and naming in DLB patients, meaning that it is more challenging to diagnose these patients with mixed pathologies accurately (987, 988, 990).

Clinically, our cohort included only 4 PD and 9 DLB cases, and pathologically, there were no cases with brainstem-only α Syn-pathology which are limitations of the study. Our study adds valuable new information about the accuracy of α Syn-SAA in the context of co-pathology and non-LBD diagnoses. In another study, CSF from 4 cases with incidental α Syn-pathology in brainstem-only have been analyzed by α Syn-SAA (977). Three of these cases were positive, suggesting that brainstem pathological α Syn shares propagation features with limbic and neocortical rather than amygdala-predominant pathological α Syn. Since brainstem-only pathological α Syn is an early event, these results are consistent detection of α Syn seeds in CSF of prodromal PD cases, like isolated REM sleep behavior disorder (iRBD) (977, 981, 991). Finally, other minor weaknesses include potential differences in interpretation of the NACC guidelines between the two institutions and the impossibility to determine if patients with α Syn-SAA negative antemortem CSF and pathological α Syn upon autopsy represent true false negatives or if the pathology developed after antemortem CSF collection. Additionally, the limbic/neocortical group was skewed towards male participants. This is congruent with numerous studies identifying a sex-link for risk of synucleinopathy (992-994). Larger numbers of cases with additional distributions of pathological α Syn, particularly brainstem-only and olfactory-only, should be further investigated to get a full picture of the relationship between brain pathology and CSF α Syn-SAA positivity. Lastly, further work is needed to fully interrogate differences in the seeding activity between pathological

α Syn from different brain regions. It is unknown if the differences reflect the conformation of the seeds (strains), interactions with co-localized co-pathology, or perhaps brain region specific components (proteins, lipids, polysaccharides, nucleic acids, etc.) that may have an effect of the α Syn-SAA. Our data suggest that AD co-pathology is unlikely to explain the differences based on CSF measures, CERAD scores, Braak-tau stages, and Thal phases.

In this large, multicentered autopsy-validated cohort of patients with a variety of stages of α Syn-pathology, our results indicate that the α Syn-SAA is highly predictive of neocortical or limbic α Syn-pathology in aging patients for whom α Syn-pathology is not clinically suspected. This feature makes α Syn-SAA a diagnostic tool with great potential for clinical trials aiming to initiate interventions early in the disease process or to select-out patients with co-incidental α Syn-pathology. However, there was substantially lower sensitivity to detect amygdala-predominant α Syn pathology in brain tissue and CSF, which may have distinct biochemical properties and seeding potential that reduces detection in current generation of α Syn-SAAs.

B.5 Methods

Patient Selection

eIRB 725 of Oregon Health and Science University ADRC gave ethical approval for this work. IRB 170957 of University of California San Diego ADRC gave ethical approval for this work. Informed consent was obtained from each subject for the retrieval of biological samples.

Participants in brain aging studies from the Oregon Alzheimer's Disease Center (OADC) (n=57) and University of California San Diego Shiley-Marcos Alzheimer's Disease Research Center (UCSD-ADRC) (n=62) who had 1) CSF collection during life, and 2) subsequent brain autopsy (n=119) were included in the study. All subjects had an annual battery of clinical, neuropsychologic, and other cognitive assessments, as described by the National Alzheimer's Coordinating Center (NACC)(995), including Mini-Mental State exam (MMSE), and Unified Parkinson's Disease Rating Scale Part III (UPDRS). Blood was drawn for the determination of APOE genotype. Clinical diagnoses, assigned at the time of CSF collection, included AD (n=75), DLB (n=9), PD (n=4), mild cognitive impairment (MCI, n=11), other dementia (n=13, including frontotemporal dementia (n=10), mixed dementia (n=1), and "other dementia" (n=2)), and cognitively normal controls (n=7). Clinical diagnoses were assigned by a multidisciplinary consensus conference at each site. Pathologically, the cohort included patients with AD pathology (n=43), AD with α Syn-pathology (n=59), α Syn-pathology in isolation (n=3), progressive supranuclear palsy (n=2), corticobasal degeneration (n=2), FTLTDP-43 (n=2), vascular disease in isolation (n=2), normal subjects (n=2), and patients with a mix of AD and other tauopathies (n=4) (Table B.3.1). Cases were grouped by α Syn-pathology distribution as below. Patient-level information can be found in Supplemental Table 1.

CSF Analysis

CSF was collected for all 119 cases by lumbar puncture in the morning fasting condition according to a standardized protocol (996). A subset of patients (n=56) had additional CSF samples obtained at the time of brain removal. CSF specimens were

divided into 0.5 ml aliquots and stored at -80°C. Antemortem CSF collection occurred 1-15 years prior to autopsy (17.6% in 0-2yr, 46.3% in 2-5yr, 18.5% in 5-8yr, 6.7% in 8-10yr, 10.9% in 10-16yr). Antemortem CSF was analyzed for A β 40, A β 42, t-tau and p-tau (Lumipulse, Fujirebio at both sites).

CSF samples were initially analyzed by the endpoint qualitative version of the α Syn-SAA that has been validated for clinical use under CLIA/CAP certifications (clinical assay, SYNTap™). Each sample was analyzed in triplicate (40 μ L CSF per well) in a 96-well plate (COSTAR, cat# 3603) with a final volume reaction of 200 μ L). The reaction mixture consisted of 0.3mg/mL rec- α Syn (Amprion, cat# S2020) in 100mM PIPES pH 6.50, 500mM NaCl, 10 μ M ThT, and a 2.5mm borosilicate glass bead per well. Plates were sealed using an Optical Adhesive Film (ThermoFisher, cat# 4311971) and shaken at 800rpm with orbital shaking for 1min every 29min of quiescent incubation in a TIMIX 5 shaker (Edmund Buehler) placed in an incubator set to 37°C. Bottom fluorescence readings at 490nm were performed using a BMG FLUOstar Omega. This clinical version of the assay was performed according to standard operational procedures in agreement with CLIA regulation. CSF samples were deemed “Detected” or “Not Detected” based on a preestablished threshold for the median maximum fluorescence of the triplicate. The research and development (R&D) kinetic α Syn-SAA was utilized to analyze CSF samples and brain tissues. The methods of the kinetic α Syn-SAA have been reported in detail elsewhere (974, 975). Briefly, CSF samples and brain homogenates (BHs) were evaluated in triplicates (40 μ L/well) in a 96-well plate (COSTAR 96, cat# 3916), in a reaction mix consisting of 0.3mg/ml rec- α Syn (Amprion, cat# S2021), 100mM PIPES pH 6.50 (Sigma, cat# 80635), 500mM NaCl (Lonza, cat# 51202), 10 μ M ThT (Sigma, cat#

T3516), and a 3/32-inch BSA-blocked Si₃N₄ bead (Tsubaki Nakashima). This assay was performed in a BMG FLUOstar Omega shaker/reader with orbital shaking at 800rpm for 1min and 29min of quiescent incubation at 37°C. Fluorescence at 490nm was measured every 30min for accurate estimation of kinetic parameters. The assay outcomes of the R&D kinetic assay are positive, inconclusive, or negative, based on a probabilistic algorithm that uses maximum fluorescence and kinetic parameters(974). Maximum fluorescence (F_{\max} , RFU) was the highest fluorescence reading within the length of the assay. A 4-parameter fit (Mars, BMG) was fit to estimate the slope (RFU/h) and the time to reach 50% of the F_{\max} (T_{50} , h) of each replicate/well. The time to threshold (TTT, h) was determined with a user defined formula (Mars, BMG); threshold was set to 5,000 RFU. Scientists performing the assay were blinded to the clinical or pathological diagnoses associated with the samples.

Brain Tissue Analysis

In a subset of patients (n=22), 500mg samples of frozen brain tissue from the middle frontal cortex and amygdala were provided for α Syn-SAA. Cases included those without α Syn-pathology (n=4), amygdala-predominant α Syn-pathology (n=10), and limbic/neocortical α Syn-pathology (n=8). All frozen samples were provided from the UCSD-ADRC.

Frontal cortex and amygdala samples were homogenized to 10% w/v in 1XPBS (Cytiva, cat# SH30256.02) with cOmplete Mini EDTA-free protease inhibitor cocktail (Roche, cat# 11836170001). Approximately 100 μ g of brain sample was homogenized in 1.5mL tubes preloaded with 1mm zirconium beads (cat# 11079110zx) in a MP FastPrep

24 homogenizer. Two rounds of homogenization were performed for all samples (15s at 4m/s and 30s at 6m/s). If additional homogenization was needed, samples were chilled on ice for 5min in between additional homogenization rounds at 6m/s for 30s. BHs were centrifuged at 800xg for 1 minute to remove cellular debris. Supernatants were collected, vortexed, aliquoted, and stored at -80°C until α Syn-SAA analysis. BH aliquots were 10-fold serially diluted in synthetic CSF (Amprion, cat# S2022) up to 10^{-9} and analyzed in triplicates. Results for 10^{-8} dilution are shown to avoid negativity by over-dilution.

Neuropathological Assessments

Neuropathological assessments were performed in a standardized manner with various pathologies assessed using hematoxylin and eosin staining and immunohistochemistry directed against tau, amyloid- β , α -synuclein, and TDP-43 species as appropriate and pathological diagnoses were assigned by expert neuropathologists (987, 997-999). MSA cases were excluded from this study given the known altered kinetics on α Syn-SAA assays compared to PD and DLB cases (1000). Alzheimer's disease neuropathological change was assigned according to NACC guidelines after Braak tau stage, CERAD stage, and Thal phase was determined (997, 1001). Distribution of LRP was determined via α -synuclein immunohistochemistry staining (OADC: α Syn MJFR1, Abcam; UCSD-ADRC: pSer129 α Syn 81A, Biogen Laboratories) using slices from pons and/or midbrain, hippocampus, amygdala, and neocortical areas including temporal cortex and/or middle frontal cortex and the following staging definitions were applied: Neocortical: midbrain+ pons+ hippocampus+ amygdala+ neocortex+; Limbic:

midbrain+ pons+ hippocampus+ amygdala+ neocortex-; Amygdala-predominant: midbrain- pons- hippocampus+/- amygdala+ neocortex- (665).

Statistical Analysis

Clinical and pathological differences between the OADC and UCSD-ADRC cohorts were assessed to determine the necessity for stratification by site. All DLB and PD patients were from UCSD. Sensitivity, specificity, and predictive values were calculated via chi-squared test with 95% confidence intervals calculated using the hybrid Wilson-Brown method. Differences in kinetic parameters were analyzed by one-way ANOVA with Tukey's multiple comparisons test or unpaired t-test. Prior to testing group differences, all outcome variables were assessed for normality. For normally distributed continuous variables, we used the General Linear Model (GLM) to test whether there were group differences in the outcome variables (age at death, onset of cognitive symptoms, and MMSE decline rate). For non-normally distributed continuous variables (UPDRS at lumbar puncture, MMSE at lumbar puncture, UPDRS at most recent visit, MMSE at most recent visit, CDR at most recent visit, lumbar puncture to autopsy interval, CSF A β 40, A β 42, t-tau, and p-tau, disease duration, postmortem interval), we used a Kruskal-Wallis test (more than two groups) or a Wilcoxon rank-sum test (two groups) to test for group differences. Post hoc pairwise comparisons were tested using the Dwass, Steel, Critchlow-Fligner Method. We used chi-square tests or Fisher's exact tests to test for group differences when outcome variables were categorical (biological sex, early-onset status, neuropathology diagnosis, clinical diagnosis, NACC variables: Thal phase for amyloid plaques, Braak stage for neurofibrillary degeneration, density of neocortical

neuritic plaques, NIA-AA Alzheimer's disease neuropathologic change (ADNC), density of diffuse plaques, cerebral amyloid angiopathy, arteriosclerosis, APOE status. For the following variables, we had data from both the OADC and UCSD-ADRC cohorts: onset of cognitive symptoms, disease duration, age at death, rate of MMSE decline, MMSE at lumbar puncture, most recent MMSE score, interval between lumbar puncture and autopsy, postmortem interval, biological sex, clinical diagnosis, Thal phase, Braak tau stage, Cerad stage, ADNC, APOE genotype, CSF A β 40, A β 42, t-tau, and p-tau. UPDRS score at lumbar puncture was only collected at UCSD. Statistical significance was set at $p < 0.05$.

B.6 Acknowledgements

We thank the patients who participated in this research, their families, and the investigators and staff at the OHSU Layton Aging and Alzheimer's Disease Research Center and Oregon VA Parkinson's Disease Research Education and Clinical Care Center; UCSD Shiley Marcos Alzheimer's Disease Research Center; Robin Guariglia and Nora Mattek for compilation of clinical and genetic data; Babett Lind for CSF sample collection. Additional thanks to the individuals at Amprion Inc. involved in this project: Frank Espin, John Middleton, Russell M. Lebovitz, and Karen MacLeod.

This study was funded in part by the Alzheimer Disease Center Clinical Core at Oregon Health and Science University (PI: Kaye; eIRB 725; supported by NIH P30 AG008017, P30 AG066518) as well as the National Center for Advancing Translational Sciences (National Institutes of Health, Grant Award Number UL1TR002369). Amprion's efforts were funded in part by the Alzheimer's Drug Discovery Foundation (ADDF)

Diagnostics Accelerator, as well as by the National Institute of Neurological Disorders and Stroke of the National Institutes of Health (Award Number U44NS111672). Moriah R. Arnold is funded through the Medical Scientist Training Program of Oregon Health & Science University (T32 GM 109835). Dr. Coughlin is funded by the National Institute of Neurological Disorders and Stroke of the National Institutes of Health (Award Number NS120038) and the National Institute on Aging (Award Number AG062429). Dr. Galasko is funded by the UCSD Shiley-Marcos ADRC (AG062429), and by the DLB Research Center of Excellence award from the Lewy Body Dementia Association. The funding sources had no role in the design and conduct of the study; collection, management, analysis, and interpretation of the data; preparation, review of approval of the manuscript; and decision to submit the manuscript for publication.

B.7 Author Contributions

MRA, DGC, DSS, LCM, DRG, and JFQ contributed to the conception and design of the study; MRA, DGC, BHB, DSS, LCM, CMF, YM, YK, ENW, JAK, AH, and RLW contributed to the acquisition and analysis of data; MRA, DGC, BHB, LCM, DRG, and JFQ contributed to drafting the text or preparing the figures.

B.8 Supplemental Material

Institution	Patient ID	Sex	Age at Death	Age at Onset	Total Disease Duration	Lumbar Puncture-Death Interval	Clinical Diagnosis	Pathology Diagnoses	LRP Group	SAA Antemortem CSF	SAA Postmortem CSF	SAA Frontal Cortex	SAA Amygdala	Harmonized Pathology
OHSU	1440	M	73	65	8	3	AD	1) AD	LRP-	-	-			AD
OHSU	2158	F	86	69	17	5	AD	1) AD	LRP-	-	-			AD
OHSU	2272	F	91	75	15	6	AD	1) AD	LRP-	-	-			AD
OHSU	2543	M	95	82	13	7	AD	1) AD	LRP-	-	-			AD
OHSU	2079	M	81	65	15	7	AD	1) AD 2) HS 3) VD	LRP-	-	-			AD + HS + VD
OHSU	3513	F	99	94	6	11	AD	1) AD 2) VD	LRP-	-	-			AD + VD
OHSU	2487	M	69	45	24	13	AD	1) AD	LRP-	-	-			AD
UCSD	5907	F	66	58	8	3	AD	1) AD 2) AA 3) VD 4) Tau	LRP-	-	-	-	-	AD + AA + VD + ARTAG
UCSD	5830	F	64	57	7	3	AD	1) Normal	LRP-	-	-			Normal
UCSD	5787	M	90			3	AD	1) AD	LRP-	-	-			AD
UCSD	5814	M	75	61	14	4	AD	1) AD	LRP-	-	-			AD
UCSD	5825	M	79	72	7	5	AD	1) AD 2) HS	LRP-	-	-			AD + HS
UCSD	5892	F	77	65	12	5	AD	1) AD 2) AA	LRP-	-	-	-	-	AD + AA
UCSD	5846	F	65	49	16	11	AD	1) AD	LRP-	-	-			AD
OHSU	3116	M	71	53	18	15	FRONTOTEMP	1) FTLD	LRP-	-	-			FTLD-TDP43
UCSD	5806	M	57	55	2	2	FRONTOTEMP	1) FTLD	LRP-	-	-			CBD
UCSD	5849	M	71	63	8	5	FRONTOTEMP	1) AD	LRP-	-	-			AD
OHSU	2790	F	84	78	5	1	MCI	1) AD 2) VD	LRP-	-	-			AD + VD
OHSU	3147	F	89	86	2	10	MCI	1) AD	LRP-	-	-			AD
OHSU	3817	F	93	85	8	11	MIXED	1) AD 2) HS 3) VD	LRP-	-	-			AD + HS + VD
OHSU	3476	F	72			10	NONE	1) AD	LRP-	-	-			AD
OHSU	3624	M	93	82	11	12	NONE	1) VD 2) AD	LRP-	-	-			AD + VD
UCSD	5828	F	71	70	1	2	NONE	1) AD 2) PART 3) METS	LRP-	-	-			AD + PART + METS
OHSU	2310	M	76	55	20	10	AD	1) AD	LRP-	-	+			AD
OHSU	1742	M	65	49	16	10	AD	1) AD	LRP-	-	+			AD
OHSU	3425	M	98	88	10	11	MCI	1) AD	LRP-	-	+			AD
OHSU	1219	M	63			1	AD	1) AD 2) CALP	LRP-	-				AD + AA
OHSU	1276	M	81	74	7	1	AD	1) AD 2) VD 3) CALP	LRP-	-				AD + AA + VD
OHSU	1399	M	85	76	8	2	AD	1) AD	LRP-	-				AD
OHSU	982	F	75	69	6	2	AD	1) AD 2) CAL	LRP-	-				AD + AA
OHSU	1510	F	66	53	13	4	AD	1) AD	LRP-	-				AD
OHSU	1610	M	62	53	9	4	AD	1) AD	LRP-	-				AD
OHSU	914	F	67	55	12	5	AD	1) FTLD	LRP-	-				FTLD-Tau
OHSU	1688	F	76	63	13	6	AD	1) AD	LRP-	-				AD

OHSU	1171	M	44	35	9	6	AD	1) AD	LRP-	-					AD
OHSU	1770	F	83	70	13	8	AD	1) AD	LRP-	-					AD
OHSU	1583	M	93	81	13	8	AD	1) AD	LRP-	-					AD
UCSD	5712	F	85	73	12	2	AD	1) AD	LRP-	-					AD
UCSD	5791	M	79			2	AD	1) AD 2) HS 3) LMN Encephalitis	LRP-	-					AD + HS + LMN Encephalitis
UCSD	5732	F	79			3	AD	1) AD	LRP-	-					AD
UCSD	5047	M	69	56	13	8	AD	1) AD	LRP-	-					AD
OHSU	850	F	48	43	6	2	FRONTOTEMP	1) PSP	LRP-	-					PSP
OHSU	1124	M	67			6	FRONTOTEMP	1) PK 2) AD	LRP-	-					AD + Pick's disease
UCSD	5766	M	81	71	10	4	FRONTOTEMP	1) FTLD	LRP-	-					PSP
OHSU	3482	F	88			10	MCI	1) AD	LRP-	-					AD
UCSD	5681	M	92	90	2	1	MCI	1) AD 2) VD	LRP-	-					AD + VD
UCSD	5687	M	85	79	6	2	MCI	1) Normal 2) VD	LRP-	-		-	-	-	VD
OHSU	1873	M	83			0	NONE	1) Normal	LRP-	-					Normal
UCSD	5816	F	83			3	NONE	1) AD 2) PART	LRP-	-					AD + PART
UCSD	5276	M	94	86	8	16	NONE	1) AD 2) VD	LRP-	-					AD + VD
OHSU	1271	M	68	59	9	7	OTHDEM	1) VD	LRP-	-					VD
UCSD	5853	M	72	65	7	3	OTHDEM	1) FTLD 2) VD 3) AA	LRP-	-		2/3	-	-	AA + VD + CBD
OHSU	1856	F	86	70	17	8	AD	1) AD 2) VD	Limbic	-	-				AD + VD
UCSD	5873	M	73	55	18	1	AD	1) AD 2) AA 3) LBD 4) TDP-43	Amygdala-predominant	-	-	-	-	-	AD + AA + FTLD-TDP43 + αSyn-Path
UCSD	5908	F	101	90	11	8	AD	1) AD 2) AA 3) LBD 4) Tau	Amygdala-predominant	-	-	-	-	-	AD + AA + αSyn-Path
UCSD	5869	F	67	56	11	4	FRONTOTEMP	1) FTLD 2) LBD	Amygdala-predominant	-	-	-	-	-	FTLD-TDP43 + αSyn-Path
UCSD	5872	M	77	69	8	6	MCI	1) AD 2) AA 3) LBD 4) TDP-43	Amygdala-predominant	-	-	-	-	-	AD + AA + FTLD-TDP43 + αSyn-Path
OHSU	3235	M	92	78	14	3	AD	1) AD 2) LBD 3) VD	Amygdala-predominant	-	+				AD + VD + αSyn-Path
OHSU	2201	M	86	71	15	10	AD	1) AD 2) VD	Amygdala-predominant	-	+				AD + VD
UCSD	5812	M	84	75	9	5	AD	1) AD 2) LBD 3) VD	Amygdala-predominant	-	+	2/3	+	+	AD + VD + αSyn-Path
UCSD	5901	F	87	79	8	5	AD	1) AD 2) AA 3) LBD	Amygdala-predominant	-	+	-	+	+	AD + AA + αSyn-Path
UCSD	5896	M	86	77	9	5	AD	1) AD 2) AA 3) LBD 4) TDP-43	Amygdala-predominant	-	+	-	+	+	AD + AA + FTLD-TDP43 + αSyn-Path
OHSU	2666	M	97			8	MCI	1) VD 2) AD	Amygdala-predominant	-	+				AD + VD
OHSU	1663	M	80	67	13	2	AD	1) AD	Amygdala-predominant	-					AD
OHSU	1454	F	86	77	9	3	AD	1) AD	Amygdala-predominant	-					AD
OHSU	832	M	61	53	9	4	AD	1) AD	Amygdala-predominant	-					AD
OHSU	1553	F	71	62	9	4	AD	1) AD	Amygdala-predominant	-					AD
OHSU	1201	M	68	57	11	7	AD	1) AD 2) CALP	Amygdala-predominant	-					AD + AA
UCSD	5731	F	84	76	8	2	AD	1) AD 2) LBD	Amygdala-predominant	-		-			AD + αSyn-Path

UCSD	5800	F	92	81	11	4	AD	1) AD	Amygdala-predominant	-		2/3	+	AD
OHSU	1034	F	59	46	13	5	FRONTOTEMP	1) PK 2) AD	Amygdala-predominant	-				AD + Pick's disease
UCSD	5704	M	78	72	6	2	DLB	1) AD	LRP-	+				AD
UCSD	5659	M	69	63	6	3	DLB	1) LBD 2) AD	Neocortical	+	-			AD + αSyn-Path
OHSU	2297	F	80	72	8	5	AD	1) AD 2) LBD 3) VD	Neocortical	+	+			AD + VD + αSyn-Path
OHSU	1729	M	58	48	10	6	AD	1) AD 2) LBD	Neocortical	+	+			AD + αSyn-Path
OHSU	1786	F	82	69	13	7	AD	1) AD 2) VD	Neocortical	+	+			AD + VD
OHSU	2034	M	82	63	18	10	AD	1) AD 2) LBD	Neocortical	+	+			AD + αSyn-Path
UCSD	5832	M	66	58	8	2	AD	1) AD 2) LBD	Neocortical	+	+			AD + αSyn-Path
UCSD	5865	M	72	66	6	2	AD	1) AD 2) LBD 3) AA	Neocortical	+	+	+	+	AD + AA + αSyn-Path
UCSD	5899	F	59	51	8	3	AD	1) AD 2) AA 3) LBD 4) TDP-43	Neocortical	+	+	+	+	AD + AA + FTLN-TDP43 + αSyn-Path
UCSD	5852	M	85	74	11	4	AD	1) AD 2) LBD	Neocortical	+	+			AD + αSyn-Path
UCSD	5831	M	87	81	6	5	AD	1) AD 2) LBD	Neocortical	+	+			AD + αSyn-Path
UCSD	5877	M	80	68	12	7	AD	1) AD 2) AA 3) LBD	Neocortical	+	+			AD + AA + αSyn-Path
UCSD	5898	M	73	52	21	10	AD	1) LBD 2) AD 3) Tau	Neocortical	+	+	+	+	AD + ARTAG + αSyn-Path
UCSD	5696	M	75	69	6	3	DLB	1) LBD 2) AD	Neocortical	+	+			AD + αSyn-Path
UCSD	5843	M	79	67	12	4	DLB	1) AD 2) LBD	Neocortical	+	+			AD + αSyn-Path
UCSD	5829	M	69			3	FRONTOTEMP	1) AD 2) LBD 3) HS	Neocortical	+	+			AD + HS + αSyn-Path
UCSD	5835	F	86	79	7	3	MCI	1) AD 2) LBD	Neocortical	+	+			AD + αSyn-Path
UCSD	5798	F	87	80	7	5	MCI	1) AD 2) LBD	Neocortical	+	+			AD + αSyn-Path
OHSU	3960	M	95	89	6	12	NONE	1) AD 2) LBD	Neocortical	+	+			AD + αSyn-Path
UCSD	5895	M	73	62	11	7	PD	1) LBD 2) AD 3) VD	Neocortical	+	+	+	+	AD + VD + αSyn-Path
OHSU	1269	M	70	61	9	2	AD	1) LBD 2) AD	Neocortical	+				AD + αSyn-Path
OHSU	1301	M	83	76	7	2	AD	1) AD 2) PD	Neocortical	+				AD + αSyn-Path
OHSU	1449	M	84	79	5	2	AD	1) AD 2) LBD	Neocortical	+				AD + αSyn-Path
OHSU	1486	M	73	66	6	3	AD	1) AD 2) LBD	Neocortical	+				AD + αSyn-Path
OHSU	1779	M	84	72	12	5	AD	1) AD 2) LBD	Neocortical	+				AD + αSyn-Path
UCSD	5851	M	71	63	8	1	AD	1) AD 2) LBD	Neocortical	+		+	+	AD + αSyn-Path
UCSD	5855	M	64	57	7	3	AD	1) AD 2) LBD 3) HS	Neocortical	+				AD + HS + αSyn-Path
UCSD	5706	M	83	77	6	3	AD	1) AD 2) LBD 3) HS	Neocortical	+				AD + HS + αSyn-Path
UCSD	5745	M	73			3	AD	1) FTLN 2) PSP 3) Corticobasal 4) HS 5) LBD	Neocortical	+				HS + PSP + CBD + αSyn-Path
UCSD	4879	M	75	62	13	4	AD	1) LBD	Neocortical	+				αSyn-Path
UCSD	5183	F	81	61	20	15	AD	1) LBD	Neocortical	+				αSyn-Path
UCSD	5688	M	88	82	6	2	DLB	1) LBD 2) AD	Neocortical	+				AD + αSyn-Path

UCSD	5729	M	70	63	7	2	DLB	1) LBD	Neocortical	+					αSyn-Path
UCSD	5815	M	84	72	12	3	DLB	1) LBD 2) AD	Neocortical	+					AD + αSyn-Path
UCSD	5505	F	68	62	6	3	DLB	1) LBD 2) AD	Neocortical	+					AD + αSyn-Path
UCSD	5778	M	72	59	13	4	DLB	1) PD 2) AD	Neocortical	+		+		+	AD + αSyn-Path
UCSD	5752	M	67	54	13	8	MCI	1) LBD 2) AD	Neocortical	+		+		+	AD + αSyn-Path
UCSD	5615	M	76	67	9	0	PD	1) LBD 2) AD 3) VD	Neocortical	+					AD + VD + αSyn-Path
UCSD	5762	M	81	72	9	4	PD	1) LBD 2) PD 3) AD	Neocortical	+		+		+	AD + αSyn-Path
OHSU	1472	M	79	64	15	2	AD	1) AD 2) HS	Limbic	+					AD + HS
OHSU	1497	M	79	65	13	3	AD	1) AD 2) VD	Limbic	+					AD + VD
OHSU	1675	M	75	65	10	3	AD	1) AD	Limbic	+					AD
UCSD	5733	M	64	59	5	0	AD	1) AD 2) LBD	Limbic	+					AD + αSyn-Path
UCSD	5875	F	72	61	11	4	AD	1) AD 2) AA 3) LBD 4) TDP-43	Limbic	+					AD + AA + FTLN-TDP43 + αSyn-Path
UCSD	5742	M	77	71	6	3	PD	1) LBD 2) PD 3) AD	Limbic	+					AD + αSyn-Path
OHSU	693	M	80	71	9	1	AD	1) AD 2) Infarcts	Amygdala-predominant	+					AD + Infarcts
OHSU	1436	F	40	37	4	2	AD	1) AD	Amygdala-predominant	+					AD
UCSD	5741	F	91	83	8	1	FRONTOTEMP	1) AD 2) PSP 3) LBD 4) VD	Amygdala-predominant	+		-		2/3	AD + VD + PSP + αSyn-Path

Table B.8.1. Summary of patient information. For pathology diagnoses, AD=Alzheimer's disease, CAL=leptomeningial congophilic angiopathy, CALP=lepto/parenchymal congophilic angiopathy, FTLN=fronto-temporal lobe degeneration, HS=hippocampal sclerosis, LBD=Lewy body dementia, Normal=no irregular pathology, PD=Parkinson's disease, PK=picks lobar sclerosis, PSP=progressive supranuclear palsy, VD=vascular disease. SAA for Table B.8.1 was performed by Amprion Inc. Neuropathology analysis was performed by Randy Woltjer and UCSD pathology.

	No α Syn-pathology (n=53)		Amygdala (n=21)		Limbic/Neocortical (n=45)			
	N	Mean (SD)	N	Mean (SD)	N	Mean (SD)	Test statistic	p value
Age at death#	53	77.2 (12.1)	21	79 (14.4)	45	76.3 (8.1)	F=0.43	0.65
Age at onset of clinical symptoms#	44	66.9 (13.8)	20	67.9 (13.7)	43	66.8 (8.9)	F=0.07	0.94
Rate of decline in MMSE score #	41	3.1 (3.3)	13	5.1 (3.7)	34	3.6 (2.8)	F=1.76	0.18
		Median (IQR)		Median (IQR)		Median (IQR)		
Onset to LP Duration	44	4.6 (2.6, 6.9)	20	5.7 (4.1, 7.0)	43	5.1 (3.5, 7.2)	$\chi^2=2.43$	0.30
Total Disease Duration	44	9.1 (6.6, 13.2)	20	9.3 (8.4, 11.8)	43	8.8 (6.2, 12.0)	$\chi^2=0.86$	0.65
UPDRS part III score at lumbar puncture##	15	0 (0, 0)	8	0 (0, 0)	21	11 (4, 25)	$\chi^2=21.59$	<0.0001
MMSE score at lumbar puncture##	53	24 (19, 29)	21	23 (14, 26)	43	22 (17, 26)	$\chi^2=5.17$	0.08
MMSE score at last visit##	53	15 (4, 22)	21	12 (9, 19)	44	15.5 (7, 21.5)	$\chi^2=0.06$	0.97
CDR score at last visit##	53	2 (1, 3)	21	2 (2, 3)	44	2 (2, 2.5)	$\chi^2=1.01$	0.60
UPDRS part III score at last visit##	40	0 (0, 0)	13	0 (0, 2)	27	8 (0, 17)	$\chi^2=14.93$	0.0006
LP to autopsy interval ##	53	4.7 (2.4, 8.4)	21	3.9 (2.4, 5.4)	45	3.2 (2.7, 5.1)	$\chi^2=2.83$	0.24
A β 42##								
OHSU	13	622 (531, 857)	5	575 (374, 705)	10	546.5 (419, 635)	$\chi^2=0.94$	0.62
UCSD	17	398 (308, 532)	10	497 (405, 519)	25	377 (298, 438)	$\chi^2=3.38$	0.18
A β 40##								
OHSU	13	10742 (8768, 13505)	5	10248 (7981, 13278)	10	9894.5 (5931, 11009)	$\chi^2=1.88$	0.39
UCSD	17	7213 (6232, 9367)	10	9143 (7375, 11203)	25	7744 (5236, 8518)	$\chi^2=4.47$	0.11
Tau##								
OHSU	13	576 (472, 720)	5	924 (585, 966)	10	506.5 (331, 731)	$\chi^2=1.56$	0.46
UCSD	17	502 (363, 763)	10	566 (535, 694)	25	353 (248, 531)	$\chi^2=4.98$	0.08
pTau##								
OHSU	13	86.7 (75.7, 100.6)	5	152.9 (94.1, 156.4)	10	84.1 (56.7, 112.4)	$\chi^2=1.99$	0.37
UCSD	17	67.6 (42.9, 102.1)	10	88.2 (80.2, 92.8)	25	54.2 (31.7, 71)	$\chi^2=4.38$	0.11
A β 42/40##								
OHSU	13	0.06 (0.05, 0.07)	5	0.05 (0.05, 0.05)	10	0.07 (0.05, 0.07)	$\chi^2=2.38$	0.30
UCSD	17	0.05 (0.05, 0.07)	10	0.05 (0.04, 0.06)	25	0.05 (0.04, 0.06)	$\chi^2=0.80$	0.67
		Percent		Percent		Percent		
Sex###							$\chi^2=6.94$	0.03
Male	31	(39.7%)	11	(14.1%)	36	(46.2%)		
Female	22	(83.7%)	10	(24.4%)	9	(37.8%)		
Clinical diagnosis##							$\chi^2=28.0$	0.002
#	6	(85.7%)	0	(0%)	1	(14.3%)		
No dementia	31	(41.3%)	16	(21.3%)	28	(37.3%)		
AD	1	(11.1%)	0	(0%)	8	(88.9%)		
DLB	0	(0%)	0	(0%)	4	(100%)		
PD	9	(69.2%)	3	(23.1%)	1	(7.7%)		
Other dementia	6	(54.6%)	2	(18.2%)	3	(27.3%)		
MCI								

Thal phase###	5	(83.3%)	1	(16.7%)	0	(0%)	$\chi^2=11.80$	0.30
0	0	(0%)	0	(0%)	1	(100%)		
1	3	(75%)	0	(0%)	1	(25%)		
2	0	(0%)	0	(0%)	2	(100%)		
3	8	(42.1%)	3	(15.8%)	8	(42.1%)		
4	11	(33.3%)	8	(24.2%)	14	(42.4%)		
Braak stage###	6	(66.7%)	1	(11.1%)	2	(22.2%)	$\chi^2=15.53$	0.21
0	2	(40%)	1	(20%)	2	(40%)		
1	0	(0%)	0	(0%)	3	(100%)		
2	4	(66.7%)	0	(0%)	2	(33.3%)		
3	2	(22.2%)	1	(11.1%)	6	(66.7%)		
4	7	(31.8%)	4	(18.2%)	11	(50%)		
5	32	(49.2%)	14	(21.5%)	19	(29.2%)		
6								
CERAD score###	12	(80%)	2	(13.3%)	1	(6.7%)	$\chi^2=11.3$	0.08
None	4	(44.4%)	1	(11.1%)	4	(44.4%)		
Sparse	12	(33.3%)	6	(16.7%)	18	(50%)		
Moderate	25	(42.4%)	12	(20.3%)	22	(37.3%)		
Frequent								
ADNC###	5	(83.3%)	1	(16.7%)	0	(0%)	$\chi^2=11.73$	0.07
None	3	(33.3%)	0	(0%)	6	(66.7%)		
Low	5	(31.3%)	1	(6.3%)	10	(62.5%)		
Intermediate	17	(40.5%)	9	(21.4%)	16	(38.1%)		
High								
Semi-CERAD score###	12	(63.2%)	4	(21.1%)	3	3 (15.8%)	$\chi^2=9.47$	0.15
None	4	(57.1%)	1	(14.3%)	2	2 (28.6%)		
Sparse	8	(33.3%)	2	(8.3%)	14	14 (58.3%)		
Moderate	26	(41.3%)	13	(20.6%)	24	24 (38.1%)		
Frequent								
Cerebral amyloid angiopathy###	18	(47.4%)	4	(10.5%)	16	(42.1%)	$\chi^2=3.17$	0.79
None	10	(43.5%)	5	(21.7%)	8	(34.8%)		
Mild	13	(37.1%)	8	(22.9%)	14	(40%)		
Moderate	9	(50%)	2	(11.1%)	7	(38.9%)		
Severe								
Arteriosclerosis###	12	(48%)	4	(16%)	9	(36%)	$\chi^2=9.16$	0.33
None	19	(52.8%)	6	(16.7%)	11	(30.6%)		
Mild	8	(33.3%)	5	(20.8%)	11	(45.8%)		
Moderate	2	(50%)	0	(0%)	2	(50%)		
Severe	3	(21.4%)	1	(7.1%)	10	(71.4%)		
Missing/Not done								
ApoE4###	26	(55.3%)	8	(17.0%)	13	(27.7%)	$\chi^2=4.47$	0.12
Non-carrier	26	(37.1%)	12	(17.1%)	32	(45.7%)		

Table B.8.2. Summary of statistical analysis between α Syn pathology groups. # general linear model used for analysis, **##** Kruskal-Wallis test used for analysis, **###** Chi-square test used for analysis. Neuropathology analysis was performed by Randy Woltjer and UCSD pathology.

[Jump Back to Table of Contents](#)

References

1. F. Tirumalasetti, L. Han, D. P. Birkett, The relationship between cancer and Alzheimer's disease. *J Am Geriatr Soc* **39**, 840 (1991).
2. A. Bajaj, J. A. Driver, E. S. Schernhammer, Parkinson's disease and cancer risk: a systematic review and meta-analysis. *Cancer Causes Control* **21**, 697-707 (2010).
3. L. G. Morris, S. Veeriah, T. A. Chan, Genetic determinants at the interface of cancer and neurodegenerative disease. *Oncogene* **29**, 3453-3464 (2010).
4. E. L. Ong, R. Goldacre, M. Goldacre, Differential risks of cancer types in people with Parkinson's disease: a national record-linkage study. *Eur J Cancer* **50**, 2456-2462 (2014).
5. K. Rugbjerg, S. Friis, C. F. Lassen, B. Ritz, J. H. Olsen, Malignant melanoma, breast cancer and other cancers in patients with Parkinson's disease. *Int J Cancer* **131**, 1904-1911 (2012).
6. J. H. Olsen *et al.*, Atypical cancer pattern in patients with Parkinson's disease. *Br J Cancer* **92**, 201-205 (2005).
7. J. H. Olsen, S. Friis, K. Frederiksen, Malignant melanoma and other types of cancer preceding Parkinson disease. *Epidemiology* **17**, 582-587 (2006).
8. J. H. Olsen, K. Tangerud, L. Wermuth, K. Frederiksen, S. Friis, Treatment with levodopa and risk for malignant melanoma. *Mov Disord* **22**, 1252-1257 (2007).
9. A. Elbaz *et al.*, Nonfatal cancer preceding Parkinson's disease: a case-control study. *Epidemiology* **13**, 157-164 (2002).
10. R. Y. Lo *et al.*, Comorbid cancer in Parkinson's disease. *Mov Disord* **25**, 1809-1817 (2010).
11. H. J. Ryu *et al.*, Parkinson's disease and skin cancer risk: a nationwide population-based cohort study in Korea. *J Eur Acad Dermatol Venereol* **34**, 2775-2780 (2020).
12. S. A. Kareus, K. P. Figueroa, L. A. Cannon-Albright, S. M. Pulst, Shared predispositions of parkinsonism and cancer: a population-based pedigree-linked study. *Arch Neurol* **69**, 1572-1577 (2012).
13. C. Becker, G. P. Brobert, S. Johansson, S. S. Jick, C. R. Meier, Cancer risk in association with Parkinson disease: a population-based study. *Parkinsonism Relat Disord* **16**, 186-190 (2010).
14. R. Constantinescu *et al.*, Malignant melanoma in early-treated Parkinson's disease: the NET-PD trial. *Mov Disord* **29**, 263-265 (2014).
15. L. A. Dalvin *et al.*, Parkinson Disease and Melanoma: Confirming and Reexamining an Association. *Mayo Clin Proc* **92**, 1070-1079 (2017).
16. J. A. Driver, G. Logroscino, J. E. Buring, J. M. Gaziano, T. Kurth, A prospective cohort study of cancer incidence following the diagnosis of Parkinson's disease. *Cancer Epidemiol Biomarkers Prev* **16**, 1260-1265 (2007).
17. J. M. Bertoni *et al.*, Increased melanoma risk in Parkinson disease: a prospective clinicopathological study. *Arch Neurol* **67**, 347-352 (2010).
18. S. R. Schwid *et al.*, Cancer incidence in a trial of an antiapoptotic agent for Parkinson's disease. *Mov Disord* **25**, 1801-1808 (2010).

19. H. Moller, L. Mellekjaer, J. K. McLaughlin, J. H. Olsen, Occurrence of different cancers in patients with Parkinson's disease. *BMJ* **310**, 1500-1501 (1995).
20. X. Zhang, D. Guarin, N. Mohammadzadehhonarvar, X. Chen, X. Gao, Parkinson's disease and cancer: a systematic review and meta-analysis of over 17 million participants. *BMJ Open* **11**, e046329 (2021).
21. D. M. Freedman, L. B. Travis, G. Gridley, R. W. Kuncl, Amyotrophic lateral sclerosis mortality in 1.9 million US cancer survivors. *Neuroepidemiology* **25**, 176-180 (2005).
22. X. Gao, K. C. Simon, J. Han, M. A. Schwarzschild, A. Ascherio, Family history of melanoma and Parkinson disease risk. *Neurology* **73**, 1286-1291 (2009).
23. P. D. Baade, L. Fritschi, D. M. Freedman, Mortality due to amyotrophic lateral sclerosis and Parkinson's disease among melanoma patients. *Neuroepidemiology* **28**, 16-20 (2007).
24. T. Pringsheim, N. Jette, A. Frolkis, T. D. Steeves, The prevalence of Parkinson's disease: a systematic review and meta-analysis. *Mov Disord* **29**, 1583-1590 (2014).
25. L. M. de Lau, M. M. Breteler, Epidemiology of Parkinson's disease. *Lancet Neurol* **5**, 525-535 (2006).
26. G. B. D. P. s. D. Collaborators, Global, regional, and national burden of Parkinson's disease, 1990-2016: a systematic analysis for the Global Burden of Disease Study 2016. *Lancet Neurol* **17**, 939-953 (2018).
27. E. R. Dorsey, B. R. Bloem, The Parkinson Pandemic-A Call to Action. *JAMA Neurol* **75**, 9-10 (2018).
28. S. K. Van Den Eeden *et al.*, Incidence of Parkinson's disease: variation by age, gender, and race/ethnicity. *Am J Epidemiol* **157**, 1015-1022 (2003).
29. E. B. Forsaa, J. P. Larsen, T. Wentzel-Larsen, G. Alves, What predicts mortality in Parkinson disease?: a prospective population-based long-term study. *Neurology* **75**, 1270-1276 (2010).
30. A. Diem-Zangerl *et al.*, Mortality in Parkinson's disease: a 20-year follow-up study. *Mov Disord* **24**, 819-825 (2009).
31. B. Pinter *et al.*, Mortality in Parkinson's disease: a 38-year follow-up study. *Mov Disord* **30**, 266-269 (2015).
32. A. Elbaz *et al.*, Risk tables for parkinsonism and Parkinson's disease. *J Clin Epidemiol* **55**, 25-31 (2002).
33. T. H. Reekes *et al.*, Sex specific cognitive differences in Parkinson disease. *NPJ Parkinsons Dis* **6**, 7 (2020).
34. B. Cholerton *et al.*, Sex differences in progression to mild cognitive impairment and dementia in Parkinson's disease. *Parkinsonism Relat Disord* **50**, 29-36 (2018).
35. R. Liu *et al.*, Potential sex differences in nonmotor symptoms in early drug-naive Parkinson disease. *Neurology* **84**, 2107-2115 (2015).
36. A. J. Noyce *et al.*, Meta-analysis of early nonmotor features and risk factors for Parkinson disease. *Ann Neurol* **72**, 893-901 (2012).
37. A. Ascherio *et al.*, Pesticide exposure and risk for Parkinson's disease. *Ann Neurol* **60**, 197-203 (2006).

38. R. Frigerio *et al.*, Chemical exposures and Parkinson's disease: a population-based case-control study. *Mov Disord* **21**, 1688-1692 (2006).
39. S. Costello, M. Cockburn, J. Bronstein, X. Zhang, B. Ritz, Parkinson's disease and residential exposure to maneb and paraquat from agricultural applications in the central valley of California. *Am J Epidemiol* **169**, 919-926 (2009).
40. J. A. Firestone *et al.*, Pesticides and risk of Parkinson disease: a population-based case-control study. *Arch Neurol* **62**, 91-95 (2005).
41. A. Elbaz *et al.*, Professional exposure to pesticides and Parkinson disease. *Ann Neurol* **66**, 494-504 (2009).
42. M. G. Weisskopf *et al.*, Persistent organochlorine pesticides in serum and risk of Parkinson disease. *Neurology* **74**, 1055-1061 (2010).
43. G. Pezzoli, E. Cereda, Exposure to pesticides or solvents and risk of Parkinson disease. *Neurology* **80**, 2035-2041 (2013).
44. S. Jo *et al.*, Association of NO₂ and Other Air Pollution Exposures With the Risk of Parkinson Disease. *JAMA Neurol* **78**, 800-808 (2021).
45. B. Krzyzanowski, S. Searles Nielsen, J. R. Turner, B. A. Racette, Fine Particulate Matter and Parkinson Disease Risk Among Medicare Beneficiaries. *Neurology* **101**, e2058-e2067 (2023).
46. B. Krzyzanowski *et al.*, Air Pollution and Parkinson Disease in a Population-Based Study. *JAMA Netw Open* **7**, e2433602 (2024).
47. W. Jiang, C. Ju, H. Jiang, D. Zhang, Dairy foods intake and risk of Parkinson's disease: a dose-response meta-analysis of prospective cohort studies. *Eur J Epidemiol* **29**, 613-619 (2014).
48. A. Ascherio, M. A. Schwarzschild, The epidemiology of Parkinson's disease: risk factors and prevention. *Lancet Neurol* **15**, 1257-1272 (2016).
49. S. M. Goldman *et al.*, Solvent exposures and Parkinson disease risk in twins. *Ann Neurol* **71**, 776-784 (2012).
50. S. M. Goldman *et al.*, Risk of Parkinson Disease Among Service Members at Marine Corps Base Camp Lejeune. *JAMA Neurol* **80**, 673-681 (2023).
51. K. M. Powers *et al.*, Parkinson's disease risks associated with dietary iron, manganese, and other nutrient intakes. *Neurology* **60**, 1761-1766 (2003).
52. Z. Lv *et al.*, Vitamin D status and Parkinson's disease: a systematic review and meta-analysis. *Neurol Sci* **35**, 1723-1730 (2014).
53. L. Wang *et al.*, Vitamin D from different sources is inversely associated with Parkinson disease. *Mov Disord* **30**, 560-566 (2015).
54. S. Shrestha *et al.*, Serum 25-hydroxyvitamin D concentrations in Mid-adulthood and Parkinson's disease risk. *Mov Disord* **31**, 972-978 (2016).
55. G. Hu *et al.*, Body mass index and the risk of Parkinson disease. *Neurology* **67**, 1955-1959 (2006).
56. G. E. Nam *et al.*, Metabolic syndrome and risk of Parkinson disease: A nationwide cohort study. *PLoS Med* **15**, e1002640 (2018).
57. E. De Pablo-Fernandez, R. Goldacre, J. Pakpoor, A. J. Noyce, T. T. Warner, Association between diabetes and subsequent Parkinson disease: A record-linkage cohort study. *Neurology* **91**, e139-e142 (2018).
58. H. Chohan *et al.*, Type 2 Diabetes as a Determinant of Parkinson's Disease Risk and Progression. *Mov Disord* **36**, 1420-1429 (2021).

59. P. W. Cullinane *et al.*, Type 2 Diabetes and Parkinson's Disease: A Focused Review of Current Concepts. *Mov Disord* **38**, 162-177 (2023).
60. S. Jafari, M. Etminan, F. Aminzadeh, A. Samii, Head injury and risk of Parkinson disease: a systematic review and meta-analysis. *Mov Disord* **28**, 1222-1229 (2013).
61. R. C. Gardner *et al.*, Traumatic brain injury in later life increases risk for Parkinson disease. *Ann Neurol* **77**, 987-995 (2015).
62. R. C. Gardner *et al.*, Mild TBI and risk of Parkinson disease: A Chronic Effects of Neurotrauma Consortium Study. *Neurology* **90**, e1771-e1779 (2018).
63. K. L. Adams-Carr *et al.*, Constipation preceding Parkinson's disease: a systematic review and meta-analysis. *J Neurol Neurosurg Psychiatry* **87**, 710-716 (2016).
64. H. Gustafsson, A. Nordstrom, P. Nordstrom, Depression and subsequent risk of Parkinson disease: A nationwide cohort study. *Neurology* **84**, 2422-2429 (2015).
65. F. Fang *et al.*, Depression and the subsequent risk of Parkinson's disease in the NIH-AARP Diet and Health Study. *Mov Disord* **25**, 1157-1162 (2010).
66. E. L. Jacob, N. M. Gatto, A. Thompson, Y. Bordelon, B. Ritz, Occurrence of depression and anxiety prior to Parkinson's disease. *Parkinsonism Relat Disord* **16**, 576-581 (2010).
67. A. Alonso, L. A. Rodriguez, G. Logroscino, M. A. Hernan, Use of antidepressants and the risk of Parkinson's disease: a prospective study. *J Neurol Neurosurg Psychiatry* **80**, 671-674 (2009).
68. L. Ishihara, C. Brayne, A systematic review of depression and mental illness preceding Parkinson's disease. *Acta Neurol Scand* **113**, 211-220 (2006).
69. J. B. Badenoch *et al.*, Neuroanatomical and prognostic associations of depression in Parkinson's disease. *J Neurol Neurosurg Psychiatry* **95**, 966-973 (2024).
70. A. B. Singleton, M. J. Farrer, V. Bonifati, The genetics of Parkinson's disease: progress and therapeutic implications. *Mov Disord* **28**, 14-23 (2013).
71. K. Marder *et al.*, Risk of Parkinson's disease among first-degree relatives: A community-based study. *Neurology* **47**, 155-160 (1996).
72. C. M. Tanner *et al.*, Parkinson disease in twins: an etiologic study. *JAMA* **281**, 341-346 (1999).
73. M. H. Polymeropoulos *et al.*, Mutation in the alpha-synuclein gene identified in families with Parkinson's disease. *Science* **276**, 2045-2047 (1997).
74. A. Zimprich *et al.*, Mutations in LRRK2 cause autosomal-dominant parkinsonism with pleomorphic pathology. *Neuron* **44**, 601-607 (2004).
75. Y. Xiong *et al.*, Overexpression of Parkinson's Disease-Associated Mutation LRRK2 G2019S in Mouse Forebrain Induces Behavioral Deficits and alpha-Synuclein Pathology. *eNeuro* **4**, (2017).
76. D. Berg *et al.*, Type and frequency of mutations in the LRRK2 gene in familial and sporadic Parkinson's disease*. *Brain* **128**, 3000-3011 (2005).
77. S. Lesage *et al.*, G2019S LRRK2 mutation in French and North African families with Parkinson's disease. *Ann Neurol* **58**, 784-787 (2005).
78. W. C. Nichols *et al.*, Genetic screening for a single common LRRK2 mutation in familial Parkinson's disease. *Lancet* **365**, 410-412 (2005).

79. A. Di Fonzo *et al.*, A frequent LRRK2 gene mutation associated with autosomal dominant Parkinson's disease. *Lancet* **365**, 412-415 (2005).
80. C. Gaig *et al.*, LRRK2 mutations in Spanish patients with Parkinson disease: frequency, clinical features, and incomplete penetrance. *Arch Neurol* **63**, 377-382 (2006).
81. A. H. Schapira, The importance of LRRK2 mutations in Parkinson disease. *Arch Neurol* **63**, 1225-1228 (2006).
82. H. Deng *et al.*, Genetic analysis of LRRK2 mutations in patients with Parkinson disease. *J Neurol Sci* **251**, 102-106 (2006).
83. A. Brice, How much does dardarin contribute to Parkinson's disease? *Lancet* **365**, 363-364 (2005).
84. L. N. Clark *et al.*, Frequency of LRRK2 mutations in early- and late-onset Parkinson disease. *Neurology* **67**, 1786-1791 (2006).
85. N. R. Whaley, R. J. Uitti, D. W. Dickson, M. J. Farrer, Z. K. Wszolek, Clinical and pathologic features of families with LRRK2-associated Parkinson's disease. *J Neural Transm Suppl*, 221-229 (2006).
86. D. M. Kay *et al.*, Parkinson's disease and LRRK2: frequency of a common mutation in U.S. movement disorder clinics. *Mov Disord* **21**, 519-523 (2006).
87. C. Paisan-Ruiz *et al.*, Familial Parkinson's disease: clinical and genetic analysis of four Basque families. *Ann Neurol* **57**, 365-372 (2005).
88. J. Trinh *et al.*, Genotype-phenotype relations for the Parkinson's disease genes SNCA, LRRK2, VPS35: MDSGene systematic review. *Mov Disord* **33**, 1857-1870 (2018).
89. D. G. Healy *et al.*, Phenotype, genotype, and worldwide genetic penetrance of LRRK2-associated Parkinson's disease: a case-control study. *Lancet Neurol* **7**, 583-590 (2008).
90. E. Tolosa, M. Vila, C. Klein, O. Rascol, LRRK2 in Parkinson disease: challenges of clinical trials. *Nat Rev Neurol* **16**, 97-107 (2020).
91. T. Kitada *et al.*, Mutations in the parkin gene cause autosomal recessive juvenile parkinsonism. *Nature* **392**, 605-608 (1998).
92. E. M. Valente *et al.*, Localization of a novel locus for autosomal recessive early-onset parkinsonism, PARK6, on human chromosome 1p35-p36. *Am J Hum Genet* **68**, 895-900 (2001).
93. V. Bonifati *et al.*, Mutations in the DJ-1 gene associated with autosomal recessive early-onset parkinsonism. *Science* **299**, 256-259 (2003).
94. C. B. Lucking *et al.*, Association between early-onset Parkinson's disease and mutations in the parkin gene. *N Engl J Med* **342**, 1560-1567 (2000).
95. E. Lohmann *et al.*, How much phenotypic variation can be attributed to parkin genotype? *Ann Neurol* **54**, 176-185 (2003).
96. N. L. Khan *et al.*, Parkin disease: a phenotypic study of a large case series. *Brain* **126**, 1279-1292 (2003).
97. K. M. Doherty *et al.*, Parkin disease: a clinicopathologic entity? *JAMA Neurol* **70**, 571-579 (2013).
98. R. Hilker *et al.*, Positron emission tomographic analysis of the nigrostriatal dopaminergic system in familial parkinsonism associated with mutations in the parkin gene. *Ann Neurol* **49**, 367-376 (2001).

99. J. Feng, Microtubule: a common target for parkin and Parkinson's disease toxins. *Neuroscientist* **12**, 469-476 (2006).
100. R. E. Burke, Recent advances in research on Parkinson disease: synuclein and parkin. *Neurologist* **10**, 75-81 (2004).
101. V. A. Morais *et al.*, PINK1 loss-of-function mutations affect mitochondrial complex I activity via NdufA10 ubiquinone uncoupling. *Science* **344**, 203-207 (2014).
102. S. R. Subramaniam, M. F. Chesselet, Mitochondrial dysfunction and oxidative stress in Parkinson's disease. *Prog Neurobiol* **106-107**, 17-32 (2013).
103. S. Hague *et al.*, Early-onset Parkinson's disease caused by a compound heterozygous DJ-1 mutation. *Ann Neurol* **54**, 271-274 (2003).
104. L. Smith, A. H. V. Schapira, GBA Variants and Parkinson Disease: Mechanisms and Treatments. *Cells* **11**, (2022).
105. E. Sidransky *et al.*, Multicenter analysis of glucocerebrosidase mutations in Parkinson's disease. *N Engl J Med* **361**, 1651-1661 (2009).
106. J. M. den Heijer *et al.*, A Large-Scale Full GBA1 Gene Screening in Parkinson's Disease in the Netherlands. *Mov Disord* **35**, 1667-1674 (2020).
107. Z. Gan-Or *et al.*, Differential effects of severe vs mild GBA mutations on Parkinson disease. *Neurology* **84**, 880-887 (2015).
108. J. A. Ruskey *et al.*, Increased yield of full GBA sequencing in Ashkenazi Jews with Parkinson's disease. *Eur J Med Genet* **62**, 65-69 (2019).
109. S. Lesage *et al.*, Large-scale screening of the Gaucher's disease-related glucocerebrosidase gene in Europeans with Parkinson's disease. *Hum Mol Genet* **20**, 202-210 (2011).
110. R. Inzelberg, S. Hassin-Baer, J. Jankovic, Genetic movement disorders in patients of Jewish ancestry. *JAMA Neurol* **71**, 1567-1572 (2014).
111. R. N. Alcalay *et al.*, Cognitive performance of GBA mutation carriers with early-onset PD: the CORE-PD study. *Neurology* **78**, 1434-1440 (2012).
112. L. M. Chahine *et al.*, Clinical and biochemical differences in patients having Parkinson disease with vs without GBA mutations. *JAMA Neurol* **70**, 852-858 (2013).
113. I. F. Mata *et al.*, GBA Variants are associated with a distinct pattern of cognitive deficits in Parkinson's disease. *Mov Disord* **31**, 95-102 (2016).
114. G. Liu *et al.*, Specifically neuropathic Gaucher's mutations accelerate cognitive decline in Parkinson's. *Ann Neurol* **80**, 674-685 (2016).
115. R. Cilia *et al.*, Survival and dementia in GBA-associated Parkinson's disease: The mutation matters. *Ann Neurol* **80**, 662-673 (2016).
116. J. Maple-Grodem *et al.*, Association of GBA Genotype With Motor and Functional Decline in Patients With Newly Diagnosed Parkinson Disease. *Neurology* **96**, e1036-e1044 (2021).
117. R. B. Postuma *et al.*, MDS clinical diagnostic criteria for Parkinson's disease. *Mov Disord* **30**, 1591-1601 (2015).
118. G. Pagano, N. Ferrara, D. J. Brooks, N. Pavese, Age at onset and Parkinson disease phenotype. *Neurology* **86**, 1400-1407 (2016).
119. G. Deuschl, P. Bain, M. Brin, Consensus statement of the Movement Disorder Society on Tremor. Ad Hoc Scientific Committee. *Mov Disord* **13 Suppl 3**, 2-23 (1998).

120. C. Marras, A. Lang, Parkinson's disease subtypes: lost in translation? *J Neurol Neurosurg Psychiatry* **84**, 409-415 (2013).
121. M. A. Thenganatt, J. Jankovic, Parkinson disease subtypes. *JAMA Neurol* **71**, 499-504 (2014).
122. J. G. Nutt, Motor subtype in Parkinson's disease: Different disorders or different stages of disease? *Mov Disord* **31**, 957-961 (2016).
123. W. J. Zetuskys, J. Jankovic, F. J. Pirozzolo, The heterogeneity of Parkinson's disease: clinical and prognostic implications. *Neurology* **35**, 522-526 (1985).
124. J. Jankovic *et al.*, Variable expression of Parkinson's disease: a base-line analysis of the DATATOP cohort. The Parkinson Study Group. *Neurology* **40**, 1529-1534 (1990).
125. L. A. Hershey, B. J. Feldman, K. Y. Kim, C. Commichau, D. G. Lichter, Tremor at onset. Predictor of cognitive and motor outcome in Parkinson's disease? *Arch Neurol* **48**, 1049-1051 (1991).
126. A. H. Rajput, A. Voll, M. L. Rajput, C. A. Robinson, A. Rajput, Course in Parkinson disease subtypes: A 39-year clinicopathologic study. *Neurology* **73**, 206-212 (2009).
127. C. H. Williams-Gray *et al.*, The CamPaIGN study of Parkinson's disease: 10-year outlook in an incident population-based cohort. *J Neurol Neurosurg Psychiatry* **84**, 1258-1264 (2013).
128. J. F. van der Heeden *et al.*, Postural instability and gait are associated with severity and prognosis of Parkinson disease. *Neurology* **86**, 2243-2250 (2016).
129. D. J. Burn *et al.*, Motor subtype and cognitive decline in Parkinson's disease, Parkinson's disease with dementia, and dementia with Lewy bodies. *J Neurol Neurosurg Psychiatry* **77**, 585-589 (2006).
130. G. Alves, J. P. Larsen, M. Emre, T. Wentzel-Larsen, D. Aarsland, Changes in motor subtype and risk for incident dementia in Parkinson's disease. *Mov Disord* **21**, 1123-1130 (2006).
131. M. A. Hely *et al.*, The sydney multicentre study of Parkinson's disease: progression and mortality at 10 years. *J Neurol Neurosurg Psychiatry* **67**, 300-307 (1999).
132. L. S. Ishihara, A. Cheesbrough, C. Brayne, A. Schrag, Estimated life expectancy of Parkinson's patients compared with the UK population. *J Neurol Neurosurg Psychiatry* **78**, 1304-1309 (2007).
133. R. Savica *et al.*, Survival and Causes of Death Among People With Clinically Diagnosed Synucleinopathies With Parkinsonism: A Population-Based Study. *JAMA Neurol* **74**, 839-846 (2017).
134. D. Backstrom *et al.*, Early predictors of mortality in parkinsonism and Parkinson disease: A population-based study. *Neurology* **91**, e2045-e2056 (2018).
135. A. D. Macleod, K. S. Taylor, C. E. Counsell, Mortality in Parkinson's disease: a systematic review and meta-analysis. *Mov Disord* **29**, 1615-1622 (2014).
136. E. Tolosa, A. Garrido, S. W. Scholz, W. Poewe, Challenges in the diagnosis of Parkinson's disease. *Lancet Neurol* **20**, 385-397 (2021).
137. R. B. Postuma, J. F. Gagnon, M. Vendette, K. Charland, J. Montplaisir, Manifestations of Parkinson disease differ in association with REM sleep behavior disorder. *Mov Disord* **23**, 1665-1672 (2008).

138. S. R. Romenets *et al.*, Rapid eye movement sleep behavior disorder and subtypes of Parkinson's disease. *Mov Disord* **27**, 996-1003 (2012).
139. R. B. Postuma *et al.*, REM sleep behavior disorder and neuropathology in Parkinson's disease. *Mov Disord* **30**, 1413-1417 (2015).
140. J. Rusz *et al.*, Quantitative assessment of motor speech abnormalities in idiopathic rapid eye movement sleep behaviour disorder. *Sleep Med* **19**, 141-147 (2016).
141. S. Rahayel *et al.*, Brain atrophy in Parkinson's disease with polysomnography-confirmed REM sleep behavior disorder. *Sleep* **42**, (2019).
142. A. Videnovic *et al.*, Increased REM sleep without atonia in Parkinson disease with freezing of gait. *Neurology* **81**, 1030-1035 (2013).
143. G. Tissingh *et al.*, Loss of olfaction in de novo and treated Parkinson's disease: possible implications for early diagnosis. *Mov Disord* **16**, 41-46 (2001).
144. G. D. Scott, M. M. Lim, M. G. Drake, R. Woltjer, J. F. Quinn, Onset of Skin, Gut, and Genitourinary Prodromal Parkinson's Disease: A Study of 1.5 Million Veterans. *Mov Disord* **36**, 2094-2103 (2021).
145. M. M. Ponsen *et al.*, Idiopathic hyposmia as a preclinical sign of Parkinson's disease. *Ann Neurol* **56**, 173-181 (2004).
146. G. W. Ross *et al.*, Association of olfactory dysfunction with risk for future Parkinson's disease. *Ann Neurol* **63**, 167-173 (2008).
147. G. Fenelon, F. Mahieux, R. Huon, M. Ziegler, Hallucinations in Parkinson's disease: prevalence, phenomenology and risk factors. *Brain* **123 (Pt 4)**, 733-745 (2000).
148. J. R. Sanchez-Ramos, R. Ortoll, G. W. Paulson, Visual hallucinations associated with Parkinson disease. *Arch Neurol* **53**, 1265-1268 (1996).
149. A. H. Lee, D. Weintraub, Psychosis in Parkinson's disease without dementia: common and comorbid with other non-motor symptoms. *Mov Disord* **27**, 858-863 (2012).
150. M. Politis *et al.*, Parkinson's disease symptoms: the patient's perspective. *Mov Disord* **25**, 1646-1651 (2010).
151. D. Aarsland *et al.*, Range of neuropsychiatric disturbances in patients with Parkinson's disease. *J Neurol Neurosurg Psychiatry* **67**, 492-496 (1999).
152. P. Barone *et al.*, The PRIAMO study: A multicenter assessment of nonmotor symptoms and their impact on quality of life in Parkinson's disease. *Mov Disord* **24**, 1641-1649 (2009).
153. L. M. Chahine, A. W. Amara, A. Videnovic, A systematic review of the literature on disorders of sleep and wakefulness in Parkinson's disease from 2005 to 2015. *Sleep Med Rev* **35**, 33-50 (2017).
154. G. Alves, T. Wentzel-Larsen, J. P. Larsen, Is fatigue an independent and persistent symptom in patients with Parkinson disease? *Neurology* **63**, 1908-1911 (2004).
155. G. Schifitto *et al.*, Fatigue in levodopa-naive subjects with Parkinson disease. *Neurology* **71**, 481-485 (2008).
156. M. Asahina, E. Vichayanrat, D. A. Low, V. Iodice, C. J. Mathias, Autonomic dysfunction in parkinsonian disorders: assessment and pathophysiology. *J Neurol Neurosurg Psychiatry* **84**, 674-680 (2013).

157. J. M. Senard *et al.*, Prevalence of orthostatic hypotension in Parkinson's disease. *J Neurol Neurosurg Psychiatry* **63**, 584-589 (1997).
158. Y. H. Hiorth, K. F. Pedersen, I. Dalen, O. B. Tysnes, G. Alves, Orthostatic hypotension in Parkinson disease: A 7-year prospective population-based study. *Neurology* **93**, e1526-e1534 (2019).
159. G. E. Lemack, R. B. Dewey, Jr., C. G. Roehrborn, P. E. O'Suilleabhain, P. E. Zimmern, Questionnaire-based assessment of bladder dysfunction in patients with mild to moderate Parkinson's disease. *Urology* **56**, 250-254 (2000).
160. A. Hand, W. K. Gray, B. J. Chandler, R. W. Walker, Sexual and relationship dysfunction in people with Parkinson's disease. *Parkinsonism Relat Disord* **16**, 172-176 (2010).
161. C. G. Goetz, C. M. Tanner, M. Levy, R. S. Wilson, D. C. Garron, Pain in Parkinson's disease. *Mov Disord* **1**, 45-49 (1986).
162. R. B. Postuma *et al.*, Validation of the MDS clinical diagnostic criteria for Parkinson's disease. *Mov Disord* **33**, 1601-1608 (2018).
163. E. Tolosa, G. Wenning, W. Poewe, The diagnosis of Parkinson's disease. *Lancet Neurol* **5**, 75-86 (2006).
164. A. J. Stoessel, W. W. Martin, M. J. McKeown, V. Sossi, Advances in imaging in Parkinson's disease. *Lancet Neurol* **10**, 987-1001 (2011).
165. G. Kagi, K. P. Bhatia, E. Tolosa, The role of DAT-SPECT in movement disorders. *J Neurol Neurosurg Psychiatry* **81**, 5-12 (2010).
166. K. P. Banks, J. G. Peacock, M. N. Clemenshaw, P. H. Kuo, Optimizing the Diagnosis of Parkinsonian Syndromes With (123)I-Ioflupane Brain SPECT. *AJR Am J Roentgenol* **213**, 243-253 (2019).
167. L. K. Teune *et al.*, Typical cerebral metabolic patterns in neurodegenerative brain diseases. *Mov Disord* **25**, 2395-2404 (2010).
168. N. Pavese, PET studies in Parkinson's disease motor and cognitive dysfunction. *Parkinsonism Relat Disord* **18 Suppl 1**, S96-99 (2012).
169. I. T. Hsiao *et al.*, Correlation of Parkinson disease severity and 18F-DTBZ positron emission tomography. *JAMA Neurol* **71**, 758-766 (2014).
170. S. Korat *et al.*, Alpha-Synuclein PET Tracer Development-An Overview about Current Efforts. *Pharmaceuticals (Basel)* **14**, (2021).
171. M. Porritt *et al.*, Dopaminergic innervation of the human striatum in Parkinson's disease. *Mov Disord* **20**, 810-818 (2005).
172. O. Hornykiewicz, The discovery of dopamine deficiency in the parkinsonian brain. *J Neural Transm Suppl*, 9-15 (2006).
173. D. J. Brooks *et al.*, Differing patterns of striatal 18F-dopa uptake in Parkinson's disease, multiple system atrophy, and progressive supranuclear palsy. *Ann Neurol* **28**, 547-555 (1990).
174. T. Murakami *et al.*, Pael-R is accumulated in Lewy bodies of Parkinson's disease. *Ann Neurol* **55**, 439-442 (2004).
175. K. Wakabayashi *et al.*, Synphilin-1 is present in Lewy bodies in Parkinson's disease. *Ann Neurol* **47**, 521-523 (2000).
176. A. Popescu, C. F. Lippa, V. M. Lee, J. Q. Trojanowski, Lewy bodies in the amygdala: increase of alpha-synuclein aggregates in neurodegenerative diseases with tau-based inclusions. *Arch Neurol* **61**, 1915-1919 (2004).

177. M. Goedert, M. G. Spillantini, K. Del Tredici, H. Braak, 100 years of Lewy pathology. *Nat Rev Neurol* **9**, 13-24 (2013).
178. J. M. Henderson, K. Carpenter, H. Cartwright, G. M. Halliday, Degeneration of the centre median-parafascicular complex in Parkinson's disease. *Ann Neurol* **47**, 345-352 (2000).
179. S. Fahn *et al.*, Levodopa and the progression of Parkinson's disease. *N Engl J Med* **351**, 2498-2508 (2004).
180. P. D. M. C. Group *et al.*, Long-term effectiveness of dopamine agonists and monoamine oxidase B inhibitors compared with levodopa as initial treatment for Parkinson's disease (PD MED): a large, open-label, pragmatic randomised trial. *Lancet* **384**, 1196-1205 (2014).
181. J. Jankovic, Pathogenesis-targeted therapeutic strategies in Parkinson's disease. *Mov Disord* **34**, 41-44 (2019).
182. A. E. Lang *et al.*, Trial of Cinpanemab in Early Parkinson's Disease. *N Engl J Med* **387**, 408-420 (2022).
183. G. Pagano *et al.*, Trial of Prasinezumab in Early-Stage Parkinson's Disease. *N Engl J Med* **387**, 421-432 (2022).
184. D. Vijayakumar, J. Jankovic, Slowing Parkinson's Disease Progression with Vaccination and Other Immunotherapies. *CNS Drugs* **36**, 327-343 (2022).
185. D. Volc *et al.*, Safety and immunogenicity of the alpha-synuclein active immunotherapeutic PD01A in patients with Parkinson's disease: a randomised, single-blinded, phase 1 trial. *Lancet Neurol* **19**, 591-600 (2020).
186. G. V. Long, S. M. Swetter, A. M. Menzies, J. E. Gershenwald, R. A. Scolyer, Cutaneous melanoma. *Lancet* **402**, 485-502 (2023).
187. M. Arnold *et al.*, Global Burden of Cutaneous Melanoma in 2020 and Projections to 2040. *JAMA Dermatol* **158**, 495-503 (2022).
188. E. H. Campbell *et al.*, Increasing Incidence and Decreasing Mortality of Cutaneous Melanoma in Middle-Aged Adults: An Epidemiologic Study in Olmsted County, Minnesota. *Mayo Clin Proc* **98**, 713-722 (2023).
189. H. G. Welch, S. Woloshin, L. M. Schwartz, Skin biopsy rates and incidence of melanoma: population based ecological study. *BMJ* **331**, 481 (2005).
190. R. A. Swerlick, S. Chen, The melanoma epidemic. Is increased surveillance the solution or the problem? *Arch Dermatol* **132**, 881-884 (1996).
191. B. A. Gilchrest, M. S. Eller, A. C. Geller, M. Yaar, The pathogenesis of melanoma induced by ultraviolet radiation. *N Engl J Med* **340**, 1341-1348 (1999).
192. J. M. Elwood, J. Jopson, Melanoma and sun exposure: an overview of published studies. *Int J Cancer* **73**, 198-203 (1997).
193. J. L. Bulliard, B. Cox, J. M. Elwood, Latitude gradients in melanoma incidence and mortality in the non-Maori population of New Zealand. *Cancer Causes Control* **5**, 234-240 (1994).
194. G. Pennello, S. Devesa, M. Gail, Association of surface ultraviolet B radiation levels with melanoma and nonmelanoma skin cancer in United States blacks. *Cancer Epidemiol Biomarkers Prev* **9**, 291-297 (2000).
195. P. J. Nelemans *et al.*, Effect of intermittent exposure to sunlight on melanoma risk among indoor workers and sun-sensitive individuals. *Environ Health Perspect* **101**, 252-255 (1993).

196. S. Wu, J. Han, F. Laden, A. A. Qureshi, Long-term ultraviolet flux, other potential risk factors, and skin cancer risk: a cohort study. *Cancer Epidemiol Biomarkers Prev* **23**, 1080-1089 (2014).
197. A. W. Kubica, J. D. Brewer, Melanoma in immunosuppressed patients. *Mayo Clin Proc* **87**, 991-1003 (2012).
198. J. D. Brewer *et al.*, Malignant melanoma in solid transplant recipients: collection of database cases and comparison with surveillance, epidemiology, and end results data for outcome analysis. *Arch Dermatol* **147**, 790-796 (2011).
199. C. S. Hollenbeak *et al.*, Increased incidence of melanoma in renal transplantation recipients. *Cancer* **104**, 1962-1967 (2005).
200. M. Ascha, M. S. Ascha, J. Tanenbaum, J. S. Bordeaux, Risk Factors for Melanoma in Renal Transplant Recipients. *JAMA Dermatol* **153**, 1130-1136 (2017).
201. S. Gandini *et al.*, Meta-analysis of risk factors for cutaneous melanoma: III. Family history, actinic damage and phenotypic factors. *Eur J Cancer* **41**, 2040-2059 (2005).
202. H. T. Lynch, B. C. Fritchot, 3rd, J. F. Lynch, Familial atypical multiple mole-melanoma syndrome. *J Med Genet* **15**, 352-356 (1978).
203. W. H. Clark, Jr., R. R. Reimer, M. Greene, A. M. Ainsworth, M. J. Mastrangelo, Origin of familial malignant melanomas from heritable melanocytic lesions. 'The B-K mole syndrome'. *Arch Dermatol* **114**, 732-738 (1978).
204. D. E. Elder, B. C. Bastian, I. A. Cree, D. Massi, R. A. Scolyer, The 2018 World Health Organization Classification of Cutaneous, Mucosal, and Uveal Melanoma: Detailed Analysis of 9 Distinct Subtypes Defined by Their Evolutionary Pathway. *Arch Pathol Lab Med* **144**, 500-522 (2020).
205. B. C. Bastian, The molecular pathology of melanoma: an integrated taxonomy of melanocytic neoplasia. *Annu Rev Pathol* **9**, 239-271 (2014).
206. K. G. Lasithiotakis *et al.*, The incidence and mortality of cutaneous melanoma in Southern Germany: trends by anatomic site and pathologic characteristics, 1976 to 2003. *Cancer* **107**, 1331-1339 (2006).
207. R. Pampena *et al.*, A meta-analysis of nevus-associated melanoma: Prevalence and practical implications. *J Am Acad Dermatol* **77**, 938-945 e934 (2017).
208. A. Breslow, Thickness, cross-sectional areas and depth of invasion in the prognosis of cutaneous melanoma. *Ann Surg* **172**, 902-908 (1970).
209. A. o. M. American Academy of Dermatology Ad Hoc Task Force for the *et al.*, Early detection of melanoma: reviewing the ABCDEs. *J Am Acad Dermatol* **72**, 717-723 (2015).
210. A. C. Geller *et al.*, Factors related to the presentation of thin and thick nodular melanoma from a population-based cancer registry in Queensland Australia. *Cancer* **115**, 1318-1327 (2009).
211. M. A. Warycha *et al.*, Changes in the presentation of nodular and superficial spreading melanomas over 35 years. *Cancer* **113**, 3341-3348 (2008).
212. M. F. Demierre, C. Chung, D. R. Miller, A. C. Geller, Early detection of thick melanomas in the United States: beware of the nodular subtype. *Arch Dermatol* **141**, 745-750 (2005).

213. S. M. Swetter, J. C. Boldrick, S. Y. Jung, B. M. Egbert, J. D. Harvell, Increasing incidence of lentigo maligna melanoma subtypes: northern California and national trends 1990-2000. *J Invest Dermatol* **125**, 685-691 (2005).
214. W. H. Clark, Jr., M. C. Mihm, Jr., Lentigo maligna and lentigo-maligna melanoma. *Am J Pathol* **55**, 39-67 (1969).
215. M. A. Weinstock, A. J. Sober, The risk of progression of lentigo maligna to lentigo maligna melanoma. *Br J Dermatol* **116**, 303-310 (1987).
216. E. K. Brunsgaard, Y. P. Wu, D. Grossman, Melanoma in skin of color: Part I. Epidemiology and clinical presentation. *J Am Acad Dermatol* **89**, 445-456 (2023).
217. W. P. Coleman, 3rd, P. R. Loria, R. J. Reed, E. T. Kremenz, Acral lentiginous melanoma. *Arch Dermatol* **116**, 773-776 (1980).
218. R. Pampena *et al.*, Clinical and Dermoscopic Features Associated With Difficult-to-Recognize Variants of Cutaneous Melanoma: A Systematic Review. *JAMA Dermatol* **156**, 430-439 (2020).
219. N. R. Abbasi *et al.*, Early diagnosis of cutaneous melanoma: revisiting the ABCD criteria. *JAMA* **292**, 2771-2776 (2004).
220. R. J. Friedman, D. S. Rigel, A. W. Kopf, Early detection of malignant melanoma: the role of physician examination and self-examination of the skin. *CA Cancer J Clin* **35**, 130-151 (1985).
221. J. Gachon *et al.*, First prospective study of the recognition process of melanoma in dermatological practice. *Arch Dermatol* **141**, 434-438 (2005).
222. J. J. Grob, J. J. Bonerandi, The 'ugly duckling' sign: identification of the common characteristics of nevi in an individual as a basis for melanoma screening. *Arch Dermatol* **134**, 103-104 (1998).
223. C. Gaudy-Marqueste *et al.*, Ugly Duckling Sign as a Major Factor of Efficiency in Melanoma Detection. *JAMA Dermatol* **153**, 279-284 (2017).
224. A. Scope *et al.*, The "ugly duckling" sign: agreement between observers. *Arch Dermatol* **144**, 58-64 (2008).
225. P. Carli *et al.*, Diagnostic and referral accuracy of family doctors in melanoma screening: effect of a short formal training. *Eur J Cancer Prev* **14**, 51-55 (2005).
226. L. Peuvrel *et al.*, Impact of a campaign to train general practitioners in screening for melanoma. *Eur J Cancer Prev* **18**, 225-229 (2009).
227. F. M. Walter *et al.*, Using the 7-point checklist as a diagnostic aid for pigmented skin lesions in general practice: a diagnostic validation study. *Br J Gen Pract* **63**, e345-353 (2013).
228. A. J. Chamberlain, L. Fritschi, J. W. Kelly, Nodular melanoma: patients' perceptions of presenting features and implications for earlier detection. *J Am Acad Dermatol* **48**, 694-701 (2003).
229. E. K. Levit, M. H. Kagen, R. K. Scher, M. Grossman, E. Altman, The ABC rule for clinical detection of subungual melanoma. *J Am Acad Dermatol* **42**, 269-274 (2000).
230. J. G. Elmore *et al.*, Concordance and Reproducibility of Melanoma Staging According to the 7th vs 8th Edition of the AJCC Cancer Staging Manual. *JAMA Netw Open* **1**, (2018).

231. J. E. Gershenwald *et al.*, Melanoma staging: Evidence-based changes in the American Joint Committee on Cancer eighth edition cancer staging manual. *CA Cancer J Clin* **67**, 472-492 (2017).
232. K. Isaksson *et al.*, Survival in 31 670 patients with thin melanomas: a Swedish population-based study. *Br J Dermatol* **184**, 60-67 (2021).
233. M. A. El Sharouni *et al.*, Development and Validation of Nomograms to Predict Local, Regional, and Distant Recurrence in Patients With Thin (T1) Melanomas. *J Clin Oncol* **39**, 1243-1252 (2021).
234. M. M. Eguchi *et al.*, Prognostic modeling of cutaneous melanoma stage I patients using cancer registry data identifies subsets with very-low melanoma mortality. *Cancer* **129**, 89-97 (2023).
235. C. M. Balch *et al.*, Age as a prognostic factor in patients with localized melanoma and regional metastases. *Ann Surg Oncol* **20**, 3961-3968 (2013).
236. C. M. Balch *et al.*, Age as a predictor of sentinel node metastasis among patients with localized melanoma: an inverse correlation of melanoma mortality and incidence of sentinel node metastasis among young and old patients. *Ann Surg Oncol* **21**, 1075-1081 (2014).
237. J. F. Thompson *et al.*, Prognostic significance of mitotic rate in localized primary cutaneous melanoma: an analysis of patients in the multi-institutional American Joint Committee on Cancer melanoma staging database. *J Clin Oncol* **29**, 2199-2205 (2011).
238. A. Joosse *et al.*, Superior outcome of women with stage I/II cutaneous melanoma: pooled analysis of four European Organisation for Research and Treatment of Cancer phase III trials. *J Clin Oncol* **30**, 2240-2247 (2012).
239. A. Joosse *et al.*, Sex is an independent prognostic indicator for survival and relapse/progression-free survival in metastasized stage III to IV melanoma: a pooled analysis of five European organisation for research and treatment of cancer randomized controlled trials. *J Clin Oncol* **31**, 2337-2346 (2013).
240. C. R. Scoggins *et al.*, Gender-related differences in outcome for melanoma patients. *Ann Surg* **243**, 693-698; discussion 698-700 (2006).
241. C. M. Balch *et al.*, Prognostic factors analysis of 17,600 melanoma patients: validation of the American Joint Committee on Cancer melanoma staging system. *J Clin Oncol* **19**, 3622-3634 (2001).
242. G. G. Callender *et al.*, Prognostic implications of anatomic location of primary cutaneous melanoma of 1 mm or thicker. *Am J Surg* **202**, 659-664; discussion 664-655 (2011).
243. N. E. Thomas *et al.*, Association Between NRAS and BRAF Mutational Status and Melanoma-Specific Survival Among Patients With Higher-Risk Primary Melanoma. *JAMA Oncol* **1**, 359-368 (2015).
244. A. L. Ji, C. K. Bichakjian, S. M. Swetter, Molecular Profiling in Cutaneous Melanoma. *J Natl Compr Canc Netw* **14**, 475-480 (2016).
245. E. C. Minca *et al.*, Comparison between melanoma gene expression score and fluorescence in situ hybridization for the classification of melanocytic lesions. *Mod Pathol* **29**, 832-843 (2016).
246. E. J. Davis, D. B. Johnson, J. A. Sosman, S. Chandra, Melanoma: What do all the mutations mean? *Cancer* **124**, 3490-3499 (2018).

247. U. E. Lang, I. Yeh, T. H. McCalmont, Molecular Melanoma Diagnosis Update: Gene Fusion, Genomic Hybridization, and Massively Parallel Short-Read Sequencing. *Clin Lab Med* **37**, 473-484 (2017).
248. F. P. Noonan *et al.*, Melanoma induction by ultraviolet A but not ultraviolet B radiation requires melanin pigment. *Nat Commun* **3**, 884 (2012).
249. F. Solano, Photoprotection and Skin Pigmentation: Melanin-Related Molecules and Some Other New Agents Obtained from Natural Sources. *Molecules* **25**, (2020).
250. S. Premi *et al.*, Photochemistry. Chemiexcitation of melanin derivatives induces DNA photoproducts long after UV exposure. *Science* **347**, 842-847 (2015).
251. A. Viros *et al.*, Ultraviolet radiation accelerates BRAF-driven melanomagenesis by targeting TP53. *Nature* **511**, 478-482 (2014).
252. D. C. Whiteman *et al.*, Melanocytic nevi, solar keratoses, and divergent pathways to cutaneous melanoma. *J Natl Cancer Inst* **95**, 806-812 (2003).
253. C. M. Olsen *et al.*, Nevus density and melanoma risk in women: a pooled analysis to test the divergent pathway hypothesis. *Int J Cancer* **124**, 937-944 (2009).
254. D. C. Whiteman, P. G. Parsons, A. C. Green, p53 expression and risk factors for cutaneous melanoma: a case-control study. *Int J Cancer* **77**, 843-848 (1998).
255. J. K. Rivers, Is there more than one road to melanoma? *Lancet* **363**, 728-730 (2004).
256. A. H. Shain *et al.*, The Genetic Evolution of Melanoma from Precursor Lesions. *N Engl J Med* **373**, 1926-1936 (2015).
257. N. Cancer Genome Atlas, Genomic Classification of Cutaneous Melanoma. *Cell* **161**, 1681-1696 (2015).
258. I. Bedrosian *et al.*, Incidence of sentinel node metastasis in patients with thin primary melanoma (< or = 1 mm) with vertical growth phase. *Ann Surg Oncol* **7**, 262-267 (2000).
259. K. Satyamoorthy *et al.*, Melanoma cell lines from different stages of progression and their biological and molecular analyses. *Melanoma Res* **7 Suppl 2**, S35-42 (1997).
260. H. Boukerche *et al.*, A new Mr 55,000 surface protein implicated in melanoma progression: association with a metastatic phenotype. *Cancer Res* **60**, 5848-5856 (2000).
261. W. H. Clark, Jr. *et al.*, Model predicting survival in stage I melanoma based on tumor progression. *J Natl Cancer Inst* **81**, 1893-1904 (1989).
262. B. C. Bastian, Understanding the progression of melanocytic neoplasia using genomic analysis: from fields to cancer. *Oncogene* **22**, 3081-3086 (2003).
263. D. Millan-Esteban *et al.*, Mutational Characterization of Cutaneous Melanoma Supports Divergent Pathways Model for Melanoma Development. *Cancers (Basel)* **13**, (2021).
264. R. Rabbie, P. Ferguson, C. Molina-Aguilar, D. J. Adams, C. D. Robles-Espinoza, Melanoma subtypes: genomic profiles, prognostic molecular markers and therapeutic possibilities. *J Pathol* **247**, 539-551 (2019).
265. M. Wang *et al.*, The genetic evolution of acral melanoma. *Nat Commun* **15**, 6146 (2024).

266. M. Krauthammer *et al.*, Exome sequencing identifies recurrent mutations in NF1 and RASopathy genes in sun-exposed melanomas. *Nat Genet* **47**, 996-1002 (2015).
267. N. Bardeesy *et al.*, Role of epidermal growth factor receptor signaling in RAS-driven melanoma. *Mol Cell Biol* **25**, 4176-4188 (2005).
268. K. A. Furge *et al.*, Suppression of Ras-mediated tumorigenicity and metastasis through inhibition of the Met receptor tyrosine kinase. *Proc Natl Acad Sci U S A* **98**, 10722-10727 (2001).
269. G. Monsel, N. Ortonne, M. Bagot, A. Bensussan, N. Dumaz, c-Kit mutants require hypoxia-inducible factor 1alpha to transform melanocytes. *Oncogene* **29**, 227-236 (2010).
270. O. Maertens *et al.*, Elucidating distinct roles for NF1 in melanomagenesis. *Cancer Discov* **3**, 338-349 (2013).
271. M. Beeram, A. Patnaik, E. K. Rowinsky, Raf: a strategic target for therapeutic development against cancer. *J Clin Oncol* **23**, 6771-6790 (2005).
272. M. J. Garnett, S. Rana, H. Paterson, D. Barford, R. Marais, Wild-type and mutant B-RAF activate C-RAF through distinct mechanisms involving heterodimerization. *Mol Cell* **20**, 963-969 (2005).
273. K. Terai, M. Matsuda, The amino-terminal B-Raf-specific region mediates calcium-dependent homo- and hetero-dimerization of Raf. *EMBO J* **25**, 3556-3564 (2006).
274. A. Sharma *et al.*, Mutant V599EB-Raf regulates growth and vascular development of malignant melanoma tumors. *Cancer Res* **65**, 2412-2421 (2005).
275. A. Fischer *et al.*, B- and C-RAF display essential differences in their binding to Ras: the isotype-specific N terminus of B-RAF facilitates Ras binding. *J Biol Chem* **282**, 26503-26516 (2007).
276. N. H. Tran, X. Wu, J. A. Frost, B-Raf and Raf-1 are regulated by distinct autoregulatory mechanisms. *J Biol Chem* **280**, 16244-16253 (2005).
277. H. Davies *et al.*, Mutations of the BRAF gene in human cancer. *Nature* **417**, 949-954 (2002).
278. Z. Yao *et al.*, BRAF Mutants Evade ERK-Dependent Feedback by Different Mechanisms that Determine Their Sensitivity to Pharmacologic Inhibition. *Cancer Cell* **28**, 370-383 (2015).
279. Z. Yao *et al.*, Tumours with class 3 BRAF mutants are sensitive to the inhibition of activated RAS. *Nature* **548**, 234-238 (2017).
280. J. K. Rivers, Melanoma. *Lancet* **347**, 803-806 (1996).
281. A. M. Goldstein *et al.*, Linkage of cutaneous malignant melanoma/dysplastic nevi to chromosome 9p, and evidence for genetic heterogeneity. *Am J Hum Genet* **54**, 489-496 (1994).
282. A. M. Goldstein *et al.*, Features associated with germline CDKN2A mutations: a GenoMEL study of melanoma-prone families from three continents. *J Med Genet* **44**, 99-106 (2007).
283. A. M. Goldstein *et al.*, Increased risk of pancreatic cancer in melanoma-prone kindreds with p16INK4 mutations. *N Engl J Med* **333**, 970-974 (1995).
284. T. Wiesner *et al.*, Germline mutations in BAP1 predispose to melanocytic tumors. *Nat Genet* **43**, 1018-1021 (2011).

285. P. Gerami *et al.*, Multiple Cutaneous Melanomas and Clinically Atypical Moles in a Patient With a Novel Germline BAP1 Mutation. *JAMA Dermatol* **151**, 1235-1239 (2015).
286. A. Piris, M. C. Mihm, Jr., M. P. Hoang, BAP1 and BRAFV600E expression in benign and malignant melanocytic proliferations. *Hum Pathol* **46**, 239-245 (2015).
287. S. Walpole *et al.*, Comprehensive Study of the Clinical Phenotype of Germline BAP1 Variant-Carrying Families Worldwide. *J Natl Cancer Inst* **110**, 1328-1341 (2018).
288. P. Valverde, E. Healy, I. Jackson, J. L. Rees, A. J. Thody, Variants of the melanocyte-stimulating hormone receptor gene are associated with red hair and fair skin in humans. *Nat Genet* **11**, 328-330 (1995).
289. D. Mitra *et al.*, An ultraviolet-radiation-independent pathway to melanoma carcinogenesis in the red hair/fair skin background. *Nature* **491**, 449-453 (2012).
290. M. T. Landi *et al.*, MC1R, ASIP, and DNA repair in sporadic and familial melanoma in a Mediterranean population. *J Natl Cancer Inst* **97**, 998-1007 (2005).
291. V. Liu, M. C. Mihm, Pathology of malignant melanoma. *Surg Clin North Am* **83**, 31-60, v (2003).
292. L. A. von Schuckmann *et al.*, Risk of Melanoma Recurrence After Diagnosis of a High-Risk Primary Tumor. *JAMA Dermatol* **155**, 688-693 (2019).
293. W. H. Clark, Jr., L. From, E. A. Bernardino, M. C. Mihm, The histogenesis and biologic behavior of primary human malignant melanomas of the skin. *Cancer Res* **29**, 705-727 (1969).
294. P. A. Ascierto *et al.*, Survival Outcomes in Patients With Previously Untreated BRAF Wild-Type Advanced Melanoma Treated With Nivolumab Therapy: Three-Year Follow-up of a Randomized Phase 3 Trial. *JAMA Oncol* **5**, 187-194 (2019).
295. M. Maio *et al.*, Five-year survival rates for treatment-naive patients with advanced melanoma who received ipilimumab plus dacarbazine in a phase III trial. *J Clin Oncol* **33**, 1191-1196 (2015).
296. J. Larkin *et al.*, Combined Nivolumab and Ipilimumab or Monotherapy in Untreated Melanoma. *N Engl J Med* **373**, 23-34 (2015).
297. J. Larkin *et al.*, Five-Year Survival with Combined Nivolumab and Ipilimumab in Advanced Melanoma. *N Engl J Med* **381**, 1535-1546 (2019).
298. L. M. Francisco *et al.*, PD-L1 regulates the development, maintenance, and function of induced regulatory T cells. *J Exp Med* **206**, 3015-3029 (2009).
299. S. Amarnath *et al.*, The PDL1-PD1 axis converts human TH1 cells into regulatory T cells. *Sci Transl Med* **3**, 111ra120 (2011).
300. Z. Eroglu, A. Ribas, Combination therapy with BRAF and MEK inhibitors for melanoma: latest evidence and place in therapy. *Ther Adv Med Oncol* **8**, 48-56 (2016).
301. C. Robert *et al.*, Five-Year Outcomes with Dabrafenib plus Trametinib in Metastatic Melanoma. *N Engl J Med* **381**, 626-636 (2019).
302. G. Bollag *et al.*, Clinical efficacy of a RAF inhibitor needs broad target blockade in BRAF-mutant melanoma. *Nature* **467**, 596-599 (2010).

303. E. W. Joseph *et al.*, The RAF inhibitor PLX4032 inhibits ERK signaling and tumor cell proliferation in a V600E BRAF-selective manner. *Proc Natl Acad Sci U S A* **107**, 14903-14908 (2010).
304. C. M. Johannessen *et al.*, COT drives resistance to RAF inhibition through MAP kinase pathway reactivation. *Nature* **468**, 968-972 (2010).
305. R. Nazarian *et al.*, Melanomas acquire resistance to B-RAF(V600E) inhibition by RTK or N-RAS upregulation. *Nature* **468**, 973-977 (2010).
306. W. D. Tap *et al.*, Pharmacodynamic characterization of the efficacy signals due to selective BRAF inhibition with PLX4032 in malignant melanoma. *Neoplasia* **12**, 637-649 (2010).
307. K. Trunzer *et al.*, Pharmacodynamic effects and mechanisms of resistance to vemurafenib in patients with metastatic melanoma. *J Clin Oncol* **31**, 1767-1774 (2013).
308. C. Montagut *et al.*, Elevated CRAF as a potential mechanism of acquired resistance to BRAF inhibition in melanoma. *Cancer Res* **68**, 4853-4861 (2008).
309. N. Wagle *et al.*, Dissecting therapeutic resistance to RAF inhibition in melanoma by tumor genomic profiling. *J Clin Oncol* **29**, 3085-3096 (2011).
310. H. Wang *et al.*, Identification of the MEK1(F129L) activating mutation as a potential mechanism of acquired resistance to MEK inhibition in human cancers carrying the B-RafV600E mutation. *Cancer Res* **71**, 5535-5545 (2011).
311. H. Shi *et al.*, Melanoma whole-exome sequencing identifies (V600E)B-RAF amplification-mediated acquired B-RAF inhibitor resistance. *Nat Commun* **3**, 724 (2012).
312. S. R. Whittaker *et al.*, A genome-scale RNA interference screen implicates NF1 loss in resistance to RAF inhibition. *Cancer Discov* **3**, 350-362 (2013).
313. P. I. Poulikakos *et al.*, RAF inhibitor resistance is mediated by dimerization of aberrantly spliced BRAF(V600E). *Nature* **480**, 387-390 (2011).
314. J. Villanueva *et al.*, Acquired resistance to BRAF inhibitors mediated by a RAF kinase switch in melanoma can be overcome by cotargeting MEK and IGF-1R/PI3K. *Cancer Cell* **18**, 683-695 (2010).
315. H. Shi *et al.*, A novel AKT1 mutant amplifies an adaptive melanoma response to BRAF inhibition. *Cancer Discov* **4**, 69-79 (2014).
316. F. Catala-Lopez *et al.*, Inverse and direct cancer comorbidity in people with central nervous system disorders: a meta-analysis of cancer incidence in 577,013 participants of 50 observational studies. *Psychother Psychosom* **83**, 89-105 (2014).
317. C. M. Roe *et al.*, Cancer linked to Alzheimer disease but not vascular dementia. *Neurology* **74**, 106-112 (2010).
318. J. P. Romero, J. Benito-Leon, E. D. Louis, F. Bermejo-Pareja, Alzheimer's disease is associated with decreased risk of cancer-specific mortality: a prospective study (NEDICES). *J Alzheimers Dis* **40**, 465-473 (2014).
319. M. Musicco *et al.*, Inverse occurrence of cancer and Alzheimer disease: a population-based incidence study. *Neurology* **81**, 322-328 (2013).
320. S. Realmuto *et al.*, Tumor diagnosis preceding Alzheimer's disease onset: is there a link between cancer and Alzheimer's disease? *J Alzheimers Dis* **31**, 177-182 (2012).

321. Y. Minami, R. Yamamoto, M. Nishikouri, A. Fukao, S. Hisamichi, Mortality and cancer incidence in patients with Parkinson's disease. *J Neurol* **247**, 429-434 (2000).
322. P. Y. Lin *et al.*, Association Between Parkinson Disease and Risk of Cancer in Taiwan. *JAMA Oncol* **1**, 633-640 (2015).
323. K. Wirdefeldt *et al.*, Parkinson's disease and cancer: A register-based family study. *Am J Epidemiol* **179**, 85-94 (2014).
324. J. L. Skibba, J. Pinckley, E. F. Gilbert, R. O. Johnson, Multiple primary melanoma following administration of levodopa. *Arch Pathol* **93**, 556-561 (1972).
325. J. A. Driver, T. Kurth, J. E. Buring, J. M. Gaziano, G. Logroscino, Prospective case-control study of nonfatal cancer preceding the diagnosis of Parkinson's disease. *Cancer Causes Control* **18**, 705-711 (2007).
326. R. Liu, X. Gao, Y. Lu, H. Chen, Meta-analysis of the relationship between Parkinson disease and melanoma. *Neurology* **76**, 2002-2009 (2011).
327. P. Huang, X. D. Yang, S. D. Chen, Q. Xiao, The association between Parkinson's disease and melanoma: a systematic review and meta-analysis. *Transl Neurodegener* **4**, 21 (2015).
328. W. H. Ward, F. Lambreton, N. Goel, J. Q. Yu, J. M. Farma, in *Cutaneous Melanoma: Etiology and Therapy*, W. H. Ward, J. M. Farma, Eds. (Brisbane (AU), 2017).
329. G. F. Wooten, L. J. Currie, V. E. Bovbjerg, J. K. Lee, J. Patrie, Are men at greater risk for Parkinson's disease than women? *J Neurol Neurosurg Psychiatry* **75**, 637-639 (2004).
330. M. Rastrelli, S. Tropea, C. R. Rossi, M. Alaibac, Melanoma: epidemiology, risk factors, pathogenesis, diagnosis and classification. *In Vivo* **28**, 1005-1011 (2014).
331. I. Sleeman *et al.*, The Role of Vitamin D in Disease Progression in Early Parkinson's Disease. *J Parkinsons Dis* **7**, 669-675 (2017).
332. Y. Sato, M. Kikuyama, K. Oizumi, High prevalence of vitamin D deficiency and reduced bone mass in Parkinson's disease. *Neurology* **49**, 1273-1278 (1997).
333. M. L. Evatt *et al.*, Prevalence of vitamin d insufficiency in patients with Parkinson disease and Alzheimer disease. *Arch Neurol* **65**, 1348-1352 (2008).
334. S. Field, J. A. Newton-Bishop, Melanoma and vitamin D. *Mol Oncol* **5**, 197-214 (2011).
335. S. Field, J. Davies, D. T. Bishop, J. A. Newton-Bishop, Vitamin D and melanoma. *Dermatoendocrinol* **5**, 121-129 (2013).
336. M. Menza, R. D. Dobkin, H. Marin, K. Bienfait, Sleep disturbances in Parkinson's disease. *Mov Disord* **25 Suppl 1**, S117-122 (2010).
337. M. A. Martinez-Garcia *et al.*, Sleep-Disordered Breathing Is Independently Associated With Increased Aggressiveness of Cutaneous Melanoma: A Multicenter Observational Study in 443 Patients. *Chest* **154**, 1348-1358 (2018).
338. M. A. Martinez-Garcia *et al.*, Association between sleep disordered breathing and aggressiveness markers of malignant cutaneous melanoma. *Eur Respir J* **43**, 1661-1668 (2014).
339. T. Pan, X. Li, J. Jankovic, The association between Parkinson's disease and melanoma. *Int J Cancer* **128**, 2251-2260 (2011).

340. B. Przybilla, U. Schwab, M. Landthaler, O. Braun-Falco, Development of two malignant melanomas during administration of levodopa. *Acta Derm Venereol* **65**, 556-557 (1985).
341. W. Pflutzner, B. Przybilla, Malignant melanoma and levodopa: is there a relationship? Two new cases and a review of the literature. *J Am Acad Dermatol* **37**, 332-336 (1997).
342. U. Dube *et al.*, Overlapping genetic architecture between Parkinson disease and melanoma. *Acta Neuropathol* **139**, 347-364 (2020).
343. H. H. Hu *et al.*, PARKIN Inactivation Links Parkinson's Disease to Melanoma. *J Natl Cancer Inst* **108**, (2016).
344. L. Levin *et al.*, Parkin Somatic Mutations Link Melanoma and Parkinson's Disease. *J Genet Genomics* **43**, 369-379 (2016).
345. Y. Sun, P. Sukumaran, A. Schaar, B. B. Singh, TRPM7 and its role in neurodegenerative diseases. *Channels (Austin)* **9**, 253-261 (2015).
346. C. Kun-Rodrigues *et al.*, A systematic screening to identify de novo mutations causing sporadic early-onset Parkinson's disease. *Hum Mol Genet* **24**, 6711-6720 (2015).
347. M. N. Murthy *et al.*, Increased brain expression of GPNMB is associated with genome wide significant risk for Parkinson's disease on chromosome 7p15.3. *Neurogenetics* **18**, 121-133 (2017).
348. M. E. Diaz-Ortiz *et al.*, GPNMB confers risk for Parkinson's disease through interaction with alpha-synuclein. *Science* **377**, eabk0637 (2022).
349. G. Tell-Marti *et al.*, The MC1R melanoma risk variant p.R160W is associated with Parkinson disease. *Ann Neurol* **77**, 889-894 (2015).
350. X. Chen *et al.*, The melanoma-linked "redhead" MC1R influences dopaminergic neuron survival. *Ann Neurol* **81**, 395-406 (2017).
351. X. Chen, D. Feng, M. A. Schwarzschild, X. Gao, Red hair, MC1R variants, and risk for Parkinson's disease - a meta-analysis. *Ann Clin Transl Neurol* **4**, 212-216 (2017).
352. W. Cai *et al.*, Melanocortin 1 receptor activation protects against alpha-synuclein pathologies in models of Parkinson's disease. *Mol Neurodegener* **17**, 16 (2022).
353. S. Raimondi *et al.*, MC1R variants, melanoma and red hair color phenotype: a meta-analysis. *Int J Cancer* **122**, 2753-2760 (2008).
354. J. A. D'Orazio *et al.*, Topical drug rescue strategy and skin protection based on the role of Mc1r in UV-induced tanning. *Nature* **443**, 340-344 (2006).
355. J. R. Davies *et al.*, Inherited variants in the MC1R gene and survival from cutaneous melanoma: a BioGenoMEL study. *Pigment Cell Melanoma Res* **25**, 384-394 (2012).
356. R. Cesari *et al.*, Parkin, a gene implicated in autosomal recessive juvenile parkinsonism, is a candidate tumor suppressor gene on chromosome 6q25-q27. *Proc Natl Acad Sci U S A* **100**, 5956-5961 (2003).
357. E. M. Valente *et al.*, Hereditary early-onset Parkinson's disease caused by mutations in PINK1. *Science* **304**, 1158-1160 (2004).
358. E. Rogaeva *et al.*, Analysis of the PINK1 gene in a large cohort of cases with Parkinson disease. *Arch Neurol* **61**, 1898-1904 (2004).

359. M. Kaghad *et al.*, Monoallelically expressed gene related to p53 at 1p36, a region frequently deleted in neuroblastoma and other human cancers. *Cell* **90**, 809-819 (1997).
360. J. Segura-Aguilar *et al.*, Protective and toxic roles of dopamine in Parkinson's disease. *J Neurochem* **129**, 898-915 (2014).
361. R. M. Slominski, M. A. Zmijewski, A. T. Slominski, The role of melanin pigment in melanoma. *Exp Dermatol* **24**, 258-259 (2015).
362. H. Fedorow *et al.*, Neuromelanin in human dopamine neurons: comparison with peripheral melanins and relevance to Parkinson's disease. *Prog Neurobiol* **75**, 109-124 (2005).
363. K. Wakamatsu, in *ICMS Journal Club*. (2021).
364. E. Greggio *et al.*, Tyrosinase exacerbates dopamine toxicity but is not genetically associated with Parkinson's disease. *J Neurochem* **93**, 246-256 (2005).
365. L. K. Marles, E. M. Peters, D. J. Tobin, N. A. Hibberts, K. U. Schallreuter, Tyrosine hydroxylase isoenzyme I is present in human melanosomes: a possible novel function in pigmentation. *Exp Dermatol* **12**, 61-70 (2003).
366. I. Carballo-Carbajal *et al.*, Brain tyrosinase overexpression implicates age-dependent neuromelanin production in Parkinson's disease pathogenesis. *Nat Commun* **10**, 973 (2019).
367. T. Pan, J. Zhu, W. J. Hwu, J. Jankovic, The role of alpha-synuclein in melanin synthesis in melanoma and dopaminergic neuronal cells. *PLoS One* **7**, e45183 (2012).
368. R. G. Perez *et al.*, A role for alpha-synuclein in the regulation of dopamine biosynthesis. *J Neurosci* **22**, 3090-3099 (2002).
369. X. Peng, R. Tehranian, P. Dietrich, L. Stefanis, R. G. Perez, Alpha-synuclein activation of protein phosphatase 2A reduces tyrosine hydroxylase phosphorylation in dopaminergic cells. *J Cell Sci* **118**, 3523-3530 (2005).
370. Y. J. Edwards *et al.*, Identifying consensus disease pathways in Parkinson's disease using an integrative systems biology approach. *PLoS One* **6**, e16917 (2011).
371. Q. Li *et al.*, Discovery of Resorcinol-Based Polycyclic Structures as Tyrosinase Inhibitors for Treatment of Parkinson's Disease. *ACS Chem Neurosci* **13**, 81-96 (2022).
372. I. Tessari *et al.*, The reaction of alpha-synuclein with tyrosinase: possible implications for Parkinson disease. *J Biol Chem* **283**, 16808-16817 (2008).
373. D. N. Dean, J. C. Lee, Linking Parkinson's Disease and Melanoma: Interplay Between alpha-Synuclein and Pmel17 Amyloid Formation. *Mov Disord* **36**, 1489-1498 (2021).
374. H. Sprong *et al.*, Glycosphingolipids are required for sorting melanosomal proteins in the Golgi complex. *J Cell Biol* **155**, 369-380 (2001).
375. C. Paisan-Ruiz *et al.*, Characterization of PLA2G6 as a locus for dystonia-parkinsonism. *Ann Neurol* **65**, 19-23 (2009).
376. C. Paisan-Ruiz *et al.*, Widespread Lewy body and tau accumulation in childhood and adult onset dystonia-parkinsonism cases with PLA2G6 mutations. *Neurobiol Aging* **33**, 814-823 (2012).

377. M. Falchi *et al.*, Genome-wide association study identifies variants at 9p21 and 22q13 associated with development of cutaneous nevi. *Nat Genet* **41**, 915-919 (2009).
378. S. Ichikawa, N. Nakajo, H. Sakiyama, Y. Hirabayashi, A mouse B16 melanoma mutant deficient in glycolipids. *Proc Natl Acad Sci U S A* **91**, 2703-2707 (1994).
379. M. Piccinini *et al.*, Deregulated sphingolipid metabolism and membrane organization in neurodegenerative disorders. *Mol Neurobiol* **41**, 314-340 (2010).
380. W. D. Bush *et al.*, The surface oxidation potential of human neuromelanin reveals a spherical architecture with a pheomelanin core and a eumelanin surface. *Proc Natl Acad Sci U S A* **103**, 14785-14789 (2006).
381. S. Ito, Encapsulation of a reactive core in neuromelanin. *Proc Natl Acad Sci U S A* **103**, 14647-14648 (2006).
382. E. M. Roider, D. E. Fisher, Red Hair, Light Skin, and UV-Independent Risk for Melanoma Development in Humans. *JAMA Dermatol* **152**, 751-753 (2016).
383. L. Zecca *et al.*, The absolute concentration of nigral neuromelanin, assayed by a new sensitive method, increases throughout the life and is dramatically decreased in Parkinson's disease. *FEBS Lett* **510**, 216-220 (2002).
384. W. S. Enochs, T. Sarna, L. Zecca, P. A. Riley, H. M. Swartz, The roles of neuromelanin, binding of metal ions, and oxidative cytotoxicity in the pathogenesis of Parkinson's disease: a hypothesis. *J Neural Transm Park Dis Dement Sect* **7**, 83-100 (1994).
385. S. Rangwala, K. Y. Tsai, Roles of the immune system in skin cancer. *Br J Dermatol* **165**, 953-965 (2011).
386. A. Passarelli, F. Mannavola, L. S. Stucci, M. Tucci, F. Silvestris, Immune system and melanoma biology: a balance between immunosurveillance and immune escape. *Oncotarget* **8**, 106132-106142 (2017).
387. M. G. Tansey, M. S. Goldberg, Neuroinflammation in Parkinson's disease: its role in neuronal death and implications for therapeutic intervention. *Neurobiol Dis* **37**, 510-518 (2010).
388. S. Vivekanantham *et al.*, Neuroinflammation in Parkinson's disease: role in neurodegeneration and tissue repair. *Int J Neurosci* **125**, 717-725 (2015).
389. G. Gelders, V. Baekelandt, A. Van der Perren, Linking Neuroinflammation and Neurodegeneration in Parkinson's Disease. *J Immunol Res* **2018**, 4784268 (2018).
390. Q. Wang, Y. Liu, J. Zhou, Neuroinflammation in Parkinson's disease and its potential as therapeutic target. *Transl Neurodegener* **4**, 19 (2015).
391. F. Garretti, D. Agalliu, C. S. Lindestam Arlehamn, A. Sette, D. Sulzer, Autoimmunity in Parkinson's Disease: The Role of alpha-Synuclein-Specific T Cells. *Front Immunol* **10**, 303 (2019).
392. N. Kustrimovic, F. Marino, M. Cosentino, Peripheral Immunity, Immunoaging and Neuroinflammation in Parkinson's Disease. *Curr Med Chem* **26**, 3719-3753 (2019).
393. V. Gopalakrishnan *et al.*, Gut microbiome modulates response to anti-PD-1 immunotherapy in melanoma patients. *Science* **359**, 97-103 (2018).
394. I. Rodriguez-Leyva *et al.*, alpha-Synuclein inclusions in the skin of Parkinson's disease and parkinsonism. *Ann Clin Transl Neurol* **1**, 471-478 (2014).

395. I. Rodriguez-Leyva *et al.*, The Presence of Alpha-Synuclein in Skin from Melanoma and Patients with Parkinson's Disease. *Mov Disord Clin Pract* **4**, 724-732 (2017).
396. C. Welinder *et al.*, Analysis of alpha-synuclein in malignant melanoma - development of a SRM quantification assay. *PLoS One* **9**, e110804 (2014).
397. Y. Matsuo, T. Kamitani, Parkinson's disease-related protein, alpha-synuclein, in malignant melanoma. *PLoS One* **5**, e10481 (2010).
398. E. Turriani *et al.*, Treatment with diphenyl-pyrazole compound anle138b/c reveals that alpha-synuclein protects melanoma cells from autophagic cell death. *Proc Natl Acad Sci U S A* **114**, E4971-E4977 (2017).
399. B. R. Lee, T. Kamitani, Improved immunodetection of endogenous alpha-synuclein. *PLoS One* **6**, e23939 (2011).
400. C. Hansen *et al.*, alpha-Synuclein propagates from mouse brain to grafted dopaminergic neurons and seeds aggregation in cultured human cells. *J Clin Invest* **121**, 715-725 (2011).
401. B. R. Lee, Y. Matsuo, A. G. Cashikar, T. Kamitani, Role of Ser129 phosphorylation of alpha-synuclein in melanoma cells. *J Cell Sci* **126**, 696-704 (2013).
402. L. Calo, M. Wegrzynowicz, J. Santivanez-Perez, M. Grazia Spillantini, Synaptic failure and alpha-synuclein. *Mov Disord* **31**, 169-177 (2016).
403. K. Pirc, N. P. Ulrih, alpha-Synuclein interactions with phospholipid model membranes: Key roles for electrostatic interactions and lipid-bilayer structure. *Biochim Biophys Acta* **1848**, 2002-2012 (2015).
404. T. Bartels *et al.*, The N-terminus of the intrinsically disordered protein alpha-synuclein triggers membrane binding and helix folding. *Biophys J* **99**, 2116-2124 (2010).
405. S. Chandra, G. Gallardo, R. Fernandez-Chacon, O. M. Schluter, T. C. Sudhof, Alpha-synuclein cooperates with CSPalpha in preventing neurodegeneration. *Cell* **123**, 383-396 (2005).
406. J. Burre, M. Sharma, T. C. Sudhof, alpha-Synuclein assembles into higher-order multimers upon membrane binding to promote SNARE complex formation. *Proc Natl Acad Sci U S A* **111**, E4274-4283 (2014).
407. J. Burre *et al.*, Alpha-synuclein promotes SNARE-complex assembly in vivo and in vitro. *Science* **329**, 1663-1667 (2010).
408. B. A. Hijaz, L. A. Volpicelli-Daley, Initiation and propagation of alpha-synuclein aggregation in the nervous system. *Mol Neurodegener* **15**, 19 (2020).
409. Z. Lv *et al.*, Assembly of alpha-synuclein aggregates on phospholipid bilayers. *Biochim Biophys Acta Proteins Proteom* **1867**, 802-812 (2019).
410. T. Bartels, J. G. Choi, D. J. Selkoe, alpha-Synuclein occurs physiologically as a helically folded tetramer that resists aggregation. *Nature* **477**, 107-110 (2011).
411. T. S. Fan, S. C. Liu, R. M. Wu, Alpha-Synuclein and Cognitive Decline in Parkinson Disease. *Life (Basel)* **11**, (2021).
412. J. Jankovic, E. K. Tan, Parkinson's disease: etiopathogenesis and treatment. *J Neurol Neurosurg Psychiatry* **91**, 795-808 (2020).
413. M. G. Spillantini *et al.*, Alpha-synuclein in Lewy bodies. *Nature* **388**, 839-840 (1997).

414. E. Maries, B. Dass, T. J. Collier, J. H. Kordower, K. Steece-Collier, The role of alpha-synuclein in Parkinson's disease: insights from animal models. *Nat Rev Neurosci* **4**, 727-738 (2003).
415. M. B. Feany, New genetic insights into Parkinson's disease. *N Engl J Med* **351**, 1937-1940 (2004).
416. B. Dehay, M. Vila, E. Bezard, P. Brundin, J. H. Kordower, Alpha-synuclein propagation: New insights from animal models. *Mov Disord* **31**, 161-168 (2016).
417. K. C. Luk *et al.*, Pathological alpha-synuclein transmission initiates Parkinson-like neurodegeneration in nontransgenic mice. *Science* **338**, 949-953 (2012).
418. K. C. Luk *et al.*, Intracerebral inoculation of pathological alpha-synuclein initiates a rapidly progressive neurodegenerative alpha-synucleinopathy in mice. *J Exp Med* **209**, 975-986 (2012).
419. J. H. Kordower, Y. Chu, R. A. Hauser, T. B. Freeman, C. W. Olanow, Lewy body-like pathology in long-term embryonic nigral transplants in Parkinson's disease. *Nat Med* **14**, 504-506 (2008).
420. J. Y. Li *et al.*, Lewy bodies in grafted neurons in subjects with Parkinson's disease suggest host-to-graft disease propagation. *Nat Med* **14**, 501-503 (2008).
421. S. Greffard *et al.*, A stable proportion of Lewy body bearing neurons in the substantia nigra suggests a model in which the Lewy body causes neuronal death. *Neurobiol Aging* **31**, 99-103 (2010).
422. L. Lu *et al.*, Gene expression profiling of Lewy body-bearing neurons in Parkinson's disease. *Exp Neurol* **195**, 27-39 (2005).
423. R. A. Bodner *et al.*, Pharmacological promotion of inclusion formation: a therapeutic approach for Huntington's and Parkinson's diseases. *Proc Natl Acad Sci U S A* **103**, 4246-4251 (2006).
424. H. J. Gertz, A. Siegers, J. Kuchinke, Stability of cell size and nucleolar size in Lewy body containing neurons of substantia nigra in Parkinson's disease. *Brain Res* **637**, 339-341 (1994).
425. C. D. Rietdijk, P. Perez-Pardo, J. Garssen, R. J. van Wezel, A. D. Kraneveld, Exploring Braak's Hypothesis of Parkinson's Disease. *Front Neurol* **8**, 37 (2017).
426. A. J. Espay *et al.*, Revisiting protein aggregation as pathogenic in sporadic Parkinson and Alzheimer diseases. *Neurology* **92**, 329-337 (2019).
427. V. R. Osterberg *et al.*, Progressive aggregation of alpha-synuclein and selective degeneration of lewy inclusion-bearing neurons in a mouse model of parkinsonism. *Cell Rep* **10**, 1252-1260 (2015).
428. B. Dehay *et al.*, Lysosomal impairment in Parkinson's disease. *Mov Disord* **28**, 725-732 (2013).
429. S. Ghavami *et al.*, Autophagy and apoptosis dysfunction in neurodegenerative disorders. *Prog Neurobiol* **112**, 24-49 (2014).
430. M. Xilouri, O. R. Brekk, L. Stefanis, Autophagy and Alpha-Synuclein: Relevance to Parkinson's Disease and Related Synucleopathies. *Mov Disord* **31**, 178-192 (2016).
431. A. H. Schapira *et al.*, Mitochondrial complex I deficiency in Parkinson's disease. *Lancet* **1**, 1269 (1989).
432. J. T. Greenamyre, T. G. Hastings, Biomedicine. Parkinson's--divergent causes, convergent mechanisms. *Science* **304**, 1120-1122 (2004).

433. J. Bove, D. Prou, C. Perier, S. Przedborski, Toxin-induced models of Parkinson's disease. *NeuroRx* **2**, 484-494 (2005).
434. S. Przedborski, K. Tieu, C. Perier, M. Vila, MPTP as a mitochondrial neurotoxic model of Parkinson's disease. *J Bioenerg Biomembr* **36**, 375-379 (2004).
435. T. B. Sherer *et al.*, Mechanism of toxicity in rotenone models of Parkinson's disease. *J Neurosci* **23**, 10756-10764 (2003).
436. J. E. Ahlskog, Challenging conventional wisdom: the etiologic role of dopamine oxidative stress in Parkinson's disease. *Mov Disord* **20**, 271-282 (2005).
437. A. E. Oakley *et al.*, Individual dopaminergic neurons show raised iron levels in Parkinson disease. *Neurology* **68**, 1820-1825 (2007).
438. P. Dusek, J. Jankovic, W. Le, Iron dysregulation in movement disorders. *Neurobiol Dis* **46**, 1-18 (2012).
439. P. Lei *et al.*, Tau deficiency induces parkinsonism with dementia by impairing APP-mediated iron export. *Nat Med* **18**, 291-295 (2012).
440. E. C. Hirsch, S. Hunot, Neuroinflammation in Parkinson's disease: a target for neuroprotection? *Lancet Neurol* **8**, 382-397 (2009).
441. E. C. Hirsch, P. Jenner, S. Przedborski, Pathogenesis of Parkinson's disease. *Mov Disord* **28**, 24-30 (2013).
442. A. J. Schaser *et al.*, Alpha-synuclein is a DNA binding protein that modulates DNA repair with implications for Lewy body disorders. *Sci Rep* **9**, 10919 (2019).
443. E. P. Rose, V. R. Osterberg, V. Gorbunova, V. K. Unni, Alpha-synuclein modulates the repair of genomic DNA double-strand breaks in a DNA-PK(cs)-regulated manner. *Neurobiol Dis* **201**, 106675 (2024).
444. C. Klein, M. G. Schlossmacher, Parkinson disease, 10 years after its genetic revolution: multiple clues to a complex disorder. *Neurology* **69**, 2093-2104 (2007).
445. R. Kruger *et al.*, Ala30Pro mutation in the gene encoding alpha-synuclein in Parkinson's disease. *Nat Genet* **18**, 106-108 (1998).
446. J. J. Zarranz *et al.*, The new mutation, E46K, of alpha-synuclein causes Parkinson and Lewy body dementia. *Ann Neurol* **55**, 164-173 (2004).
447. L. I. Golbe *et al.*, Clinical genetic analysis of Parkinson's disease in the Contursi kindred. *Ann Neurol* **40**, 767-775 (1996).
448. S. Bostantjopoulou *et al.*, Clinical features of parkinsonian patients with the alpha-synuclein (G209A) mutation. *Mov Disord* **16**, 1007-1013 (2001).
449. M. H. Polymeropoulos *et al.*, Mapping of a gene for Parkinson's disease to chromosome 4q21-q23. *Science* **274**, 1197-1199 (1996).
450. A. Dovonou *et al.*, Animal models of Parkinson's disease: bridging the gap between disease hallmarks and research questions. *Transl Neurodegener* **12**, 36 (2023).
451. R. Bussell, Jr., D. Eliezer, Residual structure and dynamics in Parkinson's disease-associated mutants of alpha-synuclein. *J Biol Chem* **276**, 45996-46003 (2001).
452. O. Coskuner, O. Wise-Scira, Structures and free energy landscapes of the A53T mutant-type alpha-synuclein protein and impact of A53T mutation on the structures of the wild-type alpha-synuclein protein with dynamics. *ACS Chem Neurosci* **4**, 1101-1113 (2013).

453. D. Ysselstein *et al.*, Effects of impaired membrane interactions on alpha-synuclein aggregation and neurotoxicity. *Neurobiol Dis* **79**, 150-163 (2015).
454. A. B. Singleton *et al.*, alpha-Synuclein locus triplication causes Parkinson's disease. *Science* **302**, 841 (2003).
455. M. C. Chartier-Harlin *et al.*, Alpha-synuclein locus duplication as a cause of familial Parkinson's disease. *Lancet* **364**, 1167-1169 (2004).
456. A. Singleton *et al.*, Association between cardiac denervation and parkinsonism caused by alpha-synuclein gene triplication. *Brain* **127**, 768-772 (2004).
457. H. A. Lashuel *et al.*, Alpha-synuclein, especially the Parkinson's disease-associated mutants, forms pore-like annular and tubular protofibrils. *J Mol Biol* **322**, 1089-1102 (2002).
458. I. Rodriguez-Leyva *et al.*, Parkinson disease and progressive supranuclear palsy: protein expression in skin. *Ann Clin Transl Neurol* **3**, 191-199 (2016).
459. V. Donadio *et al.*, Skin nerve alpha-synuclein deposits: a biomarker for idiopathic Parkinson disease. *Neurology* **82**, 1362-1369 (2014).
460. K. Doppler *et al.*, Cutaneous neuropathy in Parkinson's disease: a window into brain pathology. *Acta Neuropathol* **128**, 99-109 (2014).
461. G. Melli *et al.*, Cervical skin denervation associates with alpha-synuclein aggregates in Parkinson disease. *Ann Clin Transl Neurol* **5**, 1394-1407 (2018).
462. L. M. Chahine *et al.*, In vivo distribution of alpha-synuclein in multiple tissues and biofluids in Parkinson disease. *Neurology* **95**, e1267-e1284 (2020).
463. V. Donadio *et al.*, Skin sympathetic fiber alpha-synuclein deposits: a potential biomarker for pure autonomic failure. *Neurology* **80**, 725-732 (2013).
464. V. Donadio *et al.*, Skin nerve misfolded alpha-synuclein in pure autonomic failure and Parkinson disease. *Ann Neurol* **79**, 306-316 (2016).
465. V. Donadio *et al.*, A new potential biomarker for dementia with Lewy bodies: Skin nerve alpha-synuclein deposits. *Neurology* **89**, 318-326 (2017).
466. V. Donadio *et al.*, Skin alpha-synuclein deposits differ in clinical variants of synucleinopathy: an in vivo study. *Sci Rep* **8**, 14246 (2018).
467. L. Zange, C. Noack, K. Hahn, W. Stenzel, A. Lipp, Phosphorylated alpha-synuclein in skin nerve fibres differentiates Parkinson's disease from multiple system atrophy. *Brain* **138**, 2310-2321 (2015).
468. C. H. Gibbons, J. Garcia, N. Wang, L. C. Shih, R. Freeman, The diagnostic discrimination of cutaneous alpha-synuclein deposition in Parkinson disease. *Neurology* **87**, 505-512 (2016).
469. A. Kuzkina *et al.*, The aggregation state of alpha-synuclein deposits in dermal nerve fibers of patients with Parkinson's disease resembles that in the brain. *Parkinsonism Relat Disord* **64**, 66-72 (2019).
470. Z. Wang *et al.*, Skin alpha-Synuclein Aggregation Seeding Activity as a Novel Biomarker for Parkinson Disease. *JAMA Neurol* **78**, 1-11 (2020).
471. A. Al-Qassabi *et al.*, Immunohistochemical Detection of Synuclein Pathology in Skin in Idiopathic Rapid Eye Movement Sleep Behavior Disorder and Parkinsonism. *Mov Disord* **36**, 895-904 (2021).
472. X. Liu *et al.*, Optimization of the Detection Method for Phosphorylated alpha-Synuclein in Parkinson Disease by Skin Biopsy. *Front Neurol* **11**, 569446 (2020).

473. M. E. Jimenez-Capdeville *et al.*, Nuclear Alpha-Synuclein in Parkinson's Disease and the Malignant Transformation in Melanoma. *Neurology Research International* **2025**, 1119424 (2025).
474. K. Tsukita, H. Sakamaki-Tsukita, K. Tanaka, T. Suenaga, R. Takahashi, Value of in vivo alpha-synuclein deposits in Parkinson's disease: A systematic review and meta-analysis. *Mov Disord* **34**, 1452-1463 (2019).
475. V. A. Zuev *et al.*, Skin Fibroblasts as the Object for Clinical Diagnosis of Parkinson's Disease in Persons of Different Ages. *Bull Exp Biol Med* **167**, 177-181 (2019).
476. S. K. Mak, D. Tewari, J. W. Tetrud, J. W. Langston, B. Schule, Mitochondrial dysfunction in skin fibroblasts from a Parkinson's disease patient with an alpha-synuclein triplication. *J Parkinsons Dis* **1**, 175-183 (2011).
477. N. Rachinger *et al.*, Alpha-Synuclein and Its Role in Melanocytes. *Cells* **11**, (2022).
478. S. Shekoochi *et al.*, Knocking out alpha-synuclein in melanoma cells dysregulates cellular iron metabolism and suppresses tumor growth. *Sci Rep* **11**, 5267 (2021).
479. E. Israeli *et al.*, alpha-Synuclein expression selectively affects tumorigenesis in mice modeling Parkinson's disease. *PLoS One* **6**, e19622 (2011).
480. N. Gajendran, S. Rajasekaran, S. N. Witt, Knocking out alpha-synuclein in melanoma cells downregulates L1CAM and decreases motility. *Sci Rep* **13**, 9243 (2023).
481. E. Niederberger *et al.*, Distinct molecular mechanisms contribute to the reduction of melanoma growth and tumor pain after systemic and local depletion of alpha-Synuclein in mice. *FASEB J* **37**, e23287 (2023).
482. M. S. Parihar, A. Parihar, M. Fujita, M. Hashimoto, P. Ghafourifar, Alpha-synuclein overexpression and aggregation exacerbates impairment of mitochondrial functions by augmenting oxidative stress in human neuroblastoma cells. *Int J Biochem Cell Biol* **41**, 2015-2024 (2009).
483. W. J. Schulz-Schaeffer, The synaptic pathology of alpha-synuclein aggregation in dementia with Lewy bodies, Parkinson's disease and Parkinson's disease dementia. *Acta Neuropathol* **120**, 131-143 (2010).
484. V. Kumar *et al.*, Alpha-synuclein aggregation, Ubiquitin proteasome system impairment, and L-Dopa response in zinc-induced Parkinsonism: resemblance to sporadic Parkinson's disease. *Mol Cell Biochem* **444**, 149-160 (2018).
485. K. S. McNaught, R. Belizaire, O. Isacson, P. Jenner, C. W. Olanow, Altered proteasomal function in sporadic Parkinson's disease. *Exp Neurol* **179**, 38-46 (2003).
486. A. M. Cuervo, L. Stefanis, R. Fredenburg, P. T. Lansbury, D. Sulzer, Impaired degradation of mutant alpha-synuclein by chaperone-mediated autophagy. *Science* **305**, 1292-1295 (2004).
487. A. R. Winslow *et al.*, alpha-Synuclein impairs macroautophagy: implications for Parkinson's disease. *J Cell Biol* **190**, 1023-1037 (2010).
488. B. Greten-Harrison *et al.*, alphasynuclein triple knockout mice reveal age-dependent neuronal dysfunction. *Proc Natl Acad Sci U S A* **107**, 19573-19578 (2010).

489. J. V. Steidl, T. Gomez-Isla, A. Mariash, K. H. Ashe, L. M. Boland, Altered short-term hippocampal synaptic plasticity in mutant alpha-synuclein transgenic mice. *Neuroreport* **14**, 219-223 (2003).
490. D. J. Koss *et al.*, Nuclear alpha-synuclein is present in the human brain and is modified in dementia with Lewy bodies. *Acta Neuropathol Commun* **10**, 98 (2022).
491. L. J. Weston *et al.*, Aggregated Alpha-Synuclein Inclusions within the Nucleus Predict Impending Neuronal Cell Death in a Mouse Model of Parkinsonism. *Int J Mol Sci* **23**, (2022).
492. T. Du *et al.*, Nuclear alpha-synuclein accelerates cell senescence and neurodegeneration. *Immun Ageing* **21**, 47 (2024).
493. Z. Huang, Z. Xu, Y. Wu, Y. Zhou, Determining nuclear localization of alpha-synuclein in mouse brains. *Neuroscience* **199**, 318-332 (2011).
494. Y. Pan *et al.*, Nuclear localization of alpha-synuclein affects the cognitive and motor behavior of mice by inducing DNA damage and abnormal cell cycle of hippocampal neurons. *Front Mol Neurosci* **15**, 1015881 (2022).
495. N. M. Jensen *et al.*, MJF-14 proximity ligation assay detects early non-inclusion alpha-synuclein pathology with enhanced specificity and sensitivity. *NPJ Parkinsons Dis* **10**, 227 (2024).
496. M. L. Hegde *et al.*, Studies on genomic DNA topology and stability in brain regions of Parkinson's disease. *Arch Biochem Biophys* **449**, 143-156 (2006).
497. A. Camins *et al.*, Activation of ataxia telangiectasia muted under experimental models and human Parkinson's disease. *Cell Mol Life Sci* **67**, 3865-3882 (2010).
498. S. Sepe *et al.*, Inefficient DNA Repair Is an Aging-Related Modifier of Parkinson's Disease. *Cell Rep* **15**, 1866-1875 (2016).
499. D. Wang *et al.*, DNA damage preceding dopamine neuron degeneration in A53T human alpha-synuclein transgenic mice. *Biochem Biophys Res Commun* **481**, 104-110 (2016).
500. C. Milanese *et al.*, Activation of the DNA damage response in vivo in synucleinopathy models of Parkinson's disease. *Cell Death Dis* **9**, 818 (2018).
501. P. Garcia-Esparcia *et al.*, Altered machinery of protein synthesis is region- and stage-dependent and is associated with alpha-synuclein oligomers in Parkinson's disease. *Acta Neuropathol Commun* **3**, 76 (2015).
502. V. Vasquez *et al.*, Chromatin-Bound Oxidized alpha-Synuclein Causes Strand Breaks in Neuronal Genomes in in vitro Models of Parkinson's Disease. *J Alzheimers Dis* **60**, S133-S150 (2017).
503. S. C. Akerman *et al.*, Neurodegenerative Disease-Related Proteins within the Epidermal Layer of the Human Skin. *J Alzheimers Dis* **69**, 463-478 (2019).
504. S. Nandakumar, B. Vijayan, A. Kishore, A. Thekkuveetil, Autophagy enhancement is rendered ineffective in presence of alpha-synuclein in melanoma cells. *J Cell Commun Signal* **11**, 381-394 (2017).
505. A. Quesnel *et al.*, Uncovering potential diagnostic and pathophysiological roles of alpha-synuclein and DJ-1 in melanoma. *Cancer Med* **13**, e6900 (2024).
506. C. Fokken *et al.*, Interfering with aggregated alpha-synuclein in advanced melanoma leads to a major upregulation of MHC class II proteins. *Melanoma Res* **34**, 393-407 (2024).

507. R. Pinho *et al.*, Nuclear localization and phosphorylation modulate pathological effects of alpha-synuclein. *Hum Mol Genet* **28**, 31-50 (2019).
508. N. Sugeno *et al.*, alpha-Synuclein enhances histone H3 lysine-9 dimethylation and H3K9me2-dependent transcriptional responses. *Sci Rep* **6**, 36328 (2016).
509. E. Kontopoulos, J. D. Parvin, M. B. Feany, Alpha-synuclein acts in the nucleus to inhibit histone acetylation and promote neurotoxicity. *Hum Mol Genet* **15**, 3012-3023 (2006).
510. X. Liu *et al.*, Alpha-synuclein functions in the nucleus to protect against hydroxyurea-induced replication stress in yeast. *Hum Mol Genet* **20**, 3401-3414 (2011).
511. J. Goers *et al.*, Nuclear localization of alpha-synuclein and its interaction with histones. *Biochemistry* **42**, 8465-8471 (2003).
512. T. Nakamura *et al.*, Alpha-synuclein promotes PRMT5-mediated H4R3me2s histone methylation by interacting with the BAF complex. *FEBS J* **291**, 1892-1908 (2024).
513. S. Kim, J. M. Park, J. Moon, H. J. Choi, Alpha-synuclein interferes with cAMP/PKA-dependent upregulation of dopamine beta-hydroxylase and is associated with abnormal adaptive responses to immobilization stress. *Exp Neurol* **252**, 63-74 (2014).
514. A. Siddiqui *et al.*, Selective binding of nuclear alpha-synuclein to the PGC1alpha promoter under conditions of oxidative stress may contribute to losses in mitochondrial function: implications for Parkinson's disease. *Free Radic Biol Med* **53**, 993-1003 (2012).
515. S. E. Dent *et al.*, Phosphorylation of the aggregate-forming protein alpha-synuclein on serine-129 inhibits its DNA-bending properties. *J Biol Chem* **298**, 101552 (2022).
516. P. Vasudevaraju *et al.*, New evidence on alpha-synuclein and Tau binding to conformation and sequence specific GC* rich DNA: Relevance to neurological disorders. *J Pharm Bioallied Sci* **4**, 112-117 (2012).
517. G. P. Pfeifer, DNA Damage and Parkinson's Disease. *Int J Mol Sci* **25**, (2024).
518. V. Dileep *et al.*, Neuronal DNA double-strand breaks lead to genome structural variations and 3D genome disruption in neurodegeneration. *Cell* **186**, 4404-4421 e4420 (2023).
519. D. P. Agamanolis, J. I. Greenstein, Ataxia-telangiectasia. Report of a case with Lewy bodies and vascular abnormalities within cerebral tissue. *J Neuropathol Exp Neurol* **38**, 475-489 (1979).
520. R. Eilam, Y. Peter, Y. Groner, M. Segal, Late degeneration of nigro-striatal neurons in ATM^{-/-} mice. *Neuroscience* **121**, 83-98 (2003).
521. R. L. Warters, P. J. Adamson, C. D. Pond, S. A. Leachman, Melanoma cells express elevated levels of phosphorylated histone H2AX foci. *J Invest Dermatol* **124**, 807-817 (2005).
522. M. J. Wasco, R. T. Pu, L. Yu, L. Su, L. Ma, Expression of gamma-H2AX in melanocytic lesions. *Hum Pathol* **39**, 1614-1620 (2008).
523. L. Song *et al.*, DNA repair and replication proteins as prognostic markers in melanoma. *Histopathology* **62**, 343-350 (2013).

524. G. Puts *et al.*, Metastasis Suppressor NME1 Modulates Choice of Double-Strand Break Repair Pathways in Melanoma Cells by Enhancing Alternative NHEJ while Inhibiting NHEJ and HR. *Int J Mol Sci* **21**, (2020).
525. A. R. Harwood, B. J. Cummings, Radiotherapy for malignant melanoma: a re-appraisal. *Cancer Treat Rev* **8**, 271-282 (1981).
526. E. K. Rofstad, Radiation sensitivity in vitro of primary tumors and metastatic lesions of malignant melanoma. *Cancer Res* **52**, 4453-4457 (1992).
527. A. Trenner, A. A. Sartori, Harnessing DNA Double-Strand Break Repair for Cancer Treatment. *Front Oncol* **9**, 1388 (2019).
528. J. Biau *et al.*, A preclinical study combining the DNA repair inhibitor Dbait with radiotherapy for the treatment of melanoma. *Neoplasia* **16**, 835-844 (2014).
529. B. K. Tripathy, K. Pal, S. Shabrish, I. Mittra, A New Perspective on the Origin of DNA Double-Strand Breaks and Its Implications for Ageing. *Genes (Basel)* **12**, (2021).
530. M. Betermier, P. Bertrand, B. S. Lopez, Is non-homologous end-joining really an inherently error-prone process? *PLoS Genet* **10**, e1004086 (2014).
531. K. Rodgers, M. McVey, Error-Prone Repair of DNA Double-Strand Breaks. *J Cell Physiol* **231**, 15-24 (2016).
532. Z. Mao, M. Bozzella, A. Seluanov, V. Gorbunova, DNA repair by nonhomologous end joining and homologous recombination during cell cycle in human cells. *Cell Cycle* **7**, 2902-2906 (2008).
533. M. S. Gillespie, C. M. Ward, C. C. Davies, DNA Repair and Therapeutic Strategies in Cancer Stem Cells. *Cancers (Basel)* **15**, (2023).
534. A. Shibata *et al.*, Factors determining DNA double-strand break repair pathway choice in G2 phase. *EMBO J* **30**, 1079-1092 (2011).
535. J. Her, S. F. Bunting, How cells ensure correct repair of DNA double-strand breaks. *J Biol Chem* **293**, 10502-10511 (2018).
536. I. Brandsma, D. C. Gent, Pathway choice in DNA double strand break repair: observations of a balancing act. *Genome Integr* **3**, 9 (2012).
537. M. Shrivastav, L. P. De Haro, J. A. Nickoloff, Regulation of DNA double-strand break repair pathway choice. *Cell Res* **18**, 134-147 (2008).
538. S. Panier, S. J. Boulton, Double-strand break repair: 53BP1 comes into focus. *Nat Rev Mol Cell Biol* **15**, 7-18 (2014).
539. J. R. Chapman, M. R. Taylor, S. J. Boulton, Playing the end game: DNA double-strand break repair pathway choice. *Mol Cell* **47**, 497-510 (2012).
540. J. A. Neal, K. Meek, Choosing the right path: does DNA-PK help make the decision? *Mutat Res* **711**, 73-86 (2011).
541. C. Schofer, K. Weipoltshammer, Nucleolus and chromatin. *Histochem Cell Biol* **150**, 209-225 (2018).
542. F. Guillen-Chable, A. Bayona, L. C. Rodriguez-Zapata, E. Castano, Phase Separation of Intrinsically Disordered Nucleolar Proteins Relate to Localization and Function. *Int J Mol Sci* **22**, (2021).
543. L. Stenstrom *et al.*, Mapping the nucleolar proteome reveals a spatiotemporal organization related to intrinsic protein disorder. *Mol Syst Biol* **16**, e9469 (2020).

544. M. van Sluis *et al.*, Human NORs, comprising rDNA arrays and functionally conserved distal elements, are located within dynamic chromosomal regions. *Genes Dev* **33**, 1688-1701 (2019).
545. M. van Sluis, C. van Vuuren, H. Mangan, B. McStay, NORs on human acrocentric chromosome p-arms are active by default and can associate with nucleoli independently of rDNA. *Proc Natl Acad Sci U S A* **117**, 10368-10377 (2020).
546. M. R. King *et al.*, Macromolecular condensation organizes nucleolar sub-phases to set up a pH gradient. *Cell* **187**, 1889-1906 e1824 (2024).
547. R. W. Yao *et al.*, Nascent Pre-rRNA Sorting via Phase Separation Drives the Assembly of Dense Fibrillar Components in the Human Nucleolus. *Mol Cell* **76**, 767-783 e711 (2019).
548. D. M. Stults *et al.*, Human rRNA gene clusters are recombinational hotspots in cancer. *Cancer Res* **69**, 9096-9104 (2009).
549. V. Valori *et al.*, Human rDNA copy number is unstable in metastatic breast cancers. *Epigenetics* **15**, 85-106 (2020).
550. J. Hallgren, M. Pietrzak, G. Rempala, P. T. Nelson, M. Hetman, Neurodegeneration-associated instability of ribosomal DNA. *Biochim Biophys Acta* **1842**, 860-868 (2014).
551. K. Tomiwa, C. Nolan, J. B. Cavanagh, The effects of cisplatin on rat spinal ganglia: a study by light and electron microscopy and by morphometry. *Acta Neuropathol* **69**, 295-308 (1986).
552. L. Bigotte, Y. Olsson, Degeneration of trigeminal ganglion neurons caused by retrograde axonal transport of doxorubicin. *Neurology* **37**, 985-992 (1987).
553. S. M. Jamieson, J. Liu, B. Connor, M. J. McKeage, Oxaliplatin causes selective atrophy of a subpopulation of dorsal root ganglion neurons without inducing cell loss. *Cancer Chemother Pharmacol* **56**, 391-399 (2005).
554. I. Casafont, A. Palanca, V. Lafarga, M. T. Berciano, M. Lafarga, Effect of ionizing radiation in sensory ganglion neurons: organization and dynamics of nuclear compartments of DNA damage/repair and their relationship with transcription and cell cycle. *Acta Neuropathol* **122**, 481-493 (2011).
555. C. Rieker *et al.*, Nucleolar disruption in dopaminergic neurons leads to oxidative damage and parkinsonism through repression of mammalian target of rapamycin signaling. *J Neurosci* **31**, 453-460 (2011).
556. F. C. Baltanas *et al.*, Nucleolar disruption and cajal body disassembly are nuclear hallmarks of DNA damage-induced neurodegeneration in purkinje cells. *Brain Pathol* **21**, 374-388 (2011).
557. A. N. Lane, T. W. Fan, Regulation of mammalian nucleotide metabolism and biosynthesis. *Nucleic Acids Res* **43**, 2466-2485 (2015).
558. A. Pecoraro, M. Pagano, G. Russo, A. Russo, Ribosome Biogenesis and Cancer: Overview on Ribosomal Proteins. *Int J Mol Sci* **22**, (2021).
559. A. Zisi, J. Bartek, M. S. Lindstrom, Targeting Ribosome Biogenesis in Cancer: Lessons Learned and Way Forward. *Cancers (Basel)* **14**, (2022).
560. D. A. Kiktev *et al.*, The fidelity of DNA replication, particularly on GC-rich templates, is reduced by defects of the Fe-S cluster in DNA polymerase delta. *Nucleic Acids Res* **49**, 5623-5636 (2021).

561. D. A. Kiktev, Z. Sheng, K. S. Lobachev, T. D. Petes, GC content elevates mutation and recombination rates in the yeast *Saccharomyces cerevisiae*. *Proc Natl Acad Sci U S A* **115**, E7109-E7118 (2018).
562. D. H. Larsen *et al.*, The NBS1-Treacle complex controls ribosomal RNA transcription in response to DNA damage. *Nat Cell Biol* **16**, 792-803 (2014).
563. M. Kruhlak *et al.*, The ATM repair pathway inhibits RNA polymerase I transcription in response to chromosome breaks. *Nature* **447**, 730-734 (2007).
564. C. Mooser *et al.*, Treacle controls the nucleolar response to rDNA breaks via TOPBP1 recruitment and ATR activation. *Nat Commun* **11**, 123 (2020).
565. L. M. Korsholm *et al.*, Double-strand breaks in ribosomal RNA genes activate a distinct signaling and chromatin response to facilitate nucleolar restructuring and repair. *Nucleic Acids Res* **47**, 8019-8035 (2019).
566. M. van Sluis, B. McStay, Nucleolar DNA Double-Strand Break Responses Underpinning rDNA Genomic Stability. *Trends Genet* **35**, 743-753 (2019).
567. A. Marnef *et al.*, A cohesin/HUSH- and LINC-dependent pathway controls ribosomal DNA double-strand break repair. *Genes Dev* **33**, 1175-1190 (2019).
568. C. Siebenwirth *et al.*, Local inhibition of rRNA transcription without nucleolar segregation after targeted ion irradiation of the nucleolus. *J Cell Sci* **132**, (2019).
569. M. van Sluis, B. McStay, A localized nucleolar DNA damage response facilitates recruitment of the homology-directed repair machinery independent of cell cycle stage. *Genes Dev* **29**, 1151-1163 (2015).
570. S. M. Harding, J. A. Boiarsky, R. A. Greenberg, ATM Dependent Silencing Links Nucleolar Chromatin Reorganization to DNA Damage Recognition. *Cell Rep* **13**, 251-259 (2015).
571. Y. Shav-Tal *et al.*, Dynamic sorting of nuclear components into distinct nucleolar caps during transcriptional inhibition. *Mol Biol Cell* **16**, 2395-2413 (2005).
572. M. van Sluis, B. McStay, Nucleolar reorganization in response to rDNA damage. *Curr Opin Cell Biol* **46**, 81-86 (2017).
573. I. Mitrentsi, D. Yilmaz, E. Soutoglou, How to maintain the genome in nuclear space. *Curr Opin Cell Biol* **64**, 58-66 (2020).
574. L. M. Korsholm *et al.*, Recent advances in the nucleolar responses to DNA double-strand breaks. *Nucleic Acids Res* **48**, 9449-9461 (2020).
575. S. D'Angiolini, M. Lui, E. Mazzon, M. Calabro, Network Analysis Performed on Transcriptomes of Parkinson's Disease Patients Reveals Dysfunction in Protein Translation. *Int J Mol Sci* **25**, (2024).
576. B. Popova *et al.*, DEAD-box RNA helicase Dbp4/DDX10 is an enhancer of alpha-synuclein toxicity and oligomerization. *PLoS Genet* **17**, e1009407 (2021).
577. D. H. Ho, H. Kim, D. Nam, J. Heo, I. Son, Nuclear alpha-Synuclein-Derived Cytotoxic Effect via Altered Ribosomal RNA Processing in Primary Mouse Embryonic Fibroblasts. *Int J Mol Sci* **24**, (2023).
578. J. Vijg, Y. Suh, Genome instability and aging. *Annu Rev Physiol* **75**, 645-668 (2013).
579. V. K. Wandt *et al.*, A matter of concern - Trace element dyshomeostasis and genomic stability in neurons. *Redox Biol* **41**, 101877 (2021).
580. K. G. Paulson *et al.*, Age-Specific Incidence of Melanoma in the United States. *JAMA Dermatol* **156**, 57-64 (2020).

581. N. L. Bolick, A. C. Geller, Epidemiology and Screening for Melanoma. *Hematol Oncol Clin North Am* **38**, 889-906 (2024).
582. R. L. Siegel, A. N. Giaquinto, A. Jemal, Cancer statistics, 2024. *CA Cancer J Clin* **74**, 12-49 (2024).
583. E. Everdell *et al.*, ATLAS: A positive, high-yield review of patient symptoms most significantly associated with melanoma recurrence. *J Am Acad Dermatol* **91**, 1118-1124 (2024).
584. D. A. Munoz, M. S. Kilinc, H. B. Nembhard, C. Tucker, X. Huang, Evaluating the Cost-Effectiveness of an Early Detection of Parkinson's Disease through Innovative Technology. *Eng Econ* **62**, 180-196 (2017).
585. J. M. Fearnley, A. J. Lees, Ageing and Parkinson's disease: substantia nigra regional selectivity. *Brain* **114** (Pt 5), 2283-2301 (1991).
586. P. E. Sugier *et al.*, Investigation of Shared Genetic Risk Factors Between Parkinson's Disease and Cancers. *Mov Disord* **38**, 604-615 (2023).
587. R. Inzelberg *et al.*, Parkinson disease (PARK) genes are somatically mutated in cutaneous melanoma. *Neurol Genet* **2**, e70 (2016).
588. Y. S. Lee *et al.*, Occupational Risk Factors for Skin Cancer: A Comprehensive Review. *J Korean Med Sci* **39**, e316 (2024).
589. D. M. Freedman *et al.*, Associations between cancer and Parkinson's disease in U.S. elderly adults. *Int J Epidemiol* **45**, 741-751 (2016).
590. X. Cui *et al.*, Cancers Preceding Parkinson's Disease after Adjustment for Bias in a Danish Population-Based Case-Control Study. *Neuroepidemiology* **52**, 136-143 (2019).
591. I. Agalliu *et al.*, Cancer outcomes among Parkinson's disease patients with leucine rich repeat kinase 2 mutations, idiopathic Parkinson's disease patients, and nonaffected controls. *Mov Disord* **34**, 1392-1398 (2019).
592. M. R. Arnold *et al.*, Alpha-synuclein regulates nucleolar DNA double-strand break repair in melanoma. *bioRxiv*, (2024).
593. T. Krainc, M. H. G. Monje, M. Kinsinger, B. I. Bustos, S. J. Lubbe, Melanin and Neuromelanin: Linking Skin Pigmentation and Parkinson's Disease. *Mov Disord* **38**, 185-195 (2023).
594. S. Heinzl *et al.*, Update of the MDS research criteria for prodromal Parkinson's disease. *Mov Disord* **34**, 1464-1470 (2019).
595. A. A. o. D. Association. (2024), vol. 2024.
596. G. U. Hoglinger *et al.*, A biological classification of Parkinson's disease: the SynNeurGe research diagnostic criteria. *Lancet Neurol* **23**, 191-204 (2024).
597. C. M. Wilkowsi *et al.*, The association of seborrheic dermatitis and Parkinson's disease: A cross-sectional study. *J Am Acad Dermatol*, (2024).
598. J. H. Lee, K. Han, H. Y. Gee, The incidence rates and risk factors of Parkinson disease in patients with psoriasis: A nationwide population-based cohort study. *J Am Acad Dermatol* **83**, 1688-1695 (2020).
599. E. J. Hill *et al.*, Parkinson's disease diagnosis codes are insufficiently accurate for electronic health record research and differ by race. *Parkinsonism Relat Disord* **114**, 105764 (2023).
600. M. J. Eide *et al.*, Validation of claims data algorithms to identify nonmelanoma skin cancer. *J Invest Dermatol* **132**, 2005-2009 (2012).

601. D. Y. Hsu *et al.*, Validation of International Classification of Disease Ninth Revision codes for atopic dermatitis. *Allergy* **72**, 1091-1095 (2017).
602. C. Koros *et al.*, Double Trouble: Association of Malignant Melanoma with Sporadic and Genetic Forms of Parkinson's Disease and Asymptomatic Carriers of Related Genes: A Brief Report. *Medicina (Kaunas)* **59**, (2023).
603. S. Manne *et al.*, Blinded RT-QuIC Analysis of alpha-Synuclein Biomarker in Skin Tissue From Parkinson's Disease Patients. *Mov Disord* **35**, 2230-2239 (2020).
604. Z. Wang *et al.*, Skin alpha-Synuclein Aggregation Seeding Activity as a Novel Biomarker for Parkinson Disease. *JAMA Neurol*, (2020).
605. R. B. Postuma *et al.*, A single-question screen for rapid eye movement sleep behavior disorder: a multicenter validation study. *Mov Disord* **27**, 913-916 (2012).
606. Y. Waki, Y. Nobeyama, H. Nakagawa, A. Asahina, High prevalence of dermatophytosis of the feet in acral melanoma of the foot. *J Dermatol* **51**, 1098-1103 (2024).
607. S. Gnat, A. Nowakiewicz, D. Lagowski, P. Zieba, Host- and pathogen-dependent susceptibility and predisposition to dermatophytosis. *J Med Microbiol* **68**, 823-836 (2019).
608. M. Laurence, J. Benito-Leon, F. Calon, Malassezia and Parkinson's Disease. *Front Neurol* **10**, 758 (2019).
609. G. D. Scott, L. E. Neilson, R. Woltjer, J. F. Quinn, M. M. Lim, Lifelong Association of Disorders Related to Military Trauma with Subsequent Parkinson's Disease. *Mov Disord* **38**, 1483-1492 (2023).
610. S. van Buuren, K. Groothuis-Oudshoorn, mice: Multivariate Imputation by Chained Equations in R. *Journal of Statistical Software* **45**, 1 - 67 (2011).
611. B. Zhou, A. Latouche, V. Rocha, J. Fine, Competing risks regression for stratified data. *Biometrics* **67**, 661-670 (2011).
612. L. E. Neilson, K. M. Reavis, J. Wiedrick, G. D. Scott, Hearing Loss, Incident Parkinson Disease, and Treatment With Hearing Aids. *JAMA Neurol* **81**, 1295-1303 (2024).
613. M. S. Flynn *et al.*, Clinicopathologic Characteristics of Melanoma in Patients with Parkinson Disease. *JID Innov* **3**, 100173 (2023).
614. M. G. Spillantini, R. A. Crowther, R. Jakes, M. Hasegawa, M. Goedert, alpha-Synuclein in filamentous inclusions of Lewy bodies from Parkinson's disease and dementia with lewy bodies. *Proc Natl Acad Sci U S A* **95**, 6469-6473 (1998).
615. M. Baba *et al.*, Aggregation of alpha-synuclein in Lewy bodies of sporadic Parkinson's disease and dementia with Lewy bodies. *Am J Pathol* **152**, 879-884 (1998).
616. J. Xu *et al.*, Dopamine-dependent neurotoxicity of alpha-synuclein: a mechanism for selective neurodegeneration in Parkinson disease. *Nat Med* **8**, 600-606 (2002).
617. L. Y. Ma *et al.*, Alpha-Synuclein in Peripheral Tissues in Parkinson's Disease. *ACS Chem Neurosci* **10**, 812-823 (2019).
618. M. Fayyad *et al.*, Parkinson's disease biomarkers based on alpha-synuclein. *J Neurochem* **150**, 626-636 (2019).
619. M. W. El-Saadi *et al.*, Tracing brain genotoxic stress in Parkinson's disease with a novel single-cell genetic sensor. *Sci Adv* **8**, eabd1700 (2022).

620. Y. S. Yoon *et al.*, Senescence and impaired DNA damage responses in alpha-synucleinopathy models. *Exp Mol Med* **54**, 115-128 (2022).
621. M. Yoshida, Multiple system atrophy: alpha-synuclein and neuronal degeneration. *Neuropathology* **27**, 484-493 (2007).
622. A. N. Blackford, S. P. Jackson, ATM, ATR, and DNA-PK: The Trinity at the Heart of the DNA Damage Response. *Mol Cell* **66**, 801-817 (2017).
623. S. M. Hecht, Bleomycin: new perspectives on the mechanism of action. *J Nat Prod* **63**, 158-168 (2000).
624. A. Galbiati, C. Beausejour, F. d'Adda di Fagagna, A novel single-cell method provides direct evidence of persistent DNA damage in senescent cells and aged mammalian tissues. *Aging Cell* **16**, 422-427 (2017).
625. M. Franek, A. Kovarikova, E. Bartova, S. Kozubek, Nucleolar Reorganization Upon Site-Specific Double-Strand Break Induction. *J Histochem Cytochem* **64**, 669-686 (2016).
626. A. Gupta *et al.*, Role of 53BP1 in the regulation of DNA double-strand break repair pathway choice. *Radiat Res* **181**, 1-8 (2014).
627. A. Kakarougkas *et al.*, Opposing roles for 53BP1 during homologous recombination. *Nucleic Acids Res* **41**, 9719-9731 (2013).
628. L. S. Fink *et al.*, 53BP1 contributes to a robust genomic stability in human fibroblasts. *Aging (Albany NY)* **3**, 836-845 (2011).
629. M. Terradas, M. Martin, L. Tusell, A. Genesca, DNA lesions sequestered in micronuclei induce a local defective-damage response. *DNA Repair (Amst)* **8**, 1225-1234 (2009).
630. M. Yin, F. Hong, Q. E. Wang, in *Metastasis*, C. M. Sergi, Ed. (Brisbane (AU), 2022).
631. S. Ide, R. Imai, H. Ochi, K. Maeshima, Transcriptional suppression of ribosomal DNA with phase separation. *Sci Adv* **6**, (2020).
632. M. Somayaji, Z. Lanseur, S. J. Choi, D. Sulzer, E. V. Mosharov, Roles for alpha-Synuclein in Gene Expression. *Genes (Basel)* **12**, (2021).
633. S. Rajasekaran *et al.*, Transcriptomic analysis of melanoma cells reveals an association of alpha-synuclein with regulation of the inflammatory response. *Sci Rep* **14**, 27140 (2024).
634. H. C. Ku, C. F. Cheng, Master Regulator Activating Transcription Factor 3 (ATF3) in Metabolic Homeostasis and Cancer. *Front Endocrinol (Lausanne)* **11**, 556 (2020).
635. V. L. Fell, C. Schild-Poulter, Ku regulates signaling to DNA damage response pathways through the Ku70 von Willebrand A domain. *Mol Cell Biol* **32**, 76-87 (2012).
636. S. Deng *et al.*, The catalytic topoisomerase II inhibitor dexrazoxane induces DNA breaks, ATF3 and the DNA damage response in cancer cells. *Br J Pharmacol* **172**, 2246-2257 (2015).
637. G. Coster, M. Goldberg, The cellular response to DNA damage: a focus on MDC1 and its interacting proteins. *Nucleus* **1**, 166-178 (2010).
638. Z. Lou *et al.*, MDC1 maintains genomic stability by participating in the amplification of ATM-dependent DNA damage signals. *Mol Cell* **21**, 187-200 (2006).

639. M. Stucki *et al.*, MDC1 directly binds phosphorylated histone H2AX to regulate cellular responses to DNA double-strand breaks. *Cell* **123**, 1213-1226 (2005).
640. M. S. Lee, R. A. Edwards, G. L. Thede, J. N. Glover, Structure of the BRCT repeat domain of MDC1 and its specificity for the free COOH-terminal end of the gamma-H2AX histone tail. *J Biol Chem* **280**, 32053-32056 (2005).
641. M. S. Huen *et al.*, RNF8 transduces the DNA-damage signal via histone ubiquitylation and checkpoint protein assembly. *Cell* **131**, 901-914 (2007).
642. N. K. Kolas *et al.*, Orchestration of the DNA-damage response by the RNF8 ubiquitin ligase. *Science* **318**, 1637-1640 (2007).
643. N. Mailand *et al.*, RNF8 ubiquitylates histones at DNA double-strand breaks and promotes assembly of repair proteins. *Cell* **131**, 887-900 (2007).
644. C. Doil *et al.*, RNF168 binds and amplifies ubiquitin conjugates on damaged chromosomes to allow accumulation of repair proteins. *Cell* **136**, 435-446 (2009).
645. S. L. Sanders *et al.*, Methylation of histone H4 lysine 20 controls recruitment of Crb2 to sites of DNA damage. *Cell* **119**, 603-614 (2004).
646. M. V. Botuyan *et al.*, Structural basis for the methylation state-specific recognition of histone H4-K20 by 53BP1 and Crb2 in DNA repair. *Cell* **127**, 1361-1373 (2006).
647. S. Ray *et al.*, alpha-Synuclein aggregation nucleates through liquid-liquid phase separation. *Nat Chem* **12**, 705-716 (2020).
648. M. C. Hardenberg *et al.*, Observation of an alpha-synuclein liquid droplet state and its maturation into Lewy body-like assemblies. *J Mol Cell Biol* **13**, 282-294 (2021).
649. A. S. Sawner *et al.*, Modulating alpha-Synuclein Liquid-Liquid Phase Separation. *Biochemistry* **60**, 3676-3696 (2021).
650. Y. L. Wang *et al.*, Liquid-liquid phase separation in DNA double-strand breaks repair. *Cell Death Dis* **14**, 746 (2023).
651. X. Gai *et al.*, Pre-ribosomal RNA reorganizes DNA damage repair factors in nucleus during meiotic prophase and DNA damage response. *Cell Res* **32**, 254-268 (2022).
652. T. Nakamura *et al.*, Alpha-synuclein promotes PRMT5-mediated H4R3me2s histone methylation by interacting with the BAF complex. *FEBS J*, (2023).
653. S. Yin, L. Liu, W. Gan, PRMT1 and PRMT5: on the road of homologous recombination and non-homologous end joining. *Genome Instab Dis* **4**, 197-209 (2023).
654. J. W. Hwang *et al.*, PRMT5 promotes DNA repair through methylation of 53BP1 and is regulated by Src-mediated phosphorylation. *Commun Biol* **3**, 428 (2020).
655. M. Hamdi *et al.*, ATF3 and Fra1 have opposite functions in JNK- and ERK-dependent DNA damage responses. *DNA Repair (Amst)* **7**, 487-496 (2008).
656. K. Taketani *et al.*, Key role of ATF3 in p53-dependent DR5 induction upon DNA damage of human colon cancer cells. *Oncogene* **31**, 2210-2221 (2012).
657. F. Fan *et al.*, ATF3 induction following DNA damage is regulated by distinct signaling pathways and over-expression of ATF3 protein suppresses cells growth. *Oncogene* **21**, 7488-7496 (2002).
658. C. Charbonnel *et al.*, The Linker Histone GH1-HMGA1 Is Involved in Telomere Stability and DNA Damage Repair. *Plant Physiol* **177**, 311-327 (2018).

659. F. Pentimalli *et al.*, HMGA1 protein is a novel target of the ATM kinase. *Eur J Cancer* **44**, 2668-2679 (2008).
660. G. Baldassarre *et al.*, HMGA1 protein expression sensitizes cells to cisplatin-induced cell death. *Oncogene* **24**, 6809-6819 (2005).
661. S. Natarajan, S. Hombach-Klonisch, P. Droge, T. Klonisch, HMGA2 inhibits apoptosis through interaction with ATR-CHK1 signaling complex in human cancer cells. *Neoplasia* **15**, 263-280 (2013).
662. A. Y. Li *et al.*, Suppression of nonhomologous end joining repair by overexpression of HMGA2. *Cancer Res* **69**, 5699-5706 (2009).
663. Y. K. Chae *et al.*, Genomic landscape of DNA repair genes in cancer. *Oncotarget* **7**, 23312-23321 (2016).
664. M. Y. Hsu, L. Li, M. Herlyn, Cultivation of normal human epidermal melanocytes in the absence of phorbol esters. *Methods Mol Med* **107**, 13-28 (2005).
665. J. B. Leverenz *et al.*, Empiric refinement of the pathologic assessment of Lewy-related pathology in the dementia patient. *Brain Pathol* **18**, 220-224 (2008).
666. C. Moore, M. Xu, J. K. Bohlen, C. K. Meshul, Differential ultrastructural alterations in the Vglut2 glutamatergic input to the substantia nigra pars compacta/pars reticulata following nigrostriatal dopamine loss in a progressive mouse model of Parkinson's disease. *Eur J Neurosci* **53**, 2061-2077 (2021).
667. E. Y. Chen *et al.*, Enrichr: interactive and collaborative HTML5 gene list enrichment analysis tool. *BMC Bioinformatics* **14**, 128 (2013).
668. M. V. Kuleshov *et al.*, Enrichr: a comprehensive gene set enrichment analysis web server 2016 update. *Nucleic Acids Res* **44**, W90-97 (2016).
669. Z. Xie *et al.*, Gene Set Knowledge Discovery with Enrichr. *Curr Protoc* **1**, e90 (2021).
670. N. M. Aloy, C. Coughlan, M. W. Graner, S. N. Witt, Possible regulation of the immune modulator tetraspanin CD81 by alpha-synuclein in melanoma. *Biochem Biophys Res Commun* **734**, 150631 (2024).
671. P. M. Pollock *et al.*, Melanoma mouse model implicates metabotropic glutamate signaling in melanocytic neoplasia. *Nat Genet* **34**, 108-112 (2003).
672. H. Zhu *et al.*, Development of early melanocytic lesions in transgenic mice predisposed to melanoma. *Pigment Cell Res* **13**, 158-164 (2000).
673. H. Zhu *et al.*, Development of heritable melanoma in transgenic mice. *J Invest Dermatol* **110**, 247-252 (1998).
674. S. Chen, H. Zhu, W. J. Wetzel, M. A. Philbert, Spontaneous melanocytosis in transgenic mice. *J Invest Dermatol* **106**, 1145-1151 (1996).
675. S. Schiffner, S. Chen, J. C. Becker, A. K. Bosserhoff, Highly pigmented Tg(Grm1) mouse melanoma develops non-pigmented melanoma cells in distant metastases. *Exp Dermatol* **21**, 786-788 (2012).
676. F. J. Groelly, M. Fawkes, R. A. Dagg, A. N. Blackford, M. Tarsounas, Targeting DNA damage response pathways in cancer. *Nat Rev Cancer* **23**, 78-94 (2023).
677. A. Kauffmann *et al.*, High expression of DNA repair pathways is associated with metastasis in melanoma patients. *Oncogene* **27**, 565-573 (2008).
678. A. I. M. Sever *et al.*, Activation of caspase-9 on the apoptosome as studied by methyl-TROSY NMR. *Proc Natl Acad Sci U S A* **120**, e2310944120 (2023).

679. S. Liu, S. Yao, H. Yang, S. Liu, Y. Wang, Autophagy: Regulator of cell death. *Cell Death Dis* **14**, 648 (2023).
680. G. Kroemer, B. Levine, Autophagic cell death: the story of a misnomer. *Nat Rev Mol Cell Biol* **9**, 1004-1010 (2008).
681. Z. H. Chen *et al.*, Autophagy protein microtubule-associated protein 1 light chain-3B (LC3B) activates extrinsic apoptosis during cigarette smoke-induced emphysema. *Proc Natl Acad Sci U S A* **107**, 18880-18885 (2010).
682. J. P. Coppe *et al.*, Tumor suppressor and aging biomarker p16(INK4a) induces cellular senescence without the associated inflammatory secretory phenotype. *J Biol Chem* **286**, 36396-36403 (2011).
683. K. M. LaPak, C. E. Burd, The molecular balancing act of p16(INK4a) in cancer and aging. *Mol Cancer Res* **12**, 167-183 (2014).
684. A. Szmurlo *et al.*, The Role of Caspases in Melanoma Pathogenesis. *Curr Issues Mol Biol* **46**, 9480-9492 (2024).
685. K. Berthenet *et al.*, Failed Apoptosis Enhances Melanoma Cancer Cell Aggressiveness. *Cell Rep* **31**, 107731 (2020).
686. M. L. Hartman, Non-Apoptotic Cell Death Signaling Pathways in Melanoma. *Int J Mol Sci* **21**, (2020).
687. E. Fratta *et al.*, Autophagy in BRAF-mutant cutaneous melanoma: recent advances and therapeutic perspective. *Cell Death Discov* **9**, 202 (2023).
688. M. S. Soengas *et al.*, Inactivation of the apoptosis effector Apaf-1 in malignant melanoma. *Nature* **409**, 207-211 (2001).
689. M. S. Soengas, S. W. Lowe, Apoptosis and melanoma chemoresistance. *Oncogene* **22**, 3138-3151 (2003).
690. D. Y. Tang, R. A. Ellis, P. E. Lovat, Prognostic Impact of Autophagy Biomarkers for Cutaneous Melanoma. *Front Oncol* **6**, 236 (2016).
691. V. C. Gray-Schopfer *et al.*, Cellular senescence in naevi and immortalisation in melanoma: a role for p16? *Br J Cancer* **95**, 496-505 (2006).
692. S. Haferkamp, T. M. Becker, L. L. Scurr, R. F. Kefford, H. Rizos, p16INK4a-induced senescence is disabled by melanoma-associated mutations. *Aging Cell* **7**, 733-745 (2008).
693. S. M. Constantinou, D. C. Bennett, Cell Senescence and the Genetics of Melanoma Development. *Genes Chromosomes Cancer* **63**, e23273 (2024).
694. E. Jaune *et al.*, Discovery of a new molecule inducing melanoma cell death: dual AMPK/MELK targeting for novel melanoma therapies. *Cell Death Dis* **12**, 64 (2021).
695. A. E. M. Ibler *et al.*, Typhoid toxin exhausts the RPA response to DNA replication stress driving senescence and Salmonella infection. *Nat Commun* **10**, 4040 (2019).
696. F. M. Feringa *et al.*, Persistent repair intermediates induce senescence. *Nat Commun* **9**, 3923 (2018).
697. T. Helleday, Homologous recombination in cancer development, treatment and development of drug resistance. *Carcinogenesis* **31**, 955-960 (2010).
698. K. B. Kim *et al.*, Prevalence of Homologous Recombination Pathway Gene Mutations in Melanoma: Rationale for a New Targeted Therapeutic Approach. *J Invest Dermatol* **141**, 2028-2036 e2022 (2021).

699. Z. You *et al.*, Homologous recombination repair gene mutations as a predictive biomarker for immunotherapy in patients with advanced melanoma. *Front Immunol* **13**, 871756 (2022).
700. M. Fang *et al.*, MEN1 is a melanoma tumor suppressor that preserves genomic integrity by stimulating transcription of genes that promote homologous recombination-directed DNA repair. *Mol Cell Biol* **33**, 2635-2647 (2013).
701. W. Y. Chan, L. J. Brown, L. Reid, A. M. Joshua, PARP Inhibitors in Melanoma-An Expanding Therapeutic Option? *Cancers (Basel)* **13**, (2021).
702. F. Moisan *et al.*, Parkinson disease male-to-female ratios increase with age: French nationwide study and meta-analysis. *J Neurol Neurosurg Psychiatry* **87**, 952-957 (2016).
703. A. Joosse *et al.*, Gender differences in melanoma survival: female patients have a decreased risk of metastasis. *J Invest Dermatol* **131**, 719-726 (2011).
704. A. J. Smith, P. C. Lambert, M. J. Rutherford, Understanding the impact of sex and stage differences on melanoma cancer patient survival: a SEER-based study. *Br J Cancer* **124**, 671-677 (2021).
705. D. I. Podolskiy, A. V. Lobanov, G. V. Kryukov, V. N. Gladyshev, Analysis of cancer genomes reveals basic features of human aging and its role in cancer development. *Nat Commun* **7**, 12157 (2016).
706. N. Winkelbeiner *et al.*, A Multi-Endpoint Approach to Base Excision Repair Incision Activity Augmented by PARylation and DNA Damage Levels in Mice: Impact of Sex and Age. *Int J Mol Sci* **21**, (2020).
707. Y. Yuan *et al.*, Comprehensive Characterization of Molecular Differences in Cancer between Male and Female Patients. *Cancer Cell* **29**, 711-722 (2016).
708. A. Carusillo, C. Mussolino, DNA Damage: From Threat to Treatment. *Cells* **9**, (2020).
709. I. S. Mohiuddin, M. H. Kang, DNA-PK as an Emerging Therapeutic Target in Cancer. *Front Oncol* **9**, 635 (2019).
710. K. Komatsu, NBS1 and multiple regulations of DNA damage response. *J Radiat Res* **57 Suppl 1**, i11-i17 (2016).
711. C. Bowen, T. Zheng, E. P. Gelmann, NKX3.1 Suppresses TMPRSS2-ERG Gene Rearrangement and Mediates Repair of Androgen Receptor-Induced DNA Damage. *Cancer Res* **75**, 2686-2698 (2015).
712. A. Wilk, A. Waligorska, P. Waligorski, A. Ochoa, K. Reiss, Inhibition of ERbeta induces resistance to cisplatin by enhancing Rad51-mediated DNA repair in human medulloblastoma cell lines. *PLoS One* **7**, e33867 (2012).
713. V. Padmaraju, J. J. Bhaskar, U. J. Prasada Rao, P. V. Salimath, K. S. Rao, Role of advanced glycation on aggregation and DNA binding properties of alpha-synuclein. *J Alzheimers Dis* **24 Suppl 2**, 211-221 (2011).
714. S. Tsaridou *et al.*, 53BP1-mediated recruitment of RASSF1A to ribosomal DNA breaks promotes local ATM signaling. *EMBO Rep* **23**, e54483 (2022).
715. A. M. Grawenda, E. O'Neill, Clinical utility of RASSF1A methylation in human malignancies. *Br J Cancer* **113**, 372-381 (2015).
716. J. Fages *et al.*, JMJD6 participates in the maintenance of ribosomal DNA integrity in response to DNA damage. *PLoS Genet* **16**, e1008511 (2020).

717. E. Berkovich, R. J. Monnat, Jr., M. B. Kastan, Roles of ATM and NBS1 in chromatin structure modulation and DNA double-strand break repair. *Nat Cell Biol* **9**, 683-690 (2007).
718. M. Goldstein, F. A. Derheimer, J. Tait-Mulder, M. B. Kastan, Nucleolin mediates nucleosome disruption critical for DNA double-strand break repair. *Proc Natl Acad Sci U S A* **110**, 16874-16879 (2013).
719. D. O. Warmerdam, J. van den Berg, R. H. Medema, Breaks in the 45S rDNA Lead to Recombination-Mediated Loss of Repeats. *Cell Rep* **14**, 2519-2527 (2016).
720. B. Meyer *et al.*, Clustered DNA damage induces pan-nuclear H2AX phosphorylation mediated by ATM and DNA-PK. *Nucleic Acids Res* **41**, 6109-6118 (2013).
721. D. Menolfi, S. Zha, ATM, ATR and DNA-PKcs kinases-the lessons from the mouse models: inhibition not equal deletion. *Cell Biosci* **10**, 8 (2020).
722. D. Chowdhury *et al.*, gamma-H2AX dephosphorylation by protein phosphatase 2A facilitates DNA double-strand break repair. *Mol Cell* **20**, 801-809 (2005).
723. J. Wu *et al.*, Lewy-like aggregation of alpha-synuclein reduces protein phosphatase 2A activity in vitro and in vivo. *Neuroscience* **207**, 288-297 (2012).
724. H. Kimura *et al.*, A novel histone exchange factor, protein phosphatase 2Cgamma, mediates the exchange and dephosphorylation of H2A-H2B. *J Cell Biol* **175**, 389-400 (2006).
725. D. Chowdhury *et al.*, A PP4-phosphatase complex dephosphorylates gamma-H2AX generated during DNA replication. *Mol Cell* **31**, 33-46 (2008).
726. S. H. Moon *et al.*, Wild-type p53-induced phosphatase 1 dephosphorylates histone variant gamma-H2AX and suppresses DNA double strand break repair. *J Biol Chem* **285**, 12935-12947 (2010).
727. E. B. Kabotyanski, L. Gomelsky, J. O. Han, T. D. Stamato, D. B. Roth, Double-strand break repair in Ku86- and XRCC4-deficient cells. *Nucleic Acids Res* **26**, 5333-5342 (1998).
728. D. W. Wyatt *et al.*, Essential Roles for Polymerase theta-Mediated End Joining in the Repair of Chromosome Breaks. *Mol Cell* **63**, 662-673 (2016).
729. H. H. Y. Chang, N. R. Pannunzio, N. Adachi, M. R. Lieber, Non-homologous DNA end joining and alternative pathways to double-strand break repair. *Nat Rev Mol Cell Biol* **18**, 495-506 (2017).
730. M. Mognato, S. Burdak-Rothkamm, K. Rothkamm, Interplay between DNA replication stress, chromatin dynamics and DNA-damage response for the maintenance of genome stability. *Mutat Res Rev Mutat Res* **787**, 108346 (2021).
731. L. Zou, S. J. Elledge, Sensing DNA damage through ATRIP recognition of RPA-ssDNA complexes. *Science* **300**, 1542-1548 (2003).
732. D. Shechter, V. Costanzo, J. Gautier, Regulation of DNA replication by ATR: signaling in response to DNA intermediates. *DNA Repair (Amst)* **3**, 901-908 (2004).
733. V. Gottifredi, C. Prives, The S phase checkpoint: when the crowd meets at the fork. *Semin Cell Dev Biol* **16**, 355-368 (2005).
734. E. Cybulla, A. Vindigni, Leveraging the replication stress response to optimize cancer therapy. *Nat Rev Cancer* **23**, 6-24 (2023).

735. H. Yajima, K. J. Lee, S. Zhang, J. Kobayashi, B. P. Chen, DNA double-strand break formation upon UV-induced replication stress activates ATM and DNA-PKcs kinases. *J Mol Biol* **385**, 800-810 (2009).
736. E. Vesela, K. Chroma, Z. Turi, M. Mistrik, Common Chemical Inductors of Replication Stress: Focus on Cell-Based Studies. *Biomolecules* **7**, (2017).
737. A. D. Bolzan, M. S. Bianchi, DNA and chromosome damage induced by bleomycin in mammalian cells: An update. *Mutat Res Rev Mutat Res* **775**, 51-62 (2018).
738. J. Chen, M. K. Ghorai, G. Kenney, J. Stubbe, Mechanistic studies on bleomycin-mediated DNA damage: multiple binding modes can result in double-stranded DNA cleavage. *Nucleic Acids Res* **36**, 3781-3790 (2008).
739. W. J. Cannan, D. S. Pederson, Mechanisms and Consequences of Double-Strand DNA Break Formation in Chromatin. *J Cell Physiol* **231**, 3-14 (2016).
740. A. Montecucco, F. Zanetta, G. Biamonti, Molecular mechanisms of etoposide. *EXCLI J* **14**, 95-108 (2015).
741. D. J. Smart *et al.*, Assessment of DNA double-strand breaks and gammaH2AX induced by the topoisomerase II poisons etoposide and mitoxantrone. *Mutat Res* **641**, 43-47 (2008).
742. J. Vignard, G. Mirey, B. Salles, Ionizing-radiation induced DNA double-strand breaks: a direct and indirect lighting up. *Radiother Oncol* **108**, 362-369 (2013).
743. N. Chatterjee, G. C. Walker, Mechanisms of DNA damage, repair, and mutagenesis. *Environ Mol Mutagen* **58**, 235-263 (2017).
744. E. Mladenov, P. Kalev, B. Anachkova, The complexity of double-strand break ends is a factor in the repair pathway choice. *Radiat Res* **171**, 397-404 (2009).
745. G. L. Dianov, P. O'Neill, D. T. Goodhead, Securing genome stability by orchestrating DNA repair: removal of radiation-induced clustered lesions in DNA. *Bioessays* **23**, 745-749 (2001).
746. J. A. Kim, M. Kruhlak, F. Dotiwala, A. Nussenzweig, J. E. Haber, Heterochromatin is refractory to gamma-H2AX modification in yeast and mammals. *J Cell Biol* **178**, 209-218 (2007).
747. P. Slijepcevic, A. T. Natarajan, Distribution of X-ray-induced G2 chromatid damage among Chinese hamster chromosomes: influence of chromatin conformation. *Mutat Res* **323**, 113-119 (1994).
748. M. Falk, E. Lukasova, S. Kozubek, Chromatin structure influences the sensitivity of DNA to gamma-radiation. *Biochim Biophys Acta* **1783**, 2398-2414 (2008).
749. J. Chen, J. Stubbe, Bleomycins: towards better therapeutics. *Nat Rev Cancer* **5**, 102-112 (2005).
750. L. F. Povirk, DNA damage and mutagenesis by radiomimetic DNA-cleaving agents: bleomycin, neocarzinostatin and other enediynes. *Mutat Res* **355**, 71-89 (1996).
751. K. R. Hande, Etoposide: four decades of development of a topoisomerase II inhibitor. *Eur J Cancer* **34**, 1514-1521 (1998).
752. D. A. Koster, K. Palle, E. S. Bot, M. A. Bjornsti, N. H. Dekker, Antitumour drugs impede DNA uncoiling by topoisomerase I. *Nature* **448**, 213-217 (2007).

753. R. J. Monnat, Jr., A. F. Hackmann, M. A. Cantrell, Generation of highly site-specific DNA double-strand breaks in human cells by the homing endonucleases I-PpoI and I-CreI. *Biochem Biophys Res Commun* **255**, 88-93 (1999).
754. I. Berzsenyi, V. Pantazi, B. N. Borsos, T. Pankotai, Systematic overview on the most widespread techniques for inducing and visualizing the DNA double-strand breaks. *Mutat Res Rev Mutat Res* **788**, 108397 (2021).
755. H. Chandler *et al.*, Role of polycomb group proteins in the DNA damage response--a reassessment. *PLoS One* **9**, e102968 (2014).
756. P. Caron *et al.*, Cohesin protects genes against gammaH2AX Induced by DNA double-strand breaks. *PLoS Genet* **8**, e1002460 (2012).
757. T. Clouaire *et al.*, Comprehensive Mapping of Histone Modifications at DNA Double-Strand Breaks Deciphers Repair Pathway Chromatin Signatures. *Mol Cell* **72**, 250-262 e256 (2018).
758. E. Berkovich, R. J. Monnat, Jr., M. B. Kastan, Assessment of protein dynamics and DNA repair following generation of DNA double-strand breaks at defined genomic sites. *Nat Protoc* **3**, 915-922 (2008).
759. T. Pankotai, C. Bonhomme, D. Chen, E. Soutoglou, DNAPKcs-dependent arrest of RNA polymerase II transcription in the presence of DNA breaks. *Nat Struct Mol Biol* **19**, 276-282 (2012).
760. M. Redman, A. King, C. Watson, D. King, What is CRISPR/Cas9? *Arch Dis Child Educ Pract Ed* **101**, 213-215 (2016).
761. E. Brunner *et al.*, CRISPR-induced double-strand breaks trigger recombination between homologous chromosome arms. *Life Sci Alliance* **2**, (2019).
762. H. Ma *et al.*, CRISPR-Cas9 nuclear dynamics and target recognition in living cells. *J Cell Biol* **214**, 529-537 (2016).
763. C. D. Richardson, G. J. Ray, M. A. DeWitt, G. L. Curie, J. E. Corn, Enhancing homology-directed genome editing by catalytically active and inactive CRISPR-Cas9 using asymmetric donor DNA. *Nat Biotechnol* **34**, 339-344 (2016).
764. H. Yang *et al.*, Methods Favoring Homology-Directed Repair Choice in Response to CRISPR/Cas9 Induced-Double Strand Breaks. *Int J Mol Sci* **21**, (2020).
765. J. P. Anderson *et al.*, Phosphorylation of Ser-129 is the dominant pathological modification of alpha-synuclein in familial and sporadic Lewy body disease. *J Biol Chem* **281**, 29739-29752 (2006).
766. H. Wang *et al.*, Cerebrospinal fluid alpha-synuclein levels are elevated in multiple sclerosis and neuromyelitis optica patients during relapse. *J Neurochem* **122**, 19-23 (2012).
767. T. Stewart *et al.*, Phosphorylated alpha-synuclein in Parkinson's disease: correlation depends on disease severity. *Acta Neuropathol Commun* **3**, 7 (2015).
768. O. M. El-Agnaf *et al.*, Alpha-synuclein implicated in Parkinson's disease is present in extracellular biological fluids, including human plasma. *FASEB J* **17**, 1945-1947 (2003).
769. P. Foulds, D. M. Mann, D. Allsop, Phosphorylated alpha-synuclein as a potential biomarker for Parkinson's disease and related disorders. *Expert Rev Mol Diagn* **12**, 115-117 (2012).

770. L. Chen, M. B. Feany, Alpha-synuclein phosphorylation controls neurotoxicity and inclusion formation in a *Drosophila* model of Parkinson disease. *Nat Neurosci* **8**, 657-663 (2005).
771. M. Neumann *et al.*, Misfolded proteinase K-resistant hyperphosphorylated alpha-synuclein in aged transgenic mice with locomotor deterioration and in human alpha-synucleinopathies. *J Clin Invest* **110**, 1429-1439 (2002).
772. M. Takahashi *et al.*, Phosphorylation of alpha-synuclein characteristic of synucleinopathy lesions is recapitulated in alpha-synuclein transgenic *Drosophila*. *Neurosci Lett* **336**, 155-158 (2003).
773. M. Yamada, T. Iwatsubo, Y. Mizuno, H. Mochizuki, Overexpression of alpha-synuclein in rat substantia nigra results in loss of dopaminergic neurons, phosphorylation of alpha-synuclein and activation of caspase-9: resemblance to pathogenetic changes in Parkinson's disease. *J Neurochem* **91**, 451-461 (2004).
774. G. S. Nubling *et al.*, Modelling Ser129 phosphorylation inhibits membrane binding of pore-forming alpha-synuclein oligomers. *PLoS One* **9**, e98906 (2014).
775. A. N. Pronin, A. J. Morris, A. Surguchov, J. L. Benovic, Synucleins are a novel class of substrates for G protein-coupled receptor kinases. *J Biol Chem* **275**, 26515-26522 (2000).
776. M. A. McFarland, C. E. Ellis, S. P. Markey, R. L. Nussbaum, Proteomics analysis identifies phosphorylation-dependent alpha-synuclein protein interactions. *Mol Cell Proteomics* **7**, 2123-2137 (2008).
777. S. Appel-Cresswell *et al.*, Alpha-synuclein p.H50Q, a novel pathogenic mutation for Parkinson's disease. *Mov Disord* **28**, 811-813 (2013).
778. A. P. Kiely *et al.*, alpha-Synucleinopathy associated with G51D SNCA mutation: a link between Parkinson's disease and multiple system atrophy? *Acta Neuropathol* **125**, 753-769 (2013).
779. S. Lesage *et al.*, G51D alpha-synuclein mutation causes a novel parkinsonian-pyramidal syndrome. *Ann Neurol* **73**, 459-471 (2013).
780. P. Pasanen *et al.*, Novel alpha-synuclein mutation A53E associated with atypical multiple system atrophy and Parkinson's disease-type pathology. *Neurobiol Aging* **35**, 2180 e2181-2185 (2014).
781. C. Proukakis *et al.*, A novel alpha-synuclein missense mutation in Parkinson disease. *Neurology* **80**, 1062-1064 (2013).
782. P. Flagmeier *et al.*, Mutations associated with familial Parkinson's disease alter the initiation and amplification steps of alpha-synuclein aggregation. *Proc Natl Acad Sci U S A* **113**, 10328-10333 (2016).
783. V. Evsyukov *et al.*, Genetic mutations linked to Parkinson's disease differentially control nucleolar activity in pre-symptomatic mouse models. *Dis Model Mech* **10**, 633-643 (2017).
784. S. Vilotti *et al.*, Parkinson's disease DJ-1 L166P alters rRNA biogenesis by exclusion of TTRAP from the nucleolus and sequestration into cytoplasmic aggregates via TRAF6. *PLoS One* **7**, e35051 (2012).
785. R. W. L. So, J. C. Watts, alpha-Synuclein Conformational Strains as Drivers of Phenotypic Heterogeneity in Neurodegenerative Diseases. *J Mol Biol* **435**, 168011 (2023).

786. C. Peng, R. J. Gathagan, V. M. Lee, Distinct alpha-Synuclein strains and implications for heterogeneity among alpha-Synucleinopathies. *Neurobiol Dis* **109**, 209-218 (2018).
787. N. L. Rey *et al.*, alpha-Synuclein conformational strains spread, seed and target neuronal cells differentially after injection into the olfactory bulb. *Acta Neuropathol Commun* **7**, 221 (2019).
788. A. Li, C. Rastegar, X. Mao, alpha-Synuclein Conformational Plasticity: Physiologic States, Pathologic Strains, and Biotechnological Applications. *Biomolecules* **12**, (2022).
789. D. J. Covell *et al.*, Novel conformation-selective alpha-synuclein antibodies raised against different in vitro fibril forms show distinct patterns of Lewy pathology in Parkinson's disease. *Neuropathol Appl Neurobiol* **43**, 604-620 (2017).
790. Y. Bang, J. Lim, H. J. Choi, Recent advances in the pathology of prodromal non-motor symptoms olfactory deficit and depression in Parkinson's disease: clues to early diagnosis and effective treatment. *Arch Pharm Res* **44**, 588-604 (2021).
791. Y. Yang *et al.*, Evolving insights into erythrocytes in synucleinopathies. *Trends Neurosci* **47**, 693-707 (2024).
792. J. Matsumoto *et al.*, Transmission of alpha-synuclein-containing erythrocyte-derived extracellular vesicles across the blood-brain barrier via adsorptive mediated transcytosis: another mechanism for initiation and progression of Parkinson's disease? *Acta Neuropathol Commun* **5**, 71 (2017).
793. L. Sheng *et al.*, Erythrocytic alpha-synuclein contained in microvesicles regulates astrocytic glutamate homeostasis: a new perspective on Parkinson's disease pathogenesis. *Acta Neuropathol Commun* **8**, 102 (2020).
794. N. C. Prymaczek *et al.*, Cell-to-cell transmitted alpha-synuclein recapitulates experimental Parkinson's disease. *NPJ Parkinsons Dis* **10**, 10 (2024).
795. A. Benito-Martin, M. G. Jasiulionis, S. Garcia-Silva, Extracellular vesicles and melanoma: New perspectives on tumor microenvironment and metastasis. *Front Cell Dev Biol* **10**, 1061982 (2022).
796. J. W. Brown *et al.*, beta-Synuclein suppresses both the initiation and amplification steps of alpha-synuclein aggregation via competitive binding to surfaces. *Sci Rep* **6**, 36010 (2016).
797. J. Hayashi, J. A. Carver, beta-Synuclein: An Enigmatic Protein with Diverse Functionality. *Biomolecules* **12**, (2022).
798. M. Hashimoto *et al.*, Beta-synuclein regulates Akt activity in neuronal cells. A possible mechanism for neuroprotection in Parkinson's disease. *J Biol Chem* **279**, 23622-23629 (2004).
799. I. Surgucheva, N. Ninkina, V. L. Buchman, K. Grasing, A. Surguchov, Protein aggregation in retinal cells and approaches to cell protection. *Cell Mol Neurobiol* **25**, 1051-1066 (2005).
800. V. L. Buchman, J. Adu, L. G. Pinon, N. N. Ninkina, A. M. Davies, Persyn, a member of the synuclein family, influences neurofilament network integrity. *Nat Neurosci* **1**, 101-103 (1998).
801. L. C. Zanotti *et al.*, Synuclein Proteins in Cancer Development and Progression. *Biomolecules* **13**, (2023).

802. W. Bruening *et al.*, Synucleins are expressed in the majority of breast and ovarian carcinomas and in preneoplastic lesions of the ovary. *Cancer* **88**, 2154-2163 (2000).
803. K. M. Fung, L. B. Rorke, B. Giasson, V. M. Lee, J. Q. Trojanowski, Expression of alpha-, beta-, and gamma-synuclein in glial tumors and medulloblastomas. *Acta Neuropathol* **106**, 167-175 (2003).
804. Q. Ye *et al.*, Expression of alpha-, beta- and gamma-synuclein in colorectal cancer, and potential clinical significance in progression of the disease. *Oncol Rep* **23**, 429-436 (2010).
805. R. W. Maitta *et al.*, Alpha- and beta-synucleins are new diagnostic tools for acute erythroid leukemia and acute megakaryoblastic leukemia. *Am J Hematol* **86**, 230-234 (2011).
806. H. Ji *et al.*, Identification of a breast cancer-specific gene, BCSG1, by direct differential cDNA sequencing. *Cancer Res* **57**, 759-764 (1997).
807. T. Jia, Y. E. Liu, J. Liu, Y. E. Shi, Stimulation of breast cancer invasion and metastasis by synuclein gamma. *Cancer Res* **59**, 742-747 (1999).
808. Z. Z. Pan, W. Bruening, B. I. Giasson, V. M. Lee, A. K. Godwin, Gamma-synuclein promotes cancer cell survival and inhibits stress- and chemotherapy drug-induced apoptosis by modulating MAPK pathways. *J Biol Chem* **277**, 35050-35060 (2002).
809. A. Surguchov, R. E. Palazzo, I. Surgucheva, Gamma synuclein: subcellular localization in neuronal and non-neuronal cells and effect on signal transduction. *Cell Motil Cytoskeleton* **49**, 218-228 (2001).
810. C. Q. Zhou *et al.*, Down-regulation of gamma-synuclein in human esophageal squamous cell carcinoma. *World J Gastroenterol* **9**, 1900-1903 (2003).
811. Z. Li *et al.*, Overexpression of synuclein-gamma in pancreatic adenocarcinoma. *Cancer* **101**, 58-65 (2004).
812. N. Yanagawa *et al.*, Demethylation of the synuclein gamma gene CpG island in primary gastric cancers and gastric cancer cell lines. *Clin Cancer Res* **10**, 2447-2451 (2004).
813. H. Iwaki *et al.*, Diagnostic potential in bladder cancer of a panel of tumor markers (calreticulin, gamma -synuclein, and catechol-o-methyltransferase) identified by proteomic analysis. *Cancer Sci* **95**, 955-961 (2004).
814. H. Liu *et al.*, Loss of epigenetic control of synuclein-gamma gene as a molecular indicator of metastasis in a wide range of human cancers. *Cancer Res* **65**, 7635-7643 (2005).
815. Q. Ye *et al.*, Aberrant expression and demethylation of gamma-synuclein in colorectal cancer, correlated with progression of the disease. *Cancer Sci* **99**, 1924-1932 (2008).
816. J. Morgan *et al.*, Synuclein-gamma (SNCG) may be a novel prognostic biomarker in uterine papillary serous carcinoma. *Gynecol Oncol* **114**, 293-298 (2009).
817. P. Mhawech-Fauceglia *et al.*, Synuclein-gamma (SNCG) protein expression is associated with poor outcome in endometrial adenocarcinoma. *Gynecol Oncol* **124**, 148-152 (2012).
818. J. C. Cheng *et al.*, gamma-Synuclein Expression Is a Malignant Index in Oral Squamous Cell Carcinoma. *J Dent Res* **95**, 439-445 (2016).

819. Y. Takemura *et al.*, Gamma-synuclein is a novel prognostic marker that promotes tumor cell migration in biliary tract carcinoma. *Cancer Med* **10**, 5599-5613 (2021).
820. A. A. Hyman, C. A. Weber, F. Julicher, Liquid-liquid phase separation in biology. *Annu Rev Cell Dev Biol* **30**, 39-58 (2014).
821. M. Feric *et al.*, Coexisting Liquid Phases Underlie Nucleolar Subcompartments. *Cell* **165**, 1686-1697 (2016).
822. D. L. J. Lafontaine, J. A. Riback, R. Bascetin, C. P. Brangwynne, The nucleolus as a multiphase liquid condensate. *Nat Rev Mol Cell Biol* **22**, 165-182 (2021).
823. J. Chen, J. Shi, J. Zheng, Y. Wang, X. Wan, Liquid-liquid phase separation in DNA double-strand break repair. *Cancer Biol Med* **20**, 627-632 (2023).
824. A. K. Dunker *et al.*, The unfoldomics decade: an update on intrinsically disordered proteins. *BMC Genomics* **9 Suppl 2**, S1 (2008).
825. P. E. Wright, H. J. Dyson, Intrinsically disordered proteins in cellular signalling and regulation. *Nat Rev Mol Cell Biol* **16**, 18-29 (2015).
826. V. N. Uversky, C. J. Oldfield, A. K. Dunker, Intrinsically disordered proteins in human diseases: introducing the D2 concept. *Annu Rev Biophys* **37**, 215-246 (2008).
827. S. Mukherjee *et al.*, Liquid-liquid Phase Separation of alpha-Synuclein: A New Mechanistic Insight for alpha-Synuclein Aggregation Associated with Parkinson's Disease Pathogenesis. *J Mol Biol* **435**, 167713 (2023).
828. K. Matsuo *et al.*, RNA G-quadruplexes form scaffolds that promote neuropathological alpha-synuclein aggregation. *Cell* **187**, 6835-6848 e6820 (2024).
829. B. Xu *et al.*, Distinct Effects of Familial Parkinson's Disease-Associated Mutations on alpha-Synuclein Phase Separation and Amyloid Aggregation. *Biomolecules* **13**, (2023).
830. L. Zhang *et al.*, 53BP1 regulates heterochromatin through liquid phase separation. *Nat Commun* **13**, 360 (2022).
831. A. Agarwal *et al.*, VAMP2 regulates phase separation of alpha-synuclein. *Nat Cell Biol* **26**, 1296-1308 (2024).
832. C. Hoffmann *et al.*, Synapsin Condensates Recruit alpha-Synuclein. *J Mol Biol* **433**, 166961 (2021).
833. O. I. Povarova, I. A. Antifeeva, A. V. Fonin, K. K. Turoverov, I. M. Kuznetsova, The Role of Liquid-Liquid Phase Separation in Actin Polymerization. *Int J Mol Sci* **24**, (2023).
834. S. Yang *et al.*, Self-construction of actin networks through phase separation-induced abLIM1 condensates. *Proc Natl Acad Sci U S A* **119**, e2122420119 (2022).
835. J. X. Liu *et al.*, Liquid-liquid phase separation within fibrillar networks. *Nat Commun* **14**, 6085 (2023).
836. V. L. Sousa *et al.*, alpha-synuclein and its A30P mutant affect actin cytoskeletal structure and dynamics. *Mol Biol Cell* **20**, 3725-3739 (2009).
837. M. I. Oliveira da Silva, M. A. Liz, Linking Alpha-Synuclein to the Actin Cytoskeleton: Consequences to Neuronal Function. *Front Cell Dev Biol* **8**, 787 (2020).

838. S. Elmore, Apoptosis: a review of programmed cell death. *Toxicol Pathol* **35**, 495-516 (2007).
839. B. Kaina, DNA damage-triggered apoptosis: critical role of DNA repair, double-strand breaks, cell proliferation and signaling. *Biochem Pharmacol* **66**, 1547-1554 (2003).
840. D. De Zio, V. Cianfanelli, F. Cecconi, New insights into the link between DNA damage and apoptosis. *Antioxid Redox Signal* **19**, 559-571 (2013).
841. W. P. Roos, B. Kaina, DNA damage-induced cell death by apoptosis. *Trends Mol Med* **12**, 440-450 (2006).
842. M. Pietrzak *et al.*, Nucleolar disruption and apoptosis are distinct neuronal responses to etoposide-induced DNA damage. *J Neurochem* **117**, 1033-1046 (2011).
843. N. Lev, E. Melamed, D. Offen, Apoptosis and Parkinson's disease. *Prog Neuropsychopharmacol Biol Psychiatry* **27**, 245-250 (2003).
844. H. A. Elfawy, B. Das, Crosstalk between mitochondrial dysfunction, oxidative stress, and age related neurodegenerative disease: Etiologies and therapeutic strategies. *Life Sci* **218**, 165-184 (2019).
845. A. Nicotra, S. Parvez, Apoptotic molecules and MPTP-induced cell death. *Neurotoxicol Teratol* **24**, 599-605 (2002).
846. K. Utani, Y. Kohno, A. Okamoto, N. Shimizu, Emergence of micronuclei and their effects on the fate of cells under replication stress. *PLoS One* **5**, e10089 (2010).
847. E. Fielder, T. von Zglinicki, D. Jurk, The DNA Damage Response in Neurons: Die by Apoptosis or Survive in a Senescence-Like State? *J Alzheimers Dis* **60**, S107-S131 (2017).
848. C. Martinez-Cue, N. Rueda, Cellular Senescence in Neurodegenerative Diseases. *Front Cell Neurosci* **14**, 16 (2020).
849. K. D. van Dijk *et al.*, Changes in endolysosomal enzyme activities in cerebrospinal fluid of patients with Parkinson's disease. *Mov Disord* **28**, 747-754 (2013).
850. S. J. Chinta *et al.*, Cellular Senescence Is Induced by the Environmental Neurotoxin Paraquat and Contributes to Neuropathology Linked to Parkinson's Disease. *Cell Rep* **22**, 930-940 (2018).
851. D. K. Verma *et al.*, Alpha-Synuclein Preformed Fibrils Induce Cellular Senescence in Parkinson's Disease Models. *Cells* **10**, (2021).
852. A. Slipicevic, M. Herlyn, Narrowing the knowledge gaps for melanoma. *Ups J Med Sci* **117**, 237-243 (2012).
853. J. Quin *et al.*, Inhibition of RNA polymerase I transcription initiation by CX-5461 activates non-canonical ATM/ATR signaling. *Oncotarget* **7**, 49800-49818 (2016).
854. E. Colombo, J. C. Marine, D. Danovi, B. Falini, P. G. Pelicci, Nucleophosmin regulates the stability and transcriptional activity of p53. *Nat Cell Biol* **4**, 529-533 (2002).
855. J. C. Wong *et al.*, Nucleophosmin 1, upregulated in adenomas and cancers of the colon, inhibits p53-mediated cellular senescence. *Int J Cancer* **133**, 1567-1577 (2013).

856. Z. Li *et al.*, Impaired DNA double-strand break repair contributes to the age-associated rise of genomic instability in humans. *Cell Death Differ* **23**, 1765-1777 (2016).
857. R. R. White, J. Vijg, Do DNA Double-Strand Breaks Drive Aging? *Mol Cell* **63**, 729-738 (2016).
858. N. Rodriguez-Losada *et al.*, Overexpression of alpha-synuclein promotes both cell proliferation and cell toxicity in human SH-SY5Y neuroblastoma cells. *J Adv Res* **23**, 37-45 (2020).
859. J. Belhadj, S. Surina, M. Hengstschlager, A. J. Lomakin, Form follows function: Nuclear morphology as a quantifiable predictor of cellular senescence. *Aging Cell* **22**, e14012 (2023).
860. K. Krupina, A. Goginashvili, D. W. Cleveland, Causes and consequences of micronuclei. *Curr Opin Cell Biol* **70**, 91-99 (2021).
861. K. Suzuki, K. Kawamura, R. Ujiie, T. Nakayama, N. Mitsutake, Characterization of radiation-induced micronuclei associated with premature senescence, and their selective removal by senolytic drug, ABT-263. *Mutat Res Genet Toxicol Environ Mutagen* **876-877**, 503448 (2022).
862. M. Kirsch-Volders, M. Fenech, Towards prevention of aneuploidy-associated cellular senescence and aging: more questions than answers? *Mutat Res Rev Mutat Res* **792**, 108474 (2023).
863. E. Bochkareva *et al.*, Single-stranded DNA mimicry in the p53 transactivation domain interaction with replication protein A. *Proc Natl Acad Sci U S A* **102**, 15412-15417 (2005).
864. F. A. Derheimer *et al.*, RPA and ATR link transcriptional stress to p53. *Proc Natl Acad Sci U S A* **104**, 12778-12783 (2007).
865. M. A. Serrano *et al.*, DNA-PK, ATM and ATR collaboratively regulate p53-RPA interaction to facilitate homologous recombination DNA repair. *Oncogene* **32**, 2452-2462 (2013).
866. R. Dok *et al.*, p16INK4a impairs homologous recombination-mediated DNA repair in human papillomavirus-positive head and neck tumors. *Cancer Res* **74**, 1739-1751 (2014).
867. A. T. Vessoni, E. C. Filippi-Chiela, C. F. Menck, G. Lenz, Autophagy and genomic integrity. *Cell Death Differ* **20**, 1444-1454 (2013).
868. V. V. Eapen *et al.*, A pathway of targeted autophagy is induced by DNA damage in budding yeast. *Proc Natl Acad Sci U S A* **114**, E1158-E1167 (2017).
869. T. Juretschke, P. Beli, Causes and consequences of DNA damage-induced autophagy. *Matrix Biol* **100-101**, 39-53 (2021).
870. Y. Chen *et al.*, CHK2-FOXK axis promotes transcriptional control of autophagy programs. *Sci Adv* **6**, eaax5819 (2020).
871. G. Konstantinidis, N. Tavernarakis, Autophagy of the Nucleus in Health and Disease. *Front Cell Dev Biol* **9**, 814955 (2021).
872. M. Zhao *et al.*, CGAS is a micronucleophagy receptor for the clearance of micronuclei. *Autophagy* **17**, 3976-3991 (2021).
873. B. Levine, G. Kroemer, Autophagy in the pathogenesis of disease. *Cell* **132**, 27-42 (2008).

874. A. Fleming *et al.*, The different autophagy degradation pathways and neurodegeneration. *Neuron* **110**, 935-966 (2022).
875. X. Hou, J. O. Watzlawik, F. C. Fiesel, W. Springer, Autophagy in Parkinson's Disease. *J Mol Biol* **432**, 2651-2672 (2020).
876. E. D. Plowey, S. J. Cherra, 3rd, Y. J. Liu, C. T. Chu, Role of autophagy in G2019S-LRRK2-associated neurite shortening in differentiated SH-SY5Y cells. *J Neurochem* **105**, 1048-1056 (2008).
877. A. M. Pickrell, R. J. Youle, The roles of PINK1, parkin, and mitochondrial fidelity in Parkinson's disease. *Neuron* **85**, 257-273 (2015).
878. M. T. Rosenfeldt *et al.*, Loss of autophagy affects melanoma development in a manner dependent on PTEN status. *Cell Death Differ* **28**, 1437-1439 (2021).
879. L. Di Leo, V. Bodemeyer, D. De Zio, The Complex Role of Autophagy in Melanoma Evolution: New Perspectives From Mouse Models. *Front Oncol* **9**, 1506 (2019).
880. A. Ndoye, A. T. Weeraratna, Autophagy- An emerging target for melanoma therapy. *F1000Res* **5**, (2016).
881. C. Pangilinan, X. Xu, M. Herlyn, C. Liang, Autophagy Paradox: Strategizing Treatment Modality in Melanoma. *Curr Treat Options Oncol* **24**, 130-145 (2023).
882. F. G. Haluska *et al.*, Genetic alterations in signaling pathways in melanoma. *Clin Cancer Res* **12**, 2301s-2307s (2006).
883. N. M. Mhaidat *et al.*, Temozolomide induces senescence but not apoptosis in human melanoma cells. *Br J Cancer* **97**, 1225-1233 (2007).
884. S. Haferkamp *et al.*, Vemurafenib induces senescence features in melanoma cells. *J Invest Dermatol* **133**, 1601-1609 (2013).
885. J. Zieba *et al.*, Sensitivity of neoplastic cells to senescence unveiled under standard cell culture conditions. *Anticancer Res* **35**, 2759-2768 (2015).
886. K. A. Avery-Kiejda *et al.*, Small molecular weight variants of p53 are expressed in human melanoma cells and are induced by the DNA-damaging agent cisplatin. *Clin Cancer Res* **14**, 1659-1668 (2008).
887. K. A. Avery-Kiejda *et al.*, P53 in human melanoma fails to regulate target genes associated with apoptosis and the cell cycle and may contribute to proliferation. *BMC Cancer* **11**, 203 (2011).
888. H. Gong *et al.*, Amyloidogenicity of p53: A Hidden Link Between Protein Misfolding and Cancer. *Curr Protein Pept Sci*, (2014).
889. A. P. Ano Bom *et al.*, Mutant p53 aggregates into prion-like amyloid oligomers and fibrils: implications for cancer. *J Biol Chem* **287**, 28152-28162 (2012).
890. N. Iwahashi *et al.*, Sulfated glycosaminoglycans mediate prion-like behavior of p53 aggregates. *Proc Natl Acad Sci U S A* **117**, 33225-33234 (2020).
891. M. Brenner, V. J. Hearing, The protective role of melanin against UV damage in human skin. *Photochem Photobiol* **84**, 539-549 (2008).
892. E. Perez-Guijarro, C. P. Day, G. Merlino, M. R. Zaidi, Genetically engineered mouse models of melanoma. *Cancer* **123**, 2089-2103 (2017).
893. E. C. De Fabo, F. P. Noonan, T. Fears, G. Merlino, Ultraviolet B but not ultraviolet A radiation initiates melanoma. *Cancer Res* **64**, 6372-6376 (2004).
894. F. P. Noonan *et al.*, Neonatal sunburn and melanoma in mice. *Nature* **413**, 271-272 (2001).

895. P. Haninec, J. Vachtenheim, Tyrosinase protein is expressed also in some neural crest derived cells which are not melanocytes. *Pigment Cell Res* **1**, 340-343 (1988).
896. L. Hou, J. J. Panthier, H. Arnheiter, Signaling and transcriptional regulation in the neural crest-derived melanocyte lineage: interactions between KIT and MITF. *Development* **127**, 5379-5389 (2000).
897. S. Santhosh Kumar *et al.*, Sequential CRISPR screening reveals partial NatB inhibition as a strategy to mitigate alpha-synuclein levels in human neurons. *Sci Adv* **10**, eadj4767 (2024).
898. S. Zou, K. Scarfo, M. H. Nantz, J. G. Hecker, Lipid-mediated delivery of RNA is more efficient than delivery of DNA in non-dividing cells. *Int J Pharm* **389**, 232-243 (2010).
899. A. Yamamoto, M. Kormann, J. Rosenecker, C. Rudolph, Current prospects for mRNA gene delivery. *Eur J Pharm Biopharm* **71**, 484-489 (2009).
900. U. Gioia *et al.*, Pharmacological boost of DNA damage response and repair by enhanced biogenesis of DNA damage response RNAs. *Sci Rep* **9**, 6460 (2019).
901. N. R. Smalheiser, H. Zhang, Y. Dwivedi, Enoxacin Elevates MicroRNA Levels in Rat Frontal Cortex and Prevents Learned Helplessness. *Front Psychiatry* **5**, 6 (2014).
902. D. L. Price *et al.*, In vivo effects of the alpha-synuclein misfolding inhibitor minzasolmin supports clinical development in Parkinson's disease. *NPJ Parkinsons Dis* **9**, 114 (2023).
903. J. Pujols *et al.*, Small molecule inhibits alpha-synuclein aggregation, disrupts amyloid fibrils, and prevents degeneration of dopaminergic neurons. *Proc Natl Acad Sci U S A* **115**, 10481-10486 (2018).
904. M. Hetman, M. Pietrzak, Emerging roles of the neuronal nucleolus. *Trends Neurosci* **35**, 305-314 (2012).
905. S. Mizielinska *et al.*, Bidirectional nucleolar dysfunction in C9orf72 frontotemporal lobar degeneration. *Acta Neuropathol Commun* **5**, 29 (2017).
906. J. G. O'Rourke *et al.*, C9orf72 BAC Transgenic Mice Display Typical Pathologic Features of ALS/FTD. *Neuron* **88**, 892-901 (2015).
907. J. D. Erickson, N. G. Bazan, The nucleolus fine-tunes the orchestration of an early neuroprotection response in neurodegeneration. *Cell Death Differ* **20**, 1435-1437 (2013).
908. R. L. Hamilton, Lewy bodies in Alzheimer's disease: a neuropathological review of 145 cases using alpha-synuclein immunohistochemistry. *Brain Pathol* **10**, 378-384 (2000).
909. K. A. Jellinger, Alpha-synuclein pathology in Parkinson's and Alzheimer's disease brain: incidence and topographic distribution--a pilot study. *Acta Neuropathol* **106**, 191-201 (2003).
910. P. T. Kotzbauer, J. Q. Trojanowsk, V. M. Lee, Lewy body pathology in Alzheimer's disease. *J Mol Neurosci* **17**, 225-232 (2001).
911. J. Roudil *et al.*, Influence of Lewy Pathology on Alzheimer's Disease Phenotype: A Retrospective Clinico-Pathological Study. *J Alzheimers Dis* **63**, 1317-1323 (2018).

912. D. Twohig, H. M. Nielsen, alpha-synuclein in the pathophysiology of Alzheimer's disease. *Mol Neurodegener* **14**, 23 (2019).
913. J. B. Leverenz *et al.*, Lewy body pathology in familial Alzheimer disease: evidence for disease- and mutation-specific pathologic phenotype. *Arch Neurol* **63**, 370-376 (2006).
914. A. S. Buchman *et al.*, Nigral pathology and parkinsonian signs in elders without Parkinson disease. *Ann Neurol* **71**, 258-266 (2012).
915. D. Iacono *et al.*, Parkinson disease and incidental Lewy body disease: Just a question of time? *Neurology* **85**, 1670-1679 (2015).
916. J. Y. Lin, D. E. Fisher, Melanocyte biology and skin pigmentation. *Nature* **445**, 843-850 (2007).
917. E. R. Price *et al.*, alpha-Melanocyte-stimulating hormone signaling regulates expression of microphthalmia, a gene deficient in Waardenburg syndrome. *J Biol Chem* **273**, 33042-33047 (1998).
918. I. Rainero, L. Pinessi, Alpha-MSH and Parkinson disease. *Ital J Neurol Sci* **9**, 95-96 (1988).
919. Y. Konagaya, M. Konagaya, [Abnormality of hypothalamic dopaminergic system in neuro-degenerative diseases--evaluation of alpha-melanocyte-stimulating hormone-like immunoreactivity in cerebrospinal fluid]. *Rinsho Shinkeigaku* **31**, 821-825 (1991).
920. H. L. Dela Cruz *et al.*, New insights underlying the early events of dopaminergic dysfunction in Parkinson's Disease. *bioRxiv*, 2020.2009.2027.313957 (2023).
921. E. M. Wolf Horrell, M. C. Boulanger, J. A. D'Orazio, Melanocortin 1 Receptor: Structure, Function, and Regulation. *Front Genet* **7**, 95 (2016).
922. Z. A. Abdel-Malek *et al.*, Melanocortins and the melanocortin 1 receptor, moving translationally towards melanoma prevention. *Arch Biochem Biophys* **563**, 4-12 (2014).
923. X. Song *et al.*, alpha-MSH activates immediate defense responses to UV-induced oxidative stress in human melanocytes. *Pigment Cell Melanoma Res* **22**, 809-818 (2009).
924. V. Swope *et al.*, Significance of the melanocortin 1 receptor in the DNA damage response of human melanocytes to ultraviolet radiation. *Pigment Cell Melanoma Res* **27**, 601-610 (2014).
925. S. G. Jarrett, E. M. Wolf Horrell, M. C. Boulanger, J. A. D'Orazio, Defining the Contribution of MC1R Physiological Ligands to ATR Phosphorylation at Ser435, a Predictor of DNA Repair in Melanocytes. *J Invest Dermatol* **135**, 3086-3095 (2015).
926. A. Seluanov, Z. Mao, V. Gorbunova, Analysis of DNA double-strand break (DSB) repair in mammalian cells. *J Vis Exp*, (2010).
927. P. Mertins *et al.*, Reproducible workflow for multiplexed deep-scale proteome and phosphoproteome analysis of tumor tissues by liquid chromatography-mass spectrometry. *Nat Protoc* **13**, 1632-1661 (2018).
928. D. D. Wiredja, M. Koyuturk, M. R. Chance, The KSEA App: a web-based tool for kinase activity inference from quantitative phosphoproteomics. *Bioinformatics* **33**, 3489-3491 (2017).

929. D. M. Stults, M. W. Killen, H. H. Pierce, A. J. Pierce, Genomic architecture and inheritance of human ribosomal RNA gene clusters. *Genome Res* **18**, 13-18 (2008).
930. J. G. Gibbons, A. T. Branco, S. A. Godinho, S. Yu, B. Lemos, Concerted copy number variation balances ribosomal DNA dosage in human and mouse genomes. *Proc Natl Acad Sci U S A* **112**, 2485-2490 (2015).
931. S. Ide, T. Miyazaki, H. Maki, T. Kobayashi, Abundance of ribosomal RNA gene copies maintains genome integrity. *Science* **327**, 693-696 (2010).
932. M. Wang, B. Lemos, Ribosomal DNA copy number amplification and loss in human cancers is linked to tumor genetic context, nucleolus activity, and proliferation. *PLoS Genet* **13**, e1006994 (2017).
933. J. Xuan, K. Gitareja, N. Brajanovski, E. Sanij, Harnessing the Nucleolar DNA Damage Response in Cancer Therapy. *Genes (Basel)* **12**, (2021).
934. J. Diesch, R. D. Hannan, E. Sanij, Perturbations at the ribosomal genes loci are at the centre of cellular dysfunction and human disease. *Cell Biosci* **4**, 43 (2014).
935. A. M. Martinez, A. Kim, W. S. Yang, Detection of Ferroptosis by BODIPY 581/591 C11. *Methods Mol Biol* **2108**, 125-130 (2020).
936. U. Weyemi *et al.*, The histone variant H2A.X is a regulator of the epithelial-mesenchymal transition. *Nat Commun* **7**, 10711 (2016).
937. U. Weyemi *et al.*, Twist1 and Slug mediate H2AX-regulated epithelial-mesenchymal transition in breast cells. *Cell Cycle* **15**, 2398-2404 (2016).
938. V. Chesnokova *et al.*, Excess growth hormone suppresses DNA damage repair in epithelial cells. *JCI Insight* **4**, (2019).
939. S. J. Pearson *et al.*, ATM-dependent activation of SIM2s regulates homologous recombination and epithelial-mesenchymal transition. *Oncogene* **38**, 2611-2626 (2019).
940. M. Bozic *et al.*, Protective role of renal proximal tubular alpha-synuclein in the pathogenesis of kidney fibrosis. *Nat Commun* **11**, 1943 (2020).
941. A. R. Collins *et al.*, The comet assay: topical issues. *Mutagenesis* **23**, 143-151 (2008).
942. Z. Mao, M. Bozzella, A. Seluanov, V. Gorbunova, Comparison of nonhomologous end joining and homologous recombination in human cells. *DNA Repair (Amst)* **7**, 1765-1771 (2008).
943. D. Z. Bar *et al.*, Biotinylation by antibody recognition-a method for proximity labeling. *Nat Methods* **15**, 127-133 (2018).
944. M. Bergeron *et al.*, In vivo modulation of polo-like kinases supports a key role for PLK2 in Ser129 alpha-synuclein phosphorylation in mouse brain. *Neuroscience* **256**, 72-82 (2014).
945. K. J. Inglis *et al.*, Polo-like kinase 2 (PLK2) phosphorylates alpha-synuclein at serine 129 in central nervous system. *J Biol Chem* **284**, 2598-2602 (2009).
946. M. K. Mbefo *et al.*, Phosphorylation of synucleins by members of the Polo-like kinase family. *J Biol Chem* **285**, 2807-2822 (2010).
947. S. Goncalves, T. F. Outeiro, Assessing the subcellular dynamics of alpha-synuclein using photoactivation microscopy. *Mol Neurobiol* **47**, 1081-1092 (2013).

948. L. J. Weston *et al.*, Genetic deletion of Polo-like kinase 2 reduces alpha-synuclein serine-129 phosphorylation in presynaptic terminals but not Lewy bodies. *J Biol Chem* **296**, 100273 (2021).
949. E. P. Rose, J. S. Banga, V. K. Unni, Polo-like kinase inhibition leads to neuroprotection of neurons bearing alpha-synuclein Lewy body-like inclusions in vivo. *MicroPubl Biol* **2024**, (2024).
950. C. Cui, H. Tseng, Estimation of ribosomal RNA transcription rate in situ. *Biotechniques* **36**, 134-138 (2004).
951. L. G. Morello *et al.*, The NIP7 protein is required for accurate pre-rRNA processing in human cells. *Nucleic Acids Res* **39**, 648-665 (2011).
952. M. Gerhalter *et al.*, The novel pre-rRNA detection workflow "Riboprobing" allows simple identification of undescribed RNA species. *RNA* **30**, 807-823 (2024).
953. T. Nakamura, H. Imai, N. Tsunashima, Y. Nakagawa, Molecular cloning and functional expression of nucleolar phospholipid hydroperoxide glutathione peroxidase in mammalian cells. *Biochem Biophys Res Commun* **311**, 139-148 (2003).
954. Y. J. Wu, M. A. Pagel, L. L. Muldoon, R. Fu, E. A. Neuwelt, High alpha-v Integrin Level of Cancer Cells Is Associated with Development of Brain Metastasis in Athymic Rats. *Anticancer Res* **37**, 4029-4040 (2017).
955. T. He *et al.*, Comparative Evaluation of Proteome Discoverer and FragPipe for the TMT-Based Proteome Quantification. *J Proteome Res* **21**, 3007-3015 (2022).
956. P. V. Hornbeck *et al.*, PhosphoSitePlus: a comprehensive resource for investigating the structure and function of experimentally determined post-translational modifications in man and mouse. *Nucleic Acids Res* **40**, D261-270 (2012).
957. C. F. Orr, D. B. Rowe, Y. Mizuno, H. Mori, G. M. Halliday, A possible role for humoral immunity in the pathogenesis of Parkinson's disease. *Brain* **128**, 2665-2674 (2005).
958. L. M. Smith, M. C. Schiess, M. P. Coffey, A. C. Klaver, D. A. Loeffler, alpha-Synuclein and anti-alpha-synuclein antibodies in Parkinson's disease, atypical Parkinson syndromes, REM sleep behavior disorder, and healthy controls. *PLoS One* **7**, e52285 (2012).
959. D. Sulzer *et al.*, T cells from patients with Parkinson's disease recognize alpha-synuclein peptides. *Nature* **546**, 656-661 (2017).
960. A. Shameli *et al.*, A critical role for alpha-synuclein in development and function of T lymphocytes. *Immunobiology* **221**, 333-340 (2016).
961. W. Xiao, A. Shameli, C. V. Harding, H. J. Meyerson, R. W. Maitta, Late stages of hematopoiesis and B cell lymphopoiesis are regulated by alpha-synuclein, a key player in Parkinson's disease. *Immunobiology* **219**, 836-844 (2014).
962. C. E. Schrader, J. E. Guikema, E. K. Linehan, E. Selsing, J. Stavnezer, Activation-induced cytidine deaminase-dependent DNA breaks in class switch recombination occur during G1 phase of the cell cycle and depend upon mismatch repair. *J Immunol* **179**, 6064-6071 (2007).
963. A. Kotnis, L. Du, C. Liu, S. W. Popov, Q. Pan-Hammarstrom, Non-homologous end joining in class switch recombination: the beginning of the end. *Philos Trans R Soc Lond B Biol Sci* **364**, 653-665 (2009).

964. A. Zaheen, A. Martin, Induction and assessment of class switch recombination in purified murine B cells. *J Vis Exp*, (2010).
965. E. J. Chung *et al.*, Clinical Features of Alzheimer Disease With and Without Lewy Bodies. *JAMA Neurol* **72**, 789-796 (2015).
966. A. R. Merdes *et al.*, Influence of Alzheimer pathology on clinical diagnostic accuracy in dementia with Lewy bodies. *Neurology* **60**, 1586-1590 (2003).
967. Z. A. Sorrentino *et al.*, Unique alpha-synuclein pathology within the amygdala in Lewy body dementia: implications for disease initiation and progression. *Acta Neuropathol Commun* **7**, 142 (2019).
968. P. T. Nelson *et al.*, The Amygdala as a Locus of Pathologic Misfolding in Neurodegenerative Diseases. *J Neuropathol Exp Neurol* **77**, 2-20 (2018).
969. G. Fairfoul *et al.*, Alpha-synuclein RT-QuIC in the CSF of patients with alpha-synucleinopathies. *Ann Clin Transl Neurol* **3**, 812-818 (2016).
970. M. Shahnawaz *et al.*, Development of a Biochemical Diagnosis of Parkinson Disease by Detection of alpha-Synuclein Misfolded Aggregates in Cerebrospinal Fluid. *JAMA Neurol* **74**, 163-172 (2017).
971. B. R. Groveman *et al.*, Rapid and ultra-sensitive quantitation of disease-associated alpha-synuclein seeds in brain and cerebrospinal fluid by alphaSyn RT-QuIC. *Acta Neuropathol Commun* **6**, 7 (2018).
972. S. Manne *et al.*, alpha-Synuclein real-time quaking-induced conversion in the submandibular glands of Parkinson's disease patients. *Mov Disord* **35**, 268-278 (2020).
973. C. M. G. De Luca *et al.*, Efficient RT-QuIC seeding activity for alpha-synuclein in olfactory mucosa samples of patients with Parkinson's disease and multiple system atrophy. *Transl Neurodegener* **8**, 24 (2019).
974. L. Concha-Marambio *et al.*, Seed Amplification Assay to Diagnose Early Parkinson's and Predict Dopaminergic Deficit Progression. *Mov Disord* **36**, 2444-2446 (2021).
975. M. J. Russo *et al.*, High diagnostic performance of independent alpha-synuclein seed amplification assays for detection of early Parkinson's disease. *Acta Neuropathol Commun* **9**, 179 (2021).
976. U. J. Kang *et al.*, Comparative study of cerebrospinal fluid alpha-synuclein seeding aggregation assays for diagnosis of Parkinson's disease. *Mov Disord* **34**, 536-544 (2019).
977. M. Rossi *et al.*, Ultrasensitive RT-QuIC assay with high sensitivity and specificity for Lewy body-associated synucleinopathies. *Acta Neuropathol* **140**, 49-62 (2020).
978. W. Singer *et al.*, Alpha-Synuclein Oligomers and Neurofilament Light Chain in Spinal Fluid Differentiate Multiple System Atrophy from Lewy Body Synucleinopathies. *Ann Neurol* **88**, 503-512 (2020).
979. M. Shahnawaz, T. Bilkis, I. S. Park, Amyloid beta cytotoxicity is enhanced or reduced depending on formation of amyloid beta oligomeric forms. *Biotechnol Lett* **43**, 165-175 (2021).
980. W. Singer *et al.*, Alpha-Synuclein Oligomers and Neurofilament Light Chain Predict Phenoconversion of Pure Autonomic Failure. *Ann Neurol* **89**, 1212-1220 (2021).

981. I. Poggiolini *et al.*, RT-QuIC Using C-Terminally Truncated alpha-Synuclein Forms Detects Differences in Seeding Propensity of Different Brain Regions from Synucleinopathies. *Biomolecules* **11**, (2021).
982. C. H. Adler *et al.*, Low clinical diagnostic accuracy of early vs advanced Parkinson disease: clinicopathologic study. *Neurology* **83**, 406-412 (2014).
983. D. J. Irwin *et al.*, Neuropathologic substrates of Parkinson disease dementia. *Ann Neurol* **72**, 587-598 (2012).
984. D. J. Irwin *et al.*, Neuropathological and genetic correlates of survival and dementia onset in synucleinopathies: a retrospective analysis. *Lancet Neurol* **16**, 55-65 (2017).
985. D. Coughlin *et al.*, Cognitive and Pathological Influences of Tau Pathology in Lewy Body Disorders. *Ann Neurol* **85**, 259-271 (2019).
986. D. G. Coughlin *et al.*, Multimodal in vivo and postmortem assessments of tau in Lewy body disorders. *Neurobiol Aging* **96**, 137-147 (2020).
987. I. G. McKeith *et al.*, Diagnosis and management of dementia with Lewy bodies: Fourth consensus report of the DLB Consortium. *Neurology* **89**, 88-100 (2017).
988. G. M. Peavy *et al.*, Phenotypic differences based on staging of Alzheimer's neuropathology in autopsy-confirmed dementia with Lewy bodies. *Parkinsonism Relat Disord* **31**, 72-78 (2016).
989. M. Malek-Ahmadi *et al.*, Faster cognitive decline in dementia due to Alzheimer disease with clinically undiagnosed Lewy body disease. *PLoS One* **14**, e0217566 (2019).
990. I. G. McKeith, Consensus guidelines for the clinical and pathologic diagnosis of dementia with Lewy bodies (DLB): report of the Consortium on DLB International Workshop. *J Alzheimers Dis* **9**, 417-423 (2006).
991. A. Iranzo *et al.*, Detection of alpha-synuclein in CSF by RT-QuIC in patients with isolated rapid-eye-movement sleep behaviour disorder: a longitudinal observational study. *Lancet Neurol* **20**, 203-212 (2021).
992. J. C. Jurado-Coronel *et al.*, Sex differences in Parkinson's disease: Features on clinical symptoms, treatment outcome, sexual hormones and genetics. *Front Neuroendocrinol* **50**, 18-30 (2018).
993. M. Lubomski, R. Louise Rushworth, W. Lee, K. L. Bertram, D. R. Williams, Sex differences in Parkinson's disease. *J Clin Neurosci* **21**, 1503-1506 (2014).
994. K. M. Smith, N. Dahodwala, Sex differences in Parkinson's disease and other movement disorders. *Exp Neurol* **259**, 44-56 (2014).
995. S. Weintraub *et al.*, The Alzheimer's Disease Centers' Uniform Data Set (UDS): the neuropsychologic test battery. *Alzheimer Dis Assoc Disord* **23**, 91-101 (2009).
996. E. R. Peskind *et al.*, Safety and acceptability of the research lumbar puncture. *Alzheimer Dis Assoc Disord* **19**, 220-225 (2005).
997. T. J. Montine *et al.*, National Institute on Aging-Alzheimer's Association guidelines for the neuropathologic assessment of Alzheimer's disease: a practical approach. *Acta Neuropathol* **123**, 1-11 (2012).
998. D. W. Dickson, N. Kouri, M. E. Murray, K. A. Josephs, Neuropathology of frontotemporal lobar degeneration-tau (FTLD-tau). *J Mol Neurosci* **45**, 384-389 (2011).

999. N. J. Cairns *et al.*, Neuropathologic diagnostic and nosologic criteria for frontotemporal lobar degeneration: consensus of the Consortium for Frontotemporal Lobar Degeneration. *Acta Neuropathol* **114**, 5-22 (2007).
1000. M. Shahnawaz *et al.*, Discriminating alpha-synuclein strains in Parkinson's disease and multiple system atrophy. *Nature* **578**, 273-277 (2020).
1001. S. S. Mirra *et al.*, The Consortium to Establish a Registry for Alzheimer's Disease (CERAD). Part II. Standardization of the neuropathologic assessment of Alzheimer's disease. *Neurology* **41**, 479-486 (1991).